

DESIGN AND ANALYSIS OF RADAR ANTENNA STRUCTURE WITH
OPTIMUM DYNAMIC BEHAVIOR

A THESIS SUBMITTED TO
THE GRADUATE SCHOOL OF NATURAL AND APPLIED SCIENCES
OF
MIDDLE EAST TECHNICAL UNIVERSITY

BY

ENVER SUN

IN PARTIAL FULFILLMENT OF THE REQUIREMENTS
FOR
THE DEGREE OF MASTER OF SCIENCE
IN
MECHANICAL ENGINEERING

FEBRUARY 2016

Approval of the thesis:

**DESIGN AND ANALYSIS OF RADAR ANTENNA STRUCTURE WITH
OPTIMUM DYNAMIC BEHAVIOR**

submitted by **ENVER SUN** in partial fulfillment of the requirements for the degree
of **Master of Science in Mechanical Engineering Department, Middle East
Technical University** by,

Prof. Dr. Gülbin Dural Ünver
Dean, Graduate School of Natural and Applied Sciences

Prof. Dr. R. Tuna Balkan
Head of Department, **Mechanical Engineering**

Asst. Prof. Dr. Gökhan O. Özgen
Supervisor, **Mechanical Engineering Dept., METU**

Prof. Dr. Yavuz Yaman
Co-Supervisor, **Aerospace Engineering Dept., METU**

Examining Committee Members

Prof. Dr. F. Suat Kadioğlu
Mechanical Engineering Dept., METU

Asst.Prof. Dr. Gökhan O. Özgen
Mechanical Engineering Dept., METU

Prof. Dr. Yavuz Yaman
Aerospace Engineering Dept., METU

Asst.Prof. Dr. Kıvanç Azgın
Mechanical Engineering Dept., METU

Asst.Prof. Dr. Can Ulaş Doğruer
Mechanical Engineering Dept., Hacettepe Univ.

Date: 03.02.2016

I hereby declare that all information in this document has been obtained and presented in accordance with academic rules and ethical conduct. I also declare that, as required by these rules and conduct, I have fully cited and referenced all material and results that are not original to this work.

Name, Last name: Enver SUN

Signature:

ABSTRACT

DESIGN AND ANALYSIS OF RADAR ANTENNA STRUCTURE WITH OPTIMUM DYNAMIC BEHAVIOR

Sun, Enver

M. S., Department of Mechanical Engineering

Supervisor: Asst. Prof. Dr. Gökhan O. Özgen

Co-Supervisor: Prof. Dr. Yavuz Yaman

February 2016, 283 pages

With the advance of technology the radar antenna structures are being smaller and their design alternatives are quite numerous that they can be produced in different shapes and can be conformed to original structures such as body panel of an aircraft or car which are composed of light weight thin shell structures. Radar antennas as an integral part of the air or ground vehicles are subjected to various dynamic loadings which effects its overall radiation pattern which results overall degradation of antenna performance, especially at high amplitude resonance conditions due to low stiffness of host structures.

The passive vibration control, namely surface damping treatment methodology is one of the measurement technique that can be taken account at the initial design phase of such integration process which is based on increasing the damping capacity of host structure by adding viscoelastic materials between contacting surfaces. However adding high density materials results increase of overall weight. Therefore an extensive research activity has been carried out in order to design of surface damping

treatment with spacer layer with minimum weight and maximum damping constraints.

In this study, for simplicity and to verify the design methodology, a four layer cantilever beam that represents the host structure, was designed, analyzed and tested for optimum dynamic behavior. Mainly topology and parametric optimization methods are used in order to find best material layout of uniform spacer and best slotted configuration of spacer layer that maximize the damping performance of the design with minimum material condition. Experimental study is also conducted for layered cantilever beam with developed concept design of slotted configuration under vibration load to verify the methodology used.

Keywords: Passive vibration control, surface damping treatment, cantilever beam, spacer, topology optimization, parametric design and optimization, vibration test, finite element method, modal strain energy, loss factor.

ÖZ

EN İYİ DİNAMİK DAVRANIŞA SAHİP RADAR ANTEN YAPILARININ TASARIMI VE ANALİZİ

Sun, Enver

Yüksek Lisans, Makina Mühendisliği Bölümü

Tez Yöneticisi: Yrd. Doç. Dr. Gökhan O. Özgen

Ortak Tez Yöneticisi: Prof. Dr. Yavuz Yaman

Şubat 2016, 283 sayfa

Teknolojinin ilerlemesi ile birlikte radar anten yapıları günden güne küçülmekte ve çok farklı tasarım alternatifleri ile birlikte entegre edilebildikleri uçak veya otomobil gövdesinin dış şekline uygun olarak da üretilebilmektedirler. Bu tip radar antenlerin sinyal izdüşümü, entegre edildikleri yapıların, düşük direngenliğe sahip olmaları nedeni ile, dinamik kuvvetlerden direkt olarak etkilenen, hafif, ince kabuk yapıda olması sebebiyle özellikle yüksek genlikli yer değiştirmeye sebebiyet veren rozanans durumlarında etkilenmekte ve bu durum radar antenin performans kaybına sebebiyet vermektedir.

Yüksek genlikli bu titreşimlerin engellenmesi amacı ile sönümlenme oranını artırmaya yönelik, viskoelastik malzemelerin kullanıldığı sınırlandırılmış katmanlı titreşim sönümlenme yöntemi, pasif bir titreşim yöntemi olarak entegrasyona yönelik ve erken tasarım geliştirme evresinde uygulanabilecek önlemlerden bir tanesidir. Ancak viskoelastik malzemelerin yüksek yoğunluklu olmaları nedeni ile topyekün tasarım ağırlığında artışa neden olmaktadır. Bu sebeple düşük ağırlıklı ve yüksek titreşim

sönümleme kapasitesine sahip ara katmanlı sınırlandırılmış katmanların tasarımına yönelik geniş kapsamlı bir araştırma yürütülmüştür.

Bu çalışmada, uygulanan tasarım ve analiz yöntemlerinin basitçe doğrulanabilir bir model üzerinde gösterilmesi amacı ile, ankastre sınır koşuluna sahip dört katmanlı kiriş yapısı en iyi dinamik davranışa sahip olacak şekilde tasarlanmış, analiz ve test edilmiştir. Topoloji ve parametrik optimizasyon yöntemleri hafif ve maksimum sönümleme performansı şartları altında özellikle homojen malzeme dağılımına sahip aralayıcı katmanın minimum ağırlıklı malzeme dağılımının bulunmasında ve kanallı aralayıcının en iyi geometrik ölçülerinin bulunmasında kullanılmıştır. Geliştirilen konsept tasarımlardan kanallı yapıdaki aralayıcı katmanlı ankastre kiriş titreşim yükleri altında test edilerek, kullanılan tasarım ve analiz yönteminin geçerliliği doğrulanmıştır.

Anahtar Kelimeler: Pasif titreşim kontrolü, yüzey sönümleme, ankastre kiriş, aralayıcı katman, topoloji optimizasyonu, parametrik tasarım ve optimizasyon, titreşim testi, sonlu elemanlar yöntemi, modal gerinim enerjisi, sönümleme faktörü.

*I may be a tiny human
but
imagine beyond the stars...*

*For
My Beloved
Mother & Father
Şerife, Mahsun*

*Sisters & Brothers
Zerrin, Hamdiye, Orhan, Yusuf, Celal*

*Nephews
Berfin, Umut, Yasin, Uğur, Muhammed, Çınar, Bedirhan, Berat*

*And
Wife & Son
Aysel, Melik Baran...*

ACKNOWLEDGEMENTS

After having a long overwhelming journey of research I would like to gratefully and sincerely thank my supervisor Asst. Prof. Dr. Gökhan O. OZGEN and my co-supervisor Prof. Dr. Yavuz YAMAN for involving me to do this research from which I gained a lot as well as for their continuous support and perfect guidance from beginning to end of this thesis especially at times when I felt lost. Moreover I would like to extend my appreciation to my committee members for their comments and suggestions.

I would like express my deepest gratitude to my wife, Aysel SUN who encouraged and tolerated me throughout this long journey, without your endless support and love, this thesis would not be completed. Most importantly thanks for not only being a wife but also giving both of us our lovely baby Melik Baran SUN who is indeed treasure from Allah. I hope this study will make him inspired and it will also be a guide in his life for learning and pursuing his ambitions with confidence.

I would also like to send my special thanks to the group of people in ASELSAN, firstly, Mr.Servet KOŞAN who helped me to prepare metallic samples, Mr.Arda ÖZGEN for support in manufacturing of 3D printing samples. Also special thanks for my Dir. Mr.Tahir FIDAN for encouraging me to pursue in research and also thanks for my boss Mr.Sadık KÖŞKER for allowing and tolerating me to finish this study at busy work days. Lastly I want to thank to those who working in Environmental Condition Lab. namely, Mr.Samet, Mr.Doğuş and Mr.Umit for serving me during vibration tests.

I would like to express my special appreciation and thanks to Rebecca Brutus & Tom Burns from Soundcoat Inc.,USA, Mr.Altuğ KARADERE from Recticel Inc Turkey. for providing me the isolation samples I used in my testing phase.Also thanks to Mr.Eray ÇINAR for providing me isolation samples from Getzner GmbH.

I would like to send my special thanks to ST Engineering Support Team, Turkey for guiding me in finding solution of Hyperworks Software related problems. Special thanks to Mr. Lutz from Altair Inc., Germany.

I would like to express my deepest gratitude to workers of Republic of Turkey Prime Ministry Undersecretariat of Treasury, especially to Mr. Güvenç KALKANDELEN and Belma ÖZGOREN who had given me endless support throughout my study life and for mentoring in professional life.

Finally and most importantly, I am also very grateful to Allah who makes the impossible possible not letting me alone.

TABLE OF CONTENTS

ABSTRACT	v
ÖZ	vii
ACKNOWLEDGEMENTS	x
TABLE OF CONTENTS	xii
LIST OF FIGURES	xv
LIST OF TABLES	xxv
LIST OF SYMBOLS	xxvii
CHAPTER 1	1
1. INTRODUCTION	1
1.1 Radar Antennas	1
1.1.1 Basic Characteristics of an Antenna Element	4
1.2 Types of Antennas and Their Application Areas	8
1.2.1 Microstrip Antenna	12
1.2.2 Phased Array Antennas	14
1.2.3 Conformal Antennas	16
1.3 Motivation of the Study	20
1.4 Background	24
1.4.1 Surface Damping Treatments	25
1.4.1.1 Free Layer Damping Treatment	25
1.4.1.2 Constrained Layer Damping Treatment	26
1.4.1.3 Improved Constrained Layer Damping With Spacer Layer	29
1.5 Literature Review	32
1.5.1 Summary of Literature Review	52
1.5.2 Objective and Scope of The Thesis	55
CHAPTER 2	57
2 THEORETICAL BACKGROUND	57
2.1 Introduction	57

2.2	Damping.....	66
2.3	Viscoelastic Materials.....	68
2.3.1	Effects of Temperature and Frequency.....	69
2.3.2	Linear Dynamic Response and Energy Dissipation	70
2.3.2.1	Energy Storage and Dissipation.....	72
2.4	Analysis of Viscoelastic Damping Treatment	75
2.4.1	RKU Method.....	76
2.4.1.1	Transverse Vibration of Simple Beam.....	76
2.4.2	2D Finite Element Method	84
2.4.2.1	Modal Strain Energy Method.....	92
2.4.2.2	Direct Frequency Response Method	93
2.4.2.2.1	Half Power Bandwidth Method.....	97
CHAPTER 3		101
3	DESIGN AND ANALYSIS OF VIBRATING BEAM FOR OPTIMUM	
	DYNAMIC BEHAVIOUR	101
3.1	Introduction.....	101
3.2	Structural Optimization.....	103
3.2.1	Design Variables:.....	105
3.2.2	Constraints:	106
3.2.3	Responses:	106
3.2.4	Objective Function:.....	106
3.2.5	Topology Optimization.....	107
3.2.5.1	Density Method (SIMP).....	108
3.2.5.2	Methodology	112
3.2.5.3	Finite Element Modeling.....	117
3.2.6	Topology Optimization of Stand-off Layer	127
3.2.6.1	Case Study I:	131
3.2.6.2	Case Study II:.....	152
3.2.6.3	Case Study III:	168
3.2.6.4	Case Study IV:	183
3.2.7	Parametric Optimization.....	201

3.2.7.1	Introduction	201
3.2.7.2	Development of Methodology	202
3.2.7.3	Verification of Methodology.....	207
3.2.7.3.1	Case Study I.....	211
3.2.7.3.2	Case Study II.....	223
3.3	Comparison of Optimization Results	242
CHAPTER 4	247
4	VIBRATION TEST FOR VALIDATION	247
4.1	Experimental Study.....	247
4.1.1	Production of Test Samples	249
4.1.2	Vibration Test	252
4.2	Results and Comparisons	257
CHAPTER 5	263
5	CONCLUSION AND FUTURE WORK	263
REFERENCES	269

LIST OF FIGURES

FIGURES

Figure 1-1 Operational principle of a radar system [1].....	2
Figure 1-2 Transition between transmission line and antenna [3].....	3
Figure 1-3 Omnidirectional, semi directional and sector coverage patterns [5].....	4
Figure 1-4 Polar plot of radiation pattern [7].....	5
Figure 1-5 Directivity and Gain [8].....	7
Figure 1-6 Typical application of ground to air and air to ground radar system (Adapted from [1]).	8
Figure 1-7 The mast antenna used for car radio [10].....	9
Figure 1-8 Blade antenna attached to the skin of an aircraft [11].....	10
Figure 1-9 Radar as Airborne Warning and Control System [12].....	10
Figure 1-10 The structure of microstrip circular patch antenna (Adapted from [3]) .	12
Figure 1-11 Grid of microstrip patch antennas over design surfaces.....	13
Figure 1-12 Phased array antenna (Adapted from [6]).....	14
Figure 1-13 Sandwich smart skin (Adapted from [25])	16
Figure 1-14 Flexible conformal antenna [27]	17
Figure 1-15 Using radar sensors in the car [31].....	17
Figure 1-16 Submarine communication in the near future [35].....	18
Figure 1-17 Integration of conformal antennas on skin of aircraft [42]	19
Figure 1-18 Air vehicle body panel and possible antenna location (Adapted from: [40]).....	20
Figure 1-19 Distorted radiation pattern during vibration (Adapted from [43]).....	21
Figure 1-20 Free layer surface damping treatment	26
Figure 1-21 Constrained layer damping treatment.....	27
Figure 1-22 Application of damping treatment on aircraft fuselage [57].....	28
Figure 1-23 Application of damping solution in car body [58].....	29

Figure 1-24 Use of spacer medium as strain amplifier (a) for unconstrained layer (b) for constrained layer (<i>Adapted from [59]</i>).....	30
Figure 1-25 Distribution of damping material after topology optimization (<i>adapted from [67]</i>)	35
Figure 1-26 Segmented single and multiple constraining layer damping treatment: (<i>adapted from [70]</i>).....	37
Figure 1-27 Partial damping patches over beam with main parameters (<i>adapted from [71]</i>).....	37
Figure 1-28 Increase of radius of curvature with spacer layer (<i>Paintwork</i>).....	47
Figure 1-29 Spaced viscoelastic layer (<i>Adapted from [95]</i>)	48
Figure 1-30 Vertically oriented plates as spacer (<i>Adapted from [96]</i>).....	49
Figure 1-31 Hat section spacer with open gaps (<i>Adapted from [98]</i>)	49
Figure 1-32 Topology optimization of spacer layer (<i>Produced by Optistruct[®]</i>).....	55
Figure 2-1 Vibration of thin panel like structure (<i>Adapted from [113]</i>)	58
Figure 2-2 Single degree of freedom system under harmonic load (<i>Adapted from [113]</i>).....	59
Figure 2-3 Variance of displacement response of simple 1 DOF system $\omega = 0.8\omega_n$	63
Figure 2-4 Variance of displacement response of simple 1 DOF system: $\omega = \omega_n$... 64	64
Figure 2-5 Displacement response of simple 1 DOF system in frequency domain when $\omega = \omega_n$. [114]	65
Figure 2-6 internal energy loss mechanism: <i>hysteresis loop</i> (<i>Adapted from [113]</i>) ..	66
Figure 2-7 Variation of Modulus and Loss Factor (<i>Adapted from [119]</i>).....	69
Figure 2-8 Linear dynamic response of viscoelastic material under loading (<i>Adapted from [121]</i>)	70
Figure 2-9 Deflected shape of vibrating beam (<i>Adapted from [122]</i>).....	76
Figure 2-10 Fixed-free beam (<i>Adapted from [122]</i>).....	78
Figure 2-11 Flexural rigidity of treated layered beam	81
Figure 2-12 Topology optimization of spacer layer (<i>Adapted from [60]</i>).....	82
Figure 2-13 2D finite elements [126].....	84
Figure 2-14 2D state of strain [127]	85

Figure 2-15 2D plane elements under load [128].....	87
Figure 2-16 Extraction of damping factor from resonance peak (<i>Adapted from</i> [120])	97
Figure 2-17 Extraction of loss factor from direct frequency response functions.....	98
Figure 3-1 Optimizaton cycle (<i>Adapted from</i> : [135])	103
Figure 3-2 Simulation model for topology optimization (<i>Adapted from</i> : [136]).....	108
Figure 3-3 Material interpolation within design domain [137].....	111
Figure 3-4 Topology Optimization Steps.....	113
Figure 3-5 Topology Optimization Process	114
Figure 3-6 2D Finite element modeling.....	117
Figure 3-7 Modal analysis results: 2D modeling (Left), 3D modeling (Right)	119
Figure 3-8 Modal analysis results: 2D modeling (Left), 3D modeling (Right)	120
Figure 3-9 Modal analysis results: Analytical (RKU) (1 st to 5 th Mode)	121
Figure 3-10 Modal analysis results: Analytical (RKU) (6 th to 10 th Mode).....	122
Figure 3-11 DYAD-601 Frequency dependent material properties [144].....	126
Figure 3-12 Generation of frequency response function.....	130
Figure 3-13 Finite element model of cantilever beam	131
Figure 3-14 Layout of original (top) and optimized stand-off layer (bottom) upon minimizing compliance index	132
Figure 3-15 Refined 2D geometry of stand-off layer after topology optimization and 3D generation of final treated beam.....	134
Figure 3-16 Mode shapes of cantilever beam with optimized stand-off (Case I)....	135
Figure 3-17 Strain energy distribution of partially covered stand-off layer	136
Figure 3-18 Increased Strain Energies within VEM layer along beam.	137
Figure 3-19 Increased Strain Energies within VEM layer along beam.	137
Figure 3-20 Strain energies within viscoelastic layer along beam.....	138
Figure 3-21 Frequency response function of beam with uniform stand-off layer (H=10 mm).....	139
Figure 3-22 Frequency response function of beam with optimized stand-off layer (H=10 mm).....	139

Figure 3-23 Frequency response function of beam with equally weighted uniform stand-off layer (H=3.52 mm)	140
Figure 3-24 Frequency response functions of original uniform (dashed fade black), optimized (dark black) and equal weight (blue) uniform stand-off layer.	141
Figure 3-25 Addition of cuts into new layout of stand-off layer (partial coverage)	142
Figure 3-26 Frequency response function of beam with partially treated optimized stand-off layer	142
Figure 3-27 Overall comparison of frequency response functions	143
Figure 3-28 Thickness reduction of new layout (Topology I) of stand-off layer	145
Figure 3-29 Frequency response function of beam with optimized stand-off layer with reduced thickness.	145
Figure 3-30 Addition of cuts into stand-off layer (partial coverage) (H=3.52mm).	146
Figure 3-31 Frequency response function of beam with partially treated optimized stand-off layer with reduced thickness (Topology I).	146
Figure 3-32 Overall comparison of frequency response functions (H=3.52 mm) & (H=10 mm).....	147
Figure 3-33 Overall comparison of frequency response functions (H=3.52 mm-partially treated) & (H=10 mm-uniform fully treated).....	150
Figure 3-34 Deformation pattern of the unit cell of treated beam with stand-off layer under assumed load cases.....	153
Figure 3-35 Topology optimization result for the treated unit cell (up)-treated beam with periodic units cells (down).....	154
Figure 3-36 Mode shapes of cantilever beam with optimized stand-off (Case II)...	155
Figure 3-37 Mode shapes of cantilever beam with optimized stand-off (Case II) in the range of 8kHz-12kHz	156
Figure 3-38 Frequency response function of treated beam with stand-off layer with topology of unit cell.	157
Figure 3-39 Frequency response function of uniform stand-off layer with equivalent mass.....	157
Figure 3-40 Addition of cuts into stand-off layer with unit cell topology.	158

Figure 3-41 Frequency response function of partially treated beam with optimized stand-off layer.	158
Figure 3-42 Overall comparison of frequency response functions	159
Figure 3-43 Rebuilding of treated beam with scaled unit cell topology	162
Figure 3-44 Frequency response function of scaled stand-off layer with same unit cell topology.....	162
Figure 3-45 Frequency response function of scaled stand-off layer with partially covered same unit cell topology.....	163
Figure 3-46 Overall comparison of frequency response functions	164
Figure 3-47 Overall comparison of frequency response functions (H=3.45 mm-partially treated) & (H=10 mm-uniform fully treated)	166
Figure 3-48 Deformation pattern and new topology of the unit cell of treated beam with stand-off layer under assumed load cases.....	168
Figure 3-49 First ten mode shapes of treated cantilever beam with optimized stand-off (Case III).....	170
Figure 3-50 Mode shapes of treated cantilever beam at higher modes with optimized stand-off (Case III).....	171
Figure 3-51 Continued	172
Figure 3-52 Frequency response function of fully treated beam with optimized unit cell topology (Topology III).....	172
Figure 3-53 Frequency response function of treated beam with optimized unit cell topology with added cuts.	173
Figure 3-54 Frequency response function of beam with equally weighted uniform stand-off layer (Case III).....	173
Figure 3-55 Overall comparison of frequency response functions (Case III).....	174
Figure 3-56 Treated beam with scaled model of stand-off layer	177
Figure 3-57 Frequency response function of treated beam with reduced thickness value of stand-off layer	177
Figure 3-58 Frequency response function of partially treated beam with optimized stand-off layer with cuts.....	178

Figure 3-59 Overall comparison of frequency response functions for thinner stand-off layer with same topology (Case III).	179
Figure 3-60 Overall comparison of frequency response functions (H=2.64 mm-partially treated) & (H=10 mm-uniform fully treated).....	181
Figure 3-61 State of deformation under sinusoidal static load.....	183
Figure 3-62 Finite element model of cantilever beam under sinusoidal loading.....	184
Figure 3-63 Resulting topology and refined geometry of stand-off layer.....	184
Figure 3-64 Mode shapes of treated beam with optimized stand-off layer (Case IV)	185
Figure 3-65 Mode shapes of treated beam with optimized stand-off layer at higher modes (Case IV).....	186
Figure 3-66 Frequency response function of treated beam with optimized stand-off layer.....	187
Figure 3-67 Frequency response function of partially treated beam with optimized stand-off layer	187
Figure 3-68 Frequency response function of equally weighted treated beam with uniform stand-off layer.....	188
Figure 3-69 Overall comparison of frequency response functions (Case IV).....	189
Figure 3-70 Treated beam with scaled model of optimized stand-off layer	191
Figure 3-71 Frequency response function of treated beam with reduced thickness value of stand-off layer	191
Figure 3-72 Frequency response function of partially treated beam with optimized stand-off layer with cuts (Case IV)	192
Figure 3-73 Frequency response function of treated beam with uniform equally weighted stand-off layer (Case IV H=1.523 mm).....	192
Figure 3-74 Overall comparison of frequency response functions	193
Figure 3-75 Overall comparison of frequency response functions (H=3.79 mm-partially treated) & (H=10 mm-uniform fully treated).....	195
Figure 3-76 2D Finite element (shaded) model of cantilever vibrating beam	202
Figure 3-77 Parametric design cycle.....	203
Figure 3-78 Parametric design and optimization cycle.....	204

Figure 3-79 Parametric design of 2D treated beam in CATIA®	205
Figure 3-80 Content of HyperStudy Model.tpl file.....	205
Figure 3-81 Extraction of strain energies and modal loss factors within HyperStudy®	206
Figure 3-82 3D Finite element model of cantilever beam with viscoelastic core....	207
Figure 3-83 Definition of geometrical and material parameters as discrete design variables.	211
Figure 3-84 Cantilever sandwich beam model and its design variables (E_2 & H_2) .	211
Figure 3-85 Variation of loss factor value for different modulus value for the first ten modes ($H=1.5$ mm)- $E_{opt}=500-2200$ MPa.....	212
Figure 3-86 Variation of loss factor value for different modulus value for the first ten modes ($H=2$ mm)- $E_{opt}=500-2200$ MPa.....	213
Figure 3-87 Variation of loss factor value for different modulus value for the first ten modes ($H=2.5$ mm) - $E_{opt}=500-1100$ MPa.....	213
Figure 3-88 Variation of loss factor value for different modulus value for the first ten modes ($H=4$ mm) - $E_{opt}=500-1100$ MPa.....	213
Figure 3-89 Effect of spacer height and elastic modulus on loss factor	214
Figure 3-90 Effect of spacer height and elastic modulus on loss factor at 1 st mode	215
Figure 3-91 Effect of spacer height and elastic modulus on loss factor at 2 nd mode	215
Figure 3-92 Effect of spacer height and elastic modulus on loss factor at 3 rd mode	216
Figure 3-93 Effect of spacer height and elastic modulus on loss factor at 4 th mode	216
Figure 3-94 Effect of spacer height and elastic modulus on loss factor at 5 th mode	216
Figure 3-95 Effect of spacer height and elastic modulus on loss factor at 6 th mode	217
Figure 3-96 Effect of spacer height and elastic modulus on loss factor at 7 th mode	217
Figure 3-97 Effect of spacer height and elastic modulus on loss factor at 8 th mode	217
Figure 3-98 Effect of spacer height and elastic modulus on loss factor at 9 th mode	218
Figure 3-99 Effect of spacer height and elastic modulus on loss factor at 10 th mode	218

Figure 3-100 Effect of elastic modulus and spacer height on loss factor at 1 st mode	219
Figure 3-101 Effect of elastic modulus and spacer height on loss factor at 2 nd mode	219
Figure 3-102 Effect of elastic modulus and spacer height on loss factor at 3 rd mode	220
Figure 3-103 Effect of elastic modulus and spacer height on loss factor at 4 th mode	220
Figure 3-104 Effect of elastic modulus and spacer height on loss factor at 5 th mode	220
Figure 3-105 Effect of elastic modulus and spacer height on loss factor at 6 th mode	221
Figure 3-106 Effect of elastic modulus and spacer height on loss factor at 7 th mode	221
Figure 3-107 Effect of elastic modulus and spacer height on loss factor at 8 th mode	221
Figure 3-108 Effect of elastic modulus and spacer height on loss factor at 9 th mode	222
Figure 3-109 Effect of elastic modulus and spacer height on loss factor at 10 th mode	222
Figure 3-110 Design parameters of slotted stand-off layer	224
Figure 3-111 Parametric model of slotted configuration of treated beam	224
Figure 3-112 Design variables in parameter optimization of slotted configuration	224
Figure 3-113 Objective functions definitions in optimization	225
Figure 3-114 Built-in optimization algorithms	226
Figure 3-115 Evaluation history of optimization method	226
Figure 3-116 Optimized slotted configuration of stand-off layer (H=2.513 mm)	227
Figure 3-117 Mode shapes of treated cantilever beam with optimized slotted stand-off layer (H ₂ =2.513 mm)	228
Figure 3-118 Displacement response of treated beam with uniform stand-off (H=10 mm)	229

Figure 3-119 Displacement response of treated beam with uniform stand-off (H=4 mm).....	229
Figure 3-120 Displacement response of treated beam with uniform stand-off (H=1.32 mm).....	230
Figure 3-121 Displacement response of treated beam with optimized slotted stand-off (H=2.513 mm -Full Coverage).....	230
Figure 3-122 Displacement response of treated beam with optimized slotted stand-off (H=2.513 mm -Partial Coverage).....	231
Figure 3-123 Overall comparison of treated beams with uniform and optimized stand-off.....	232
Figure 3-124 Mode shapes of treated cantilever beam with optimized slotted stand-off layer (H ₂ =3.12 mm).....	235
Figure 3-125 Comparison of results of optimization algorithms: GRSM vs GA	236
Figure 3-126 Comparison of results of optimization algorithms: GRSM-GA-MOGA	239
Figure 3-127 Frequency response function comparison of best candidate designs.	242
Figure 3-128 Continued	243
Figure 3-129 Frequency response function of bare and treated beam with optimum stand-off layer	244
Figure 3-130 (Continued).....	245
Figure 3-131 Frequency response function of bare and treated beam with optimum design candidates for stand-off layer	245
Figure 3-132 (Continued).....	246
Figure 3-133 Frequency response function of bare and treated beam with optimum stand-off layer	246
Figure 4-1 3D view of treated beam with optimized configuration of slotted stand-off layer.....	248
Figure 4-2 Cutting and machining of aluminum sheets.....	249
Figure 4-3 3D prototypes of optimized slotted stand-off layer.....	250
Figure 4-4 Assemblage of each individual layers to form treated beams	251

Figure 4-5 Manufactured treated beam samples: (a) 10 mm uniform, (b) 4 mm uniform, (c) 1.32 mm uniform,(d) 2.513 mm slotted-full coverage, (e) 2.513 mm slotted partially covered stand-off layer.....	252
Figure 4-6 Modal analysis of test fixture: 1 st Mode: 1958 Hz (Up), 2 nd Mode: 2609 Hz (Down).....	253
Figure 4-7 Treated beam attached to the shaker in fixed-free boundary condition .	254
Figure 4-8 Data acquisition system used in vibration test	255
Figure 4-9 Generation of frequency response function.....	256
Figure 4-10 Vibration test results: Frequency response functions of each sample..	257
Figure 4-11 Acceleration response of treated beams with uniform and optimized slotted stand-off: (a) GRSM vs GA , (b) GRSM,GA,MOGA, (c) GRSM vs Uniform Spacer	258
Figure 4-12 (Continued).....	259
Figure 4-13 Comparison of numerical and experimental results	260

LIST OF TABLES

TABLES

Table 2-1 Roots of shape function for the cantilever (fixed-free) beam [123]	81
Table 2-2 Correction factor for shear parameter for specific boundary condition [124]	83
Table 3-1 Material and Geometrical Properties Three Layer Treated Beam.....	118
Table 3-2 Comparison of Modal Analysis Results	123
Table 3-3 Material and Geometric Cards in Hypermesh [143].....	125
Table 3-4 Isotropic Frequency Dependent Material Property Card [143]	125
Table 3-5 Material and Geometric Properties of Individual Layers	127
Table 3-6 Comparison of Original and Optimized Beam	133
Table 3-7 Summary of the optimization results (CASE I-H=10mm)	144
Table 3-8 Summary of the optimization results (CASE I-H=3.52 mm)	149
Table 3-9 Results of Optimization for H=10mm and H=3.52 mm Stand-off Layer	151
Table 3-10 Summary of the optimization results (CASE II-H=10mm).....	161
Table 3-11 Summary of the optimization results (CASE II-H=3.45 mm).....	165
Table 3-12 Results of Optimization for H=10mm and H=3.45 mm Stand-off Layer	167
Table 3-13 Summary of the optimization results (CASE III-H=10mm)	176
Table 3-14 Summary of the optimization results (CASE III-H=2.64 mm)	180
Table 3-15 Results of Optimization for H=10mm and H=2.64 mm Stand-off Layer	182
Table 3-16 Summary of the optimization results (CASE IV-H=10mm)	190
Table 3-17 Summary of the optimization results (CASE IV-H=3.79 mm)	194
Table 3-18 Results of Optimization for H=10mm and H=3.79 mm Stand-off Layer	196
Table 3-19 Relative Damping Performance of Fully Treated Uniform Thinner Stand- off Layers	197

Table 3-19 Continued.....	198
Table 3-20 Summary of Relative Damping Improvement w.r.t. Thick Uniform Stand-off Layer (H=10mm)	199
Table 3-21 Material properties of sandwich beam [114].....	208
Table 3-22 Comparison of the loss factor results.....	209
Table 3-23 Optimum values of parameters for the slotted configuration (GRSM). ..	227
Table 3-24 Relative damping performance of optimized slotted stand-off layer	233
Table 3-25 Optimum values for slotted configuration: Genetic Algorithm (GA) ...	234
Table 3-26 Relative damping performance of optimized slotted stand-off layer (GA)	237
Table 3-27 Optimum values for slotted configuration: Multi Objective Genetic Algorithm (MOGA)	238
Table 3-28 Relative damping performance of optimized slotted stand-off layer (MOGA).....	240
Table 3-29 Relative damping performance of optimized slotted stand-off layers with respect to thick uniform spacer (H=10 mm)	241
Table 3-30 Overall comparison of optimized designs in terms of damping	243
Table 4-1 Loss factors and frequency results for optimized beam with slotted stand-off (Numerical Results).....	260
Table 4-2 Relative comparison of damping performances of tested beams	261

LIST OF SYMBOLS

SYMBOLS

k : Wave number

λ : Wave length

ω : Angular frequency

m : Mass

c : Damping coefficient

k : Stiffness term

X : Displacement amplitude

ζ : Damping ratio

D : Internal strain energy due to hysteresis

σ : Stress

ϵ : Strain

$E'(\omega), G'(\omega)$: Storage Young's and Shear Modulus (Frequency Dependent)

$E''(\omega), G''(\omega)$: Loss Young's and Shear Modulus (Frequency Dependent)

$\eta(\omega)$: Loss factor (Frequency Dependent)

ρ : Density

β : Root of shape function (flexural modes)

I : Area moment of inertia of cross section

H_i : Layer thickness ($i=1,2..n$)

g^* : shear parameter

ϵ_i : Normal strain term ($i=x,y,z$)

γ_{ij} : Shear strain in ij -plane

U: Internal strain energy

N_i =Shape functions

M: Mass matrix

K: Stiffness matrix

B: Damping matrix

A: Magnitude of response amplitude

CHAPTER 1

INTRODUCTION

1.1 Radar Antennas

Advances in modern technology together with expanding needs have made possible various practical applications in communication field either in military and civilian sector. Especially the wireless technology is one of the growing field that allows us to send, convey and receive data regardless of location and distances without the need of cables or any other forms of electrical conductors through the use of a source of electrical energy, antenna elements and conductive space, which is usually open atmosphere, altogether forming a communication network.

In military applications one of the application area of wireless communication is, radio detection and ranging, shortly RADAR which was developed in World War II to detect the enemy targets. Through the years the application areas and their functions have been widened and they have been used for tactical, intelligence, surveillance, and reconnaissance purposes as well as keeping air routes safe by tracking air traffic, detecting moving targets such as missiles, vehicles for speed measurement and even in image generation purposes.

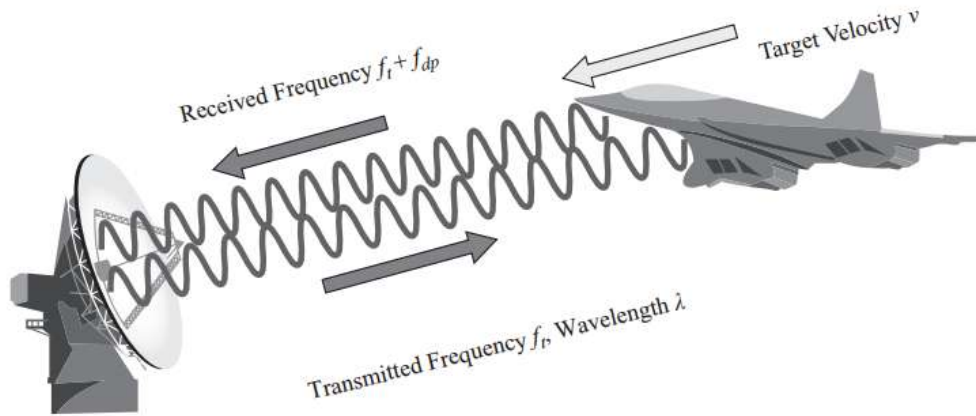


Figure 1-1 Operational principle of a radar system [1]

In radar systems, the generated electromagnetic waves are directed to an object or an area from which the required information will be collected. This process resembles the illumination of a region by a light. The waves collide, bounce and scattered back from the target locations then the antenna elements collect those bounced waves back again in order to gather desired information from it via signal processing. A radar system performs this action continuously and simultaneously for stationary or moving targets [1].

The antenna is the first element in the transmitting or receiving those signals which are described as travelling electromagnetic waves in space/air. Depending on the purpose, antennas can work either in transmitter or receiver modes. Basically the electrical energy is converted into electromagnetic waves and antennas are used to radiate those waves in the form of a beam that is received by another antenna at which the electromagnetic waves are then converted into electrical signals after signal processing [2].

Basic principle of radiation of electromagnetic waves through antennas can be illustrated as in Figure 1-2. The electrical field is generated in source by simply creating an unbalanced charge and in transmitter mode the generated signals with certain amplitude guided to the antenna element and radiated to the free space to the

required direction. Conversely in receiving mode the energy received is transformed into another wave to be processed to extract the information from it [3]. From this perspective, antennas have critical role as they provide the fundamental link between free space and target.

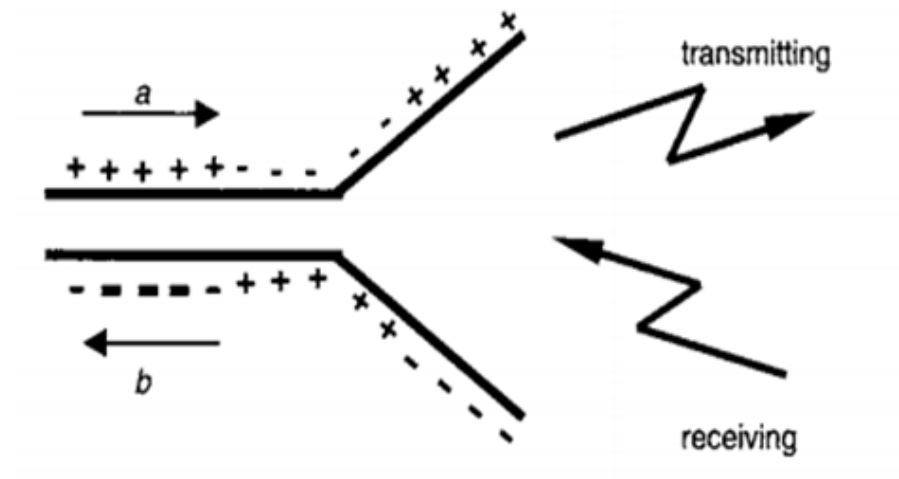


Figure 1-2 Transition between transmission line and antenna [3]

Antenna elements basically focus and transmit the RF energy into a specific direction and based on their transmitting characteristics the antennas are grouped into two part [4, 5];

- Omnidirectional
- Directional and Semi-Directional

Omnidirectional Antennas:

This type of antenna elements creates a toroidal uniform coverage area around its axis and its simple form is known as dipole antenna (Figure 1-3). When intended to have uniform coverage of RF signals such as the case for the radio broadcasting applications this type of antennas are selected.

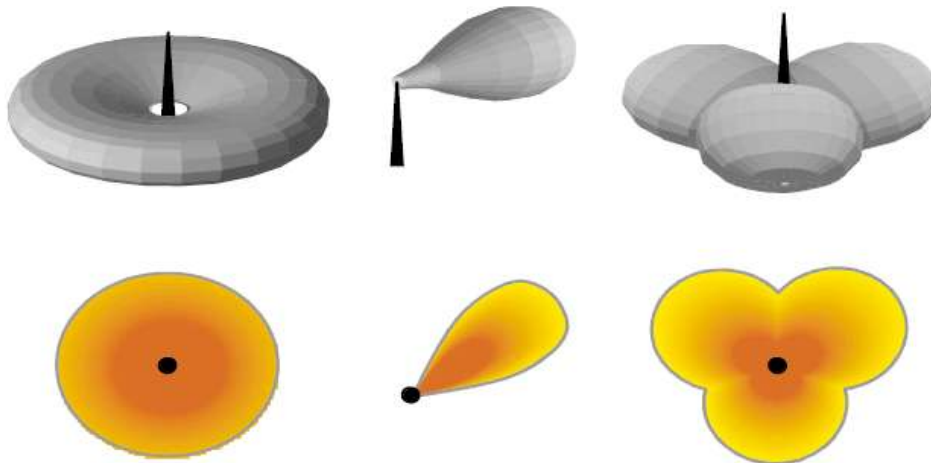


Figure 1-3 Omnidirectional, semi directional and sector coverage patterns [5]

Directional and Semi-Directional:

In this type of antennas the radiated energy concentrated into specific direction with narrower band width, patch and panel like antennas are within this group. Using more than one antenna the coverage area in certain direction can be increased (Figure 1-3).

1.1.1 Basic Characteristics of an Antenna Element

The performance of antennas is described with various radiation characteristics. Some of the important basic characteristics of an antenna element are listed below [6].

Radiation Pattern:

Antennas emit electromagnetic energy in certain modes and the radiation strength can be different in one direction compared to other direction. Radiation pattern is visualization of propagated wave which shows in which direction an antenna directs the energy it radiates. This information can be provided either in the form of polar or

rectangular plots. An example of polar graph shows a sample radiation pattern (Figure 1-4).

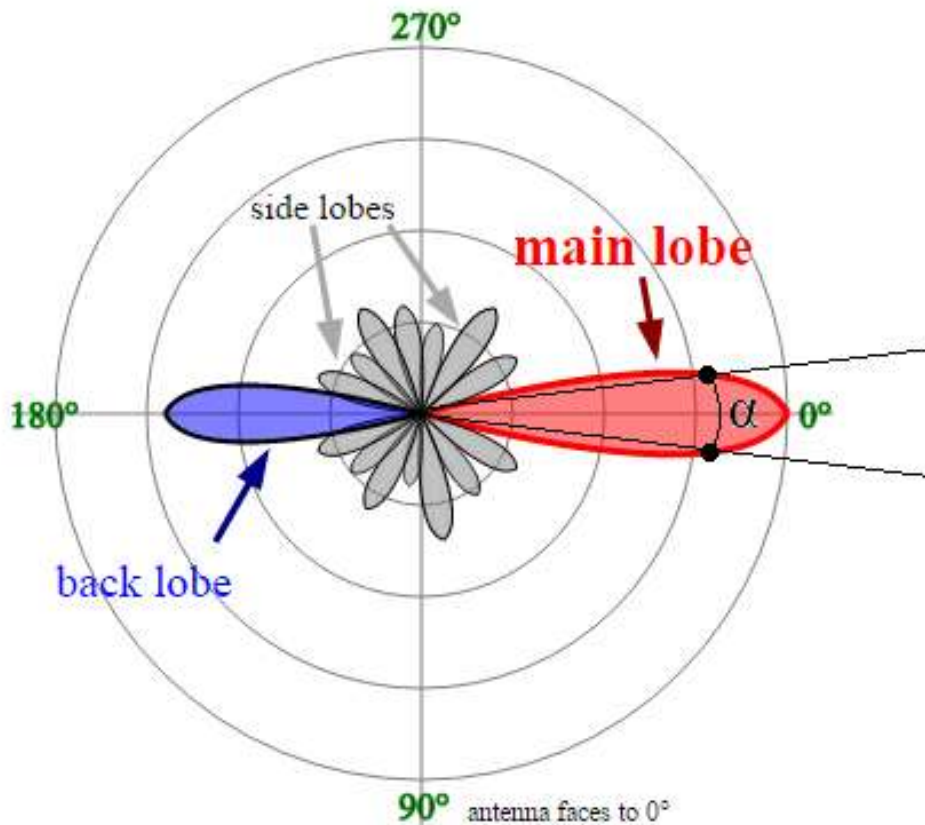


Figure 1-4 Polar plot of radiation pattern [7]

The *main lobe* shows the maximum radiation direction whereas the *side lobes* shows the least energy propagation directions with smaller beams which are usually radiation in undesired directions in varying intensity which can create various problems that will be defined in subsequent section. Another side lobe is called *back lobe* which is the portion of radiation pattern that is directed opposing the main beam direction.

Beam width:

Defines the maximum angular range of emitted pattern α (Figure 1-4) in which the strength of antenna at its half power.

Band width:

Antennas operate over wide frequency ranges and bandwidth defines the effective operation frequency where its performance is set for.

Directivity and Gain:

Antennas are designed for the specific purpose and mostly intend is to focus its radiation energy to a particular direction while minimizing in other direction. The gain is known as the ratio of maximum energy emitted to that particular direction to the least energy portion in other direction. On the other hand directivity is focusing action or increase of strength in specific direction. If we consider radiation pattern as a beam of light coming from out of a torch, focusing action corresponds to narrowing beam pattern and increasing directivity [8]. Increasing directivity of antenna elements provides long range capability for the radar antenna.

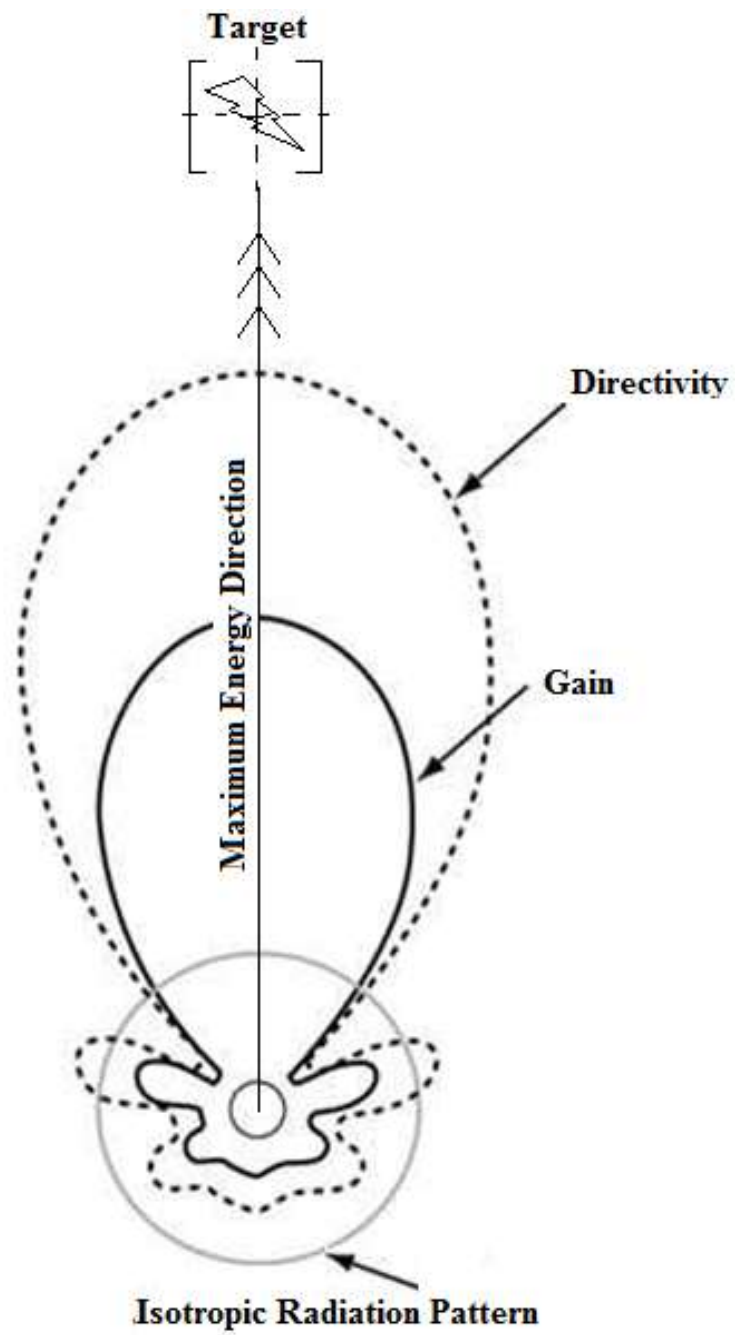


Figure 1-5 Directivity and Gain [8]

1.2 Types of Antennas and Their Application Areas

Using various types of antennas with the help of their radiation characteristics described above, radars perform various operational functions.

During search or surveillance function, a radar antenna forms the generated radiation energy into a shape called directive beams or a pattern which illuminates and scans the wide angular region in short or long range for detection and extraction of information from targets that may exist on ground or in sky as illustrated in Figure 1-6. During operation radar antenna simply radiates its energy in form of a beam (Figure 1-3) that focus on over an area or on a target like a light source and scans repeatedly. If any exists, upon reflection of scattered energy from the objects, radar antenna picks up those reflections as receiver. In addition to search function some radars also perform tracking function which requires specially designed antennas i.e. airborne radar antennas [9].

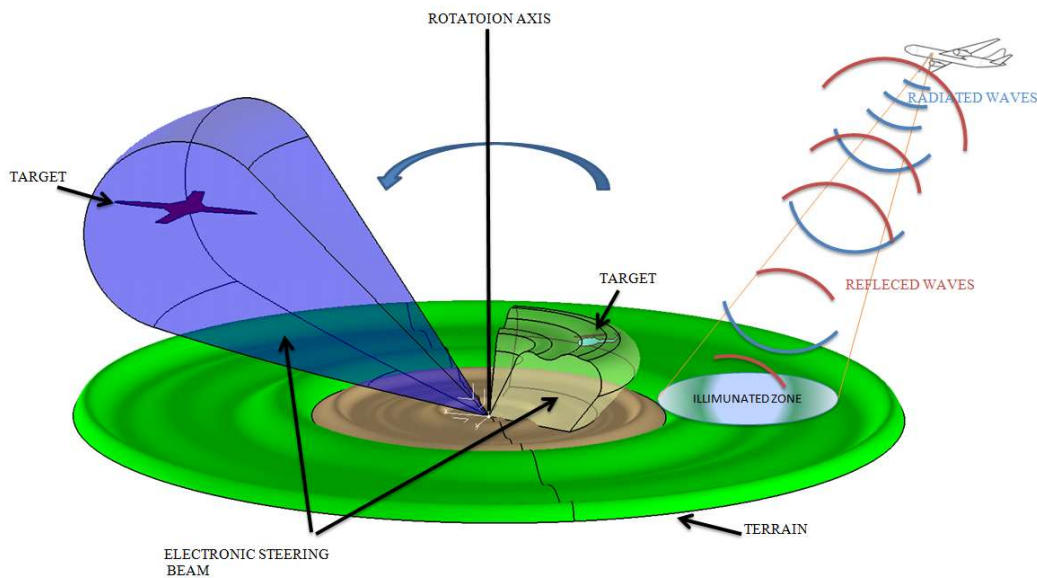


Figure 1-6 Typical application of ground to air and air to ground radar system (Adapted from [1]).

Radar antennas are installed on various platforms ranging from land vehicles, submarines, missiles and aircrafts, helicopters and automobiles in various sizes and shapes to provide essential functions as part of communication, navigation, tracking, monitoring, electronic warfare and collision avoidance systems [9].

One of the most common antenna type that is conventionally used over automobiles is the mast antenna. This type of antenna creates uniform radiation pattern around the car for best performance for car radio (Figure 1-7).



Figure 1-7 The mast antenna used for car radio [10]

Aircrafts also use many types of antennas attached over their body in order to communicate and route its path based on the information gathered from air traffic control and also to navigate to the exact location using global positioning system via creating a link between satellites-ground and aircraft. They can be small enough in size like blade antennas attached over the skin of a civil aircraft (Figure 1-8) and also huge enough as part of early warning warfare systems in military aircrafts (Figure 1-9).



Figure 1-8 Blade antenna attached to the skin of an aircraft [11]



Figure 1-9 Radar as Airborne Warning and Control System [12]

The location, size, number and shape of these antennas are selected based on specific functional requirements and some performance criteria as well as their reliability and maintainability. Small or big in size, the antennas protruding from the outer mold

line of the aircraft involves modifications on the aircraft surface and the ones as shown in (Figure 1-9) greatly increase the cross section of aircraft resulting an increased cost, weight and aerodynamic drag with increased fuel consumption. In case of improper design and integration of antennas some mechanical problems arise such that due to severe loading environment such as vibration and buffeting phenomena encountered during flight may cause delamination, cracks and rupture at the vicinity of the attached zone or on the antenna itself which in turn may also cause the loss of antenna. Thin blade antennas, especially those attached to the critical zone of disturbing aerodynamic flow, are more prone to vibrate and rupture under this kind of excitations [13,14]. In addition, this type of antennas increases the risk of detection by other radars due to increased vehicle signature [15].

Fortunately with the advances in electronic and production technology have led to the creation of new form of antenna that extends the application areas with diverse advantages over classical radar antennas in terms of performance over wide frequency range, cost, weight, ease of installation, low profile and conformable which is the key important property enabling of integration electronics on various curved or planar surfaces which are special type of radiator elements termed as microstrip patch antenna which can be printed over or embedded into the design domain.

1.2.1 Microstrip Antenna

The microstrip antenna element simply composed of printed metallic conductor over the dielectric substrate which creates a cavity between another larger ground plane (Figure 1-10). The basic radiation mechanism of patch antennas relies on generation of electric field between patch and ground plane at its resonant frequency. When it is triggered with electrical current, it radiates in some certain modes or in other words in a different shape of beam of electromagnetic energy perpendicular to its surface.

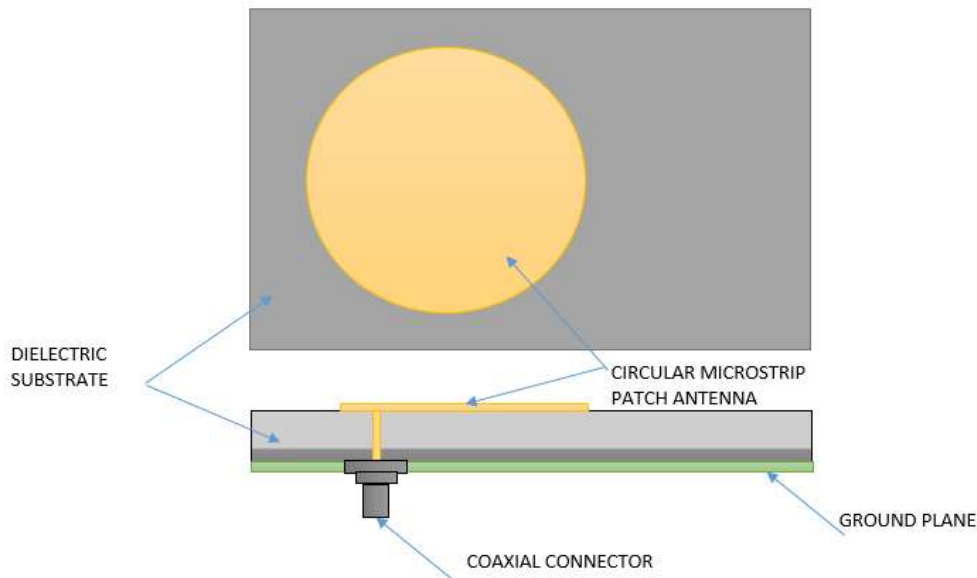


Figure 1-10 The structure of microstrip circular patch antenna (*Adapted from* [3])

Microstrip patch antenna provides numerous advantages over conventional radar antennas thanks to its smaller size, light weight, thin profile simpler form as well as their low cost and ease of production. Their shapes can be changed and they are suitable for various geometrical configurations. They can be either planar in circular, rectangular, square, triangular or any other irregular shape [16]. Moreover their conformability over intended design domain makes them more attractive for various military and civil industries.

Their radiation characteristics can be controlled through incorporation of complex signal processing algorithms and together with construction of miniature fractal grid pattern of microstrip patch antenna arrays, which are known as phased array antennas, their radiation coverage area can be increased. Also making use of their conformability and new photolithographic production process enables this single patch antennas printed over any geometrical surface making them best alternative choice instead of using heavy and bulky traditional antennas (Figure 1-11) [17, 18].

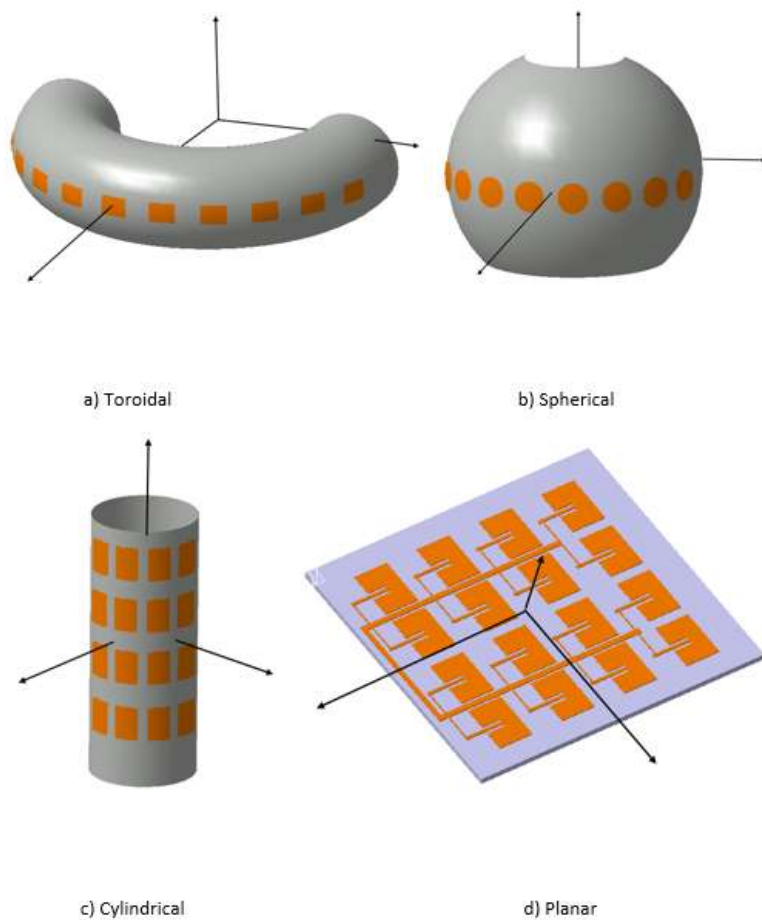


Figure 1-11 Grid of microstrip patch antennas over design surfaces
(Adapted from [16])

1.2.2 Phased Array Antennas

In practical applications a single element antenna is unable to meet the gain or highly directive radiation pattern requirements especially suited for long distance communication. Therefore a group of single patch radiator antenna elements are joined together with certain distances in order to form an array with individual phase shifter (Figure 1-12). The radiation pattern is built creating a time delay between each single elements radiation pattern such that phase difference occurs providing necessary target illumination with improved gain and broad angular coverage over desired direction with additional beam steering capability. Grouping each individual element in such concept also improves its beam width and performance [19]

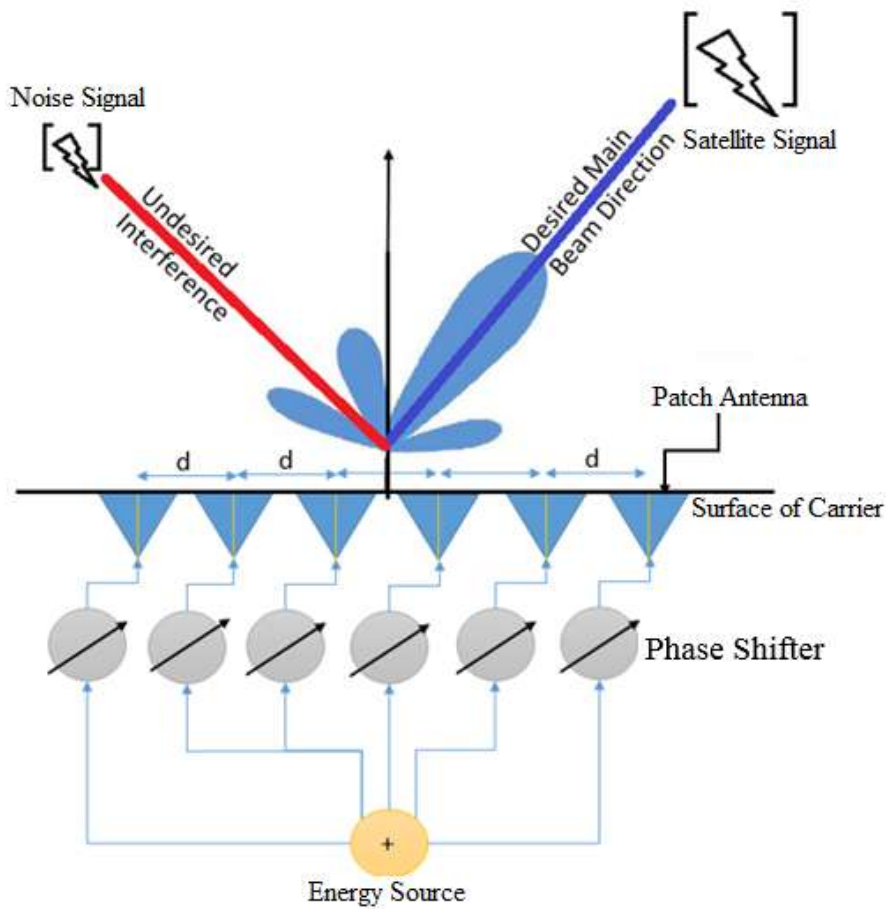


Figure 1-12 Phased array antenna (Adapted from [6])

The relative distribution of each antenna elements effects the overall performance of antenna. Change in distance between radiators effects the radiation pattern. When the space between individual patch increase the beam widths of all major lobes get narrower and the strength of minor lobes increases which are in undesired directions (Figure 1-12) [20].

Phased array antenna has many technical advantages: high power efficiency with increased gain, shaped beam, fast tracking by electric scanning, high stealth performance. Moreover they can be in various geometrical configurations integrated on circularly symmetric surfaces, such as cylinders, cones or spheres. If the array elements distribute on the carrier surface, the shape of the array is the same as the carrier contour, then the array is a conformal phased array. Conformal phased array has many advantages compared to planar phased array:

- Low profile, smaller volume,
- No effect to aerodynamic performance of aircrafts, automobiles and high speed trains
- Wider scanning range [21].

1.2.3 Conformal Antennas

The microstrip antenna technology together with phased array concept extends the application areas of antennas one step further. Due to light weight constructions of microstrip antennas and most importantly the conformable array form which reduce the aerodynamic drag together with flexibility of application over diverse surfaces make them first choice in automotive, high speed train, submarine, aircraft with “smart skin” concept [22]. Moreover compared to planar antennas their angular coverage and beam steering range is higher [23]. For example it is possible to have a coverage of 360° with cylindrical or spherical antenna array.

The smart skin concepts introduce the application of antennas in compact form over the surface having same shape or within the sandwich structure as an additional layer (Figure 1-13) [24,25,26] which may contain microstrip patch or array of radiator elements as an integral part of the structure for electromagnetic applications.

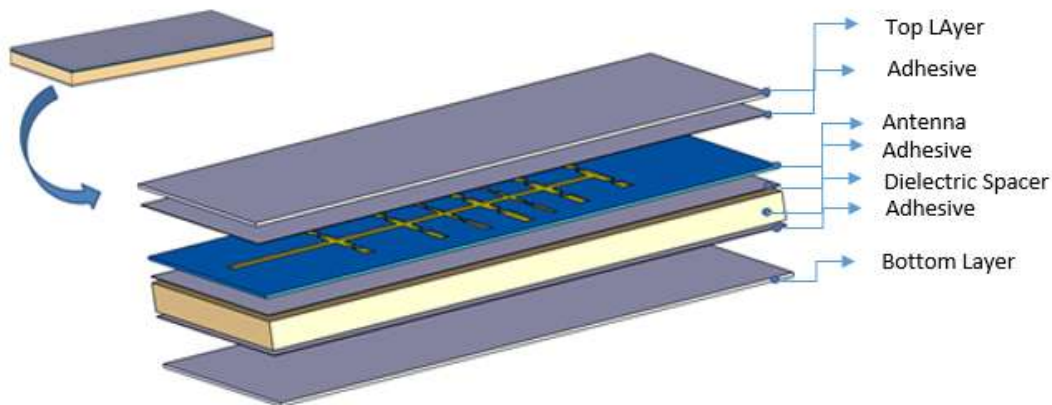


Figure 1-13 Sandwich smart skin (*Adapted from* [25])

In today's printed manufacturing technology allows production of largely flexible antenna elements for the future multifunctional smart structures [27]. This

technology enables the radiator elements to be printed over complex surfaces leading to more aerodynamically improved structures as well as styling.

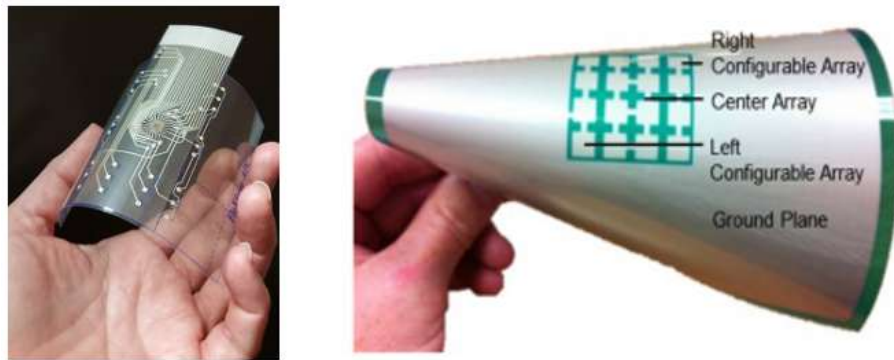


Figure 1-14 Flexible conformal antenna [27]

One of the important applications of conformal phased array antenna is automotive collision avoidance radar or adaptive cruise control technology that can be integrated to body panels. Using radar sensors integrated over the surface of a car provide increased traffic safety by continuously scanning the roadway and conformal shape of antennas reduce aerodynamic drag together with decrease of fuel consumption [28, 29, 30]. Also some concepts are being developed to use roof of a car as GPS antenna.

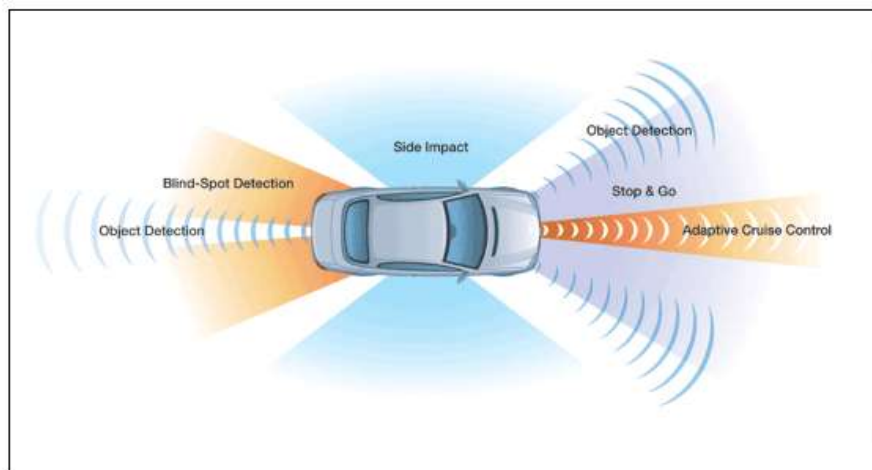


Figure 1-15 Using radar sensors in the car [31]

Future submarine designs take the advantages of conformal phased sonar arrays [32] as well as long range communication with satellites (Figure 1-16) [33,34]. Under sea environment conformal shape of antenna reduces surface wakes that minimize the detectability leading a stealth characteristic.

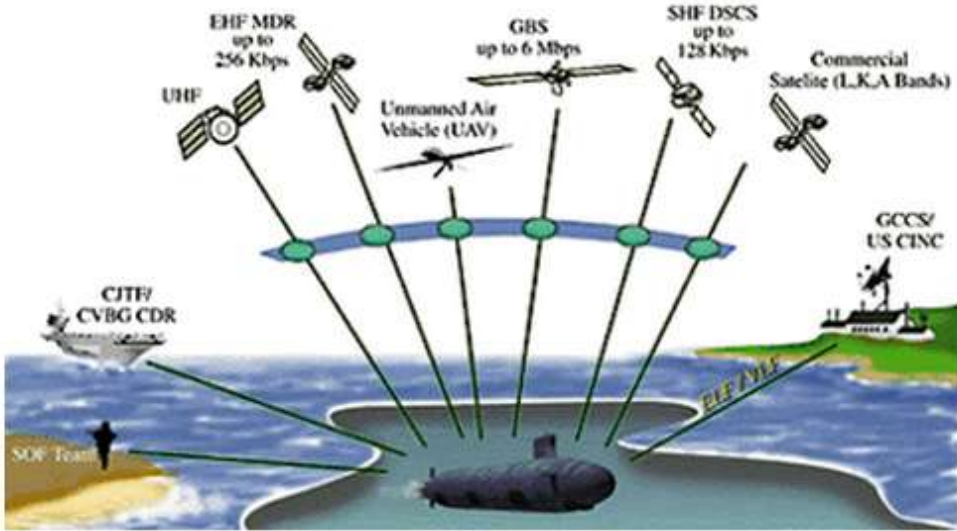


Figure 1-16 Submarine communication in the near future [35]

Civil or military an aircraft has several antennas protruding from its structure and they are performing in various frequency ranges for different avionics functions such as navigation, communication, instrument landing systems, electronic counter measure, radar altimeter, and so on. Some radar antennas also covered with radome that may even change shape of an air vehicle causing significant air drag and some structural instabilities [36]. Integration and replacing those protruding bulky types of radar antennas with patch antennas and embedding them into the aircraft skin has certainly a potential benefit in cancellation of the disturbing effect on air flow caused by protruding antenna types (Figure 1-17) as well as considerable weight reduction, smaller size and minimal cost.

In combat aircraft application these embedded antennas will give rise to very low radar cross section or can be completely 'hidden' to tracking radar. In addition, they can be used to detect, monitor or even jam other unwanted electromagnetic field signatures.

Current goal in aviation industry is to embed those protruding antennas into the aircraft skin by replacing them with microstrip patch antennas. For that purpose many attends have been carried out for the design of such conformal antenna structures [37, 38, 39, 40, 41]

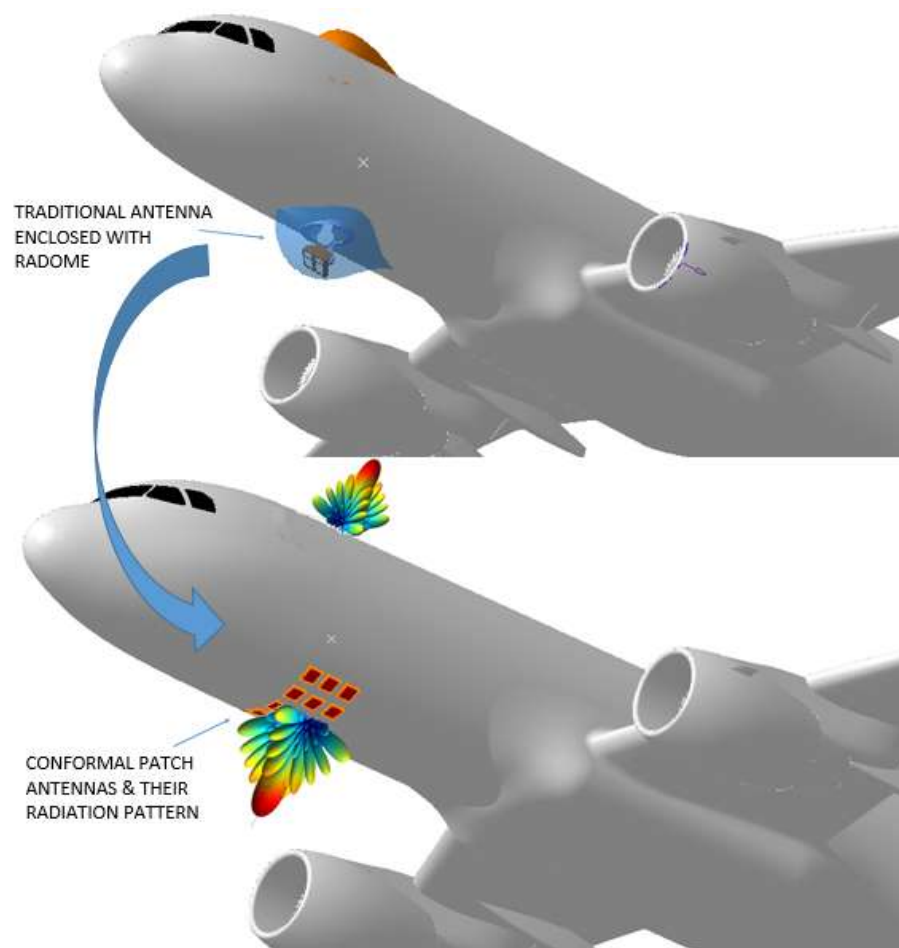


Figure 1-17 Integration of conformal antennas on skin of aircraft [42]

1.3 Motivation of the Study

Radar antennas are integrated on various platforms over which they are subjected to various kinds of harsh static and dynamic environmental loadings at their operational conditions. Besides, efforts to increase the performance and decrease the cost of production as well as to reduce fuel consumption, the designers are forced to create weight efficient solutions which lead to lightweight design of structural components such as high speed train and automotive body panels, aircraft and helicopter skin, stringer and frame combination. Hence, this makes those structures weak and much more prone to be effected under those loading conditions due to reduced thickness (stiffness) that in turn results the structural instabilities like low and high frequency structural deformation problems known as vibration. These deformations are at their highest value especially when the structural resonances are triggered.

When the antenna locations are considered the effects of deformations caused by static and dynamic loads are numerous. In aircraft or helicopters for example the whole structure is made up of as a combination of skin, stringer and frame as shown in (Figure 1-18).

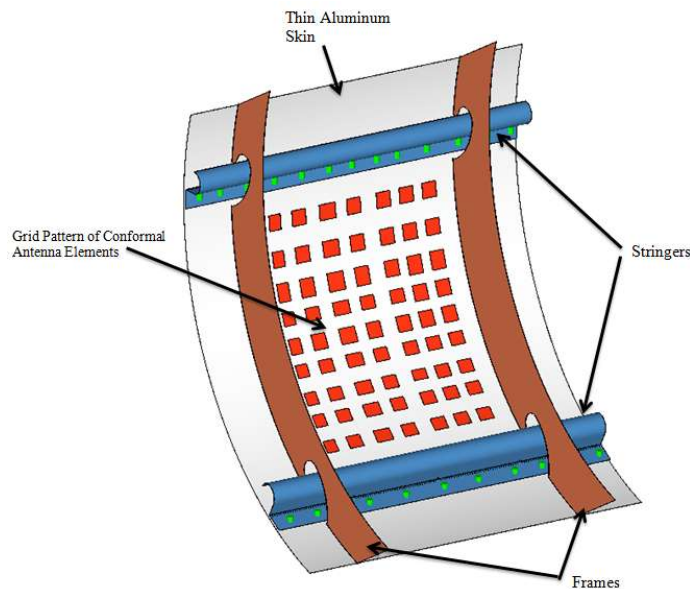


Figure 1-18 Air vehicle body panel and possible antenna location (*Adapted from: [40]*)

Integration of conformal antennas on vehicle platforms lets the choice of antenna locations such as the skin of the aircraft, helicopter and automobile body panels which are locally thin and weak compared to other components. In operational conditions, the aerodynamic fluctuating normal pressure loads cause the panels to deform. Moreover due to structural resonances excited at distinct frequencies different dynamic deformations known as mode shapes also occur. As a result of these flexible deformations the antenna elements are disoriented and the distance between individual antenna elements, which defines the overall radiation patterns are changed especially at low frequency oscillations. This in turn causes the distortion of radiation pattern with reduced gain, increased side lobe levels, which are considered as waste of energy. This can be illustrated by combining deformed mode shape of panel geometry, which is obtained by analysis of panel in Hypermesh, with scattered radiation pattern on top of it using paint shop program (Figure 1-19). The increased side lobe levels are the main cause of interference of transmitted signals with other electromagnetic waves in undesired directions as well as increased risk of detection in military applications and reduced performance, especially for highly directional antenna elements [43, 44, 45, 46, and 47].

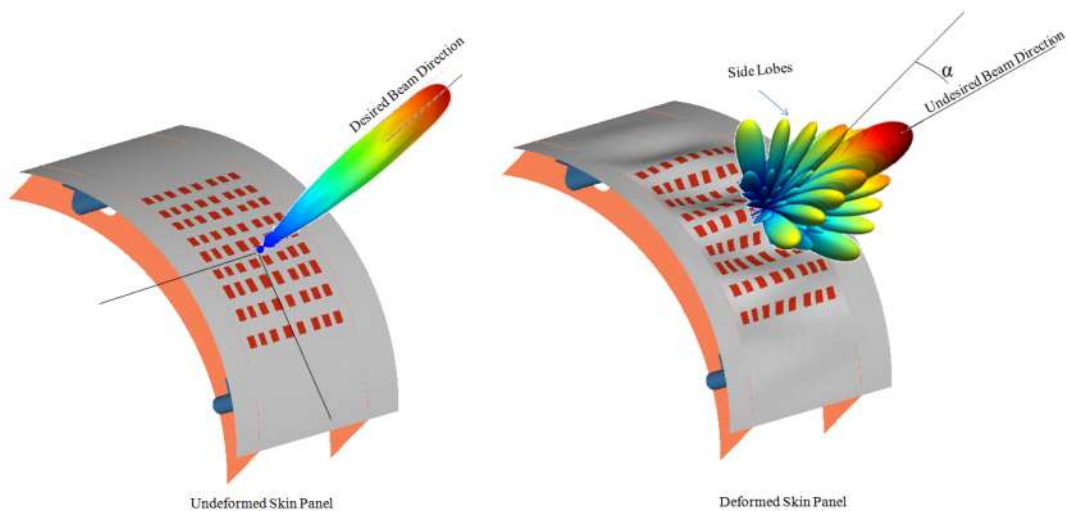


Figure 1-19 Distorted radiation pattern during vibration (*Adapted from [43]*)

Additionally when there is an obstacle such as part of a carrier in the direction of side lobes, the transmitted signals backscattered creating mutual coupling which results an alteration of radiation pattern [48].

In practice there are several methods available to suppress the effects of vibration on antenna performance and the methodologies can be grouped as ;

- Mechanical Suppression,
- Mechanical and Electronic Suppression
- Electronic Suppression

In this field the first study is the one conducted by NATO Research Task Groups [49, 50, 51]. This group shows effects of vibration on antenna pattern and proposes mechanical and electronic suppression technique which involves using some measurement sensors, cables located at the vicinity of vibrating antenna elements. The mechanical sensing devices, namely accelerometers, strain gauges are used to detect and capture the physical location of antenna instantly during cycling motion then using electronically controlled piezoelectric patches appropriate resistive motion is induced simultaneously to stop the vibration.

Another suppression method is electronic compensation using algorithms to correct the shape of beam pattern and minimize side lobes. Again using some sensors the mutual positions are dynamically measured then the amplitude and phase shifts are compensated using appropriate mathematical algorithms electronically with correction factors [52, 53].

The above two method involves measurement of antenna position in very harsh dynamic environment simultaneously with instrumentation of heavy, expensive external attached sensors, cables. This brings also the calibration of each sensor and lack of reliable signal processing algorithms which may be another possibility of error source.

Local deformations of conformal antenna structures caused by high or low frequency vibrations can also be suppressed via following pure mechanical suppression techniques which are grouped in passive vibration control techniques. In passive methods, the structural mass and stiffness distribution, which are the key parameters that defines the dynamic behavior of the structure, are varied in order to get rid of resonances via shifting the natural frequencies of structure out of disturbing frequency range. However, increase of stiffness is generally not acceptable due to associated additional weight. Moreover, in some cases, due to random nature and wide frequency spectrum range of the loadings there are unavoidable coincidence with those forcing frequencies. In such cases increase of damping utilizing damping treatments with viscoelastic materials has considerable effects in lowering high amplitudes especially at resonance frequencies.

In practice, viscoelastic materials, which are mostly polymers, cannot be used to build a structure because they are not strong enough to tolerate loads. However, they can be efficiently added on top of a structure or embedded into. This vibration control approach (damping treatment) is after adding viscoelastic materials to a structural system in such a way that maximum possible energy is dissipated to achieve the highest vibration suppression therefore the minimum distortion.

In this study, the fundamental motivation is to design, improve and apply that passive damping treatment methodology in suppression of excessive vibration response encountered in thin vibrating conformal antenna surfaces. For that purpose it is aimed to design novel passive damping device that utilize viscoelastic material with maximum damping capacity using parametric design and optimization strategies.

1.4 Background

The light weight construction and lack of damping in metallic structures lead structural resonance problems with high amplitudes when a few of natural frequencies are matched with those of forcing frequencies. These resonances not only cause the degradation of antenna performance but also cause noise and fatigue problems due to high amplitude cyclic displacements which result alternating stresses. This in turn necessitates a vibration control strategy to get rid of or at least decrease the effects of those unwanted resonances. Introducing damping or in other words adding energy dissipation mechanism within the structural components is one of the popular method in control of excessive vibration.

The viscoelastic materials possess inherent property of energy dissipation characteristic especially when they are subjected to mechanical deformations like tension, compression, shear or any other combination of these loadings. The energy exposed within the elastic medium is converted into heat through hysteresis loop. Therefore when some portion of energy is moved away continuously along with cyclic deformation, in the form of heat, the cyclic motion dies out gradually or the resonance peaks are lowered to a certain acceptable value.

To take the advantage of this energy dissipation property of the viscoelastic materials they are incorporated into designs in order to reduce dynamic response and minimize induced stress by dynamic loads. The viscoelastic materials used as dampers in various forms of configurations which are classified under surface damping treatments as;

- Free Layer Surface Damping Treatment
- Constrained Layer Surface Damping Treatment
- Improved Constrained Layer With Standoff Layer

This section provides a draft summary about surface damping treatments then a review of literature on the study of designing and analysis of passive viscoelastic constrained layer damping treatment either with or without standoff layer, specifically applied to vibrating beams and shell like structures.

1.4.1 Surface Damping Treatments

The polymers or rubber like materials inherently dissipate energy through hysteresis loop. In other words they must be subjected to dynamically varying stress and strains in order to convert mechanical energy into the heat. Therefore when a layer of metallic structure deforms in its vibration modes the best place for the attachment of the damping layer is the highest point of stress and strains within or over the vibrating structure. Generally speaking, this is the aim of all design strategies being followed in control of vibration when using viscoelastic materials.

1.4.1.1 Free Layer Damping Treatment

This is the most basic form of application of viscoelastic materials over one or two free surface of the beam or plate like structures. During flexural bending motion under vibration, the top or bottom layers are exposed to cyclic direct tensile and compressive strains, parallel to the surface of the structure and whose values are directly proportional to the distance from the neutral plane of bending (Figure 1-20). Those cyclic strains force the flexible layer of viscoelastic material to dissipate energy in the form of heat and since the strains induced is also proportional to the distance from neutral plane it is wise to locate the layer away from neutral plane as far as possible to induce more strains. Moreover the energy dissipation is directly proportional to the thickness and modulus of viscoelastic layer.

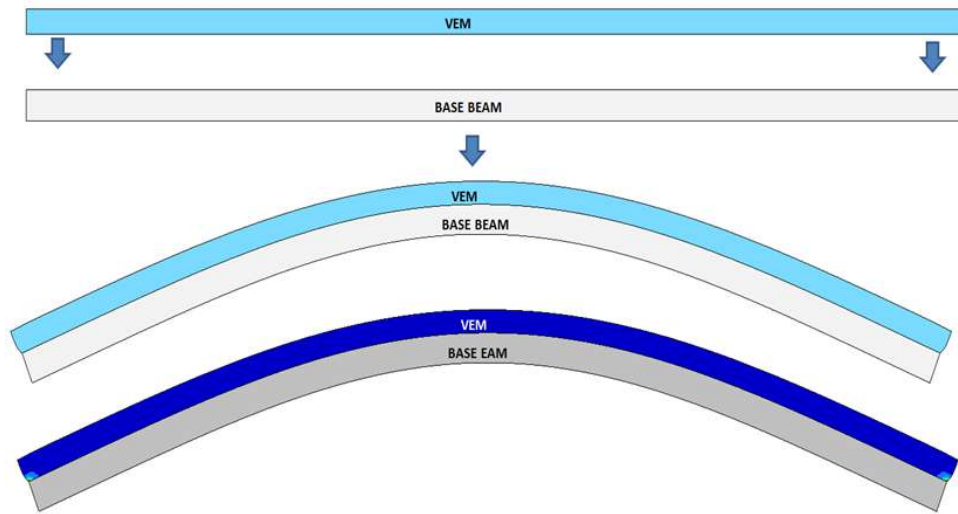


Figure 1-20 Free layer surface damping treatment

1.4.1.2 Constrained Layer Damping Treatment

Forming a sandwich type structure by placing the flexible layer of viscoelastic material between two stiff layers, close to neutral plane is another option of damping treatment because the transverse shear strain is maximum at this neutral surface. Incorporation of damping layer on this surface cause damping layer to deform in shear mode which is the basic mechanism of energy dissipation. Moreover compared to free layer as the structure vibrates, the external stiff layer constrains top free motion of polymer layer causing high shear deformation within the middle layer due to cyclic relative motion exists between top and bottom stiff layers during vibration [54] (Figure 1-21). The study [55] shows the effectiveness of constrained layer over free layer damping treatment.

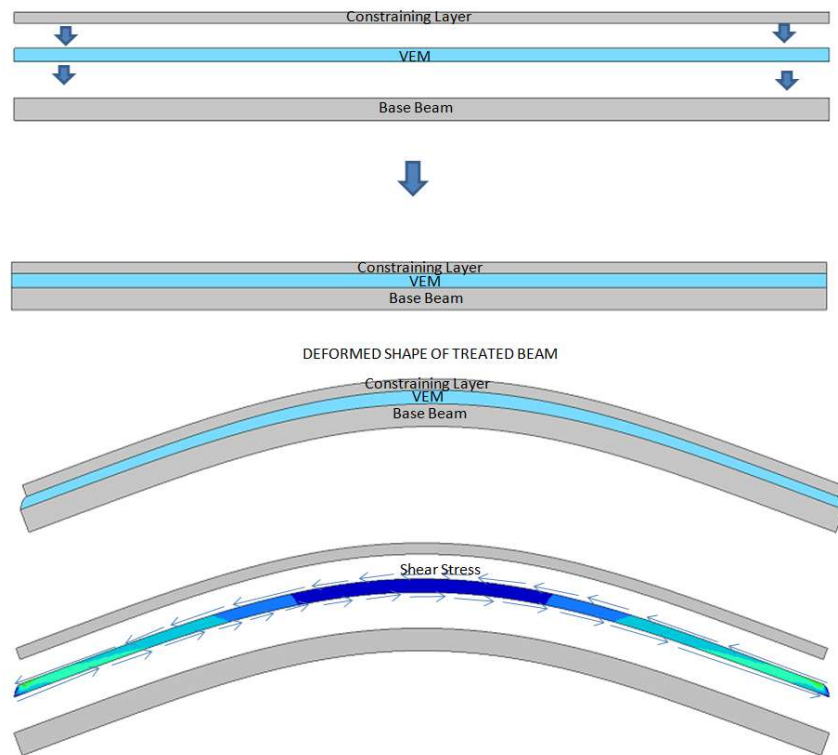


Figure 1-21 Constrained layer damping treatment

In practice, the viscoelastic layer is bonded to a sheet of metal with adhesive which forms the constraining layer and this combination can be cut into pieces in various forms depending on the application surface area which can later be applied to the vibrating structure. Constrained layer damping treatment is applied to a wide range of structures including aircraft skin (Figure 1-22), automotive body panels (Figure 1-23) with stringers and stiffeners, vehicle engine covers and brake pad insulators [56].

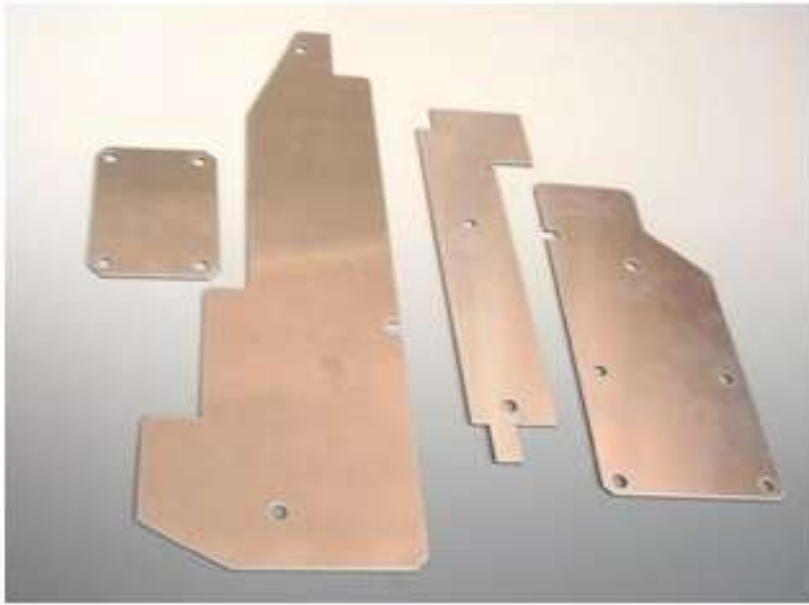


Figure 1-22 Application of damping treatment on aircraft fuselage [57]

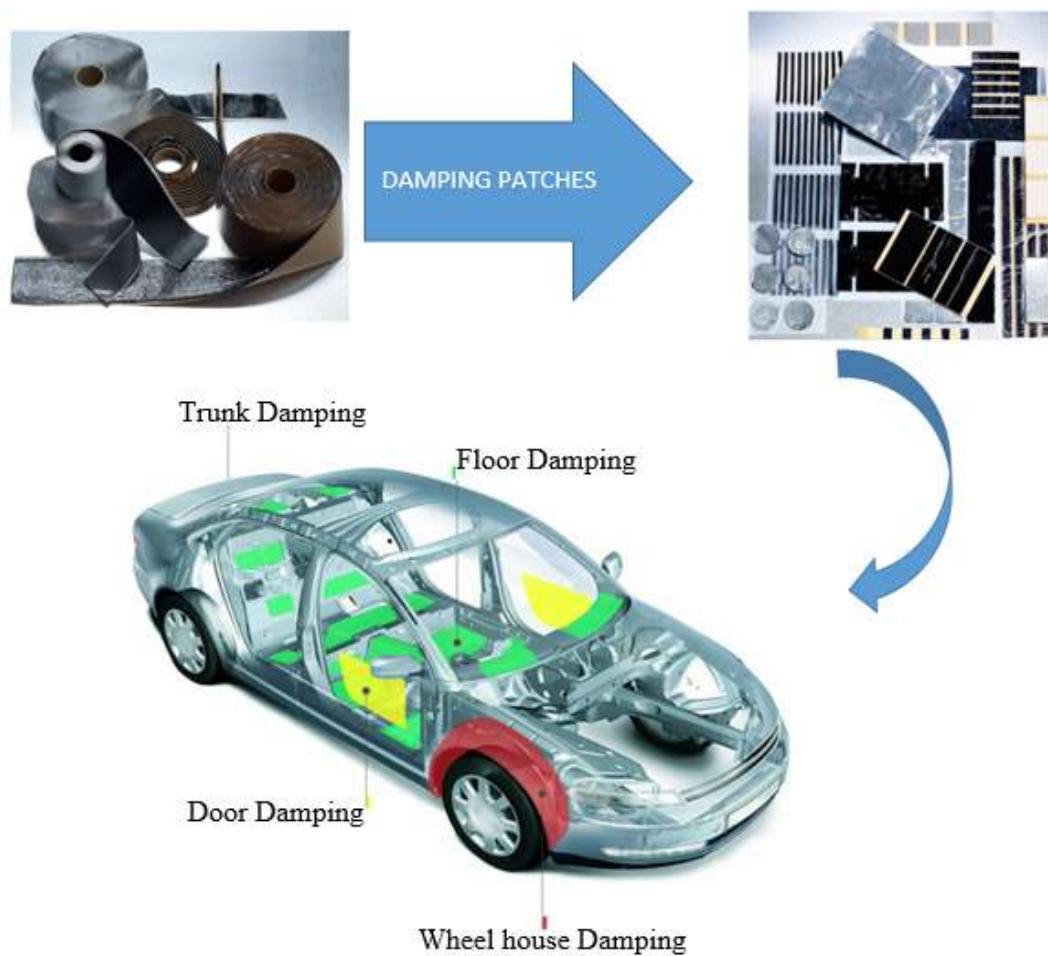
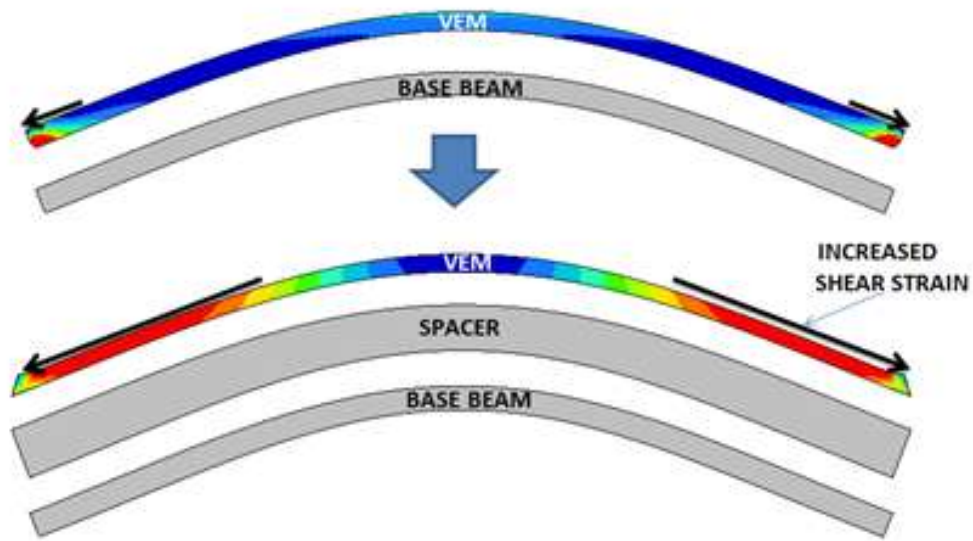


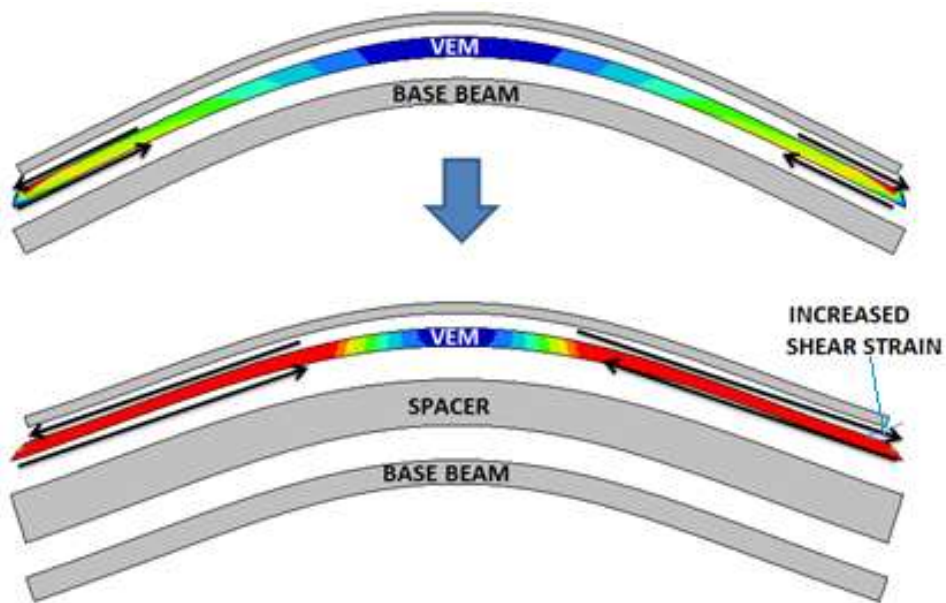
Figure 1-23 Application of damping solution in car body [58]

1.4.1.3 Improved Constrained Layer Damping With Spacer Layer

Since the exposed strain within the viscoelastic layer is directly proportional to its distance from the neutral plane of sandwiched plate or beam under flexural deformation, the effectiveness of damping can be increased by simply placing the damping layer away from the neutral plane as much as possible via using a spacer medium between damping layer and vibrating structure. In this configuration the spacer layer behaves as strain magnifier, therefore the energy dissipation capacity of both free and constrained layer damping treatments increases (Figure 1-24).



(a)



(b)

Figure 1-24 Use of spacer medium as strain amplifier (a) for unconstrained layer (b) for constrained layer (*Adapted from [59]*)

Effectiveness depends on a number of different parameters including material properties, layer thickness, location, surface coverage and the distribution of dynamic strain on the host structure [58].

In order to achieve larger loss factor various configurations and a number of practical applications are explored all of them are simply the shear-dependent configurations in order to induce larger shear strain into VEM and as a result, to gain higher energy dissipation characteristic for the whole system. Some of them can be classified as follows:

- Segmented constraining layer (Partial coverage)
- Multiple constrained layer treatments and
- Combination of segmented and multiple constrained layers overlapped over eachother.
- and Stand-off layer configuration.

The idea behind all configuration is to induce shear motion so the shear strain in the viscoelastic layer can be increased. Moreover tailoring the design parameters together with the frequency and temperature dependence of VEM material, a design can be achieved for wide frequency and temperature range of applications [58].

In the following section the studies carried out by various researchers in order to improve the damping performance or increase of loss factor of vibrating structures using constrained layer damping treatment has been reviewed. After extensive review of literature it is seen that numerous methodologies have been used such as modal strain energy method, analytical methods and finite element method and optimization algorithms in order to increase the damping capacity of vibrating host structures.

1.5 Literature Review

The pioneering work in design and analysis of constrained layer damping treatment was first conducted by Kerwin [59], Ross et al. [60], Ungar and Kerwin [61], who developed a simplified theory to calculate the damping factor of a bar (plate) with constrained layer damping. With those first studies, it was observed theoretically that the main mechanism behind the damping was mainly the cause of shear deformation exists between two stiff layers which implied that as long as the shear deformation at viscoelastic layer is increased the damping capacity can also be increased. The study also revealed other factors effecting the performance of such constrained layer damping system such as; wavelength of bending waves, the thicknesses, different geometrical configurations of elastic and viscoelastic components and elastic modulus of individual layers as well as temperature and frequency of loading environment.

Theoretical background for constrained layer beam with various boundary conditions is formed by Mead and Markus [62] who developed the theoretical models for the axial and bending vibrations of sandwich beams with viscoelastic core. Based on these earlier works, some of the important and similar investigations were carried out by various researchers using different methodologies together with numerical techniques aiming to maximize the damping capacity of vibrating simple beam and shell like structures. The effects of geometrical parameters as well as geometrical configurations for free, constrained layer and treatment with spacer layer on damping performance over the vibrating structures were investigated and optimum conditions were sought by the following studies.

For the simplest treatment, free layer damping treatment, the maximum loss factor has been sought as well as for minimum material distribution while keeping the dynamic response minimum. Lumsdaine et.al. [63] optimized the unconstrained viscoelastic layer thickness distribution yielding an optimal shape over the beam and plate type structures that minimize the central displacement of base laminate under harmonic loading. The height of each viscoelastic element that covers the structure being analysed was selected as design variable within prescribed lower and upper limits with overall constant volume constraint. Sequential Quadratic Programming algorithm was used to find the optimum values of those element height under objection of minimum peak displacement at first mode. The methodology repeated for different structures possessing different thicknesses and boundary conditions. Results showed that compared to uniform coating, optimal distribution with minimal mass greatly reduces the peak responses in all studied cases. In addition it was noted that for optimum configuration of damping distribution the results were in close proximity of each other namely, for the case of constant or frequency dependent material properties for viscoelastic material

In another study Lumsdaine presents the topology optimization technique for the maximization of loss factor of first resonance mode of beam. Sequential Quadratic Programming algorithm was adopted for the study as well as Modal Strain Energy method [64] which does not necessitate the use of viscoelasticity and require inclusion of frequency dependent material properties, with this method instead, the real part of complex modulus is used and the dissipative energy terms are calculated from undamped real natural mode shapes from which the strain energies are calculated and used in calculation of loss factor through finite element method. The calculated modal loss factors were also verified using half-power bandwidth method upon performing two dimensional, direct frequency response finite element simulation. The results obtained through the optimization reveals an improvement of modal loss factor up to 300% [65].

For free layer damping treatment, Koruk et.al.[66] proposes random search algorithm based on big bang–big crunch optimization method in order to optimize damping capacity of simple beam type structure. They combined again the modal strain energy method with their algorithm and they showed the effectiveness of methodology conducting a case study using simple cantilever beam. Specifically the beam was divided into 10 sub-regions in which individual damping layer exist, whose material properties were assumed to be average, and with allowable maximum thickness value. As an objection maximum loss factor for the first mode was sought via varying the thickness values, which are defined as design variable, through random search algorithm at each sub-region. Their results showed that modal strain energy method has sufficient accuracy within %4 error. They carried out single and multi-mode optimization analysis for the cantilever beam yielding minimum of 3.9 times higher modal loss factors compared to uniform treatment.

Since the damping treatment requires addition of extra material to the host structure, the weight is another concern in design strategy. To minimize the material consumption therefore the weight of vibrating structure, while maintaining maximum damping for the particular modes, topology optimization technique utilized by various researchers. The topology optimization method gives the optimal material distribution or layout of treatment (Figure 1-25) under material consumption and dynamic response constraints with an objection of maximum loss factor. The density of material is used as design parameter and at maximum strain energy locations the density value of 1 indicates existence of material while value of 0 indicates empty regions. With this methodology there is no need to fully treat the structures for maximum damping.

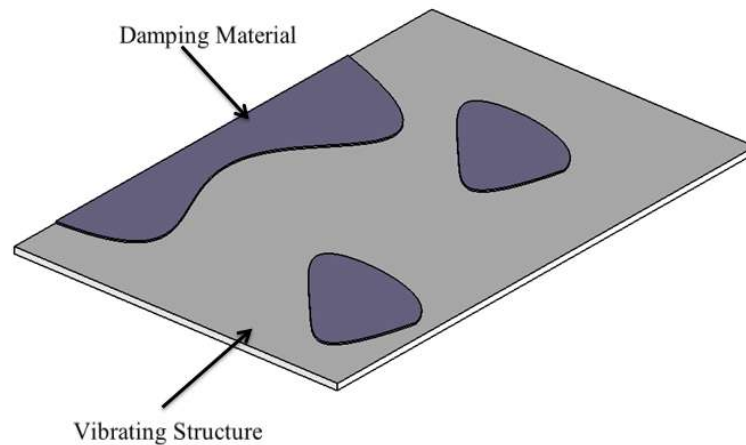


Figure 1-25 Distribution of damping material after topology optimization (*adapted from [67]*)

Kang et. al. [67] have demonstrated that the optimum layout of treatment over the vibrating plate obtained using topology optimization technique gives higher damping performance yielding a reduced vibration response. In their analysis damping material distribution obtained for the cantilever plate that was subjected to unit harmonic force at its tip. A similar approach used in SIMP method was proposed using artificial damping material model in order to define design variables as density of elements which are defined as design domain. The objective was selected as the minimization of sum of squares of displacement amplitudes at loading point. Their investigation included the effects of loading frequency and damping coefficients defined as Rayleigh damping coefficients which combines the effect of stiffness and damping matrices. the results showed that for increase in loading frequency yields much more complex layouts. Moreover the damping coefficients have significant effect in distribution of damping material over the design surface

Fang and Zheng [68] proposed an improved sensitivity analysis method as part of topology optimization methodology. In their study cantilever and fixed plate covered with constrained layer damping treatment were considered as case studies and the material distribution was optimized under broadband harmonic loading condition via minimizing the square of displacement of target point at resonance frequency under

material volume constraint. They emphasize the importance of improved sensitivity analysis by showing improved optimum material distribution and higher reduction in response compared to traditional sensitivity analysis. Also the study shows the fact that applied boundary condition effects the optimized material layout dramatically.

Chia et. al. [69] propose another design strategy in order to efficiently cover vibrating structures with constrained layer damping treatment. The study use different sets of cellular automata algorithms used to cover aluminum plate for known optimum coverage and compare their results in which different coverage shapes and areas of damping distribution exist especially for those bending and torsional modes. Also a curved composite plate was selected as one of case study to find its optimal coverage with constrained layer damping treatment

Apart from free layer damping optimization studies some others concerning constrained layer damping treatment has been studied by various researchers yielding extensive configurations that maximize the damping capacity of vibrating structure. In order to increase the shear strain therefore the energy dissipation within viscoelastic layer, D.J.Mead [70] proposed cutting constraining layer at certain distances. It was shown by Parfitt et al. [70] that during flexural deformation, the local shear strains were successfully increased around those cuts (Figure 1-26).

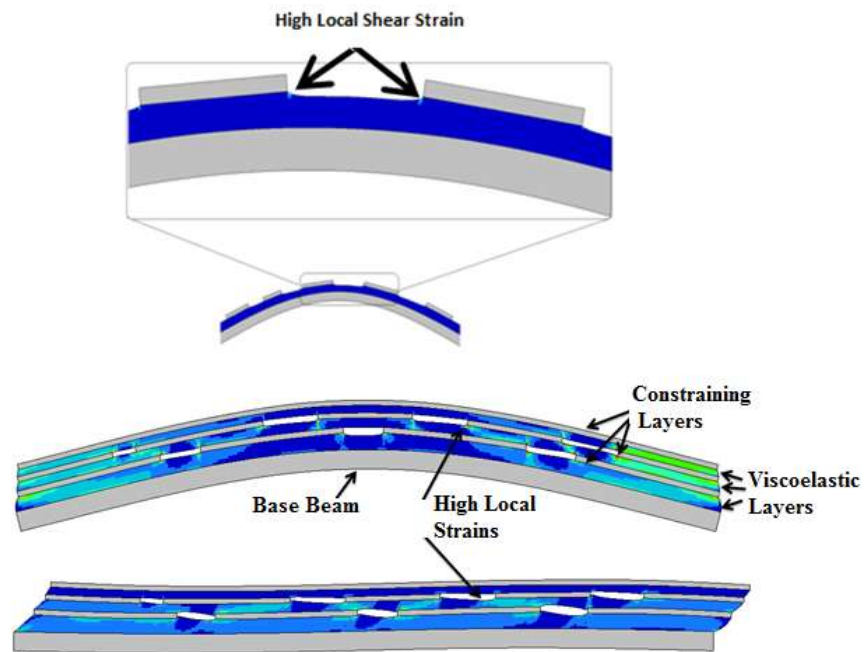


Figure 1-26 Segmented single and multiple constraining layer damping treatment: (adapted from [70]).

Nokes and Nelson [71] provided one of weight efficient and maximum damping solution by completely diving damping layers into patches. In their theoretical and experimental study it was shown that instead of covering whole beam, spreading damping patches, with stiff viscoelastic layer and certain dimension, over the beam was adequate for maximizing damping capacity (Figure 1-27).

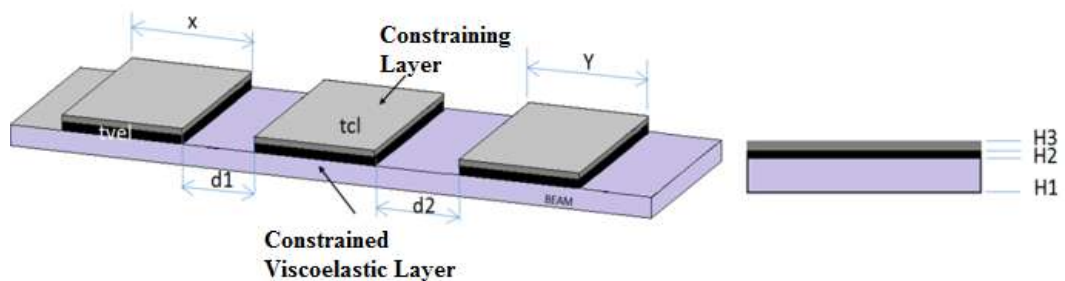


Figure 1-27 Partial damping patches over beam with main parameters (adapted from [71]).

Plunkett et.al. [72] performed an optimization study to find the effective length for those distributed damping patches which are X and Y parameters in (Figure 1-27). They investigated performance of symmetrically arranged segmented damping treatment theoretically by assuming sinusoidal deformation pattern over the cantilever beam structure and compared their final results with experiments. They also investigated interaction of multiple damping layers (Figure 1-26) for optimum configuration. Their results show that there is an optimum length of patches which provides maximum damping.

A similar study was conducted by Trompette et.al.[73]. They showed that the dissipated strain energy therefore the damping capacity can be increased via application of cuts in constraining layer. In their study, the shear stress distribution within the viscoelastic medium was changed by simply adding a single cut over both constraining layer and viscoelastic layer. They investigated influence of this single cut location on loss factor. For that purpose they sought the best position for that cut and the optimum coverage area to maximize the first modal loss factor. The cut position was varied along the dimension of the beam and loss factors were calculated using modal strain energy method. Genetic Algorithm was used to find the best cut position for target modes using the cut position as the design variable. According to their results, extracted from a simple cantilever beam model, with an optimal coverage area and best location of cut the modal loss factor for the first modes can be increased.

Marchelin et. al. [74] performed a new strategy using Genetic algorithm to find the best number, location and thickness of constrained layer damping patches over the beam which is modeled via finite element method. The undamped mode shapes were used to calculate energy dissipation ratio namely loss factor for its maximum value at first mode. Results were compared with loss factors obtained by experimental modal test for free-free beam structure. Their study shows that the patches are cumulated around middle of the beam at which the shear strain energy is high due to the flexure.

Kung and Singh [75] theoretically investigated partial damping treatment and followed a parametric design strategy. The study proposes an analytical energy based approach for analyzing harmonic response of beams with multiple constrained-layer viscoelastic patches. Several damping configurations such as damping patches with cutouts together with boundary condition effects for the cantilever beam are investigated. The result of study shows that for fixed end boundary condition both the natural frequency and loss factor are higher due to additional constraint added that increase the shear deformation within viscoelastic layer. Moreover study reveals that the loss factor is sensitive to cutout size and location. For the shorter cuts the loss factor has higher values compared to larger cutout size that yields monotonic decrease of loss factor.

Zheng et.al.[76] studied the vibration response of partially covered simply supported beam is minimized through parametric and optimization study. The passive constrained layer damping patch was attached to the center of the beam and the governing equations of motion was derived using energy approach with the geometrical and material parameters of partially covered beam as a whole system. The most critical design parameter was extracted through sensitivity analysis as well as the optimum location, length and core shear modulus of the patch by employing Genetic Algorithm search method for the minimal vibration energy of the whole system in appropriate frequency range, taking into account the multiple resonant modes. The results showed that the most crucial parameters were the location, length and the core shear modulus compared to core and constraining layer thickness and also with a shorter coverage length, reduction of resonant response was higher compared to longer patches which was shown to be one of the advantages for the weight critical applications

Lepoittevin et.al.[77] incorporates several cuts over the constrained and constraining layer in order to increase the shear strain at vicinity of cuts which is termed as “edge effect” and investigates the effects of those cuts on damping performance of 2D modelled vibrating cantilever beam. Optimization algorithm based on deterministic

mathematical programming, Nelder-Mead simplex method, together with modal strain energy method were used to find the optimal location and number of those cuts that maximize the modal loss factor. According to the results obtained reveals that for the single cut positioned at the highest radius of flexural curvature has much more effect on the loss factor. Additionally there is a certain number of those cuts that yields maximum loss factor. Results also proves that via addition of cuts at certain position and numbers, up to 92% increase of loss factor is achievable. Another conclusion given is that the difference is minimal for simultaneous damping optimization of multi-mode case with certain weights and single mode optimization run seperately

Zheng et.al [78] compared various optimization methodologies each other by simply evaluating the damping performance of partially treated simply supported beam. After building the analytical formulation the best patch layout was sought which minimize the transverse displacement and material consumption by using sub-problem approximation method, the first-order method, sequential quadratic programming (SQP) and genetic algorithm (GA). It was proved that genetic algorithm was best solution method out of four. The design variables are selected as number of patches as well as length and location of each individul patches.

In the following studies the finite element method also successfully applied in conjunction with modal strain energy method in order to find the value of best design parameters for the optimum damping treatment. Moreover different finite element modelling techniques are used such as 2D and 3D. Also in those studies the viscoelastic material properties are simply used as constant with respect to frequency of loading environment.

In reference [79] the damping performance of constrained layer damping treatment was investigated via performing parametric design and analysis procedure. The thickness of viscoelastic layer was selected as design variable for the cantilever beam model. The analysis was carried out for two different viscoelastic material. For finite

element analysis CHEXA solid element are used for VEM layer. The modal loss factor was obtained by Modal Strain Energy Method. The results showed that the performance of PCLD treatment is mainly affected by thickness of VEM material.

Shepard et al. [80] combined single layer finite element model that has the shear and extensional damping capability as well as frequency dependent material property with Genetic Algorithm to find the best geometrical parameters, namely the thicknesses for the sandwich damped beam. The thickness of viscoelastic core and constraining layer were selected as design parameters and were varied between prescribed upper and lower limits to extract the best option that minimize the dynamic response, specifically sum of squares of peak response of the beam, especially for the first three mode while targeting either simultaneously or individually. The results show that objection of minimum response for the multi-mode case gives deficient results compared to single mode objection. Moreover the study reveals that the optimal damping configuration which is lower in weight has higher performance in reducing vibration amplitudes.

Veley and Rao [81] applied a new finite element modelling technique for the constrained layer damping applications that increases numerical modeling efficiency. Based on the proposed model, the effect of viscoelastic layer and constraining layer thicknesses together with location of treatment on loss factor was studied. The analysis carried out for beams and plates was revealed that the curvature of the vibrating structure defines the best location at which the strain energy is maximum and this location was mode dependent. Also it was found that both the constraining and viscoelastic layer thicknesses were selected as two parameters that maximize the loss factor of the treated structure for lower modes. Addition to this result it was noted that increase in viscoelastic layer thickness has negative effect on higher modes. Moreover the parametric study was carried out for unconstrained and constrained layer damping treatment to find out the best location of single and multiple partial patch of damping treatment that maximizes the loss factor in

vibrating structure. The results show that as the patches moves away from the root of cantilever, where the strains are high, the first modal loss factor decreases

Subramanian et.al [82] proposes a methodology of damping optimization based on finite element and modal strain energy method in finding the best size and location for the damping material over the vibrating automobile body panels through an iterative design cycle. The methodology used identifies the high strain energy regions over the design domain upon performing a modal analysis technique and optimize the applied damping treatment in terms of area, size and thickness under manufacturing constraints aiming to minimize acoustic noise radiation due to vibration. They shows the effectiveness of the methodology over panels by comparing analysis results for treated case and non-treated baseline model with experimental test conducted using laser vibrometer. Their results shows 16 % noise reduction over the baseline without treatment .

Maoût et. al. [83] studied the optimization of composite sandwich beam with viscoelastic core embedded inside aiming to maximize damping capability of sandwich beam type structure that has also sufficient stiffness under static loading .The design variables chosen for that purpose are total number of layers, their orientations and thickness as well as the position of viscoelastic layer. The analysis was carried out under stiffness and mass increase constraints. While having sufficient stiffness under 3-point loading, the modal strain energies were calculated using modal strain energy method and used in linear search algorithm developed to maximize the loss factor of hybrid beam

Wang et.al [84] propose evolutionary structural optimization methodology in conjunction with finite element method and modal strain energy method to find best constrained layer damping distribution over clamped plate. Starting from full coverage of plate the optimal distribution of constrained layer damping was found via deletion of unnecessary elements which are defined as design variables under maximum allowable volume ratio. The first and second modal loss factors were

maximized within single mode optimization strategy. Then multi-mode optimization study carried out assigning some certain weight factors for each mode. The results showed improved modal loss factors as well as it was clearly revealed that single and multi-mode optimization yields different material topologies over the plate.

Serabatir et.al [85] propose a methodology using finite element method with random search technique, namely, Genetic Algorithm to find the optimum distribution of damping layer. In their method the finite element model of cantilever beam is developed with controlled number of sub regions. Using Genetic algorithm, at each region existence of element of viscoelastic layer with parameterized thickness and location value is represented with particular coding called “Chromosome” which possess a special representation of design variables in the form of numerical strings that can be of either 1 or 0 for each element.

Based on calculated vibration modes and modal damping ratios algorithm changes the design parameters by selecting among the best population of design variables until global optimum that represents the maximum damping condition is reached. Specifically the algorithm assigns 1 or 0 for the element that represents the viscoelastic layer. Upon convergence yields the optimal distribution of damping layer in discrete form. Their result verifies that the optimal damping locations are those regions where possess high strain energy. Also study suggests that local and thicker coating of damping layer is much more effective way of treatment.

Optimum distribution of viscoelastic and elastic materials within vibrating structures by topology optimization has also been studied by many researchers. Boucher et. al [86] performed analytical and numerical design methodologies in order to increase deformation pattern of viscoelastic material that is embedded into honeycomb structure under static and dynamic loading together with an optimum material distribution and minimal weight. For that purpose they performed topology optimization under various in-plane static loadings and extracted the architecture of filled viscoelastic material with minimum volume fraction by minimizing

compliance of full and partially filled 2D unit honeycomb cell geometry under the fact that for linear analysis maximum strain location is same for static and dynamic cases. In addition for this static analysis constant viscoelastic material properties were utilized which is also independent of maximum strain location. They obtained improved damping capacity up to %45 via partial filling. It was also noted that improvement in damping was dependent on cell geometry and mode of deformation of the unit cell. This study also shows the applicability of static analysis method in damping maximization purpose via topology optimization.

Agnese and Scarpa [87] constructed bi-phasic 2D composite unit cell geometry at micro-mechanical level to be used in forming macro-scale structure by periodic multiplication and compares the performance of inclusion of matrix material, which is responsible of energy dissipation, for different volume fraction ratios in two different shape namely, star and cylindrical, in terms of damping capacity for honeycomb structure. Study shows that for minimum fiber fraction star shaped matrix material provides higher damping capacity.

Pai [88] in his master thesis carried out parametric study combined with topology optimization in two dimension aiming to find best elastic and viscoelastic material distribution for maximum loss factor. The simply supported and cantilever beam under static loading taken as case study. Specifically the finite element simulation technique was linked with optimization algorithm, which uses an SQP. The sandwich beam was modeled using 2D plane stress elements some of which are assigned as design space, namely constraining and viscoelastic layer whose densities and elastic modulus values were varied between lower and upper bounds. The objective function was selected as maximization of loss factor calculated using modal strain energy method through finite element simulation. The effect of boundary condition applied as fixed or free for the cantilever beam was also studied. The whole process was repeated for different material fraction values and base beam thickness as well as for each boundary condition. The study reveals some design alternatives that were extracted through the interpretation of optimized material distribution which were

also tested in another study of author [89]. Results shows tendency of distribution, for the the stiff material, at upper portion of the design domain forming a column like topology over viscoelastic layer. The results also show up to %1250 improvement of loss factor by simply optimizing the material distribution over the vibrating medium using topology optimization.

Kim et. al. [90] showed the effectiveness of topology optimization over two other approaches namely, mode shape and strain energy distribution method. In their study damping material distribution was found using all three methods for the quarter and semi cylindrical shell structure under fixed-fixed boundary condition to achieve maximum modal loss factor under limited damping material volume.

The design variable was selected as density of material which represents the overall distribution of design domain using rational approximation for material properties whose values were updated using optimality criteria. Qualitative analysis determines that topology optimization offers up to % 61.14 better damping performance.

Rong et. al.[91] proposed a new topology optimization model which suppress the localized modes of vibrating structures which originates from low stiffness regions during optimizatation of material distribution.The 2D material distribution was obtained under random vibraiton load and response constraints for limited material volume fraction.

Lei et.al. [92] employed topology optimization method to reduce the sound radiation of thin plate. In their study the optimal distribution of passive constrained layer damping patches over the surface of thin plate was found by assigning density of damping material as design variable using SIMP method. This is one of the method in which the existence of elements over the surface defined as numerical 1 which means damping material should apply for that element location, conversely the assigned numerical value of 0 represents a void case that is the deletion of element for that location. The objective of optimization was selected as minimization of

square of normal velocity of each finite element node. They obtained the optimal patch distribution over the square aluminum plate for different volume fraction ratios. Results shows that application of damping treatment over the critical points of a design area can greatly reduce the overall sound radiation.

Chen and Liu [93] extracted different microstructural configuration using topology optimization method in order to obtain an improved damping properties out of new topology of damping layer. First the optimum shear storage modulus of the viscoelastic material that maximizes the loss factor for the first three modes was found via parametric study of a cantilever beam.

This optimum shear property was used in design of 2D viscoelastic layer using SIMP method that yields best topological pattern of the damping layer. The optimization was carried out for the 2D periodic unit cell from which the overall structural pattern was assumed to be built. The density of the elements and volume fraction of viscoelastic material were selected as design variable and constraint respectively. The resulting different microstructures were used in modelling of constrained layer treated cantilever beam. Vibration response curves showed that optimum microstructure of damping layer enhances the modal loss factors as well as reducing the resonant response level as the compliance (flexibility) of the whole structure increases.

Al Ajmi [94] tried to achieve optimum cellular material topology in two dimensions that gives both distribution of material and target shear modulus level that maximize the damping capacity of composite structures using homogenization and topology optimization strategies. In his study microstructure of design space out of mixture of elastic and viscoelastic material combination were found in two dimension and showed performance of extracted topologies by conducting experiments over beam type structure. In addition he made performance comparisons of traditional design method, modal strain approach, and proposed homogenization approach. He concluded that topologies found using modal strain energy and proposed method

maximized the damping capacity significantly over the full coverage but homogenization method yielded much improved results in terms of material consumption.

Up now from the extensive literature review it is inferred that the damping can be increased by increasing shear strain energy of the viscoelastic layer that is incorporated over or into vibrating structures. Moreover changing geometrical configurations, location, dimensional parameters, microstructural and layout topologies of elastic and viscoelastic materials has been shown to be possible to increase the damping capacity of vibrating beam or shell like structures using various analytical and systematic numerical techniques by inspected studies.

In addition to those methodologies by inclusion of spacer layer between vibrating structure and viscoelastic layer inherently increases the strain energy of the damping layer by increasing the distance from the neutral plane [60]. During flexural motion increase of radius of curvature directly expose higher shear deformation within the viscoelastic layer compared to traditional free and constrained layer damping treatments (Figure 1-28).

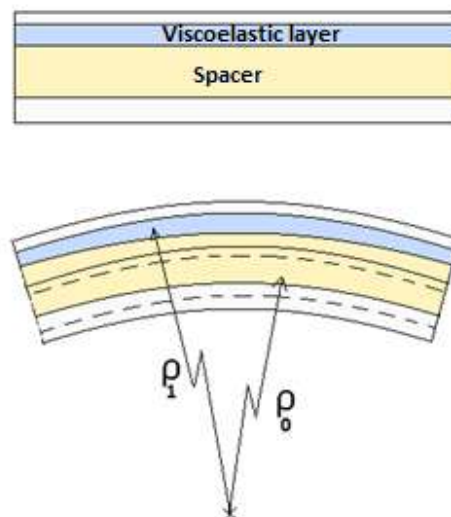


Figure 1-28 Increase of radius of curvature with spacer layer (*Paintwork*)

In literature there is a few number of studies concerning the design and analysis of spacer layer. Whitter’s [95] arched truss one of the earliest design example for this type of damping treatment. The viscoelastic layer is trapped between two curved section with certain distance from the neutral plane of vibrating beam or plate. This configuration is effective especially in low frequency oscillations by inducing shear by the relative motion of upper and lower arches.

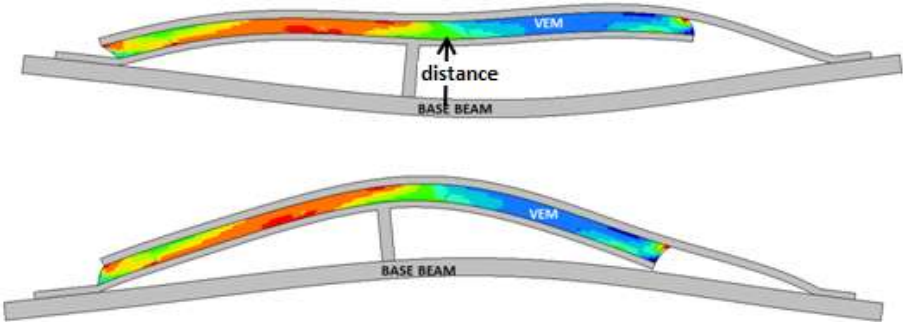


Figure 1-29 Spaced viscoelastic layer (*Adapted from [95]*)

Patel et.al [96] proposes a new structural damping configuration to increase the effectiveness of damping material which consists of a series of rows of vertically oriented platelets with continuous strips of damping material sandwiched between them. Adjacent rows of platelets may overlap each other to enhance the deformation of the damping material. The damping mechanism behind the proposed design is that during flexural deformation the attached vertical plates tend to separate from each other which in turn results the shear deformation in viscoelastic medium among them.

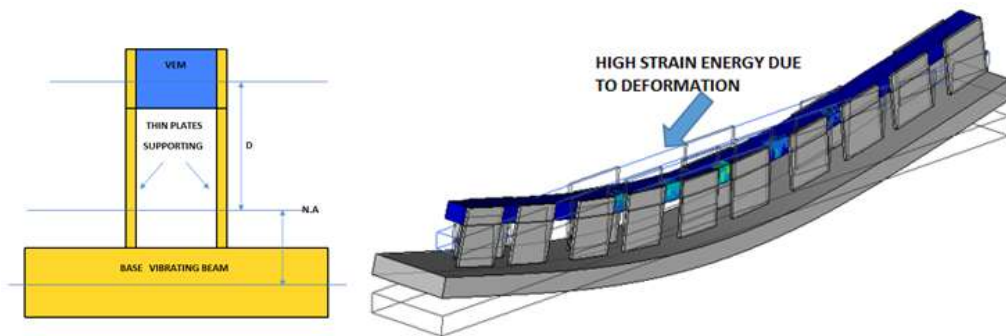


Figure 1-30 Vertically oriented plates as spacer (*Adapted from [96]*)

For the maximum damping capacity the ideal spacer layer is the one that possesses high shear resistance as well as minimum bending stiffness [97] which implies there is an optimum dimensional characteristic for the spacer geometry. The geometric configuration has been considered by Painter [98] for constrained layer damping treatment is another example which possesses low flexural stiffness due to opening gaps as shown in Figure 1-31.

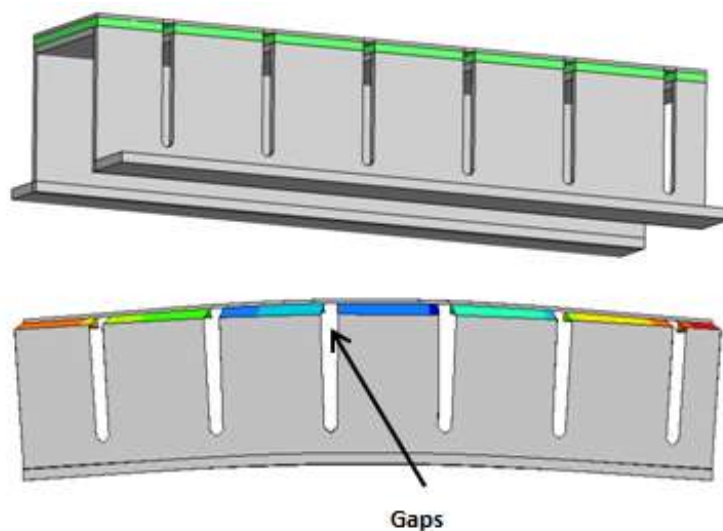


Figure 1-31 Hat section spacer with open gaps (*Adapted from [98]*)

For the designing and analysis of damping treatment with stand-off layer numerous analytical, experimental and numerical studies have also been carried out for maximization of damping by various researchers. Fallugi et.al [99] performed an experimental approach using commercial slotted spacer geometries to investigate the effectiveness of this type of configuration over the plates and airplane wings. Rogers and Parin [100,101] conducted a parametric study using analytical technique to extract the relationship between basic geometrical parameters of layers and material modulus values of simply supported plate for maximum damping. Moreover they conducted sensitivity analysis to find the dominant parameter and concluded that for maximum damping the height of spacer layer should be increased to a practical value. The effectiveness of damping treatment with stand-off layer has been shown with their extensive test campaign by applying their damping designs on pressurized fuselage skin, airplane outer wing skin in order to reduce the negative effects of resonances during flight. Their quantitative analysis results also showed that due to decrease of amplitude of vibration with integrated damping treatment with stand-off layer the stress levels were decreased therefore the fatigue life of skin structure was improved 34 times. More recently in order to predict the dynamic response of such spaced layer damping treatment Yellin et.al [102] proposed a new analytical model for fully and uniformly treated beam using Euler-Bernoulli beam theory. They showed the capability of newly developed model in prediction of the dynamic response by performing numerical examples and comparing three configurations of cantilever beam, namely, untreated, conventional constrained layer and with stand-off layer damping treatment. The ideal spacer layer condition was also sought by assigning different shear stiffness values for the spacer layer. They also concluded that in order to have the highest damping capacity the spacer layer should have high stiffness in shear and low bending stiffness. Vuure et.al [103] tried to incorporate low weight fabric panels as spacer layer to investigate this ideal condition and proposed injection of foam into fabric panel cores to tailor or increase the shear stiffness of layer. Moreover as a spacer layer position in four layer system they showed that using spacer layer as a third layer from down to top can yield %10 higher damping compared to conventional spaced layer damping treatment. For the same purpose

Huang et.al [104] used low weight microcellular foam type structure as spacer layer. They noted that by tailoring the micro-mechanical properties of cellular foams it is possible to have high shear and low bending stiffness. With their experimental study conducted with cantilever treated beam it was shown that foam type spacer layer can increase the damping by %80 with %3 additional weight. Yellin et.al [105] extended the previous analytical study [102] by conducting experiments on cantilever beams using viscoelastic spacer layer that has sufficient shear stiffness and inherent damping property to increase the overall damping performance. It is also emphasized that geometric and material manipulations can greatly increase the damping. In another and recent study of Yellin et.al [106] contributes in development of analytical model for the slotted stand-off layer using their previous analytical methodology. In their study the governing equation of motion of the four layer unit cell geometry, which is the building block of slotted configuration, composed of void and spacer material derived and used to predict overall system damping performance by assuming a beam structure composed of periodic unit cells. In addition to theoretical study in [107] they investigated the effect of number of slots within spacer geometry numerically and experimentally for the beams having prescribed constant spacer height as 2.55 mm, slot widths as 1.59 mm, 3.35 mm and 7.54 mm and number of slots as 19, 9 and 5. The results of all, having the same mass were compared to beam with solid uniform spacer with same total mass. In this study however the final comparison results between those cases were not reported quantitatively other than giving frequency response plots. Pavanasam [108] in his master thesis sought best parameters in order to minimize RMS vibration response with noise reduction goal by conducting parametric study using certain number of prescribed stand-off heights and different viscoelastic and constraining layer thicknesses by MSE method with constant viscoelastic material properties. The study finds best choice for stand-off height out of a known certain dimensions. It was reported that the resulting greatest damping factor value was 0.39.

Chaudry and Baz [109] developed a finite element model as an extension of study carried out by Yellin [106]. They performed numerical and experimental studies to validate their models with certain slotted dimensions for the spacer layer.

1.5.1 Summary of Literature Review

From the extensive literature review it is inferred that dynamic analysis and design of damping treatments with viscoelastic materials requires calculations of complex mode shapes and iterations which is time consuming due to frequency dependent mechanical properties of such polymeric materials [110]. As an alternative to this method, it is seen that the Modal Strain Energy Method proposed by Johnson and Kienholz [64] has been extensively used. Compared to other methods this method utilizes undamped real mode shapes from which the dissipative strain energies within viscoelastic layer is extracted and the loss factors are calculated for each mode as the ratio of dissipated energy and total strain energies of all individual components. For this purpose the Finite Element Method greatly helps in determination of mode shapes and extraction of strain energies of all components that forms the damping treatment system, at each mode. Since this method uses the undamped real modes, it does not require the use of frequency dependent material properties, instead, use of constant average material properties are well enough for design and optimization purposes to get rough estimate of initial design parameters [66].

In addition to parametric studies by MSE method, topology optimization technique one of the effective method used to find the material distribution for both maximum damping and minimum material consumption for minimal weight. These conditions are the main concern for the automotive and aerospace industry. Moreover for maximum damping it is also referred from the studies that geometrical configuration greatly affects the damping capacity of vibrating structures. Therefore most of the studies sought the optimum parameters, mostly dimensions, and layout of either free or constrained layer damping treatments over simple beams and plates especially for the first three modes since they are most critical ones in terms of high amplitudes and

stress values that cause structural problems. The common aim for those studies was either to increase the strain energy of damping treatment inherently or locate them to the most effective regions that induce high strain energy within the treatment.

Apart from traditional free and constrained layer damping treatments, the ones that use stand-off layer is another effective method that inherently increase the shear strain within the viscoelastic layer which is located at the top of this kind of spacer which is used as strain magnifier as it increase the curvature radii of flexural deformation that induce higher shear deformation. It is noted in literature that this kind of application has advantages over conventional treatments. For this layer to be more and more effective it has also been noted that it should have high shear resistance together with low bending stiffness. One of the configurations of this type of spacer layer is reported as the one having slotted stand-off layer which has also weight efficient since some portion of material is removed and it contains gaps within its domain.

It may be inferred from the literature review that insight into the variation of spacer layer configurations has not been clearly and systematically defined. It seems quite possible to seek the best slotted configuration and geometrical parameters with a more systematic approach other than methodologies followed by initial guesses, trial and error for the geometric parameters of this type of damping treatment [107]. However based on knowledge extracted from the earlier studies it is quite possible to create parametric design strategy for maximum damping as well as minimum weight condition by combining Modal Strain Energy Method and Finite Element Method as calculation methods while using Global Response Surface Method, Genetic Algorithm as an optimization algorithms. In purpose of parameter optimization of stand-off layer, the study of Koruk et.al [66] and Yellin et.al [107] can be adopted such that the spacer layer can be divided into certain sub regions that forms slotted configuration and the dimensions of those configuration can easily be found between lower and upper bounds via one click parametric design strategy instead of trial and error procedure yielding more quantitative results. For this purpose the HyperStudy®

software that controls all simulation process by combining different CAE platforms and mathematical optimization algorithms can be of best choice.

Moreover theoretical works and parametric studies on PCLD treatments for vibration and noise suppression really assist design decision. On the other hand, studies based on the topology optimization are very few, particularly, to the author's best knowledge, extensive research reveals that none of the studies concerns topology optimization of spacer layer for maximum damping and minimum weight condition other than slotted configuration. Again from the literature the following studies can be adopted in using topology optimization method for finding best material distribution of spacer layer. Boucher et. al [86] which use 2D topology optimization method under static loading for honeycomb unit cells to find best viscoelastic material distribution to be embedded into honeycombs. Also the study of Pai [88] who sought 2D material distribution for conventional three layer constrained layer damping treatment using topology optimization method. Kim et. al. [90] shows the effectiveness of topology optimization compared to modal strain energy method. Rong et. al.[91] finds 2D material distribution under dynamic loads. Chen and Liu [93], Al Ajmi [94], Huang et. al. [111] finds 2D microstructural distribution of elastic and viscoelastic mediums for constrained layer damping treatments. It is also quite possible defining spacer layer as design space and find the material distribution in 2D (Figure 1-32) under assumed static flexural deformation [72] to investigate the performance of final design in terms of damping capacity. Moreover as followed in Yellins study [107] the periodic unit cells of topologically optimized stand-off layer can be used as building block of a treated beam. Once having the optimized configurations both numerical and experimental validation can be performed by production of final design.

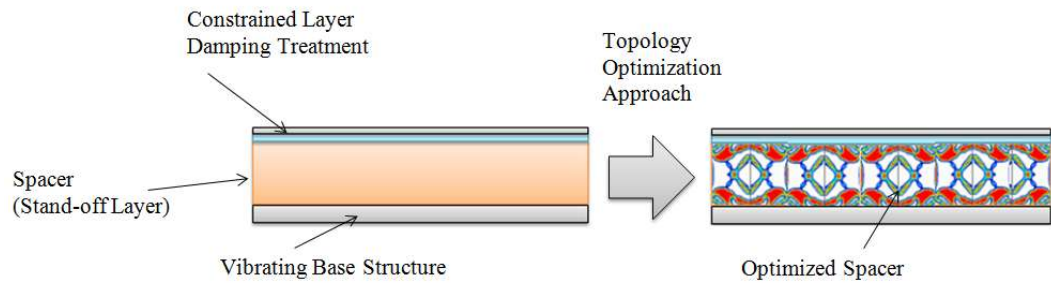


Figure 1-32 Topology optimization of spacer layer (*Produced by Optistruct[®]*)

1.5.2 Objective and Scope of The Thesis

The purpose of this study is to gain theoretical and practical knowledge about design and analysis of sandwich type structures with viscoelastic materials. More specifically the focus of this study is damping improvement of structures with stand-off layer or spacer geometry between flexible viscoelastic layer and vibrating structure using parametric and topology optimization methodologies which is in the end to get a design that may be used for vibration suppression of conformal radar antennas attached over vibrating thin shell structures.

Two different optimization methodology is going to be used namely as topology and parameter optimization methods. The aim with the use of method of topology optimization is to get the best optimal material distribution of spacer layer with minimal weight that will yield maximum damping loss factor for the first three modes of vibrating structure by combining the methodologies used by previous researchers. As a second design approach, parametric optimization method with which it is also aimed to develop robust, flexible design methodology by extending the work conducted by others to reach quantitative results specifically in design of stand-off layer.

CHAPTER 2

THEORETICAL BACKGROUND

2.1 Introduction

Thin shell like elastic structures whose thickness dimensions are much less than the other dimensions tend to vibrate more easily in the direction of surface normal. The pattern of this out of plane motion is sinusoidal in shape and they are called mode shapes of vibration or structural waves. These waves can be of transverse, longitudinal and bending form and are result of energy imparted to the medium and they can be characterized as the relative displacement with respect to the rest position of structure and with their direction, speed etc. These waves have the ability of carrying energy from one point to another and they occur at some fixed frequencies which are also called natural frequency of vibration or resonance frequencies. In other words, the energy imparted to the structures travels in the form of elastic waves at certain frequencies and one special case exists when the forcing frequency coincides with those structural natural frequencies, this coincidence is termed as the resonance at which the amplitude of those waves that is the displacement in normal direction, tends to be large. Such kind of structural deformations have many drawbacks which were explained in previous chapter such as deviation of antenna pattern due to change of distance between antenna patches over the surface, disturbing sound radiation due to coupling of structural waves with free surrounding air waves, fatigue due to cyclic stress generated at deformed zones (Figure 2-1) etc [112].

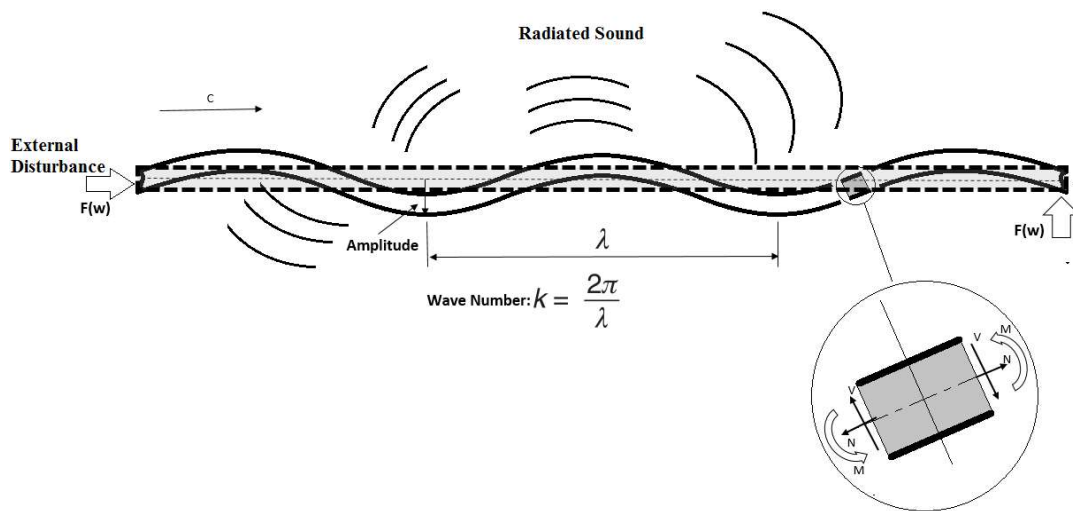


Figure 2-1 Vibration of thin panel like structure (*Adapted from [113]*)

The vibration of structures can be grouped in two categories [113] such that when a harmonic external force continuously disturb the medium, the structure is said to be under forced vibration and since the disturbing energy continuously imparted to structure the elastic waves formed are also continuously propagated over the domain varying sinusoidally at the same frequency of oscillation with a spatial period of λ , described as wavelength.

The response associated under forced vibration is termed as a combination of transient response and steady-state response, the latter is completely dominated by the excitation frequency and it prevails until the force is removed. When the excitation force is removed and the structure is left to vibrate freely, the structure vibrates at its one or combination of certain modes but with a decaying response over time until it is completely motionless. The reason for such decaying free response is the inherent energy dissipation mechanism involved during vibrating motion such as friction caused by surrounding air or interaction of mechanical components with each other. The phenomena called *damping* which is the energy dissipation and one of the important parameter in vibration control measurements.

Structures subjected to dynamic loads, generally show structural damping values which are capable of reducing oscillations amplitude. In aerospace field, low structural damping or high oscillations amplitude, may impact negatively on structural stability and emitted noise as well as the performance of attached antenna elements over the vibrating surface as explained previous chapter. By increasing damping it is possible to obtain a considerable noise and vibration reduction. For this purpose the most popular form of increase of damping is to embed viscoelastic layer into structural components. Before going into details of viscoelastic materials and their damping characteristic, it is aimed to give insight into how the damping parameter effects the dynamic behaviour of the complex structure by considering dynamic behaviour of the simplest dynamic model, that is, single degree of freedom system.

Dynamic behaviour of structures as well as effects of the parameter involved in calculation of response of complex structures can easily be explained/visualized by considering the dynamic response of single degree of freedom system under harmonic excitation.

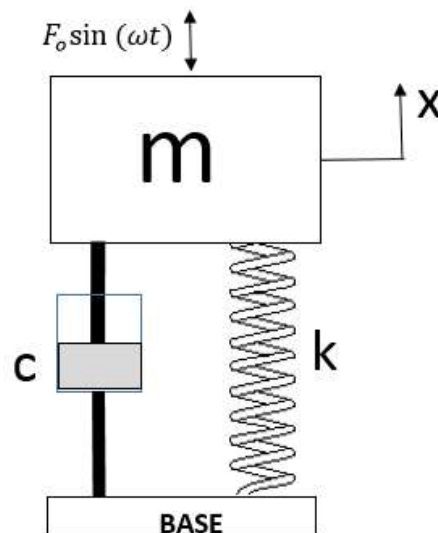


Figure 2-2 Single degree of freedom system under harmonic load (*Adapted from [113]*)

The dynamic response calculation of single degree of freedom system in theoretical form given as follows [113].

$$m\ddot{x} + c\dot{x} + kx = F_o \sin(\omega t) \quad (2-1)$$

$$F(t) = F_o \sin(\omega t) \quad (2-2)$$

Where F_o represents the amplitude the applied load and ω is frequency of applied load or deriving frequency (rad/s).

The solution of this equation of motion composed of two solution as an homogenous which is transient part and a particular solution which is referred as steady state response. For the linear systems the output response is proportional to the input forcing, that is, the sinusoidal input will produce a sinusoidal output of the same frequency which corresponds the the particular solution of the problem and area given as follows [113];

$$x_p(t) = X \sin(\omega t - \theta) \quad (2-3)$$

$$x_h(t) = e^{-2\zeta\omega_n t} (A \sin(\omega_d t) - B \cos(\omega_d t)) \quad (2-4)$$

Where X is the steady state amplitude and θ is the phase shift at steady state. The coefficients A and B are the constants found by initial condition of the system such as initial applied displacement and velocity of mass m.

$$X = \frac{F_o/k}{\sqrt{(1 - m\omega^2)^2 + (c\omega/k)^2}} \quad (2-5)$$

This equation can be rewritten as follows;

$$X \frac{k}{F_o} = \frac{1}{\sqrt{\left[1 - \left(\frac{\omega}{\omega_n}\right)^2\right]^2 + \left[2\zeta\left(\frac{\omega}{\omega_n}\right)\right]^2}} \quad (2-6)$$

$$\tan(\theta) = \frac{2\zeta(\omega/\omega_n)}{1 - (\omega/\omega_n)^2} \quad (2-7)$$

Here in these equations;

$\omega_n = \sqrt{k/m}$ is the natural frequency of the undamped system when (c=0),

$\omega_d = \omega_n\sqrt{1 - \zeta^2}$ is the natural frequency of the damped system,

$\zeta = \frac{c}{c_c}$ is the damping ratio of the system and $c_c = 2\sqrt{km}$.

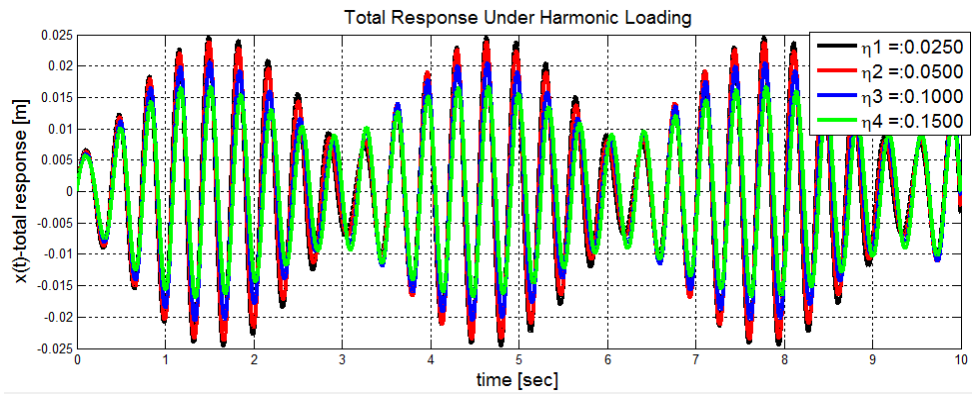
Also for the linear system, the total solution can also be regarded as the sum of independent individual solutions therefore the total response of the system becomes [113];

$$X(t) = e^{-\zeta\omega_n t} (A \sin(\omega_d t) - B \cos(\omega_d t)) + X \sin(\omega t - \theta) \quad (2-8)$$

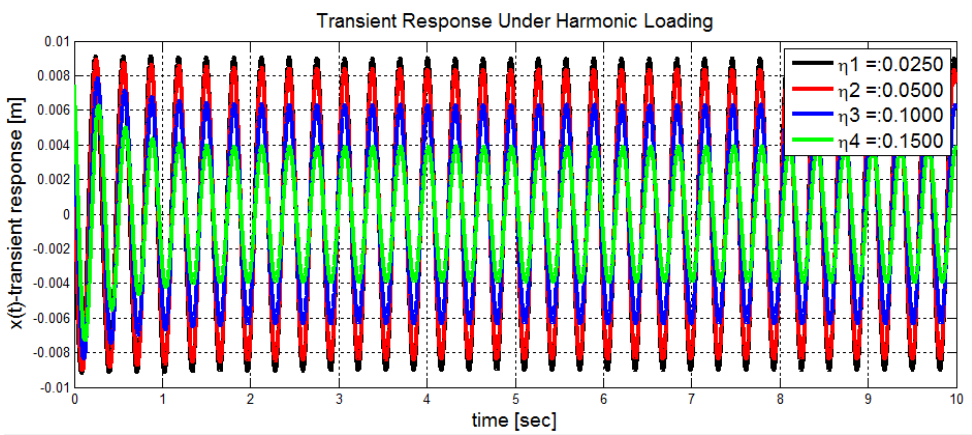
One of the important conclusion that can be derived from the above equation is that larger the time, t, smaller the free response and the forced response, which dominates the total response of the system. Another important phenomena for the dynamic behaviour of the structures that can be drawn from this simple system is that when the forcing frequency approaches to the undamped natural frequency of the system, that is, when $\omega \approx \omega_n$ the response of the system, lets say the displacement, tends to be very large which is called *resonance* condition and represents the unstable

condition for the system under consideration and this result unwanted noise and deflections which need to be suppressed.

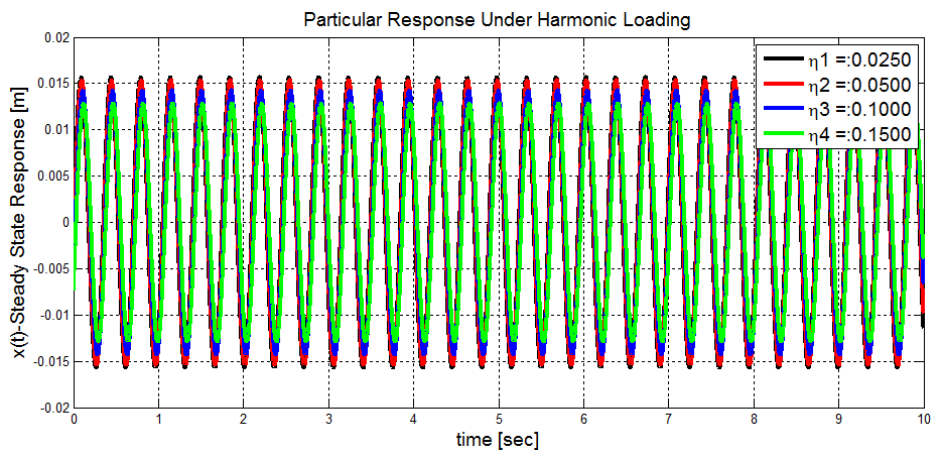
The solution of this dynamic equation has been programmed and solved for the particular initial conditions in MATLAB[®] [114] and the results will be given in time domain for the case at which the forcing frequency close to the natural frequency and for the other case at which both forcing and natural frequencies exactly matches eachother. In Figure 2-3 the response of the dynamic system was plotted for the condition that the forcing frequency very close the natural frequency of the total system, that is $\omega \approx 0.8\omega_n$. The resulting response called *beat phenomena* which generally results before and after resonance condition and can be regarded as early warning of advancing resonance. In the same plot the influence of damping parameter is also given and it can be noticed that as we increase the damping parameter, the resulting amplitudes are less for total and each of individual solutions.



(a)

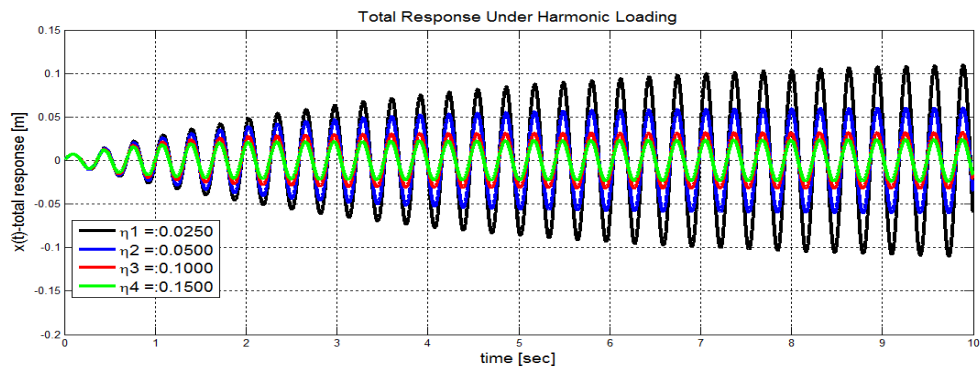


(b)

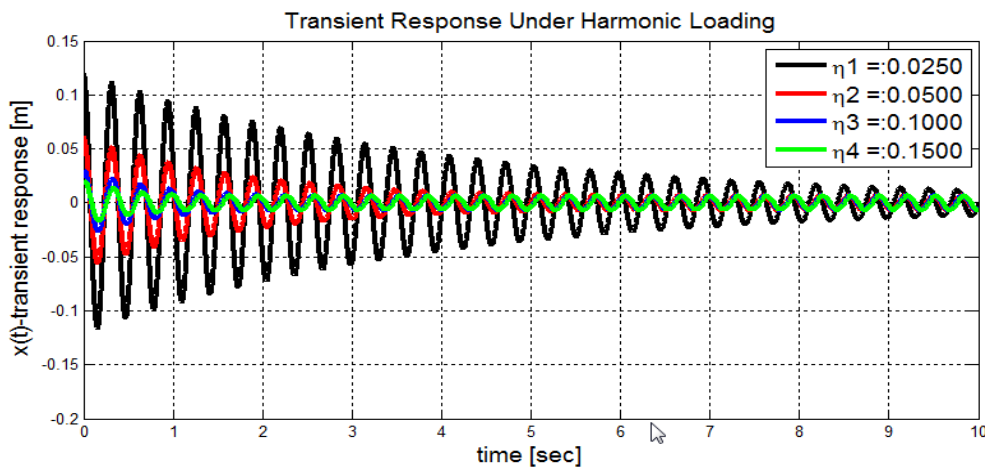


(c)

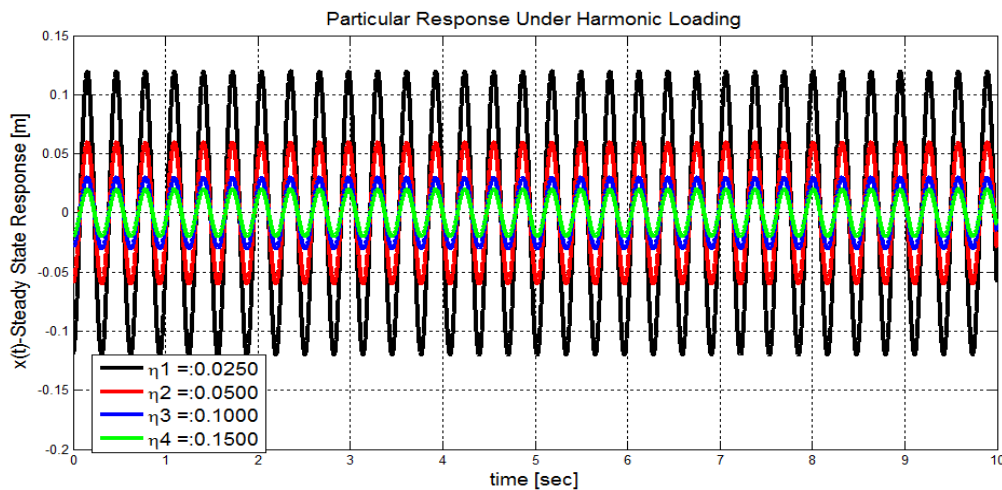
Figure 2-3 Variance of displacement response of simple 1 DOF system $\omega = 0.8\omega_n$
 (a) Total Response (Beat Phenomena). (b) Free Response (Transient), (c) Steady – State Response (Forcing Frequency)



(a)



(b)



(c)

Figure 2-4 Variance of displacement response of simple 1 DOF system: $\omega = \omega_n$

(a) Total Response (Resonance Phenomena), (b) Free Response (Transient),

(c) Steady-State Response (Forcing Frequency)

The most critical condition occurs when the forcing frequency exactly matches with natural frequency of the system, that is, $\omega = \omega_n$. The amplitude of total vibration response tends to be very large with time (Figure 2-4-a). The influence of damping can also be seen from each individual response solutions (Figure 2-4-b,c). Again as we increase the damping parameter the amplitude of responses get lower and lower. The same result can also be visualized in frequency domain. The time domain solution has an equivalent frequency domain representation, which is much more useful in design of structures, for linear dynamic system and for the particular resonance frequency it is shown in (Figure 2-5). From such frequency response plots one can easily see that in case of lack of damping, that is, $\zeta = 0$, the displacement response is maximum at resonance frequency and as we increase damping factor ζ the amplitude is lowered. Inversely, from such frequency response plot one can identify resonance frequency at which the peaks occur together with damping parameter involved in system response by considering the peak response and half power bandwidth points in frequency response function. Because the peak region is fully damping controlled. The details will be given in following pages.

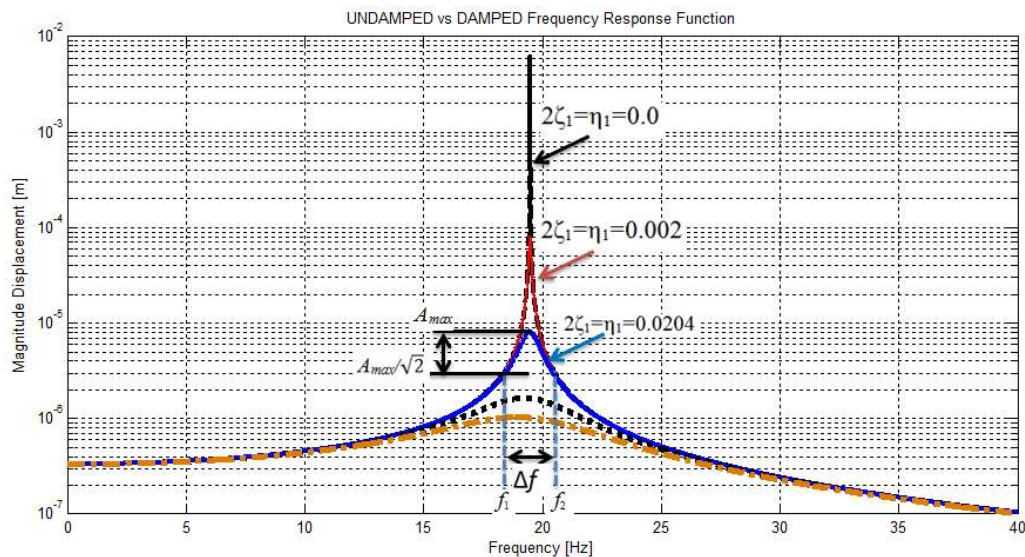


Figure 2-5 Displacement response of simple 1 DOF system in frequency domain when $\omega = \omega_n$. [114]

2.2 Damping

As previously explained the damping greatly reduces the vibration response amplitudes. The mechanism behind the damping phenomena is simply the dissipation of excess energy imparted into the vibrating structure in terms of heat which in turn lessens the total mechanical energy within the vibrating system. Damping occur in many different ways in vibrating structures either in the form of friction due to relative motion exists during vibration between individual components of an assembly contacting each other at joints and this mechanism known as *structural damping*. The dissipation of energy can also be accomplished by utilizing drag force generated within a fluid like medium known as *viscous damping*. In this study we will focus on another damping mechanism that is due to the inherent material property which relies on the internal heat generation under cyclic deformation that is *material (internal) damping*. Material damping results from internal interaction of microstructures within body and mechanical energy is dissipated during cyclic deformation in elastic range in all engineering materials. This mechanism of energy dissipation is explained as the interaction of stress and strain, occurring (Figure 2-1) due to internal forces under cyclic loading, as the *hysteresis loop* (Figure 2-6). All the mechanisms involved in vibration damping are simply the energy loss mechanisms.

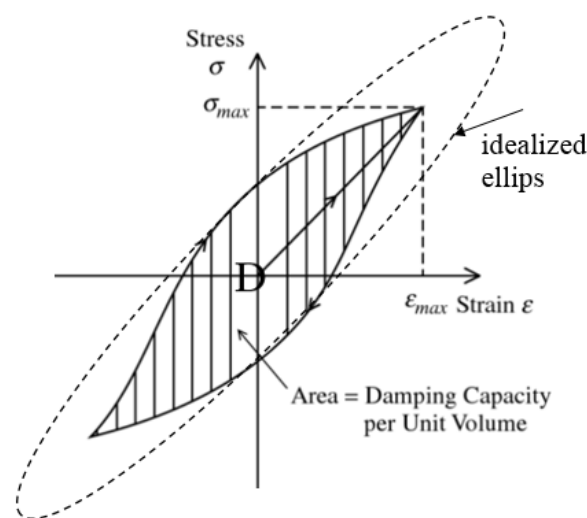


Figure 2-6 internal energy loss mechanism: *hysteresis loop* (Adapted from [113])

The energy dissipation per unit volume of the material, per stress cycle, is given by the area of the hysteresis loop. This is termed specific energy D ,

$$D = \oint \sigma d\varepsilon \quad (2-9)$$

In an engineering system, a structure should stay stable and undamaged despite of the internal and external vibrations. The stability of a system depends on its damping ability, which can be affected by design. Damping is defined as the energy dissipation of a system in vibration and it can be presented by various parameters, one of which is the loss factor. Loss factor η characterize the energy dissipation of treated vibrating structures and is defined as the ratio of specific damping capacity D , which is average energy dissipated, per radian of the damping cycle [113, 61] to the total amount of energy stored per cycle.

$$\eta = \frac{\Delta U}{2\pi U_{max}} = \frac{1}{2\pi} \frac{\text{Energy dissipated per cycle}}{\text{Maximum energy stored per cycle}} \quad (2-10)$$

Where ΔU is the energy loss per cycle and U_{max} is the total stored reversible energy of the system. Parameters ΔU and U_{max} can be measured through the area and the shape of the hysteresis loop.

For the metallic structures the energy dissipation rate is so small. For aluminum alloys for example the average loss factor is measured to be around 0.00197, 0.00079, and 0.00057 for mode I, II, and III, respectively. This leads the researchers on finding new material and design configurations that maximize the damping capacity of structures [115,116,117].The polymeric based viscoelastic materials are good candidates in this manner. Because they have large and inherent energy dissipation capacity therefore the high loss factor, especially when they are subjected to the cyclic shear deformation and this makes them attractive in vibration control applications [56, 59].

2.3 Viscoelastic Materials

In order to avoid large dynamic amplification during vibration the structures should be able to dissipate energy. This means that the material either should have high internal damping or composed of high loss mechanism that makes viscoelastic materials unique choice for passive vibration control.

Viscoelastic materials are mainly polymeric and due to their low stiffness property they cannot be used as structural load carrying members however their composition of randomly arranged large molecular chains, which are known as amorphous polymers, interact and deform easily under load, causing large energy dissipation due to high internal friction among chains compared to metals. In other words they have large area of hysteresis loop under cyclic stress which results high energy loss mechanism. Moreover depending on the operational conditions, the bonds between uncross-linked polymeric molecules can be strong, moderate or weak. Degradation of bonds allows slippage of each molecules with each other which results large deformation capability. Therefore the viscoelastic materials exhibit both elastic and viscous behaviour which means they can both store and dissipate energy [118].

2.3.1 Effects of Temperature and Frequency

The environmental operational condition strongly affects the dynamic behavior and dissipation characteristic of the viscoelastic materials. The mechanical properties such as modulus and energy dissipation characteristic vary with temperature and frequency of loading due to the change of strength of intermolecular connections. Three different phase of composition takes place for different temperature and frequency of loading as shown in (Figure 2-7)

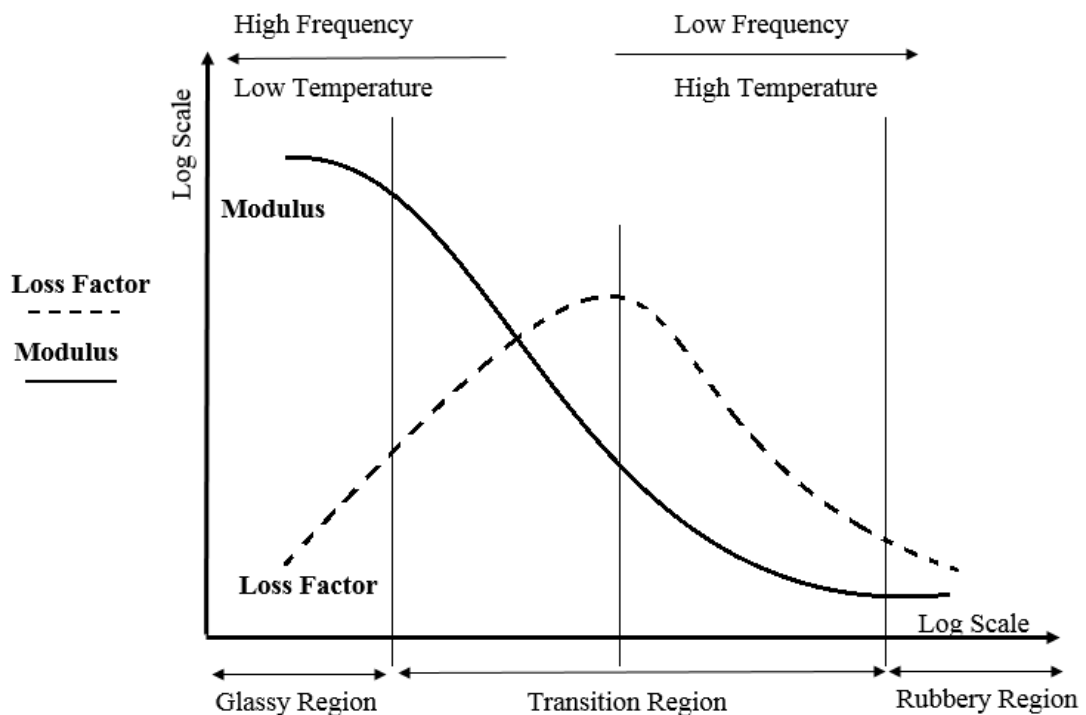


Figure 2-7 Variation of Modulus and Loss Factor (*Adapted from* [119])

The bonds between molecules of polymers are strong in cold environment which results a stiff and less energy dissipation characteristic which is also dominating from low frequency to high frequency of oscillations at constant temperature. This state of material is called *glassy phase* due to increased stiffness. As we increase the temperature the strength of bonds between molecular polymeric networks degrades gradually resulting less stiff, soft structure but with an increase of energy dissipation

characteristic at the state of material called *transition phase*. Further increase of temperature results decreasing both stiffness and loss mechanism at the state called *rubbery phase* which is also dominating at low frequency of oscillations at constant temperature. In terms of damping performance the viscoelastic materials exhibit higher damping capacity at their transition phase.

2.3.2 Linear Dynamic Response and Energy Dissipation

When a purely elastic material is submitted to oscillatory stress σ , the measured strain ϵ occurs in phase. In a viscoelastic material however, strain lags behind stress. Consider a bar of viscoelastic material is subjected to time varying harmonic tension or shear load of maximum value of F_0 at which the maximum stress and strain were σ_0 and ϵ_0 respectively. When a viscoelastic material is subjected to an alternating stress, it is observed that the strain associated with given stress is not in phase with each other [120].

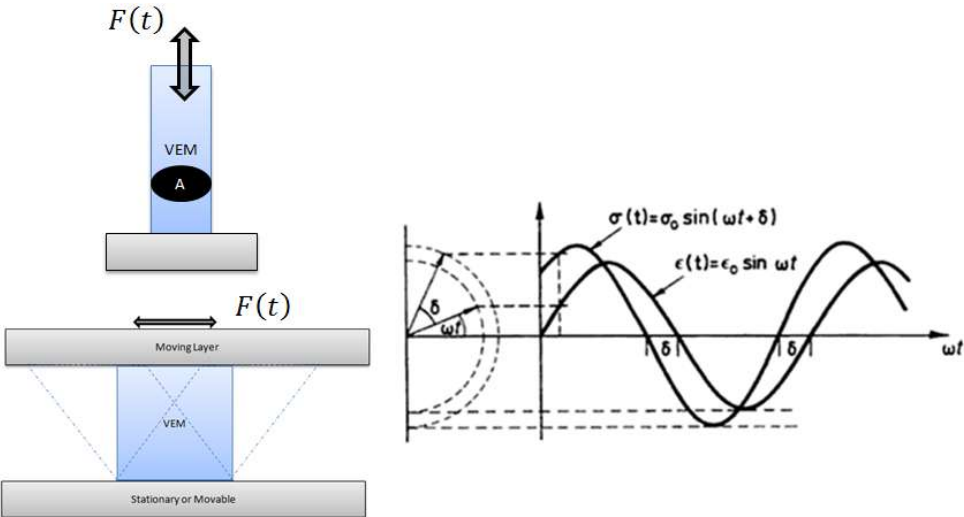


Figure 2-8 Linear dynamic response of viscoelastic material under loading (*Adapted from [121]*)

$$\sigma(t) = \frac{F(t)}{A} = \sigma_o \sin(\omega t + \delta) \quad (2-11)$$

$$\epsilon(t) = \epsilon_o \sin(\omega t) \quad (2-12)$$

$$\sigma = \sigma_o \cos(\delta) \sin(\omega t) + \sigma_o \sin(\delta) \sin(\omega t + \pi/2) \quad (2-13)$$

in which the first term of stress equation is in phase while the second term is out of phase with a phase angle $\pi/2$. A usual way to characterize the material is then to define a complex Young's modulus E^* after rewriting (2-13) in complex form and dividing it by strain (2-12) yields;

$$\sigma = \sigma_o \cos(\delta) \sin(\omega t) + i \sigma_o \sin(\delta) \sin(\omega t) \quad (2-14)$$

$$\text{Complex Modulus} = \frac{\sigma}{\epsilon} = \frac{\sigma_o}{\epsilon_o} \cos(\delta) + i \frac{\sigma_o}{\epsilon_o} \sin(\delta) \quad (2-15)$$

and knowing the fact that the modulus is frequency dependent the complex young modulus can be written as;

$$E^*(\omega) = E'(\omega) + iE''(\omega) \quad (2-16)$$

where E' is the elastic or storage modulus and E'' is loss modulus, and the ratio of loss modulus over storage modulus is called loss factor and defined as;

$$\tan(\delta) = \frac{E''}{E'} = \eta(\omega) \quad (2-17)$$

$$E^*(\omega) = E(\omega)(1 + i\eta(\omega)) \quad (2-18)$$

The same is true for shear modulus. Assuming that the Poisson ratio of the viscoelastic materials is constant in frequency, the complex shear modulus yields

$$G^*(\omega) = G'(\omega) + iG''(\omega) = G(\omega)(1 + i\eta(\omega)) \quad (2-19)$$

Where $G' = G$ shear modulus, G'' the shear loss modulus, and η the loss factor defined as;

$$\eta(\omega) = \frac{G''(\omega)}{G'(\omega)} \quad (2-20)$$

2.3.2.1 Energy Storage and Dissipation

Dissipation of energy by means of viscoelastic materials is essentially due to hysteresis effect takes place within the molecular structure under cyclic loading. The storage and dissipative characteristic, as an enclosed area in hysteresis loop (Figure 2-6), in more theoretical form is given in [120]; as follows

Let the harmonic loading be as follows;

$$\sigma = \sigma_o \sin(\omega t) \quad , \quad \epsilon = \epsilon_o \sin(\omega t - \delta) \quad (2-21)$$

The stored energy is found by simply integrating the stress-strain loop over the quarter cycle as [120];;

$$\begin{aligned}
\int_0^{\epsilon_o} \sigma d\epsilon &= \int_0^{\pi/2\omega} \sigma \frac{d\epsilon}{dt} dt \\
&= \omega \epsilon_o \sigma_o \int_0^{\pi/2\omega} [\cos(\omega t) \sin(\omega t) \cos(\delta) \\
&\quad + \sin^2(\omega t) \sin(\delta)] dt \\
&= \epsilon_o \sigma_o \left[\frac{\cos(\delta)}{2} + \frac{\pi \sin(\delta)}{4} \right]
\end{aligned} \tag{2-22}$$

For $\delta=0$

$$\int_0^{\epsilon_o} \sigma d\epsilon = \epsilon_o \sigma_o \tag{2-23}$$

This is known as recoverable stored energy. The second term represents the dissipated energy and for $\delta=0$ it vanishes since all energy is recovered. The above equation can be rewritten in terms of storage modulus such that [120];

$$E' = \frac{\sigma_o}{\epsilon_o} \cos(\delta) \quad , \sigma_o = \frac{E' \epsilon_o}{\cos(\delta)} \tag{2-24}$$

Therefore the **storage energy** is;

$$W_s = \int_0^{\epsilon_o} \sigma d\epsilon = \frac{1}{2} E' \epsilon_o^2 \tag{2-25}$$

We can also find the dissipated energy by integrating stress-strain loop over full cycle since the dissipated energy is equal to the area of enclosed hysteresis loop. Taking the one quarter of full cycle yields [120];;

$$\begin{aligned}
 \int_0^{\epsilon_o} \sigma d\epsilon &= \frac{1}{4} \int_0^{2\pi/\omega} \sigma \frac{d\epsilon}{dt} dt \\
 &= \frac{1}{4} \omega \epsilon_o \sigma_o \int_0^{2\pi/\omega} [\cos(\omega t) \sin(\omega t) \cos(\delta) \\
 &\quad + \sin^2(\omega t) \sin(\delta)] dt \\
 &= \frac{1}{4} \epsilon_o \sigma_o \pi \sin(\delta)
 \end{aligned} \tag{2-26}$$

Recalling E'' from (2-15) the **dissipated energy** is;

$$W_d = \frac{\pi}{4} E'' \epsilon_o^2 \tag{2-27}$$

From the definition the ratio of dissipated energy in one cycle to the total energy stored in medium is loss factor and is yielded as;

$$\frac{W_s}{W_d} = \frac{\pi}{2} \tan(\delta) \tag{2-28}$$

The phase angle between stress and strain creates hysteresis effect that can be related to damping which is termed as loss tangent and it is a measure of internal friction or material damping under cyclic motion.

2.4 Analysis of Viscoelastic Damping Treatment

Design of damping treatment requires prediction of dynamic behavior of treated structure accurately. In literature there are well documented approaches to simulate the dynamic response of the structures. In this part of the study some of the methodologies, either analytical or numerical approaches, used in damping prediction of complex structures will be explained.

The simplest analytical method developed for the analysis of damping treatment has been proposed by Ross, Ungar, Kerwin known as RKU Method which was also shown to be well correlated with experiments conducted for constrained and unconstrained damping treatments [60]. The methodology based on estimation of complex flexural bending stiffness which depends on material and geometrical properties of individual layers and the wavelength of vibration. The method is also applicable for various classical boundary conditions.

Another method proposed by Johnson and Kienholtz [64] based on the modal analysis of treated structure from which the undamped modes shapes are used to extract the dissipated energy in terms of modal strain energies for each layers at each mode. Since the undamped modes are used in calculation of dissipated energies the constant material properties can be utilized as an advantage of this method compared to method requires use of frequency dependent complex modulus for the viscoelastic material, which is not practical for the huge structural problems since it requires time consuming iterative solution [110]. Instead the Modal Strain Energy method (MSE) calculates the average damping factor and it is valuable method to find optimum design in practically short time.

Among all methods the Direct Frequency Response Analysis (DFRA) is another method used in conjunction with finite element method (FEM) and utilize frequency dependent material properties of viscoelastic material. The solution of this methodology yields the frequency response functions of treated structure for any

location over the design from which one can extract the damping factors for each modes accurately upon using Half Power Bandwidth Method.

2.4.1 RKU Method

This method was developed in the early of 1969 by Ross et.al. [60] and is experimentally proved for use in design applications. It is the simplest method of analysis for the damping performance of the treated beam and shell like structures. Since the methodology is based on finding the flexural stiffness of vibrating, let’s say, beam like structure, it is important first to consider transverse vibration of beam before going into details of this methodology.

2.4.1.1 Transverse Vibration of Simple Beam

The analytical model of transverse vibration of beam like structures is given in many textbooks [122] and will be explained here in order to understand the RKU method. Below the governing equation of motion for the transverse vibration of continuum beam is given and solved under the cantilever boundary condition for the first 10 modes of the beam.

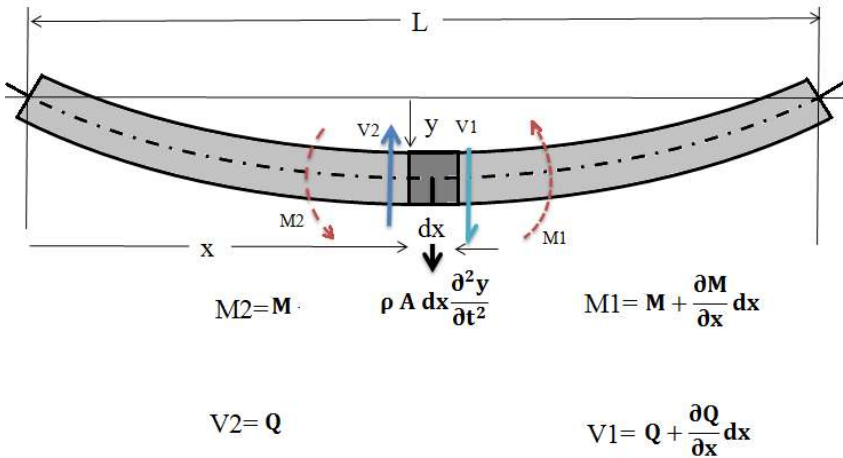


Figure 2-9 Deflected shape of vibrating beam (Adapted from [122])

Neglecting rotary inertia and shear of infinitesimal element, taking moment with respect to center yields;

$$Q = \partial M / \partial x \quad (2-29)$$

And summing forces in the y direction yields;

$$\frac{\partial Q}{\partial x} dx = \rho A dx \frac{\partial^2 y}{\partial t^2} \quad (2-30)$$

Hence

$$\frac{\partial^2 M}{\partial x^2} = \rho A \frac{\partial^2 y}{\partial t^2} \quad (2-31)$$

For uniform cross section of beam the bending rigidity **EI** is constant [122], so

$$M = -EI \frac{\partial^2 y}{\partial x^2} \text{ and } \frac{\partial^2 M}{\partial x^2} = -EI \frac{\partial^4 y}{\partial x^4} \quad (2-32)$$

$$\frac{\partial^4 y}{\partial x^4} + \left(\frac{\rho A}{EI} \right) \frac{\partial^2 y}{\partial t^2} = 0 \quad (2-33)$$

This equation is the general equation of motion for the transverse vibration of a uniform beam. Moreover when a beam performs one of its normal modes during vibration, the deflection at any point of the beam also varies harmonically with time, therefore it can be written;

$$y = X(B_1 \sin(\omega t) + B_2 \cos(\omega t)) \quad (2-34)$$

where **X** is a function of x which defines the beam shape of the normal mode of vibration. Hence;

$$\frac{\partial^4 X}{\partial x^4} = \left(\frac{\rho A}{EI}\right) \omega^2 X = \beta^4 X \quad (2-35)$$

where

$$\beta^4 = \left(\frac{\rho A}{EI}\right) \omega^2 \quad (2-36)$$

And the general solution to the beam equation finally yields as follows [122]);

$$X = C_1 \cos h(\beta x) + C_2 \sinh(\beta x) + C_3 \cos(\beta x) + C_4 \sin(\beta x) \quad (2-37)$$

In this final equation the coefficients C_1 to C_4 are determined from the applied boundary condition for two ends of the beam.

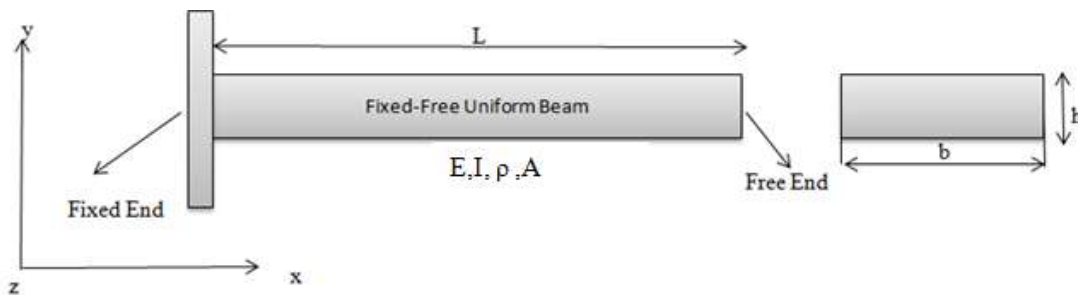


Figure 2-10 Fixed-free beam (*Adapted from [122]*)

Considering the transverse vibration of fixed-free thin uniform cross section beam with length of L, the boundary condition for this beam can be written as follows;

$$\text{B.C 1 : } y(0) = 0 \quad (2.37 \text{ a})$$

$$\text{B.C 2: } \theta(0) = 0 \quad \text{at } \frac{dy}{dx} |_{@x=0} = 0 \quad (2.37 \text{ b})$$

$$\text{B.C 3 : } M(L) = 0 \quad \text{at } EI \frac{\partial^2 y}{\partial x^2} |_{@x=L} \quad (2.37 \text{ c})$$

$$\text{B.C 4 : } V(L) = 0 \quad \text{at } EI \frac{\partial^3 y}{\partial x^3} |_{@x=L} \quad (2.37 \text{ d})$$

$$\begin{aligned} \frac{dX(x)}{dx} &= C_1 \beta \sinh(\beta x) + C_2 \beta \cosh(\beta x) \\ &\quad - C_3 \beta \sin(\beta x) + C_4 \beta \cos(\beta x) \end{aligned} \quad (2.37 \text{ e})$$

$$\begin{aligned} \frac{d^2 X(x)}{dx^2} &= C_1 \beta^2 \cosh(\beta x) + C_2 \beta^2 \sinh(\beta x) \\ &\quad - C_3 \beta^2 \cos(\beta x) - C_4 \beta^2 \sin(\beta x) \end{aligned} \quad (2.37 \text{ f})$$

$$\begin{aligned} \frac{d^3 X(x)}{dx^3} &= C_1 \beta^3 \sinh(\beta x) + C_2 \beta^3 \cosh(\beta x) \\ &\quad + C_3 \beta^3 \sin(\beta x) - C_4 \beta^3 \cos(\beta x) \end{aligned} \quad (2.37 \text{ g})$$

After substitution of the boundary conditions ;

$$\begin{aligned} C_1 + C_3 &= 0 \\ C_2 + C_4 &= 0 \end{aligned} \quad (2.37 \text{ h})$$

$$C_1 \cosh(\beta L) + C_2 \sinh(\beta L) - C_3 \cos(\beta L) - C_4 \sin(\beta L) = 0 \quad (2.37 \text{ i})$$

$$C_1 \sinh(\beta L) + C_2 \cosh(\beta L) + C_3 \sin(\beta L) - C_4 \cos(\beta L) = 0 \quad (2.37 \text{ ii})$$

Eliminating C_1 and C_3 from (2-37) and (2-37) by substitution of (2-37) yields;

$$[\cosh(\beta L) + \cos(\beta L)]C_3 + [\sinh(\beta L) + \sin(\beta L)]C_4 = 0 \quad (2.37 \text{ iii})$$

$$[\sinh(\beta L) - \sin(\beta L)]C_3 + [\cosh(\beta L) + \cos(\beta L)]C_4 = 0 \quad (2.37 \text{ iv})$$

Rearranging above equations in matrix form;

$$\begin{bmatrix} \cosh(\beta L) + \cos(\beta L) & \sinh(\beta L) + \sin(\beta L) \\ \sinh(\beta L) - \sin(\beta L) & \cosh(\beta L) + \cos(\beta L) \end{bmatrix} \begin{bmatrix} C_3 \\ C_4 \end{bmatrix} = \begin{bmatrix} 0 \\ 0 \end{bmatrix} \quad (2.37 \text{ v})$$

The solution of above equation yields the shape function of

$$\cos(\beta L) \cosh(\beta L) = 1 \quad (2.37 \text{ vi})$$

Recalling beam equation (2-36); the natural frequency of cantilever beam thus can be written as;

$$\omega_i = \beta_i^2 \sqrt{\frac{EI}{\rho A}} \quad (2-38)$$

The first 10 roots of shape function (2.37 vi) for the cantilever (fixed-free) beam is found to be as given in Table 2-1 [123];

Table 2-1 Roots of shape function for the cantilever (fixed-free) beam [123]

Order	1st	2nd	3rd	4th	5th	6th	7th	8th	9th	10th
$\beta_i L$	1.875	4.694	7.855	10.996	14.137	17.28	20.42	23.56	26.70	29.85

To relate the frequency at which attenuation begins, the frequency–wavelength relationship for transverse waves propagating through a beam is given as;

$$\omega_i = \left(\frac{2\pi}{\lambda}\right)^2 \sqrt{\frac{\mathbf{EI}}{\rho A}} \quad (2-39)$$

Where I, E, A, and ρ are the physical parameters of the beam layer and λ is the wavelength of vibration. One can easily conclude from the derived frequency formula for the simple beam that increase of frequency results shorter wavelength of vibration. The flexural rigidity \mathbf{EI} in this formula is calculated using RKU equations for the treated beams using the analytical formula given below [60]

For the three layer constrained layer damping treatment the complex flexural rigidity \mathbf{EI}^* is approximated as follows [60];

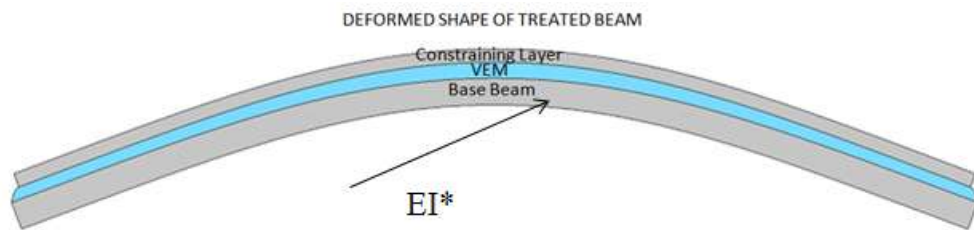


Figure 2-11 Flexural rigidity of treated layered beam

$$\begin{aligned}
EI^* &= E_1 \frac{H_1}{12} + E_2^* \frac{H_2}{12} + E_3 \frac{H_3}{12} - E_2^* \frac{H_2^2}{12} \left(\frac{H_{31} - D}{1 + g^*} \right) \\
&+ E_1 H_1 + E_2^* H_2 (H_{21} - D)^2 + E_3 H_3 (H_{31} - D)^2 \\
&- \left(\frac{E_2^* H_2}{2} (H_{21} - D) + E_3 H_3 (H_{31} - D) \right) \left(\frac{H_{31} - D}{1 + g^*} \right)
\end{aligned} \tag{2-40}$$

where

$$D = \frac{E_2^* H_2 \left(H_{21} - \frac{H_{31}}{2} \right) + g(E_2^* H_2 H_{21} + E_2^* H_2 H_{31})}{E_1 H_1 + E_1 H_2 / 2 + g(E_1 H_1 + E_2^* H_2 + E_3 H_3)} \tag{2.40a}$$

$$H_{31} = \frac{(H_1 + H_3)}{2} + H_2 \tag{2.40b}$$

$$H_{21} = \frac{(H_1 + H_2)}{2} \tag{2.40c}$$

$$g^* = \frac{G_2^*}{E_3 H_2 H_3 (\beta_i)^2 \sqrt{C_n}} \tag{2.40d}$$

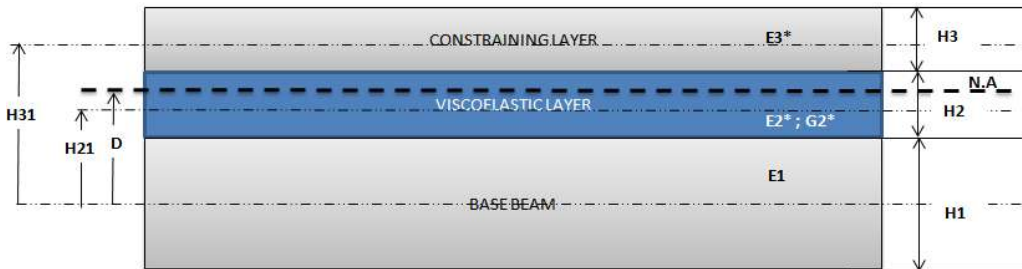


Figure 2-12 Topology optimization of spacer layer (*Adapted from [60]*)

Where g^* is shear parameter and C_n is the correction factor for the considered boundary condition given (Table 2-2).

Table 2-2 Correction factor for shear parameter for specific boundary condition [124]

Boundary Conditions	Correction Factor	
	Mode 1	Mode 2+
Pinned-Pinned	1	1
Clamped-Clamped	1.4	1
Clamped-Pinned	1	1
Clamped-Free	0.9	1
Free-Free	1	1

The loss factor associated with damping treatment is finally found as the ratio of imaginary part and real part of complex rigidity as follows;

$$\eta = \frac{\text{imag}(EI^*)}{\text{real}(EI^*)} \quad (2-41)$$

The solution of RKU equation is iterative since the complex modulus E^* has frequency dependency as explained before.

The latter methodologies requires the use of finite element method (FEM) therefore this numerical procedure will be explained for the 2D plain strain case since in this study the design of vibrating structure considered in 2D.

2.4.2 2D Finite Element Method

The strain energy distribution should also be represented by the finite elements for the loss factor calculation using Modal Strain Energy Method. The 2D plane shell elements, namely, QUAD4 can also be used in order to extract strain energy through stress-strain field. The theoretical formulation together with deformation pattern of plain strain element, for the stress-strain calculations using nodal displacement field is given in (Figure 2-14). The general two dimensional state of strain for an infinitesimal element is direct function of nodal displacement in x and y only and this can be represented by rectangular QUAD4 element. [126]

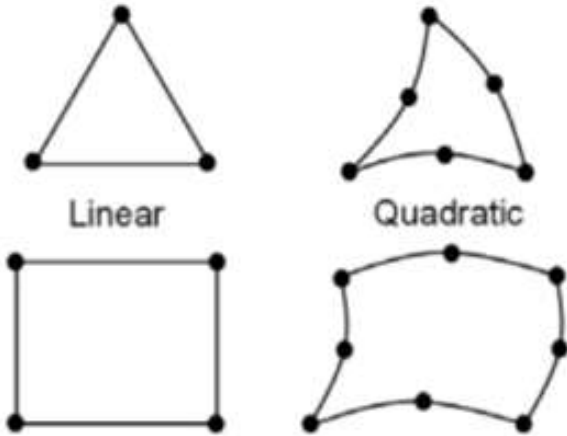


Figure 2-13 2D finite elements [126]

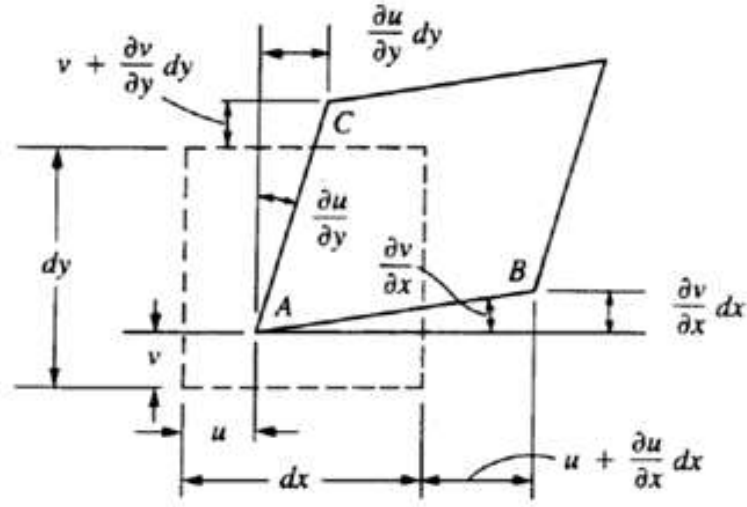


Figure 2-14 2D state of strain [127]

In 2D assumption the deformation takes place only in x-y plane .Theoretically the plain strain modeling strategy is defined by the following formulations [127].

$$\varepsilon_x = \frac{\partial u}{\partial x} \quad ; \quad \varepsilon_y = \frac{\partial v}{\partial y} \quad ; \quad \gamma_{xy} = \frac{\partial u}{\partial y} + \frac{\partial v}{\partial x} \quad (2-42)$$

$$\varepsilon_z = \frac{\partial w}{\partial z} = 0 \quad ; \quad \gamma_{xz} = \frac{\partial w}{\partial x} + \frac{\partial u}{\partial z} = 0 \quad ; \quad \gamma_{yz} = \frac{\partial w}{\partial y} + \frac{\partial v}{\partial z} \quad (2-43)$$

From equations, one can see that ε_x is a function of x, ε_y is a function of y and γ_{xy} is a function of both x and y and the stress relations are given as [127];

$$\begin{aligned} \sigma_x &= \frac{E}{1+\nu} \left[\varepsilon_x + \frac{\nu}{1-2\nu} (\varepsilon_x + \varepsilon_y) \right] \\ \sigma_y &= \frac{E}{1+\nu} \left[\varepsilon_y + \frac{\nu}{1-2\nu} (\varepsilon_x + \varepsilon_y) \right] \\ \tau_{xy} &= \frac{E}{2(1+\nu)} \gamma_{xy} = G \gamma_{xy} \end{aligned} \quad (2-44)$$

and

$$\sigma_z = \nu(\sigma_x + \sigma_y)$$

For plain strain condition the thickness direction is taken as unity under the condition that either load, if exist, acts perpendicular to the plane of model and it is equally distributed along each cross section which is same in z direction. Moreover under the load or deformation, the displacement in z direction, $w \approx 0$ and the Poisson's effect is so small that $\sigma_z \approx 0$ based on the linear small deformation theory. For the case of analysis of constrained layer damping in 2D, the plain strain modeling assumption is therefore applicable for simple cantilever beam since we are interested only in flexural small deformations, which create shear deformation within the viscoelastic layer, omitting out of plane or torsional modes during its dynamic or static motion. The associated error analysis for the plain strain assumption compared to 3D as well as analytical solution is given in Chapter 3.

The stresses are also given in matrix form as;

$$\begin{Bmatrix} \sigma_x \\ \sigma_y \\ \tau_{xy} \end{Bmatrix} = [D] \begin{Bmatrix} \varepsilon_x \\ \varepsilon_y \\ \gamma_{xy} \end{Bmatrix} \quad (2-45)$$

Where for plain strain condition, elastic property matrix, D is;

$$[D] = \frac{E}{(1+\nu)(1-2\nu)} \begin{bmatrix} 1-\nu & \nu & 0 \\ \nu & 1-\nu & 0 \\ 0 & 0 & 0.5-\nu \end{bmatrix} \quad (2-46)$$

E is elastic modulus of isotropic material and ν is Poisson's ratio. Then the strain energy of an element can be found using the stress-strain law as follows;

$$U = \frac{1}{2} \int_V \underline{\sigma}^T \underline{\varepsilon} dV = \frac{1}{2} \int_V \underline{\varepsilon}^T \underline{D} \underline{\varepsilon} dV \quad (2-47)$$

In 2D plain strain case [127];

$$\begin{aligned}
 U &= \frac{1}{2} \int_V \underline{\sigma}^T \underline{\varepsilon} dV \\
 &= \frac{1}{2} \int_V \begin{Bmatrix} \sigma_x \\ \sigma_y \\ \tau_{xy} \end{Bmatrix}^T \begin{Bmatrix} \varepsilon_x \\ \varepsilon_y \\ \gamma_{xy} \end{Bmatrix} dV \\
 &= \frac{1}{2} \int_V (\sigma_x \varepsilon_x + \sigma_y \varepsilon_y + \tau_{xy} \gamma_{xy}) dV
 \end{aligned} \tag{2-48}$$

In order to compute the strain energy of elements we need to know the displacement at each nodal point. The finite element method is used to compute those nodal displacements under loading at each element by solving a set of linear functions arranged in the form of equation of (2-49). The forcing column vector, $\underline{\mathbf{F}}$ is related with displacement vector, $\underline{\mathbf{u}}$ through the global stiffness matrix, $\underline{\mathbf{K}}$ which is built by assembling all individual element's stiffness matrix, \mathbf{k} . The finite element formulation to calculate unknown displacements through calculating element stiffness matrix is given as follows [128];

$$\underline{\mathbf{F}} = \underline{\mathbf{K}} \underline{\mathbf{u}} \tag{2-49}$$

where \mathbf{F} is forcing either in the form of nodal load vector (f_N) or surface traction (S_t) as depicted in (Figure 2-15), \mathbf{k} is stiffness matrix and $\underline{\mathbf{u}}$ is nodal unknown displacement vector.

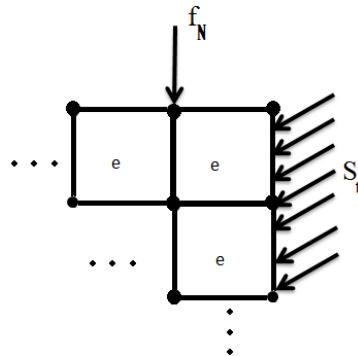


Figure 2-15 2D plane elements under load [128]

Strain –Displacement Relation:

$$\underline{\varepsilon} = \underline{\partial u} \quad (2-50)$$

Stress-Strain Law:

$$\underline{\sigma} = \underline{D\varepsilon} = \underline{D\partial u} \quad (2-51)$$

The displacement terms from (Figure 2-14) are approximated within the 2D finite elements using the shape functions N_i as [128];

$$\begin{aligned} u(x,y) &\approx N_1(x,y)u_1 + N_2(x,y)u_2 + N_3(x,y)u_3 + N_4(x,y)u_4 \\ v(x,y) &\approx N_1(x,y)v_1 + N_2(x,y)v_2 + N_3(x,y)v_3 + N_4(x,y)v_4 \end{aligned} \quad (2-52)$$

The same expression can be written in matrix form as [128];

$$\underline{u} = \begin{Bmatrix} u(x,y) \\ v(x,y) \end{Bmatrix} = \begin{bmatrix} N_1 & 0 & N_2 & 0 & N_3 & 0 & N_4 & 0 \\ 0 & N_1 & 0 & N_2 & 0 & N_3 & 0 & N_4 \end{bmatrix} \begin{Bmatrix} u_1 \\ v_1 \\ u_2 \\ v_2 \\ u_3 \\ v_3 \\ u_4 \\ v_4 \end{Bmatrix} \quad (2-53)$$

And in more compact form as;

$$\underline{u} = \underline{N d} \quad (2-54)$$

Then the approximated strain distribution in terms of displacement is [128];

$$\begin{aligned}
 \varepsilon_x &= \frac{\partial u(x, y)}{\partial x} \approx \frac{\partial N_1(x, y)}{\partial x} u_1 + \frac{\partial N_2(x, y)}{\partial x} u_2 + \frac{\partial N_3(x, y)}{\partial x} u_3 + \frac{\partial N_4(x, y)}{\partial x} u_4 \\
 \varepsilon_y &= \frac{\partial v(x, y)}{\partial y} \approx \frac{\partial N_1(x, y)}{\partial y} v_1 + \frac{\partial N_2(x, y)}{\partial y} v_2 + \frac{\partial N_3(x, y)}{\partial y} v_3 + \frac{\partial N_4(x, y)}{\partial y} v_4 \\
 \gamma_{xy} &= \frac{\partial u(x, y)}{\partial y} + \frac{\partial v(x, y)}{\partial x} \approx \frac{\partial N_1(x, y)}{\partial y} u_1 + \frac{\partial N_1(x, y)}{\partial x} v_1 + \dots
 \end{aligned} \quad (2-55)$$

The same expression can be written in matrix form as [128];

$$\underline{\varepsilon} = \begin{Bmatrix} \varepsilon_x \\ \varepsilon_y \\ \gamma_{xy} \end{Bmatrix} = \underbrace{\begin{bmatrix} \frac{\partial N_1(x, y)}{\partial x} & 0 & \frac{\partial N_2(x, y)}{\partial x} & 0 & \frac{\partial N_3(x, y)}{\partial x} & 0 & \frac{\partial N_4(x, y)}{\partial x} & 0 \\ 0 & \frac{\partial N_1(x, y)}{\partial y} & 0 & \frac{\partial N_2(x, y)}{\partial y} & 0 & \frac{\partial N_3(x, y)}{\partial y} & 0 & \frac{\partial N_4(x, y)}{\partial y} \\ \frac{\partial N_1(x, y)}{\partial y} & \frac{\partial N_1(x, y)}{\partial x} & \frac{\partial N_2(x, y)}{\partial y} & \frac{\partial N_2(x, y)}{\partial x} & \frac{\partial N_3(x, y)}{\partial y} & \frac{\partial N_3(x, y)}{\partial x} & \frac{\partial N_4(x, y)}{\partial y} & \frac{\partial N_4(x, y)}{\partial x} \end{bmatrix}}_{\mathbf{B}} \begin{Bmatrix} u_1 \\ v_1 \\ u_2 \\ v_2 \\ u_3 \\ v_3 \\ u_4 \\ v_4 \end{Bmatrix} \quad (2-56)$$

In short form as;

$$\underline{\varepsilon} = \underline{\mathbf{B}} \underline{\mathbf{d}} \quad (2-57)$$

Now we have three approximations from which the element stiffness matrix can be derived for single 2D plane strain element as follows [128];

$$\underline{\mathbf{k}} = \int_{V^e} \underline{\mathbf{B}}^T \underline{\mathbf{D}} \underline{\mathbf{B}} dV \quad (2-58)$$

Once the element stiffness matrix is found, the global stiffness matrix can easily built and used in finding unknown displacement using equation (2-49).

In dynamic case the governing equations are given, for 2D plane case, as follows [110].

$$\begin{aligned}\frac{\partial \sigma_{xx}}{\partial x} + \frac{\partial \tau_{xy}}{\partial y} &= \rho \frac{\partial^2 u}{\partial t^2} \\ \frac{\partial \tau_{xy}}{\partial x} + \frac{\partial \sigma_{yy}}{\partial y} &= \rho \frac{\partial^2 v}{\partial t^2}\end{aligned}\quad (2-59)$$

Where u and v are the displacements in the x and y-direction, respectively, as shown in Figure 2-14.

Assuming that every layer is isotropic, so the stress-strain relation can be written as [110];

$$\begin{bmatrix} \sigma_{xx} \\ \sigma_{yy} \\ \tau_{xy} \end{bmatrix} = \begin{bmatrix} C_{11} & C_{12} & 0 \\ C_{12} & C_{22} & 0 \\ 0 & 0 & C_{66} \end{bmatrix} \begin{bmatrix} \varepsilon_{xx} \\ \varepsilon_{yy} \\ \gamma_{xy} \end{bmatrix}\quad (2-60)$$

The above square matrix is complex due to complex shear and elastic modulus of viscoelastic layer. Using the strain displacement relations given in (2-42) and (2-43) together with equation (2-59), the equation (2-60) takes the following form [110];

$$\begin{aligned}\frac{\partial}{\partial x} (C_{11} \frac{\partial u}{\partial x} + C_{12} \frac{\partial v}{\partial y}) + \frac{\partial}{\partial y} (C_{66} \frac{\partial u}{\partial y} + C_{66} \frac{\partial v}{\partial x}) &= \rho \frac{\partial^2 u}{\partial t^2} \\ \frac{\partial}{\partial x} (C_{66} \frac{\partial u}{\partial y} + C_{66} \frac{\partial v}{\partial x}) + \frac{\partial}{\partial y} (C_{12} \frac{\partial u}{\partial x} + C_{22} \frac{\partial v}{\partial y}) &= \rho \frac{\partial^2 v}{\partial t^2}\end{aligned}\quad (2-61)$$

The equation of motion that is derived using the solution given in [129] more explicitly in familiar matrix form and it is given as [110];

$$\begin{bmatrix} \mathbf{M} & 0 \\ 0 & \mathbf{M} \end{bmatrix} \begin{Bmatrix} \ddot{\mathbf{u}} \\ \ddot{\mathbf{v}} \end{Bmatrix} + \begin{bmatrix} \mathbf{K}^{11} & \mathbf{K}^{12} \\ \mathbf{K}^{21} & \mathbf{K}^{22} \end{bmatrix} \begin{Bmatrix} \mathbf{u} \\ \mathbf{v} \end{Bmatrix} = 0\quad (2-62)$$

$$\mathbf{M}\ddot{\mathbf{x}} + \mathbf{K}^*\mathbf{x} = \mathbf{0}$$

The displacement terms are approximated using interpolation functions $\varphi_i^e(x, y)$ element by element using finite element method yields [110];

$$u \approx \sum_{i=1}^n b_i^e \varphi_i^e(x, y)$$

$$y \approx \sum_{i=1}^n a_i^e \varphi_i^e(x, y)$$
(2-63)

The $[\mathbf{M}]$ is the mass matrix which represents mass of each element while the $[\mathbf{K}^i]$ represents the stiffness matrix and it is also complex. Both terms are calculated by integration over the domain of finite element as given below [110].

$$M_{ij} = \int_{\Omega^e} \rho t \varphi_i \varphi_j dx dy$$

$$K^{11}_{ij} = \int_{\Omega^e} t (C_{11} \frac{\partial \varphi_i}{\partial x} \frac{\partial \varphi_j}{\partial x} + C_{66} \frac{\partial \varphi_i}{\partial y} \frac{\partial \varphi_j}{\partial y}) dx dy$$

(2-64)

$$K^{12}_{ij} = K^{21}_{ji} = \int_{\Omega^e} t (C_{12} \frac{\partial \varphi_i}{\partial x} \frac{\partial \varphi_j}{\partial y} + C_{66} \frac{\partial \varphi_i}{\partial y} \frac{\partial \varphi_j}{\partial x}) dx dy$$

$$K^{22}_{ij} = \int_{\Omega^e} t (C_{66} \frac{\partial \varphi_i}{\partial x} \frac{\partial \varphi_j}{\partial x} + C_{22} \frac{\partial \varphi_i}{\partial y} \frac{\partial \varphi_j}{\partial y}) dx dy$$

2.4.2.1 Modal Strain Energy Method

MSE method is energy formulation and one of the practical method proposed by Johnson and Kienholz [64] that utilize the undamped mode shapes of vibrating structure to extract the strain energy which is dissipated by the viscoelastic layer. The loss factors are calculated for each mode as the ratio of dissipated energy and total strain energies of all individual components. For this purpose the Finite Element Method greatly helps in determination of mode shapes and extraction of strain energies of all components that forms the damping treatment system, at each mode. Since this method uses the undamped real modes, it does not require the use of frequency dependent material properties, instead, use of constant average material properties are well enough for design and optimization purposes to get rough estimate of initial and optimum design parameters.

In this method classical modal analysis is performed using average constant material properties. The damping of the structure is approximated as the ratio of sum of product of loss factors for each of the layers over to total strain energies associated for each mode as follows [93].

$$\eta_k = \frac{\sum_{i=1}^n \eta_{i,k} U_{i,k}}{U_{total,k}}$$

$$U_{total,k} = \sum_{i=1}^n U_{i,k}$$

$$\eta_1 = \frac{(\eta_{1,1} U_{1,1}) + (\eta_{2,1} U_{2,1}) + (\eta_{3,1} U_{3,1})}{U_{1,1} + U_{2,1} + U_{3,1}} \quad (2-65)$$

$$\eta_2 = \frac{(\eta_{1,2} U_{1,2}) + (\eta_{2,2} U_{2,2}) + (\eta_{3,2} U_{3,2})}{U_{1,2} + U_{2,2} + U_{3,2}}$$

$$\eta_3 = \frac{(\eta_{1,3} U_{1,3}) + (\eta_{2,3} U_{2,3}) + (\eta_{3,3} U_{3,3})}{U_{1,3} + U_{2,3} + U_{3,3}}$$

$$\dots$$

Where $\eta_{i,k}$ is the material loss factor of the layer i at mode k , $U_{i,k}$ is the modal strain energy of the layer i at mode k . $U_{total,k}$ is the total modal strain energy at mode k .

An alternative and potentially more accurate method to calculate the modal loss factor is the Half-Power Bandwidth approach which requires the computation of frequency response functions [130]. Therefore direct frequency response analysis best choice for this purpose and one of the method utilized in this study.

2.4.2.2 Direct Frequency Response Method

In direct frequency response analysis, structural response is computed at discrete excitation frequencies by solving a set of coupled matrix equations using complex algebra under harmonic loading. The damped forced vibration equation of motion with harmonic excitation given in [131].

$$[\mathbf{M}]\{\ddot{x}\} + [\mathbf{B}]\{\dot{x}\} + [\mathbf{K}^*]\{x\} = \{\mathbf{P}(\omega)\}e^{j\omega t} \quad (2-66)$$

Where;

$[\mathbf{M}]$: Global Mass Matrix

$[\mathbf{B}]$: Global Damper Matrix

$[\mathbf{K}^*]$: Global Structural Stiffness Matrix with Complex Terms

$\{\mathbf{P}(\omega)\}$: Loading Vector

ω : Angular loading frequency

The response of the system under harmonic loading is assumed to be same as loading such that for linear system if the forcing function is harmonic, the response is also harmonic as stated below [131];

$$\{x\} = \{X(\omega)\}e^{j\omega t} \quad (2-67)$$

where $\{X(\omega)\}$ is complex displacement vector. Taking the first and second derivatives of above equation

$$\begin{aligned} \{\dot{x}\} &= j\omega \{X(\omega)\}e^{j\omega t} \\ \{\ddot{x}\} &= -\omega^2 \{X(\omega)\}e^{j\omega t} \end{aligned} \quad (2-68)$$

Substitution of above terms into equation of motion the following is obtained [131].;

$$-\omega^2 [\mathbf{M}]\{X(\omega)\}e^{j\omega t} + j\omega [\mathbf{B}]\{\dot{x}\}e^{j\omega t} + [\mathbf{K}]\{X(\omega)\}e^{j\omega t} = \{\mathbf{P}(\omega)\}e^{j\omega t} \quad (2-69)$$

This simplifies as below [131];

$$([\mathbf{K}^* - \omega^2 \mathbf{M}] + j\omega \mathbf{B})\{X(\omega)\} = \{P(\omega)\} \quad (2-70)$$

This expression represents a general system of equations with complex coefficients if damping is included which is the energy dissipation characteristics of the system. The ratio of output displacement to the input force is termed as Receptance and it represents the transfer function of the system. In matrix form it can be stated as follows [114];

$$[\alpha] = [[\mathbf{K}^* - \omega^2 \mathbf{M}] + j\omega \mathbf{B}]^{-1} \quad (2-71)$$

The damping in direct frequency response analysis is incorporated in several ways, the damping matrix $[B]$ represents viscous damping generated by damper elements and is composed of two forms as [131].

$$B = [B^1] + [B^2] \quad (2-72)$$

$[B^1]$ represents the viscous terms added via CVISC and CDAMPi Bulk Data cards used in Optistruct[®] solver, that is, via damping element properties. $[B^2]$ is another input matrix via DMIG Bulk Data card if the model contains discrete damper elements. Another method is to use uniform Global Structural Damping Coefficient, G through PARAM, G Bulk data card. On the other hand the frequency dependent viscoelastic material stiffness and damping properties can also be embedded into the solution of equation of motion through MATF1 card in which the TABLEDi tabular entries for each of stiffness and damping properties form the complex stiffness matrix as follows [131];

$$K^* = [K^1] (1 + jG) + [K^2] + j[K^4] \quad (2-73)$$

$[K^1]$ is the stiffness matrix for elastic structural elements. If there were no viscoelastic components and all components had same damping properties it would be quite appropriate to use only uniform structural damping parameter, G, however inclusion of viscoelastic layer, whose material properties are frequency dependent, makes the analysis complicated. $[K^2]$ is stiffness terms added via direct matrix input via DMIG card. The last term $[K^4]$ created via multiplication of individual element stiffness matrices with input GE, that is, viscoelastic element damping [131].

In this study both elastic, $[K^1]$, viscoelastic components, $[K^4]$, are used utilizing the advantage of inserting the viscoelastic frequency dependent material properties as tabular functions of $TR(f)$ and $TI(f)$ such that [131];

$$\mathbf{K}^* = [\mathbf{K}^1](1 + j\mathbf{G}) + \{\mathbf{TR}(f) + j\mathbf{TI}(f)\} [\mathbf{K}^4] \quad (2-74)$$

where $TR(f)$ and $TI(f)$ is real and imaginary part of complex modulus, that is G' and G'' , respectively. Since the elastic components such as structural Aluminum have quite low damping capacity [115] the G terms are taken as almost zero. In Hypermesh environment the viscoelastic material properties can be incorporated through use of TABLEDi entries together with MATF1 Isotropic Frequency Dependent Material card [132].

Upon completion of direct frequency response analysis the frequency response function, i.e. receptance, can be generated as outputs from which the damping factors can be extracted via using Half Power Bandwidth Method. This method is one of the well known and accepted one in extracting the loss factors from measured or calculated FRF curves obtained either from experimental or numerical studies respectively especially at or close to resonance peaks [133]. The following section gives the methodology in finding loss factor near resonance region.

2.4.2.2.1 Half Power Bandwidth Method

From previous theoretical study of single degree of freedom system we conclude that the peak locations in frequency response functions are damped controlled regions and therefore the damping parameters can easily be extracted by simply using half power bandwidth method which requires the detection of value of each peaks as well as the corresponding natural frequencies together with half power bandwidth points on frequency axis as depicted in (Figure 2-16) [120]

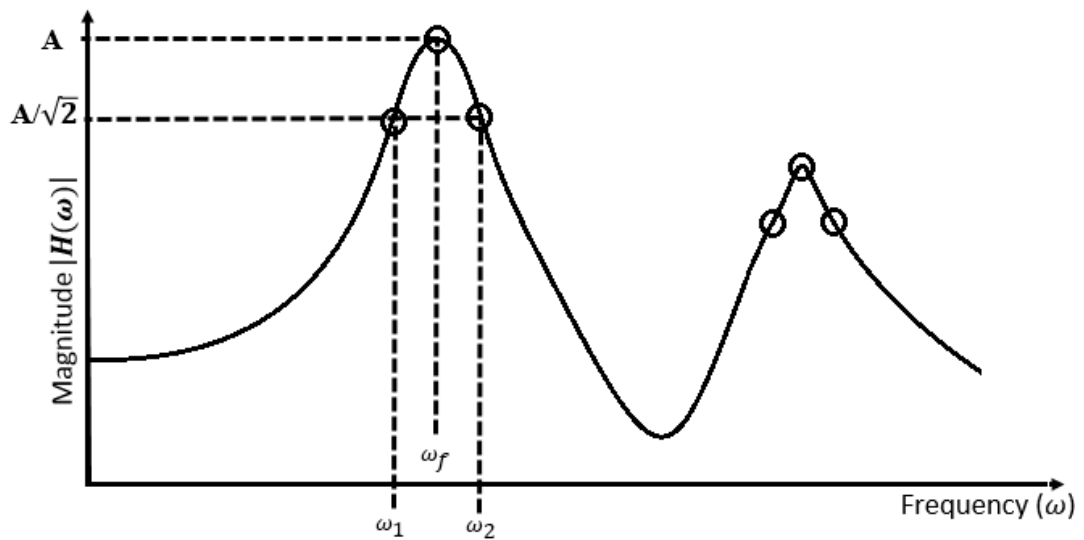


Figure 2-16 Extraction of damping factor from resonance peak (*Adapted from*[120])

According to the methodology, the half power bandwidth points are found by simply dividing peak value of response to $1/\sqrt{2}$ and find the intersection points at resulting amplitude level on curve which gives the lower and upper bound of frequency band on frequency axis. Upon detection of all numerical values, the loss factor is related with those parameters as follows;

$$\eta = \frac{\omega_2 - \omega_1}{\omega_r} = 2\zeta \quad (2-75)$$

For this purpose a special MATLAB code has been written to accomplish this task such that the code finds the peaks of FRF plots and detects half-power bandwidth points from which it calculates the loss factors. The flowchart for this task is shown in (Figure 2-17). The frequency response functions were exported out of Hypergraph[®] into MATLAB environment at which the specially coded routine, for detection of resonance frequencies as well as calculation of damping factors, has been utilized.

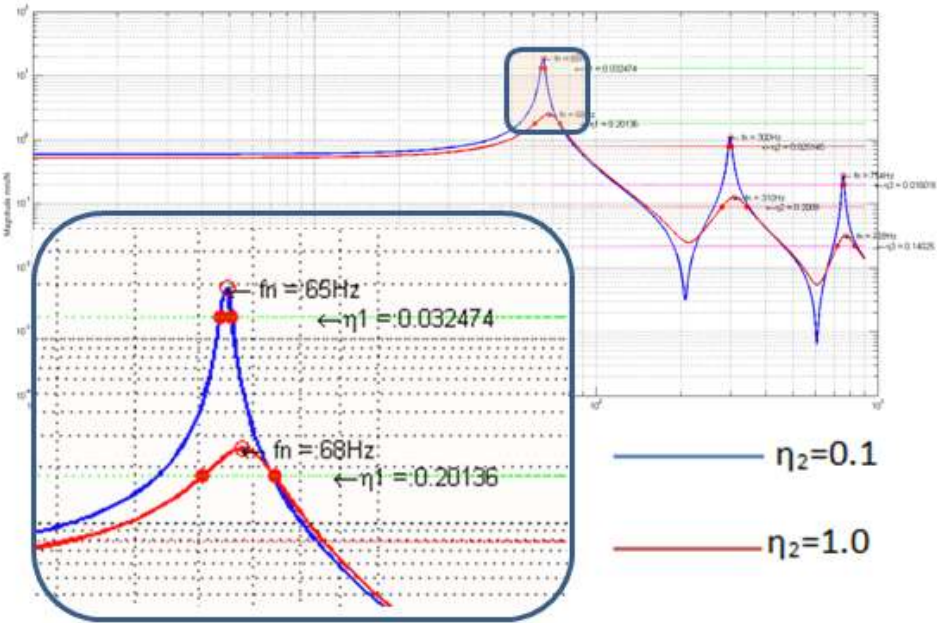
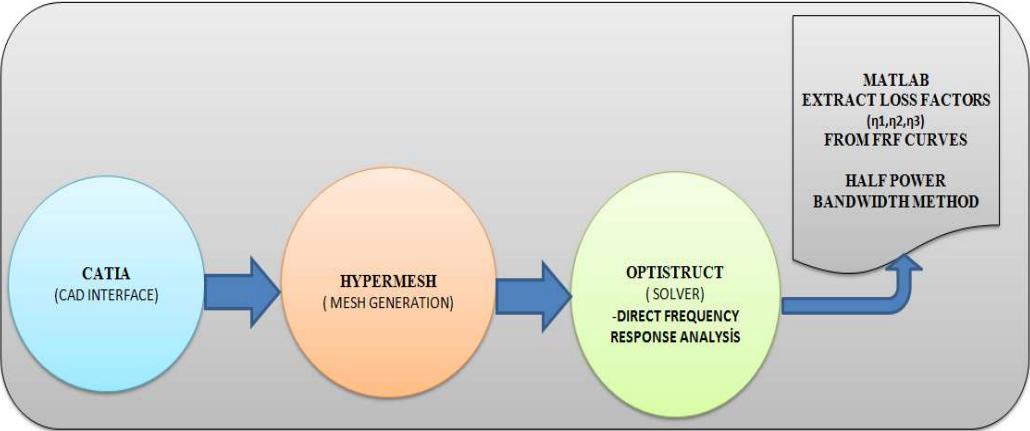


Figure 2-17 Extraction of loss factor from direct frequency response functions

In this study the research activity is composed of three parts and they are given in subsequent chapters. In the first part, one of the numerical method namely topology optimization technique has been utilized in order to find best material distribution of stand-off layer with minimal weight using different modelling technique and objective function as well as constraints. Then the overall damping performance of the resulting topologies has been investigated and compared to each other in terms of total weight and damping loss factors extracted from frequency response functions using Half Power Bandwidth method upon performing direct frequency response analysis which computes the harmonic forced response of each candidate design. In the second part, another numerical method which is parametric design strategy together with known optimization algorithms have been used to find best optimum geometrical and material parameters that maximize the loss factor for the first three modes since the first modes dominate the overall structural dynamic response. The Modal Strain Energy (MSE) has been used in conjunction with Finite Element Method to calculate the loss factors. Moreover to see the effects of extracted geometries from numerical studies in higher modes, the frequency of interest has been selected such a way that it covers the first 10 modes of the vibrating structure. Throughout the numerical studies cantilever boundary condition has been used for layered beam structure since it is easy to model, simulate and also create in experimental study conducted at the third and last part of the research in order to validate the design procedure that has been followed. Also, the objective of experiment has been primarily to qualify the design, manufactured based on numerical results that were achieved in the second part of the study.

CHAPTER 3

DESIGN AND ANALYSIS OF VIBRATING BEAM FOR OPTIMUM DYNAMIC BEHAVIOUR

3.1 Introduction

Inclusion of spacer layer in purpose of vibration attenuation through strain energy maximization leads to the increase of weight of total structure which is a disadvantage for the weight critical applications such as automotive and aerospace applications. Therefore there is always compromise between weight and damping performance of the weight critical vibrating structures. This is in turn results to seek feasible design alternatives for the damping treatment with stand-off layer. However the design of damping layer treatment an iterative process to find best geometrical configuration with minimum weight together with maximum damping performance among several parameters such as thickness, material properties, layout of damping layer etc. Fortunately there are mathematical design strategies that manage such numerous design parameters efficiently and they can be followed to investigate the effectiveness in optimization of spacer layer for maximum damping and minimum weight constraints.

In recent years with advance of computer technology it is quite possible to use mathematical optimization algorithms effectively to seek best options among those parameters within minutes. Moreover the numerical simulation techniques such as Finite Element Method (FEM) enables the designers to model the real physical problem in computer environment by utilizing commercial software tools virtually under a set of boundary and loading conditions. In this method the design domain virtually created through CAD software and divided into mathematically formulated

number of smaller domains which are called “finite elements” connected by “nodes” which forms grid like 2D for plane or shell type structures or 3D for volumetric mathematical model which is later solved by numerical approaches. The result of finite element analysis solutions are extracted at nodes and can be of any type like displacement, velocity and acceleration for dynamic problems while can be of temperature for thermal analysis. The accuracy of latter method in prediction of real physical behavior directly related to the modeling assumptions and boundary and loading conditions [129].

Improving design that satisfies certain functional requirements necessitates determination and evaluation of many possible designs; this also requires time consuming, exhausting trial-and-error stages among several design possibilities. Incorporation of optimization algorithms with computers enables the automated search for finding the best design parameters based on the requirements imposed into the solution.

Specifically the optimization methods utilize the numerical search techniques which are performed within a range of certain design parameter values starting from an initial design that is being improved through the selection of design candidates created out of bounded design space. The search continuous until all constraints and given objection is satisfied. Combining FEM with optimization methods greatly improves the practical application of such kind of search algorithms within selected design domains and enables the flexibility of evaluation of several design possibilities in a short time. The design is continuously altered based on constraints and assigned design parameters seeking the best target solution that satisfies the objectives.

The simulation models are built by linking finite element model and optimization algorithms. The finite element model functionally represents the parameterized numerical model of physical problem containing geometric, material and boundary condition information. The design engineer is capable of defining several design

parameters, constraints, responses and target objective out of this model that affects the response of structure in hand (Figure 3-1) [134].

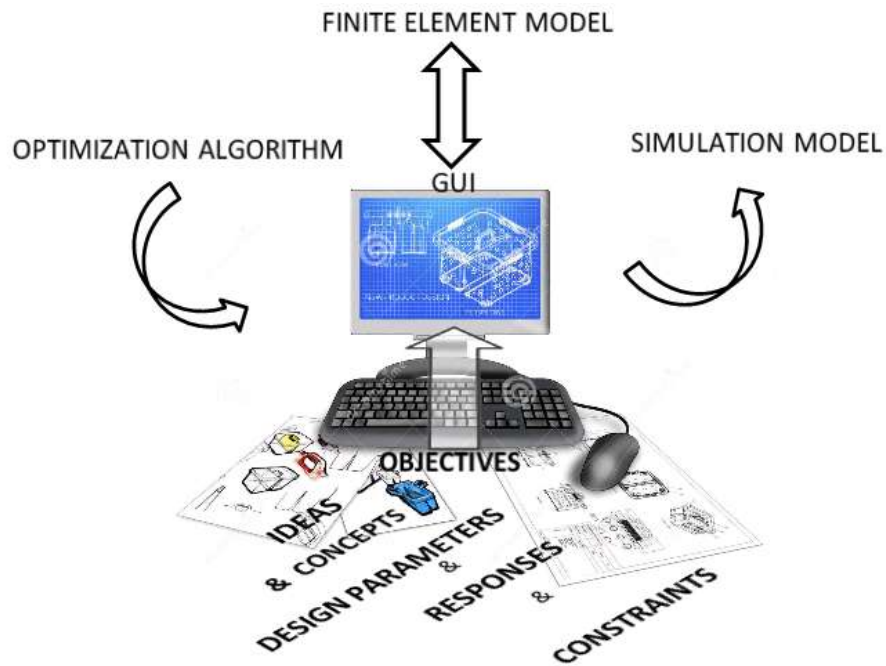


Figure 3-1 Optimizaton cycle (*Adapted from:* [135])

3.2 Structural Optimization

In computational mechanics structural optimization aims to increase the structural performance of mechanical systems and their sub components in a systematic way following an effective and reliable path. Especially the weight concerns, performance and reliability requirements as well as competition in automotive and aerospace industry urgently needs such type of optimization methodology in order to manufacture weight efficient and functionally increased performance of products.

Structural optimization starts with conceptual design and modeling phase at which the boundary of the system is defined. At this stage creativity, material selection, size and location of structural members play an important role in final response of the structure. In analysis and evaluation stage the numerical finite element model is developed in order to calculate the response of components simulating the operational conditions. This process usually followed by automated modifications to tune the response such as displacement, stress etc. The aim is to keep the response of the structure at a certain acceptable levels, minimize or maximize with certain constraints [136]. At another stage the process continues with formulation of the problem.

A general structural optimization problem utilizes mathematical algorithms to solve the following form of standard formulation [134]:

$$\text{S.O.} \left\{ \begin{array}{l} \text{minimize or maximize } f(x, y) \text{ with respect to } x \text{ and } y \\ \text{subject to} \left\{ \begin{array}{l} \text{behavioral constraints on } y \\ \text{design constraints on } x \\ \text{equilibrium constraints} \end{array} \right. \end{array} \right. \quad (3-1)$$

In a more general form;

$$\begin{aligned} & \text{maximize or minimize } f(\mathbf{x}) \\ & \text{such that} \quad g_j(\mathbf{x}) \geq 0, j = 1, \dots, n \\ & \quad \quad \quad h_k(\mathbf{x}) = 0, j = 1, \dots, n \\ & \quad \quad \quad x_i^L \leq x_i \leq x_i^U \\ & \mathbf{x} = (x_1, x_2, x_3, x_4, \dots, x_n) \end{aligned} \quad (3-2)$$

Where \mathbf{x} represents a vector of design variables with components $x_i, i = 1, 2, \dots, n$, the $g_j(\mathbf{x})$ and $h_k(\mathbf{x})$ are the constraints and can be equality or inequality form. x_i^L and x_i^U are the lower and upper bounds of design variables x_i .

Objective of structural optimization problem most generally are minimizing over all mass or volume of the components, production cost as well as stress distribution, also maximizing stiffness etc. In general terms the aim is to find optimum geometrical configuration ensuring manufacturability of structure for the specific problem [136].

3.2.1 Design Variables:

The improving of structural performance under given constraints necessitates the change of structure to seek best solution for the specific task. For the structural design process such changes are accomplished by selecting and assigning the building block of main design parameters as design variable within optimization algorithm. Design variables can be of geometric sizes of a structural member such as its length, height, width, thickness, area and even a nodal coordinate of finite element mesh or material properties like modulus, density etc.

Also they can take continuous or discrete forms. Continuous variables can be varied between prescribed lower and upper bound and can be of any numerical value within that bounds while discrete forms i.e. material modulus values, can take only specific values as per predefined material choices because of existing material source. In practice because of its easiness compared to discrete form solution, the continuous design variables are preferred and can be tailored upon optimization calculation to a nearest best practical discrete value. Mostly the parameters that affect the response much are the key design variables that derive the design process.

3.2.2 Constraints:

Design process generally contains some limitations such as limited material volume for minimum weight concern and mostly the design variables are subjected to those constraints. Minimum or zero displacement constraints due to limited sway space in dynamic problem. The selection of minimum standard structural beam cross section under static loading condition requires also the variation of height, width, thickness within certain range. For the same problem, the maximum allowable stress value over the cross section can also be chosen as constraint in order to guarantee the final stress level below that threshold value. Therefore constraints should impose physically possible design space otherwise the area of cross section would be chosen as minimum as possible which may not be practically manufacture or would possess high local stress value over the impractical final section. Quantities that are usually used as constraints are stress, strain, displacement, frequency, acceleration, volume etc. Those are can also be defined as objective function such as minimum displacement, minimum frequency objections.

3.2.3 Responses:

The responses are generally the output of simulation stage and are tracked throughout the calculations and checked whether they satisfy the objective function. From the structural point of view, response can be of structural displacement, stress, strain or reaction force, compliance etc..

3.2.4 Objective Function:

In general a mathematical formulation the represents the overall response of the structure under consideration and that can be minimized and maximized in order to improve the structural performance based on the values of design variables. The weight of a structural component, displacement or stress of a specific location within

design domain, modal frequencies basic responses in objection function that can be minimized or maximized [136]

Today, the decision on how a new design should look like is mostly based on a benchmark design or on previous designs. The decision-making is based on the experience of those involved in the design process. However, preliminary design tools such as topology optimization can be introduced to enhance the process. The concept can be based on results of a computational optimization rather than guessing by using topology

3.2.5 Topology Optimization

Topology optimization is one of the popular technique used in structural design process at the early phase of product development stage. The method generates the best material distribution under prescribed boundary and loading conditions as depicted in Figure 3-2. The term best can be in terms of weight or in terms of stiffness or some other criteria such as minimum vibration frequency for dynamic problems or maximum load carrying capacity for buckling criteria. Thus one can define number of measurable parameters as structural performance criteria while determining the final topology of design.

The finite element mesh of the evenly distributed uniform material within the design domain is used as link in creation of final distribution of design by considering the element density values as continuous design variable (Figure 3-2). The design domain divided into number of regions as design and non-design domain. Only the elements belongs to design domain or domains are considered as design variable. Other regions are kept as constant distribution. Upon completion of topology optimization the new path of material distribution is obtained while removing some portion of whole design based on the design objective. Therefore the methodology helps to figure out the layout of final design with best, in terms of functional requirements, such as maximum load carrying capacity or maximum lowest natural

frequency with minimum material distribution without performing time consuming trial-and-error procedures.

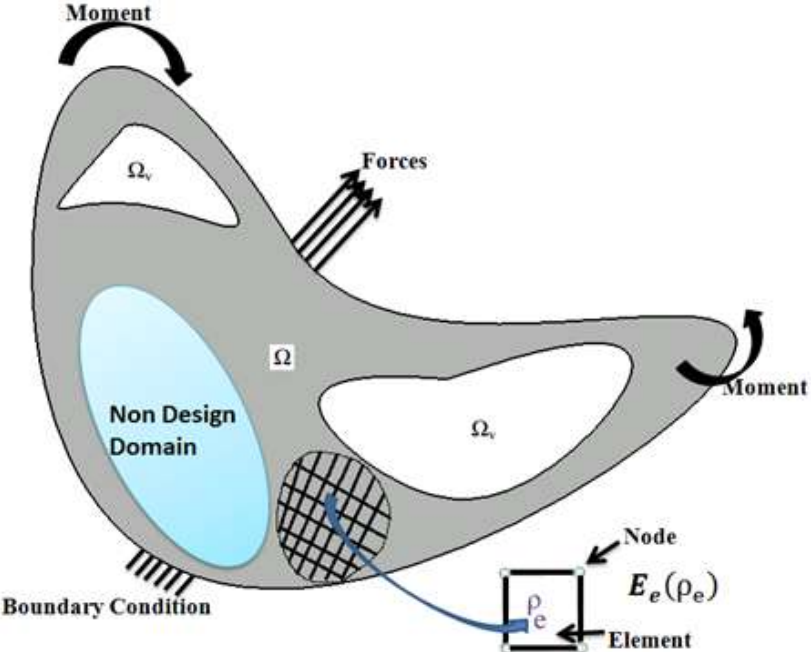


Figure 3-2 Simulation model for topology optimization (Adapted from: [136])

3.2.5.1 Density Method (SIMP)

As previously mentioned the aim is to distribute material as efficient as possible within selected design space. For this purpose several methodologies are developed. Among them the SIMP (Solid Isotropic Microstructures with Penalization) proposed by Bendsøe [137] is very popular method in which stiffness of material is directly proportional to the pseudo density of material. The density value is continuously varied as design variable between 0 and 1 representing the void and solid material respectively. For 2D models the density is also represented as the thickness of the shell elements [132]. In this method the objective is usually to minimize the

compliance of the structure considering load cases, material volume fraction constraints.

SIMP is a density-stiffness interpolation scheme of density method which forms the non-linear relation between modulus of elasticity and relative density of each individual finite element (Figure 3-2) by penalizing the intermediate density values of individual finite elements to force their density value to be either 1 or 0.

According to the SIMP model, the finite element elasticity matrix \mathbf{E}_e is expressed in terms of the element volumetric material density $\rho_e, 0 \leq \rho_e \leq 1$ in a power $p, p \geq 1$ as [134]

$$\mathbf{E}_e(\rho_e) = \rho_e^p \mathbf{E}_e^* \quad (3-3)$$

where \mathbf{E}_e^* is the elasticity matrix of a corresponding element with the fully solid elastic material the structure is to be made of. The power p in (3-3), which is termed the penalization power, is introduced with a view to yield distinctive “0-1” designs, and is normally assigned values increasing from 1 to 3 during the optimization process. Such values of p have the desired effect of penalizing intermediate densities $\rho_e, 0 \leq \rho_e \leq 1$ since the element material volume is proportional to ρ_e , while the interpolation (3-3) implies that the element stiffness is less than proportional

By analogy with (3-3), for a vibrating structure the finite element stiffness and mass matrix may be expressed as [138]

$$\begin{aligned} \mathbf{K}_e(\rho_e) &= \rho_e^p \mathbf{K}_e^* \\ \mathbf{M}_e(\rho_e) &= \rho_e^q \mathbf{M}_e^* \end{aligned} \quad (3-4)$$

where \mathbf{K}_e^* and \mathbf{M}_e^* represents the element stiffness and mass matrix corresponding to fully solid material, and the power $q_e \geq 1$.

The global stiffness matrix \mathbf{K} and mass matrix \mathbf{M} for the finite element based structural response analyses behind the optimization, can now be calculated by the following summations [138].

$$\begin{aligned}\mathbf{K} &= \sum_{e=1}^{Ne} \rho_e^p \mathbf{K}_e^* \\ \mathbf{M} &= \sum_{e=1}^{Ne} \rho_e^q \mathbf{M}_e^*\end{aligned}\tag{3-5}$$

Using SIMP method the typical topology optimization formulation can therefore be stated as follows [132];

$$\mathbf{find}: \mathbf{x} = \{\rho_1, \rho_2, \rho_3, \dots \dots \rho_{Ne}\}$$

$$\rho_i = \begin{cases} \rho_{\min} & \text{void} \\ 1 & \text{solid} \end{cases}$$

$$(i = 1, 2, 3, \dots, Ne)$$

(3-6)

while $\mathbf{Min\ or\ Max} : \mathbf{f}(\mathbf{x})$

Under $\mathbf{s.t.}: V = \sum_{i=1}^{Ne} V_i \leq V^*$

where V is the total volume of simulation model achieved by summing all individual element volumes V_i 's. V^* is the maximum allowable total limit of final design domain. The objective function $\mathbf{f}(\mathbf{x})$ can be regarded as total compliance or first natural frequency of vibrating beam. Ne is the total number of elements in design space.

In Figure 3-3 the distribution of material within prescribed design domain is illustrated as elastic modulus versus density values for the isotropic 2D rectangular domain. The black areas indicate the total initial uniform elastic domain where the density value is 1 which represents the existence of material. On the other hand as the density value approaches to the value of 0, which corresponds to the removal of elastic material, based on the volumetric constraints and objective function the material from the design domain is removed yielding a truss like structure as final design. Here the density of each elements, which are the building block of the structural domain, are considered as design variable and varied between 0 and 1. The aim of structural topology optimization is to find the best possible material distribution over the design domain that is necessary for the functional target performance value defined via objection function. From the Figure 3-3 one can also see the effect of penalty factor in variation of elastic modulus.

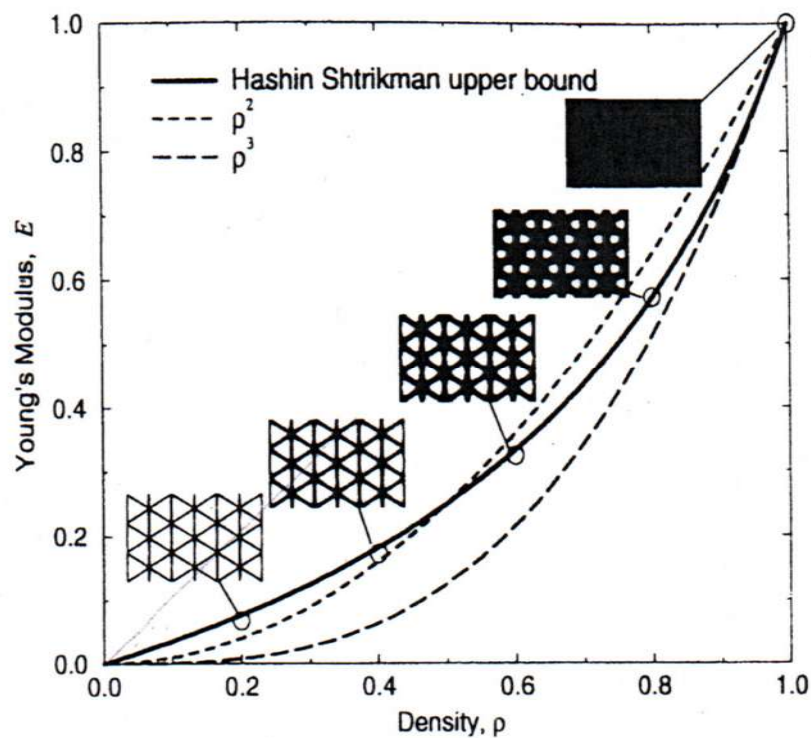


Figure 3-3 Material interpolation within design domain [137]

The result of topology optimization is a rough layout of final design with its inner and outer boundaries of optimum material distribution. Therefore it needs to be reinterpreted by the designer to approach final material distribution which is much more practical to produce. The process consists of several steps and will be explained in the following sections.

3.2.5.2 Methodology

In design, analysis and optimization procedures, defining rough estimate of design and formulation of physical problem is first essential two steps. For this purpose after having the CAD design, the finite element method, which divides the design domain into structural mesh, is used for the pre-processing part of the optimization procedure. The Hyperworks suit 13.0 from Altair Engineering gives an extensive opportunity for the engineers to model, analyze and optimize the structural components using Hypermesh as pre-processor, Optistruct as solver and Hyperview as post-processing platforms [132].

Mainly the optimization methodology requires four different phase of design steps to be performed step by step as shown in Figure 3-4. In *phase I* the geometry of problem is transformed into finite element mesh on which the boundary conditions and loads are applied from which the specific load cases are created. Then the material properties are assigned to each corresponding portion of design domains are also identified and base analysis step which will be used by the optimization algorithm is defined. For example if the frequency of the component is concerned, then the modal analysis step to extract those frequencies of interest should be defined. After performing base analysis, in *phase II* the total design domain divided into design and non-design spaces explicitly. At this phase the target finite elements are selected as design elements out of global structural mesh. Generally the boundary of the global mesh is considered as non-design space. The setup of optimization is also takes place at this phase; the responses, constraints and objective function are defined such that the design space elements are selected as design variable, and the

material property of each element within that space, namely the pseudo-density values, are calculated through SIMP method by Optistruct [132] based on constraints and objective.

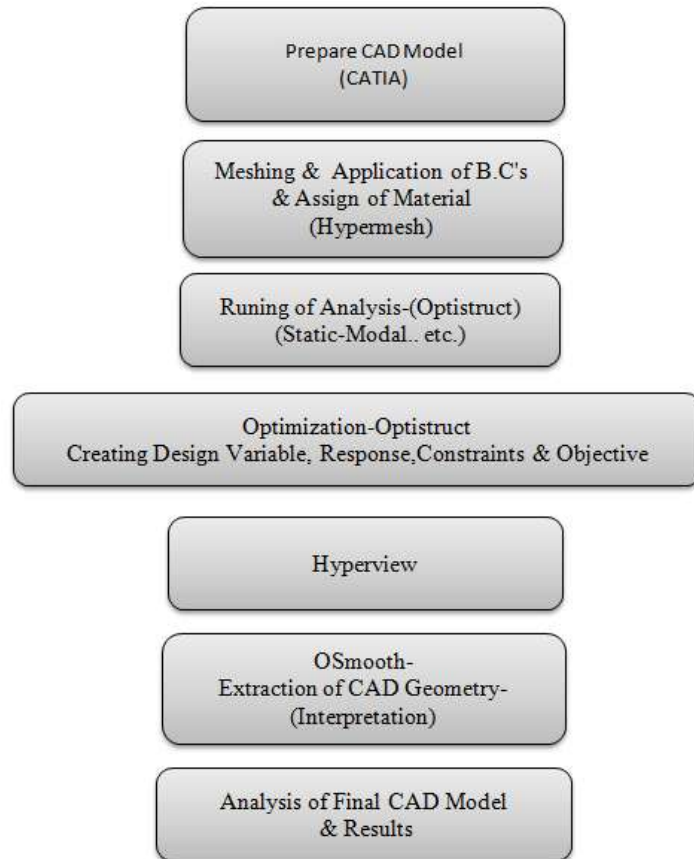


Figure 3-4 Topology Optimization Steps

Phase III includes visualization of calculated topology of design space. The density of each element is plotted giving rough estimate of final design as voids or solid material. Since the topology results are rough, generally the result of topology optimization results needs to be interpreted by the designer based on the experience. In *phase IV* some tuning process takes place such that the boundary of final design shape is obtained through some modifications and interpretations. OSsmooth function in Hypermesh interface enables an automatic 2D or 3D surface or solid

generation to be modified at this phase, from finite elements that represents the calculated topology of the structure.

An example of 2D topology optimization of cantilever beam type structure has been analyzed and shown in Figure 3-5 to summarize the above mentioned phases. The beam is modeled as 2D plane structure and imported into Hypermesh environment at which the total domain divided into finite element mesh (*phase I*) as well as two sub groups namely, design space and non-design space are defined respectively (*phase II*). In order to show effect of selection of different design space two different portion of beam selected as design space. As a load case static analysis step is defined under a tip load over the beam (*phase II*). The truss like material distribution is found through global compliance minimization setup under volume fraction constraint with which maximum allowable volume is defined (*phase III*). This step can be interpreted as weight minimization under load. After having rough topology OSsmooth functionality of Hypermesh is used to extract final geometry based on designer’s interpretation (*phase IV*).

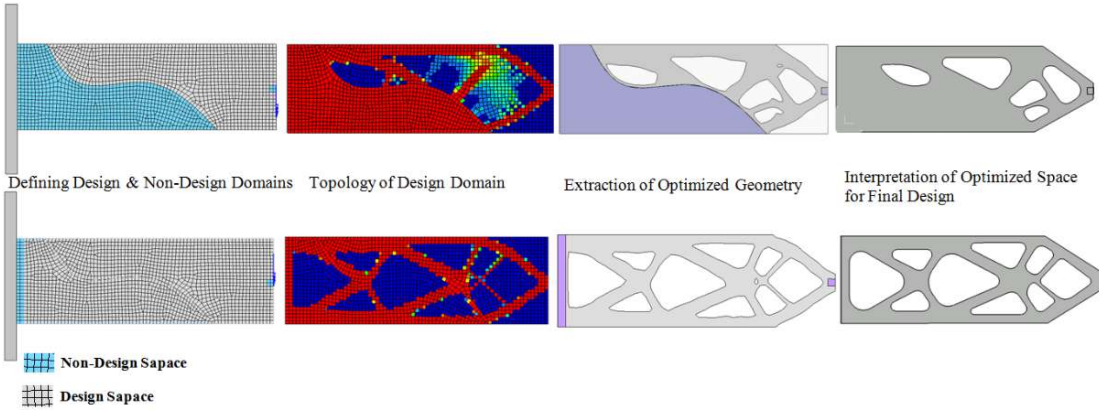


Figure 3-5 Topology Optimization Process

Since the topology optimization gives the effective load path together with optimum material distribution along this path, the compliance minimization strategy for 2D honeycomp cell filled with viscoelastic material is successfully applied by Boucher

et. al [86] in order to find the minimal material distribution of viscoelastic domain that is subjected to highest strain energy, along extracted topologies under static in plane loads that mimics the deformation pattern of unit cell under vibration. The solution gives the optimum viscoelastic material topology within unit honeycomp cell in order to increase vibration attenuation capacity of honeycomp panels.

Inclusion of spacer layer in purpose of vibration attenuation through strain energy maximization leads to the increase of weight of total structure which is a disadvantage for the weight critical applications such as automotive and aerospace applications. Therefore there is always compromise between weight and damping performance of the weight critical vibrating structures. This is in turn results to seek feasible design alternatives for the damping treatment with stand-off layer.

The next sections contain the detailed analysis steps for the optimization of stand-off layer carried out in this study. Two optimization strategies have been investigated by analyzing simple cantilever layered beam type structure since its modeling quite easy and its dynamic behavior can easily be analyzed. First, the topology optimization method has been utilized in order to find best material distribution under assumed sinusoidal distributed static loading that force the beam structure to deform in its assumed modes. The first mode shape is quite achievable via this methodology. Moreover the assumed unit cell geometry was also modeled with certain length and the extracted unit cell topology was used as building block of whole beam that is composed of repeated unit cells. The unit cell is a representative volume of material for the periodic construction of whole beam and the concept is used in this study based on the fact that the response of 2D periodic whole structure can be characterized by unit cell which is known as Bloch Theorem [139]. The material layout of unit cell found by topology optimization and upon creation of composite periodic structure effects the frequency response characteristics such a way that response can be reduced in specific frequency ranges [140]. This construction methodology has also special characteristic advantages especially at some frequency ranges of loading, when the corresponding wavelength of the vibration matches with

unit cell length. The associated transverse waves at the corresponding frequency ranges creates amplified local deformation zones, in other words, local resonance [141] at each unit cell such that the attached viscoelastic material can undergo large deformation, such that the energy dissipation due to high strain, expected to be also magnified at mid or high frequencies [142] at which the attenuation zones exists in the frequency response functions.

The topology optimization for the design volume was carried out using constant material properties for the viscoelastic layer and upon extracting the candidate topologies for the final design, the performance of extracted topologies in terms of damping and weight was later inquired by incorporating frequency dependent material properties for the viscoelastic layer through direct frequency response analysis using Optistruct[®] as solver and Hypermesh[®] as pre-processor from Altair Engineering Inc.

In the second method, the cantilever beam has been modeled parametrically using CATIAV5-R22[®] environment as design tool such that the thickness and material properties of stand-off layer were defined as design variables in HyperStudy[®] environment. Generation of layered cantilever beam and its finite element model as well as modal analysis steps were performed automatically through macros and utilizing capability of well recognized HyperStudy[®] software again from Altair Engineering Inc. Modal Strain Energy Method was used together with finite element method to calculate modal loss factors via extracting strain energy distribution of each individual layers such that the loss factors are linked numerically with the geometrical and material parameters of stand-off layer. This methodology enables the designer to link the final numerical values of loss factors for the first three modes with the geometrical and material parameters of design in hand. Performing DOE (Design of Experiment) studies and utilizing build-in optimization algorithms within HyperStudy[®] the best geometrical parameters for maximum damping for the cantilever beam were found.

3.2.5.3 Finite Element Modeling

The finite element method was used as the base of two optimization methodologies that has been followed throughout the thesis study. The modeling strategy is common for both of the optimization studies. Therefore it will be explained in this section before giving details and results of two methods.

The 2D finite element modeling strategy has been followed in order to create analysis models. This assumption is efficient in terms of modeling and analysis cost since the number of elements are drastically reduced. Specifically the plain strain condition is simulated assuming the section of beam represents the dynamic behavior of cantilever beam (Figure 3-6). For topology optimization method 2D assumption is applicable for finding distribution of material within stand-off layer using PSHELL element cards [132].

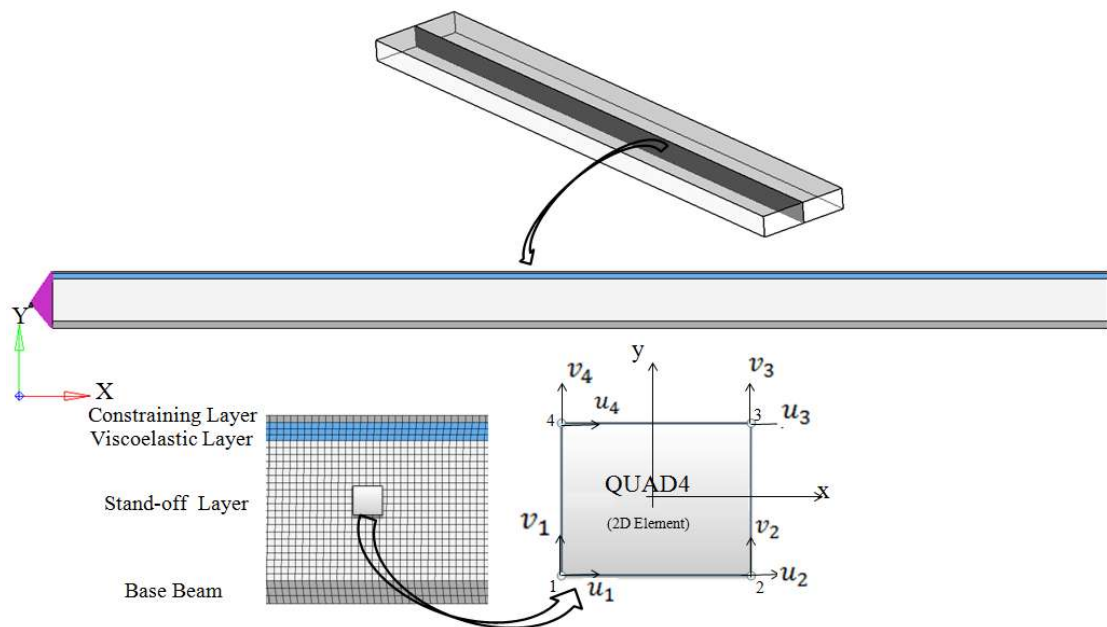


Figure 3-6 2D Finite element modeling

Numerical 2D and 3D as well as analytical (RKU) solutions for the modal analysis of cantilever three layer beam were performed for the first 10 modes. In 2D modeling Quad4 elements are used under the plain strain condition while in 3D case the elements were selected to be 3D HEX8. Moreover RKU equations are used for the same geometrical and constant material parameters for all three layers and modeling approach (Table 3-1). Analytical solution was performed in MATLAB® by calculating equal flexural rigidity of layered beam via using RKU equations for fixed-free boundary condition. The resulting stiffness value was used in frequency equation given in Chapter 2 to calculate approximate value of natural frequencies of layered beam together with the corresponding mode shapes for the first ten modes (Figure 3-9). The results for mode shapes and corresponding natural frequencies are compared to each other (Table 3-2).

Table 3-1 Material and Geometrical Properties Three Layer Treated Beam

Properties	Base Beam Layer (Aluminum)	Damping Layer (Dyad-601)	Constraining Layer (Aluminum)
Length [mm]	250	250	250
Thickness [mm]	1.6	1.27	0.5
Material Young Modulus [MPa](Constant)	70000	50	70000
Poisson's Ratio (ν)	0.3	0.49	0.3
Density (kg/m ³)	2770	1040	2770

It was seen from the modal analysis that 2D modeling approach captures the flexural mode shapes quite well while the order of each mode may have difference compared to 3D modeling results. For example the 3rd mode shape in 2D model corresponds to the 4th mode shape extracted by 3D modeling. Also the 2D model only captures the flexural mode shapes except other modes, i.e. torsional, and this is acceptable for our design considerations since the viscoelastic damping dominantly amplified by shear

deformation due to the flexural motion of vibrating structure and the motivation was to reduce flexural response of the structure.

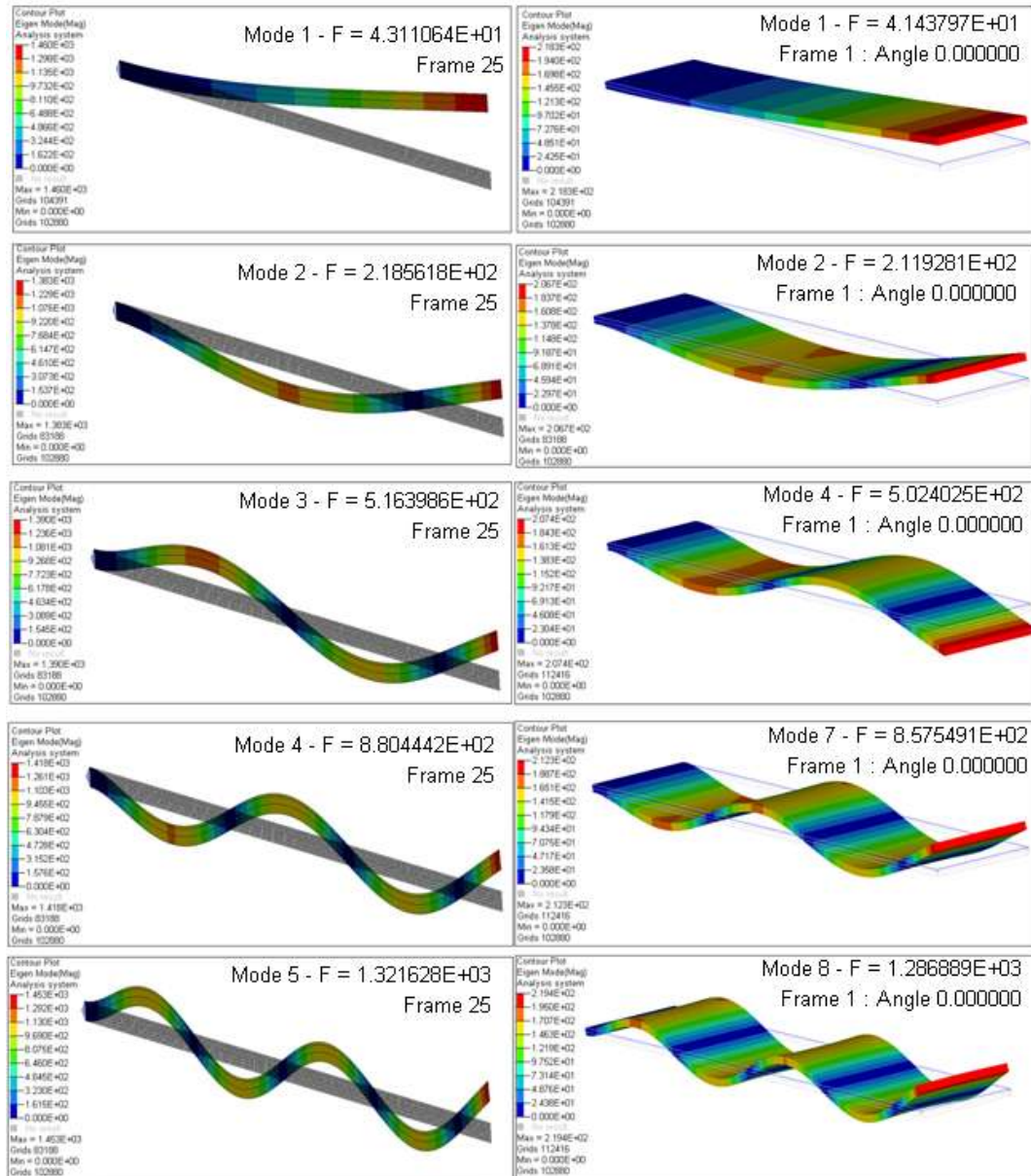


Figure 3-7 Modal analysis results: 2D modeling (Left), 3D modeling (Right)

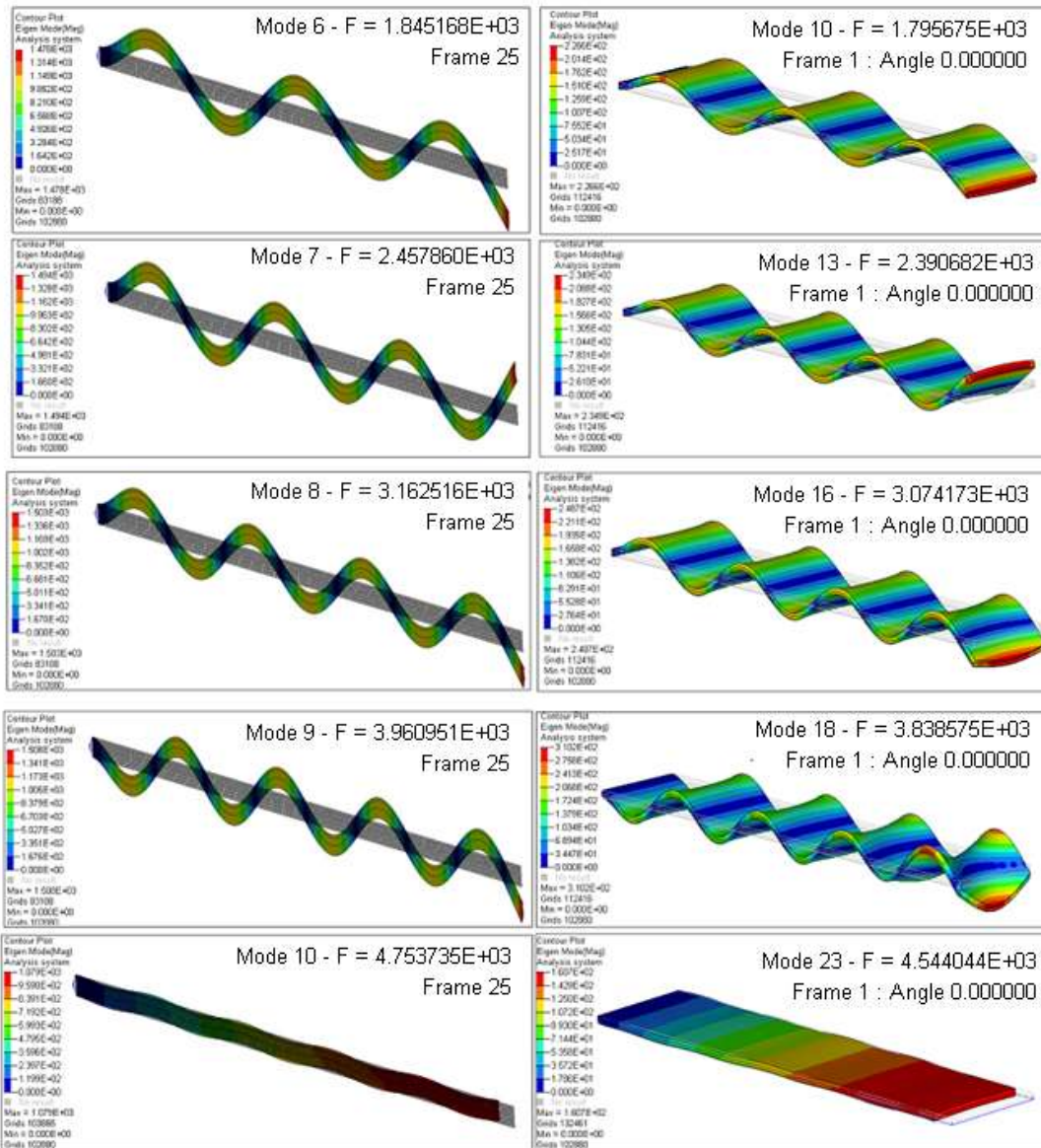


Figure 3-8 Modal analysis results: 2D modeling (Left), 3D modeling (Right)

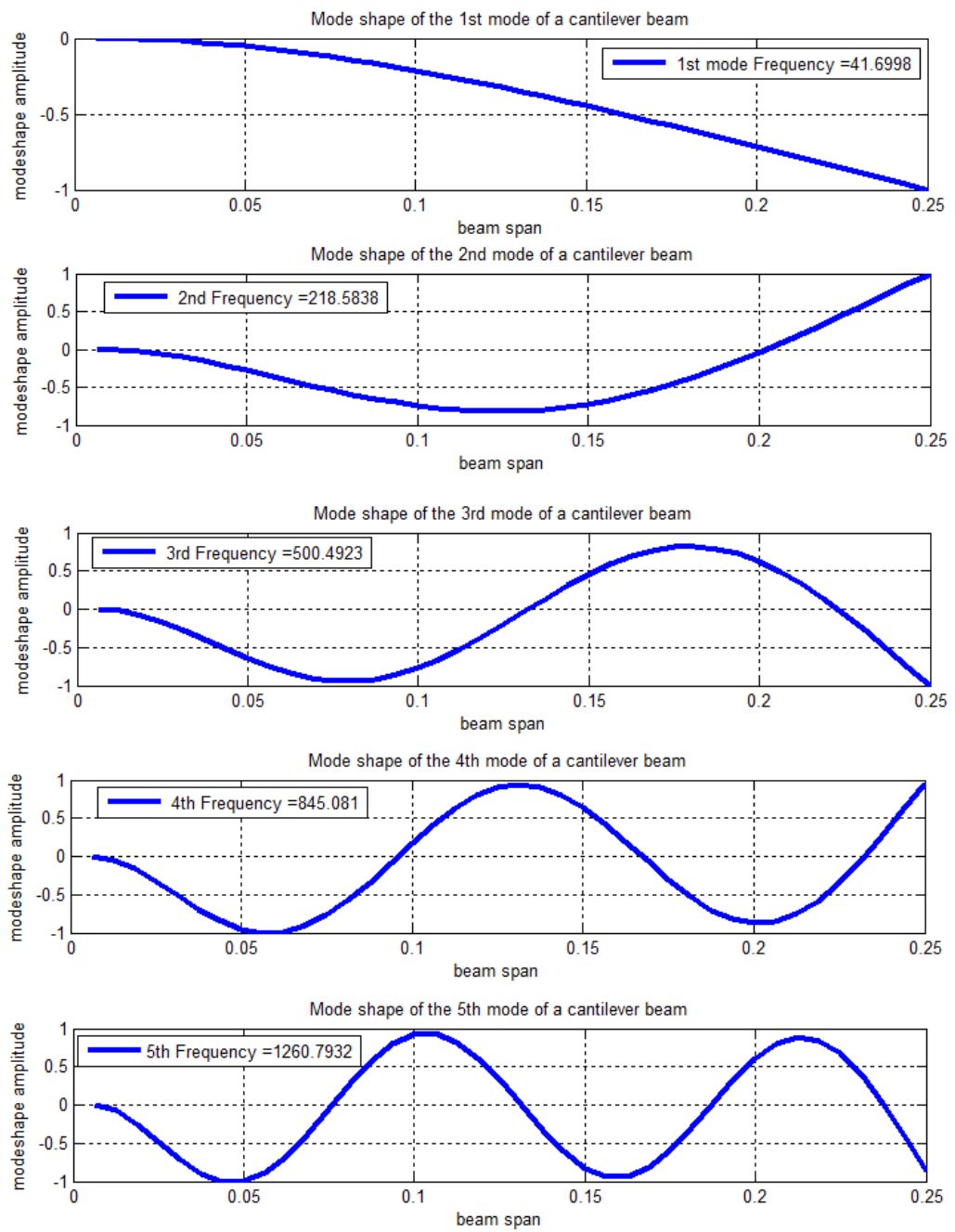


Figure 3-9 Modal analysis results: Analytical (RKU) (1st to 5th Mode)

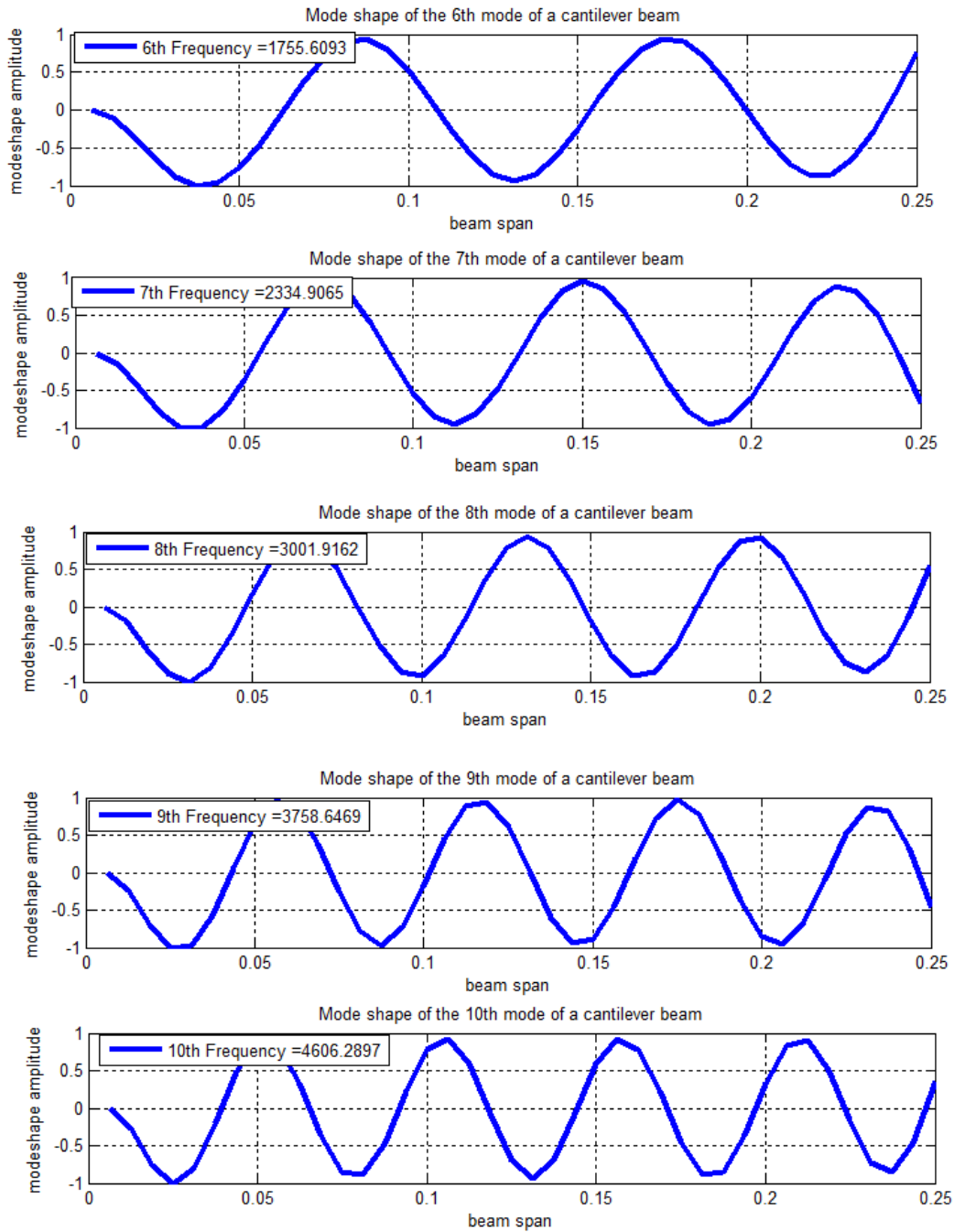


Figure 3-10 Modal analysis results: Analytical (RKU) (6th to 10th Mode)

Table 3-2 Comparison of Modal Analysis Results

Mode Number (2D;3D;RKU)	2D QUAD4		Analytical RKU	Abs. Pret. Err. (%)		
	Plain Strain FEM	3D HEX8 FEM		2D	3D	RKU
	(1;1;1)	43.11		41.44	41.70	-
(2;2;2)	218.56	211.93	218.58	-	3.13	0.01
(3;4;3)	516.40	502.40	500.49	-	2.79	3.18
(4;7;4)	880.44	857.55	845.08	-	2.67	4.18
(5;8;5)	1321.63	1286.89	1260.80	-	2.70	4.82
(6;10;6)	1845.17	1795.68	1755.60	-	2.76	5.10
(7;13;7)	2457.86	2390.68	2334.90	-	2.81	5.27
(8;16;8)	3162.52	3074.17	3001.90	-	2.87	5.35
(9;18;9)	3960.95	3838.58	3758.60	-	3.19	5.38
(10;23;10)	4753.74	4544.04	4606.30	-	4.61	3.20

The natural frequencies for the same three layer beam calculated using three modeling approach were in quite well agreement with each other with a percentage error of 2D model was maximum %5.38 that was considered to be small enough. Therefore 2D plain strain condition was used throughout the study.

The base beam corresponding to vibrating antenna element, the stand-off layer, viscoelastic layer and constraining layers were all modeled using linear QUAD4 isoparametric 4-noded shell type finite elements. QUAD4 shell elements are defined by 4-nodes with two degrees of freedom at each node, namely, translations in nodal $-x$ and $-y$ directions (Figure 3-6). The number of finite element used in modeling quite affects the accuracy of the analysis results. Also topology optimization requires sufficient numbers of elements to finely distribute material within design space.

Bearing in mind this fact together with analysis run cost sufficient number of elements in modeling such that two elements through the thinnest viscoelastic layer thickness were used.

The geometric and material properties of 2D plane shell elements, namely, QUAD4, were assigned using PSHELL property cards together with MAT1 material cards which have the following formats given in Table 3-3. MAT1 card is used to define isotropic constant material properties for the elements within individual layers. PSHELL card also is used for defining section properties of each layer, such as material (MID1), thickness (T) etc. The plain strain case is also set in this card by assigning MID2= -1 at 5th column while setting MID3 as blank at 7th column of this card [143]. For topology optimization the T0 is set to 0 which is the minimum base thickness.

Table 3-3 Material and Geometric Cards in Hypermesh [143]

(1)	(2)	(3)	(4)	(5)	(6)	(7)	(8)	(9)	(10)
MAT1	MID	E	G	NU	RHO	A	TREF	GE	
	ST	SC	SS						

(1)	(2)	(3)	(4)	(5)	(6)	(7)	(8)	(9)	(10)
PSHELL	PID	MID1	T	MID2	12I/T3	MID3	TS/T	NSM	
	Z1	Z2	MID4	T0	ZOFFS				

Upon completion of topology and parametric optimization studies, the performance of designs is investigated by incorporating the frequency dependent material properties for the viscoelastic material. For this purpose Direct Frequency Response Analysis has been performed. In this type analysis method isotropic frequency dependent material properties are assigned to viscoelastic elements using MATF1 card which uses tabulated form of material properties with respect to frequency, as Modulus of Elasticity $E(f)$, Shear Modulus, $G(f)$ and damping factor $GE(f)$ as TABLEDi entries which are shown T(E), T(G) and T(GE) in Table 3-4 in column 3th, 4th and 9th respectively.

Table 3-4 Isotropic Frequency Dependent Material Property Card [143]

(1)	(2)	(3)	(4)	(5)	(6)	(7)	(8)	(9)	(10)
MATF1	MID	T(E)	T(G)	T(NU)	T(RHO)	T(A)		T(GE)	
	T(ST)	T(SC)	T(SS)						

The material for the viscoelastic layer is selected as DYAD-601 Souncoat[®] from the Soundcoat company located at USA [144],. The frequency dependent material properties at 23 C (room temperature) is given in Figure 3-11.

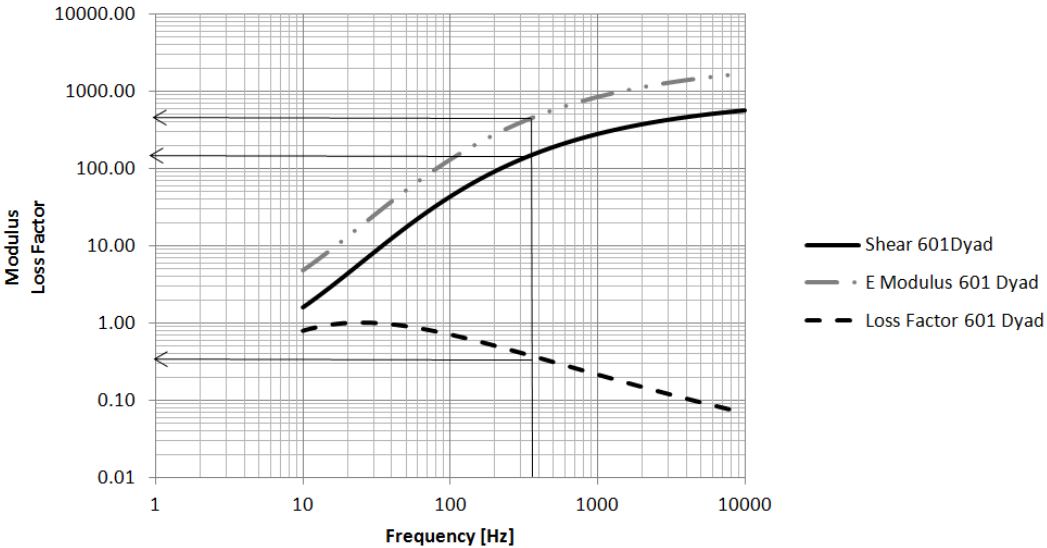


Figure 3-11 DYAD-601 Frequency dependent material properties [144]

Optimization studies started from an initial design model that has certain constant material and geometric properties. Design model of a long four layered beam model has been created using CATIAVS-R22[®] and finite element model is created in Hypermesh[®] using the initial constant material parameters and geometric properties for the topology optimization are given in Table 3-5.

Table 3-5 Material and Geometric Properties of Individual Layers

Properties	Base Beam Layer (Aluminum)	Stand-off Layer (ABS-P430)	Damping Layer (Dyad-601)	Constraining Layer (Aluminum)
Elastic Modulus, E (GPa)	70	2.2	-	70
Shear Modulus, G (GPa)	-	-	0.05(*)	-
Density, ρ (kg/m ³)	2770	1040	1120	2770
Poisson's Ratio, ν	0.3	0.38	0.49	0.3
Loss Factor, η	0.001	0.08	0.8	0.001
Length [mm]	250	250	250	250
Thickness [mm]	1.6	10	1.27	0.5

(*) Modulus value is chosen, from material data plot (Figure 3-11), to correspond fundamental frequency of reference layered beam, $\omega_1 = 137 \text{ Hz}$.

For the stand-off layer the ABS P430 type material was selected since complex topologies can easily be manufactured using rapid prototyping technology from 2D to 3D [145]. Since the topology optimization requires sufficient design space, a 10 mm stand-off height was selected to be as base reference analysis model.

3.2.6 Topology Optimization of Stand-off Layer

In this part of the study it is aimed to investigate the effectiveness of topology optimization method in finding the best material distribution for the stand-off layer with minimum weight as well as with maximum damping capacity via adapting the study of Boucher et.al [86]. The reference study uses minimization of compliance for the topology optimization of 2D viscoelastic medium. Here in this study the stand-off layer was selected as design space to be optimized under assumed flexural sinusoidal static load to mimic deformation pattern as is the case in reference [72] under vibration. Upon finding the material distribution for the stand-off layer the damping performance of cantilever four layer treated beam will be investigated using frequency dependent material properties for the viscoelastic layer. The beam

represents the structure over which the antenna elements are thought to be attached and our aim is to minimize weight of damping treatment with stand-off layer while increasing the damping capacity of it.

In classical topology optimization minimizing the compliance while constraining the material volume can be solved using the density method, assuming linear elasticity. This methodology can simply be stated mathematically as follows [136]

$$\left\{ \begin{array}{l} \min_{\boldsymbol{\rho}} C(\boldsymbol{\rho}) = \mathbf{F}^T \mathbf{u}(\boldsymbol{\rho}) \\ \text{s. t.} \left\{ \begin{array}{l} \boldsymbol{\rho}^T \mathbf{a} = V \\ \rho_{min} = 0.01 \leq \rho_e \leq \rho_{max} = 1 \end{array} \right. \end{array} \right. \quad (3-7)$$

$$e = 1, \dots, n$$

where n is the number of element within design domain and $\boldsymbol{\rho} = [\rho_1, \rho_2, \dots, \rho_n]^T$ is design variable vector which contains individual element densities to be varied between 0 and 1. \mathbf{a} is the vector of element areas. Also \mathbf{F} is loading vector. Recalling element nodal displacement formulation of each individual element, the global displacement vector \mathbf{u} can also be stated as follows [132];

$$\mathbf{u}(\boldsymbol{\rho}) = \mathbf{K}^{-1}(\boldsymbol{\rho})\mathbf{F} \quad (3-8)$$

And compliance minimization under load takes the final form of [132];

$$\min_{\boldsymbol{\rho}} C(\boldsymbol{\rho}) = \mathbf{F}^T \mathbf{K}^{-1}(\boldsymbol{\rho})\mathbf{F} \quad (3-9)$$

Above equation reflects that under constant static force compliance is inversely proportional with stiffness of the structure that is minimizing compliance is simply means the increase of stiffness of the structure. Increase of stiffness has positive effect in decreasing the vibration amplitude [119] and also weight reduction is

another advantage through any combination of constraints in compliance minimization problems [146].

Multiple load cases such as static and modal analysis steps can also be combined in topology optimization enabling the modification of frequency of structure. For this purpose compliance index and weighted compliance responses are used. The combined compliance index is a method to consider multiple frequencies and static subcases (loadsteps, load cases) combined in a classical topology optimization. The index is formulated as follows [132]:

$$S = \sum W_i C_i + NORM \frac{\sum W_j l \lambda_i}{\sum W_j} \quad (3-10)$$

This is a global response that is defined for the whole structure. The normalization factor, *NORM*, is used for normalizing the contributions of compliances and eigenvalues. The quantity *NORM* is typically computed using the formula [132]:

$$NF = C_{\max} \lambda_{\min} \quad (3-11)$$

The weighted compliance method considers multiple static loads. In this method different weight factors are assigned for each of static load cases according to dominant characteristic of loading. The weighted compliance is formulated as follows [132];

$$C_w = \sum W_i C_i = 1/2 \sum W_i u_i^T f_i \quad (3-12)$$

In the following sections some practical applications of topology optimization methodology are given by either minimizing compliance responses with material volume and displacement constraints or by maximizing the first modal frequency. It is aimed to investigate effectiveness of topology optimization in finding best layout

of stand-off layer that maximize the damping capacity of simple cantilever beam structure with minimum overall mass by comparing damping performance of resulting topologies through direct frequency response analysis in which the frequency dependent material properties are used. The Half Power Bandwidth Method is used to extract the damping factors of first three modes of the beam using a MATLAB code that has been developed in order to calculate corresponding damping factors automatically from frequency response functions in evaluation of damping performances (Figure 3-12). Moreover a uniform stand-off layer that has equivalent weight with new topology is recreated with reduced thickness and compared with original base model to quantify the increase of damping. In order to investigate the effect of height of the stand-off layer; the extracted same topologies, for each case study, are rescaled to reduced thickness values and their damping performances are also reported.

The displacement frequency response functions (Receptance) were generated upon performing direct frequency response analysis from the tip of simple cantilever beam, namely from tip of base beam whose vibration to be suppressed, as shown in (Figure 3-12) by exciting beam with harmonic unit force (1N) from same location in the frequency range of 5Hz to 14 kHz in order to evaluate the damping performance of design alternatives.



Figure 3-12 Generation of frequency response function

3.2.6.1 Case Study I:

In first case study a 250 mm long four layered treated cantilever beam model in 2D is modeled using QUAD4 shell elements in Hypermesh[®] finite element software environment using material and geometrical data given in Table 3-5. One end of the beam is restrained in all degrees of freedom to a one single node that represents the cantilever boundary condition using RBE2 rigid elements. The static in-plane sinusoidal flexural distributed load is applied at top row of the nodes to induce deformation that mimics the vibration deformation as well to induce shear deformation within the viscoelastic layer as shown in (Figure 3-13). The motivation behind this methodology is to find material distribution with minimum weight that will yield the induced state of deformation therefore the high strain energy within damping layer during its vibration motion with less bending rigidity while having higher shear stiffness in stand-off layer which are the properties of ideal stand-off layer [107]. The less bending rigidity can be achieved due to removal of material taking into account the induced load path in static load case, which was also selected to be in the form of sinus load that induce state of shear within damping layer for maximum damping, under volume constraints and lastly higher stiffness due to maximization of frequency at modal analysis step at this optimization case study.

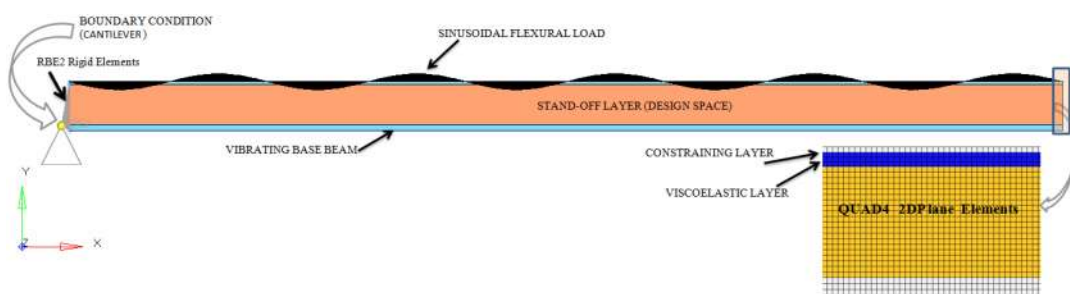


Figure 3-13 Finite element model of cantilever beam

Static and modal analysis steps are performed prior to the optimization step as base analysis. In optimization step, the property card of stand-off layer is selected as design domain using DESVAR cards in Optistruct. Then the compliance index response card DESRP1 card that will be used as objective function was created. This first response uses previous static analysis together with modal analysis steps simultaneously to take the frequency of the structure into account. Each of frequency and static load cases are equally weighted as $\omega_f = 1; \omega_s = 1$, respectively at this step. For constraining the material volume to be used in final optimized layout, the VOLFRAC response was also created using same card. This card represents the upper bounds of material volume fraction compared to original volume of total design. Therefore in this case the maximum value of 0.30 was set for this response.

Finally as an objective function minimize option was selected for the first response of the topology optimization, namely compliance index which will take account both static and modal analysis steps. The original and resulting treated beam is shown in the following Figure 3-14. The elements that has pseudo density value of 1 (red in color) were left while the ones that have 0 (blue in color) values were all deleted from the original design space. One can see the periodic nature of stand-off layer due to periodic sinus load as well as the shape that is yielded for maximum natural frequency, that is, in other words for high shear stiffness.

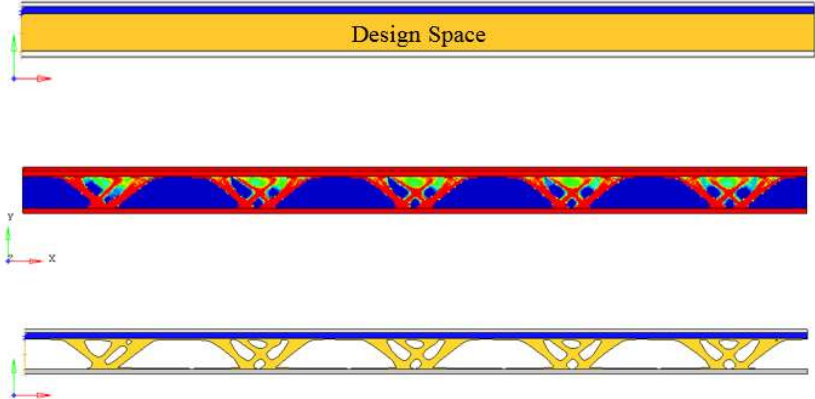


Figure 3-14 Layout of original (top) and optimized stand-off layer (bottom) upon minimizing compliance index

Table 3-6 Comparison of Original and Optimized Beam

	Uniform	Optimized
Spacer Mass [TON]	5.200e-06	0.7824e-06 (%15)
Total Mass [TON]	9.841e-06	3.103e-06 (%30)
Modal Frequency (1 st) [Hz]	137.34 Hz	148.19 Hz
Static Tip Displacement [mm]	11.3 mm	7.16 mm

In Table 3-6 comparison of static and modal analysis results of beam with uniform and optimized stand-off layer is given. Upon optimization the static tip displacement is reduced while the first natural frequency is shifted to higher level as expected. Also the total mass of the beam structure is reduced as being approximately %30 of total initial structure as was set in VOLFRAC card. As previously explained the result of topology optimization cannot be used directly since it needs to be refined to get final design space. In Hypermesh Smooth functionality was used to extract the surface geometry from the topology of stand-off layer. Then it was exported to the CATIAV5-R22 environment to tune the shape of voids and solids portions. This stage completely depends on the designer interpretation. The final geometry of the stand-off layer was recreated considering solid elements ($\rho=1$) periodically distributed as the solution implies. And this configuration was given as shown in (Figure 3-15) as well as its 3D geometry via extruding in perpendicular direction of the paper. The 3D geometry is given for demonstration purpose only to show how generated 2D topologies could be used in producing real 3D products with less weight.

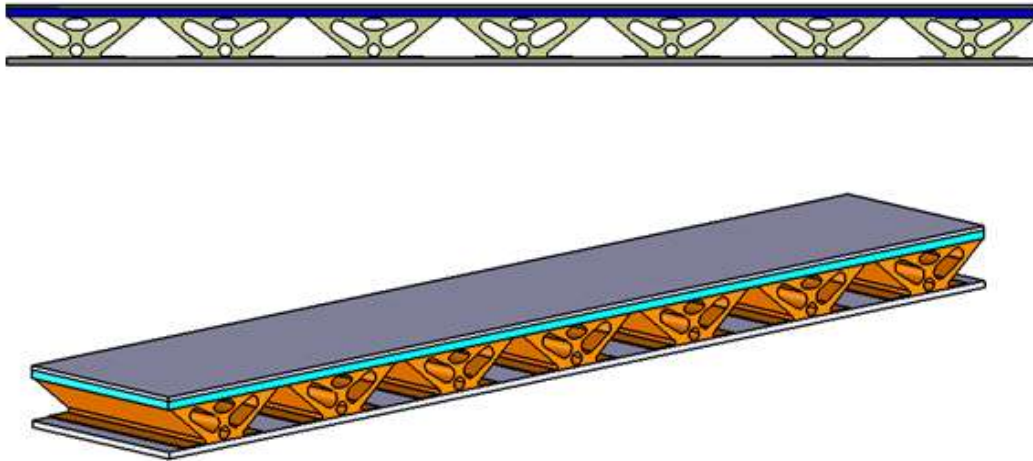


Figure 3-15 Refined 2D geometry of stand-off layer after topology optimization and 3D generation of final treated beam.

This tuned final 2D geometry was then used to investigate the dynamic behavior of cantilever beam in terms of damping capacity. It is already known that increase of modal strain energy in viscoelastic layer greatly increase the damping capacity. Regarding to increase of damping capacity, the modal analysis has been performed to visualize the deformation pattern within viscoelastic layer by simply extracting strain energy distribution. Modal analysis results (Figure 3-16) show that irregular deformation patterns exist at top portion of the beam, where the viscoelastic layer located. This irregularity creates induced shear deformation within the viscoelastic layer during vibration and as the frequency of vibration increase this irregularities shows themselves more along the entire beam.

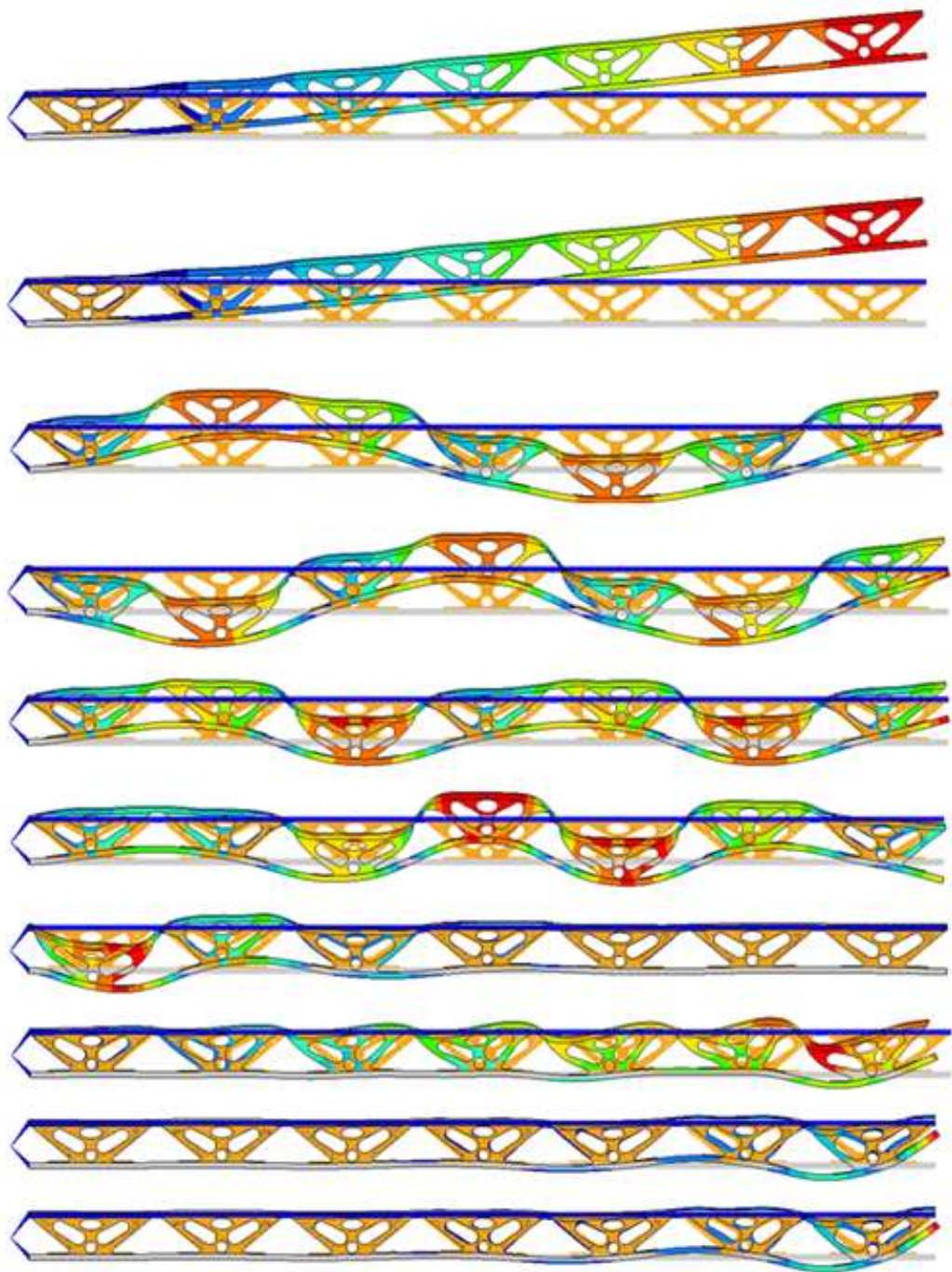


Figure 3-16 Mode shapes of cantilever beam with optimized stand-off (Case I)

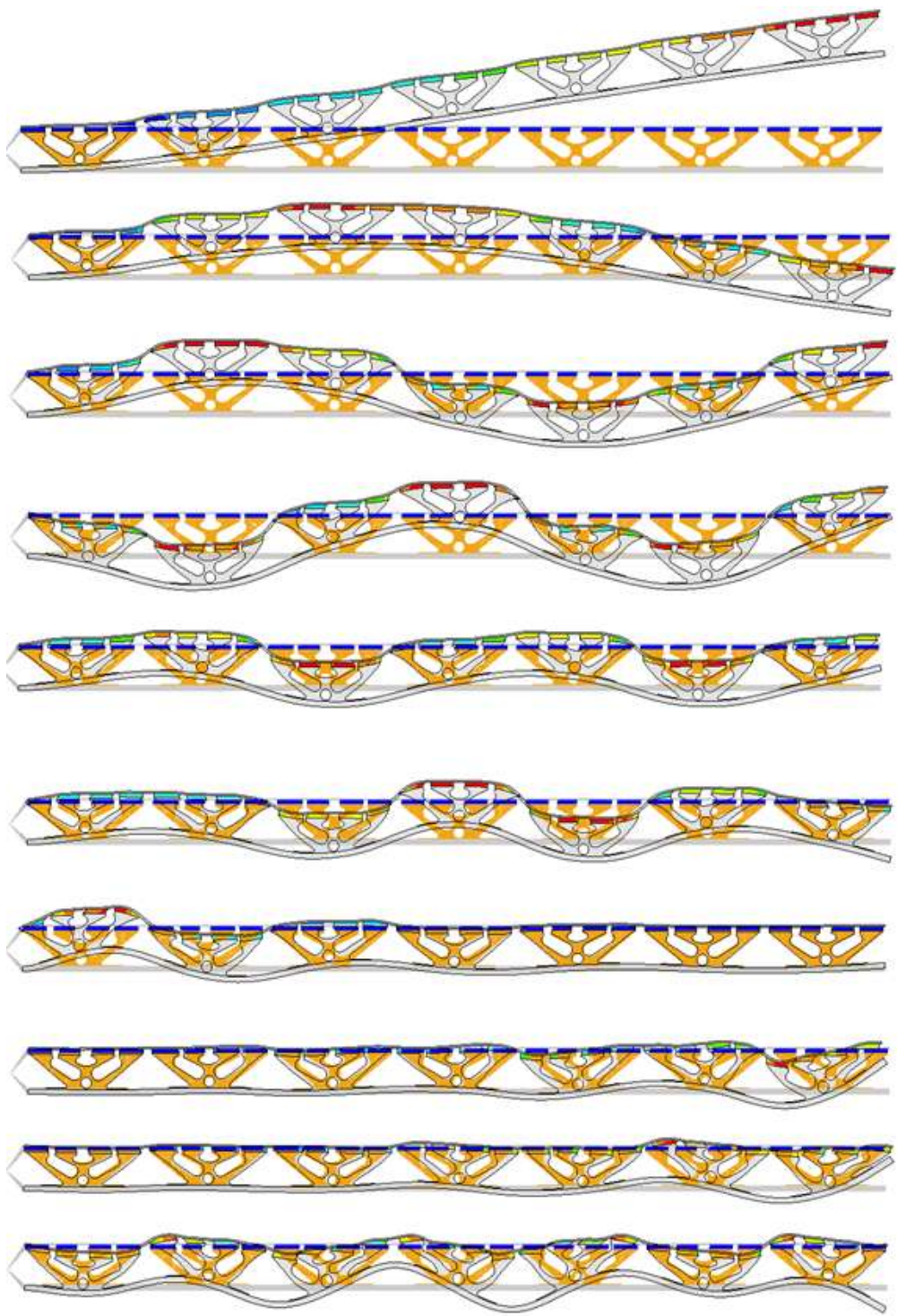


Figure 3-17 Strain energy distribution of partially covered stand-off layer

The increase of strain energies within viscoelastic layer can also be seen more easily from plots given below (Figure 3-18 to Figure 3-20) for the first three modes due to the new stand-off configuration. In the following plots the smooth line (red) represents the strain energy values for each element positioned above uniform stand-off layer while randomly distributed line (blue) shows the strain energy values for the same elements above optimized new configuration. It is clear that new configuration induce higher shear strain within the viscoelastic layer compared to uniform one. Moreover the new stand-off configuration possesses less weight than original uniform case.

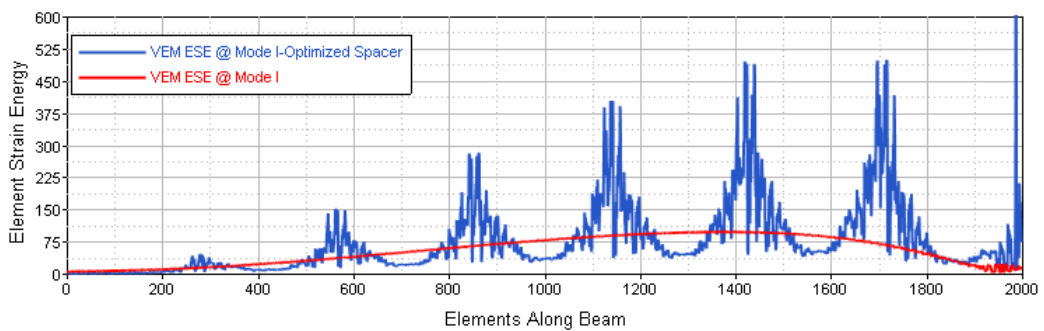


Figure 3-18 Increased Strain Energies within VEM layer along beam.

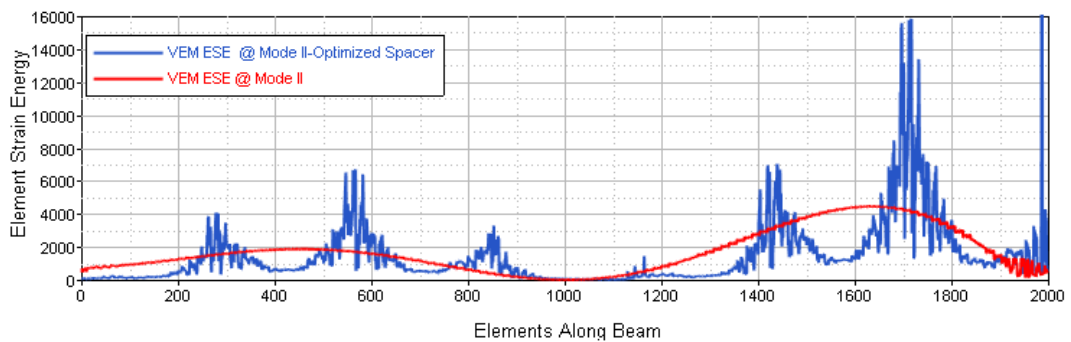


Figure 3-19 Increased Strain Energies within VEM layer along beam.

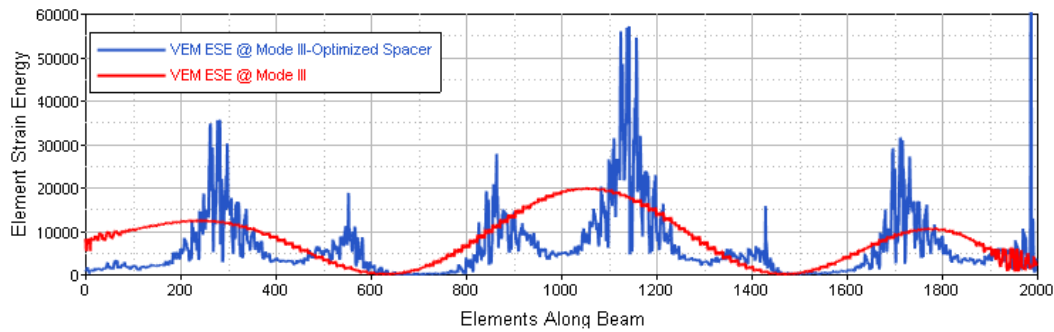


Figure 3-20 Strain energies within viscoelastic layer along beam.
 (Red: Uniform Stand-off, Blue: Optimized Stand-off)

Up to now the constant material properties are used for the viscoelastic layer since the topology optimization method used as concept design generation. Fortunately it is obvious from above results that new stand-off configuration induce higher shear strain which in turn the final geometry has higher modal loss factors. Now in order to quantify the damping performance of the new configuration accurately, frequency dependent material properties are incorporated into direct frequency response analysis with which we can able to extract damping factors using Half Power Bandwidth Method from frequency response functions. The following Figure 3-21 and Figure 3-22 shows the frequency response functions, namely receptance plots, of original beam with uniform and optimized stand-off layer for the first 10 modes respectively. The peaks represent the displacement response of tip of the base beam at resonance frequencies at each mode. The loss factors as well as frequencies were detected via using specially written MATLAB[®] code and all were attached on curve for each of those peaks.

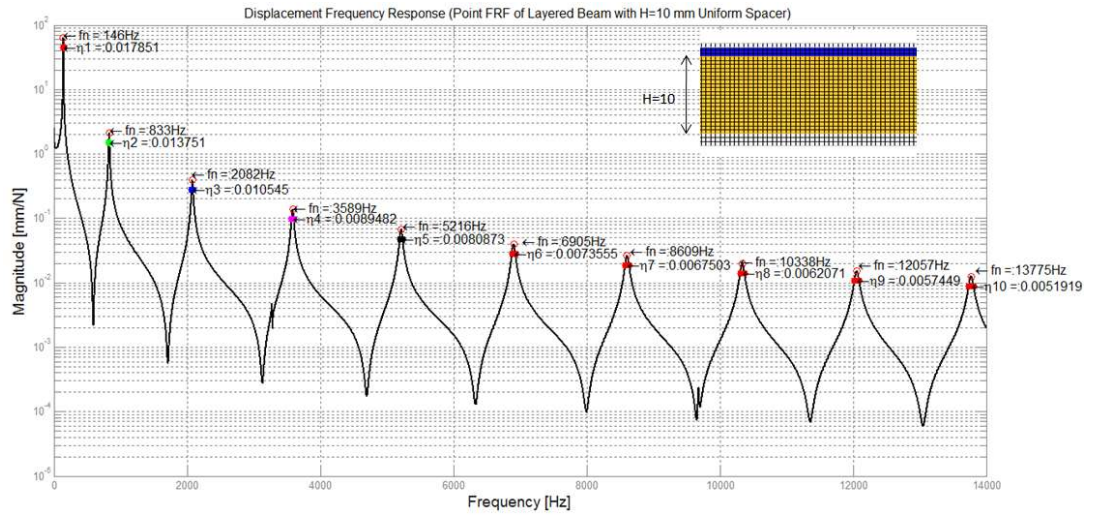


Figure 3-21 Frequency response function of beam with uniform stand-off layer (H=10 mm)

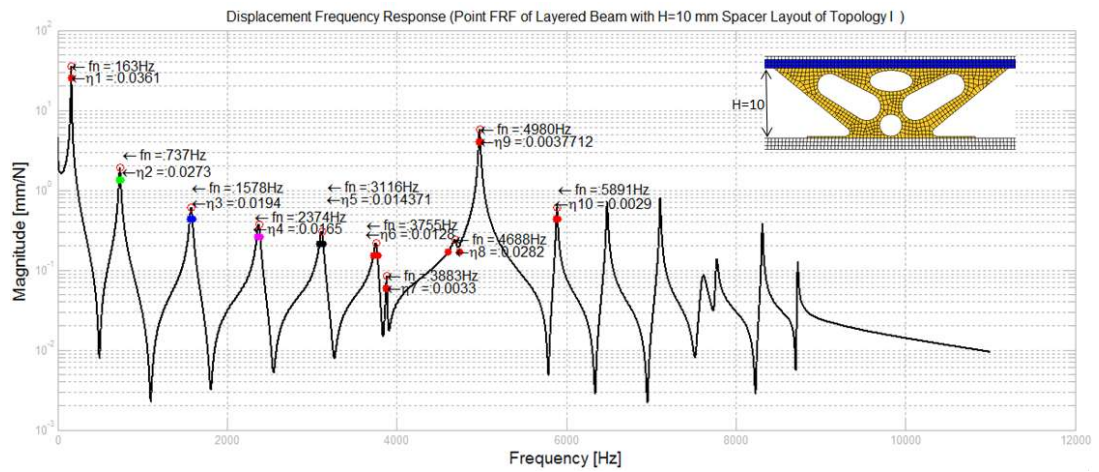


Figure 3-22 Frequency response function of beam with optimized stand-off layer (H=10 mm)

The new stand-off layer configuration has less weight compared to uniform layer. Therefore in order to compare the performance of this newly generated layer with layer that has equivalent mass, a new uniform layer is modeled with less thickness but same weight. The following Figure 3-23 shows the frequency response function of beam with equally weighted uniform stand-off layer.

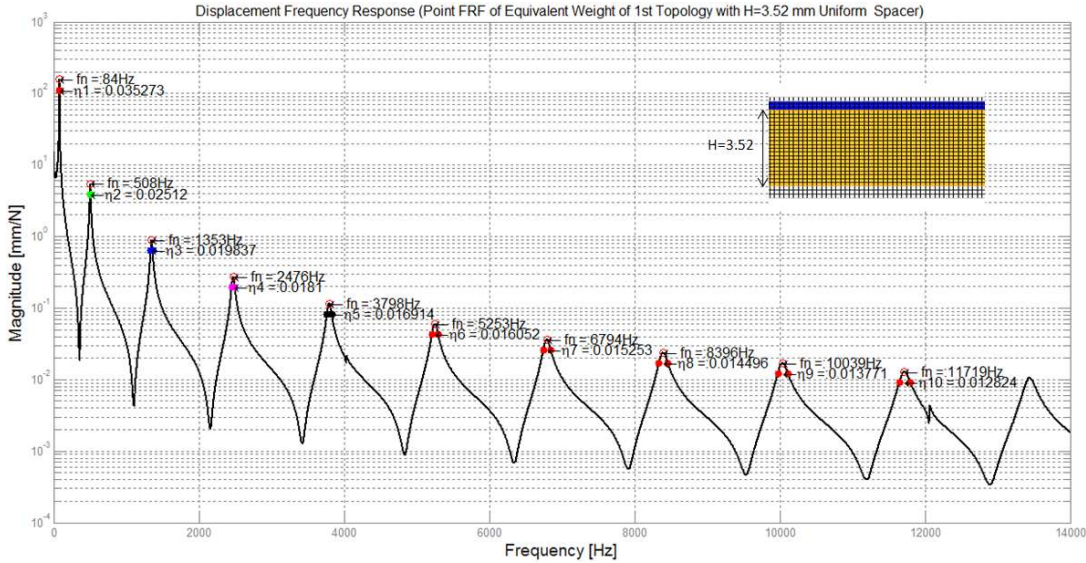


Figure 3-23 Frequency response function of beam with equally weighted uniform stand-off layer (H=3.52 mm)

The following Figure 3-24 shows overall comparison of frequency response functions for fully treated original uniform (dashed fade black), optimized (dark black) and equal weight (blue) uniform stand-off layer.

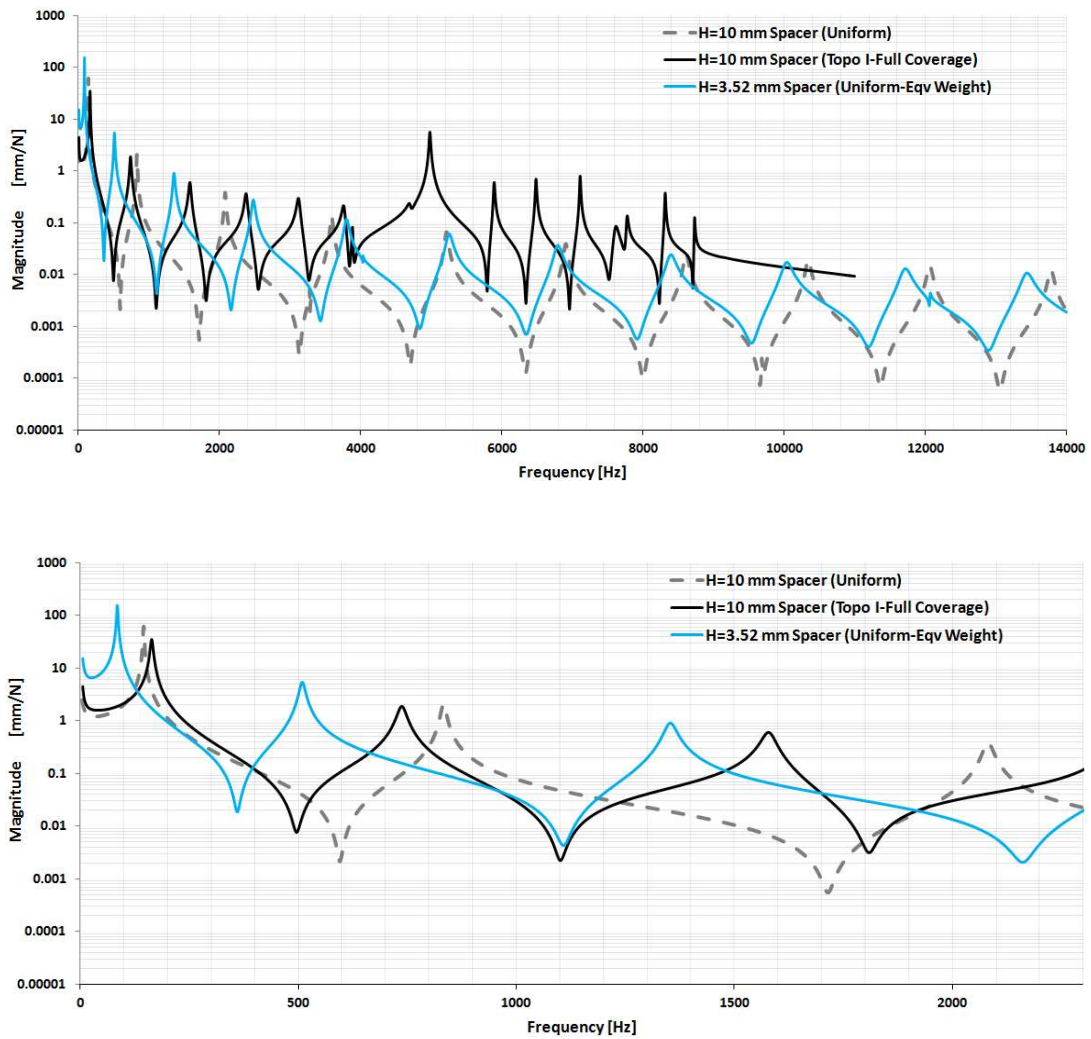


Figure 3-24 Frequency response functions of original uniform (dashed fade black), optimized (dark black) and equal weight (blue) uniform stand-off layer.

One can see from Figure 3-24 that the new topology of stand-off layer has lower amplitude compared to original beam structure with uniform and equally weighted uniform stand-off layer. However upon 4 kHz there are visible high amplitudes in response function while weight equivalent thinner uniform layer has stable dynamic characteristic. However it is quite visible from response function that thinner layer has higher response amplitude especially in lower frequencies but they are gradually diminished at higher frequencies. The shape of response curve tends to be broader due to increased damping.

From the literature it is known that addition of cuts into viscoelastic layer as well as partial coverage further increases damping capacity. Such modification was also incorporated into new layout of stand-off layer as depicted in Figure 3-25. The viscoelastic layer is also covered partially. It is expected to increase the shear strain at the vicinity of the cuts within stand-off layer.

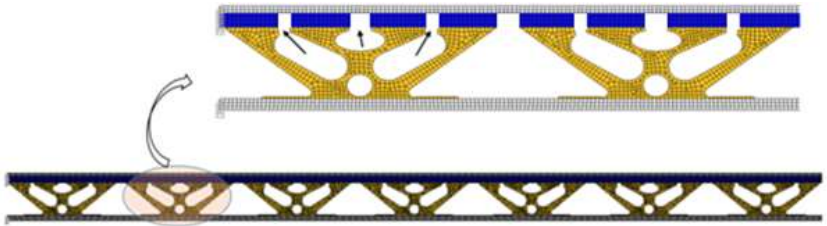


Figure 3-25 Addition of cuts into new layout of stand-off layer (partial coverage)

The following Figure 3-26 shows the frequency response function of beam with optimized stand-off layer with cuts.

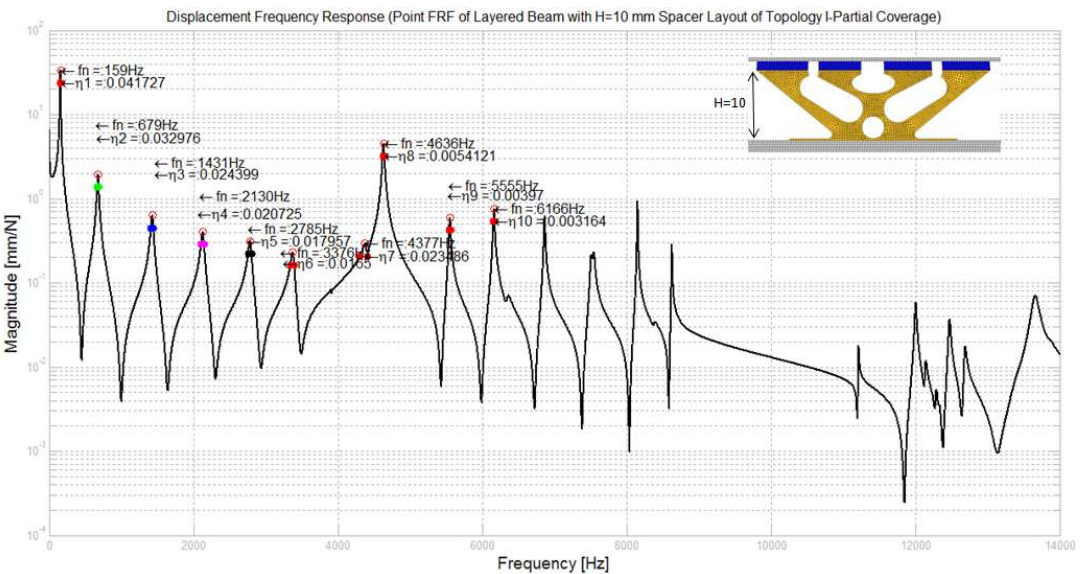


Figure 3-26 Frequency response function of beam with partially treated optimized stand-off layer

The comparison of all above cases is given in the following Figure 3-27, it is seen that new topology of stand-off layer with cuts has improved the damping capacity of beam especially at lower frequencies with shallower and broader response curve. However upon 4 kHz there are visible high amplitudes with narrow peaks in response function for the thick spacer with new layout of spacer.

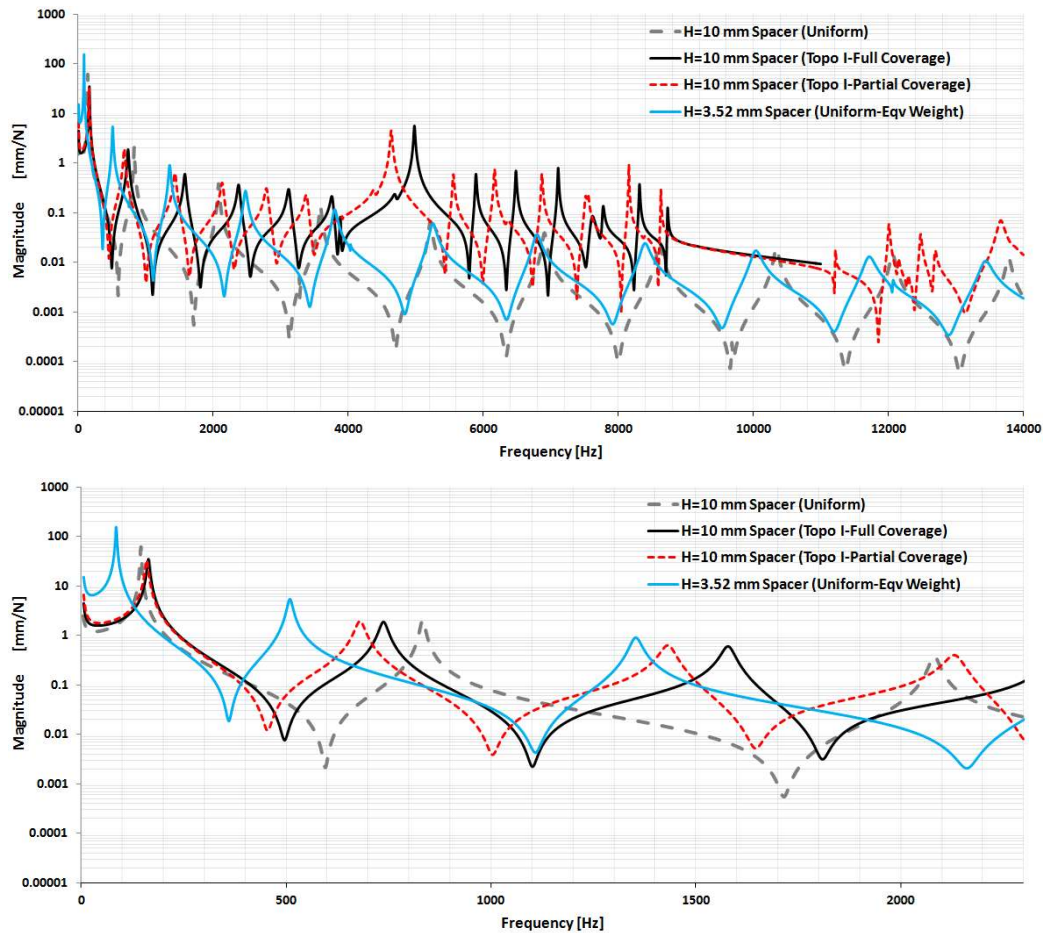



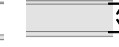




Figure 3-27 Overall comparison of frequency response functions
(H=10 mm & H=3.52 mm)

The numerical results are given for each of the cases considered previously in the following Table 3-7. The results include comparison in terms of total weight percentage, frequency and loss factors for the first ten modes. The damping performance of optimized fully and partially treated beam compared to uniform case which is considered to be reference configuration. Minimizing compliance index

results %38.34 mass reduction as well as damping improvement %101.68 for the first mode, %97.1 for the second mode, %84.76 for the third mode for fully treated case and the relative improvement is until 7th mode. Additionally for the partial case with same topology, %41.2 mass reduction as well as dampin improvement of %132.96 for the first mode, %139.13 for the second mode, %132.38 for the third mode compared to reference model with 10 mm uniform stand-off layer, was achieved. The improvement is continous until 7th mode for the partial treatment. The first mode is shifted to a higher value while all others were lowered.

Table 3-7 Summary of the optimization results (CASE I-H=10mm)

(CASE I-H=10mm)						
1st Topology Relative Damping Performance w.r.t. Uniform Stand-Off Layer						
Frequency f [Hz]			Loss Factor $\eta=2\zeta$			
H=10						
						
Mode #	Uniform Full Coverage	Optimized Full Coverage	Optimized Partial Coverage	Uniform Full Coverage Weight=100%	Optimized Full Coverage Weight=61.66%	Optimized Partial Coverage Weight=58.80%
1++	146.00	163.00	159.00	0.018	0.036	0.042
				-	↑ 101.68%	↑ 132.96%
2++	833.00	737.00	679.00	0.014	0.027	0.033
				-	↑ 97.10%	↑ 139.13%
3++	2082.00	1578.00	1431.00	0.011	0.019	0.024
				-	↑ 84.76%	↑ 132.38%
4++	3589.00	2374.00	2130.00	0.009	0.016	0.021
				-	↑ 84.27%	↑ 132.58%
5++	5216.00	3116.00	2785.00	0.008	0.014	0.018
				-	↑ 77.78%	↑ 122.22%
6++	6905.00	3755.00	3376.00	0.007	0.013	0.017
				-	↑ 72.97%	↑ 122.97%
7+-	8609.00	3883.00	4377.00	0.007	0.003	0.024
				-	↓ -51.47%	↑ 245.59%
8+-	10338.00	4688.00	4636.00	0.006	0.028	0.005
				-	↑ 354.84%	↓ -12.90%
9--	12057.00	4980.00	5555.00	0.006	0.004	0.004
				-	↓ -33.33%	↓ -29.82%
10--	13775.00	5891.00	6166.00	0.005	0.003	0.003
				-	↓ -44.23%	↓ -38.46%

From Figure 3-23 one can see that the reduced uniform thickness for the stand-off layer yields almost higher modal loss factor for the first three mode and even higher beyond the 3rd mode. Therefore in the following case the same topology is scaled down to a lower thickness value of 3.52 mm stand-off height and pattern of new layout was covered along the beam (Figure 3-28) and the same analyzes were also repeated for this new thickness value. The results were also reported in the following pages.

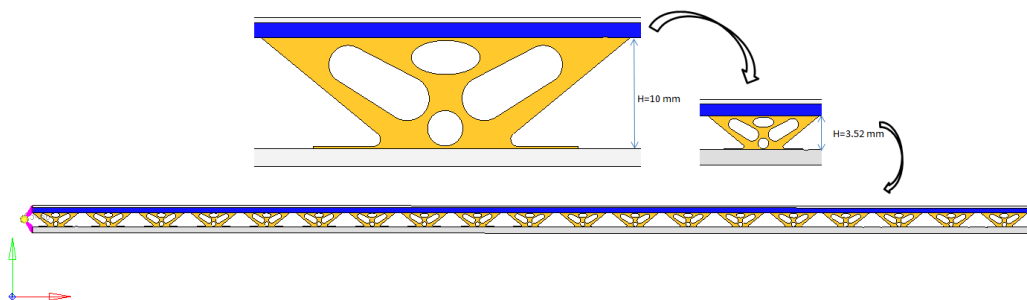


Figure 3-28 Thickness reduction of new layout (Topology I) of stand-off layer

The following Figure 3-29 shows the frequency response function for the same topology with reduced thickness.

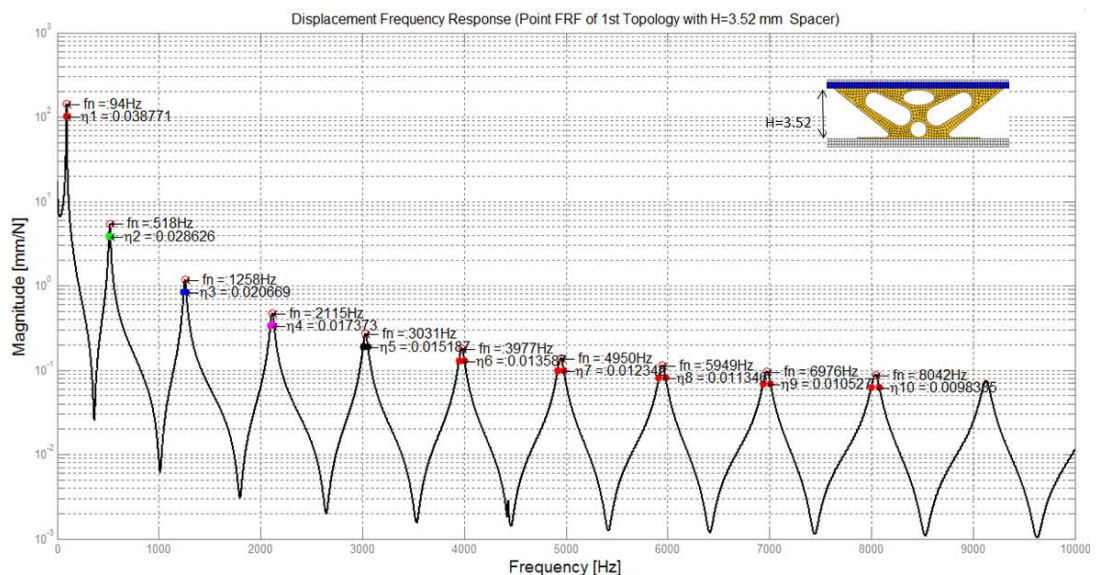


Figure 3-29 Frequency response function of beam with optimized stand-off layer with reduced thickness.

Like in the previous case, the cuts were added into stand-off layer with reduced thickness as depicted in Figure 3-30. The coverage of viscoelastic layer was done partially using the area left over the stand-off layer.

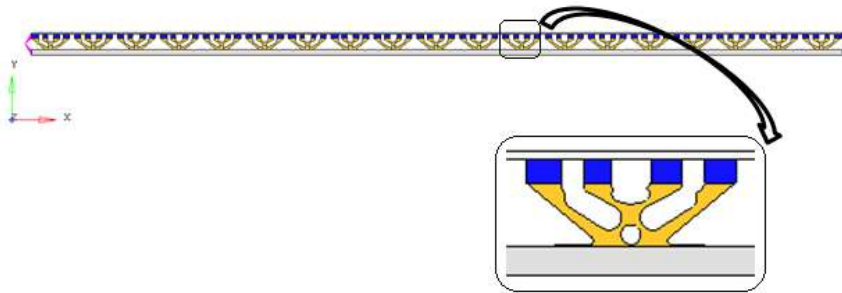


Figure 3-30 Addition of cuts into stand-off layer (partial coverage) (H=3.52mm)

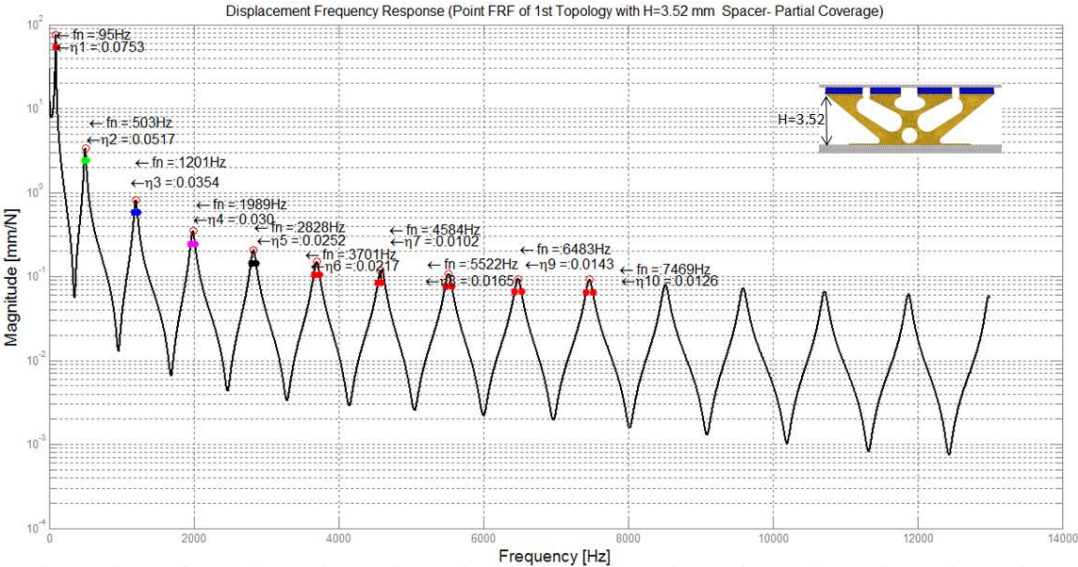


Figure 3-31 Frequency response function of beam with partially treated optimized stand-off layer with reduced thickness (Topology I).

Comparison of frequency response functions for the beam with optimized and uniform stand-off layer with a thickness value of 3.52 mm is given in the following (Figure 3-32). Scaling the stand-off layer down to a reduced thickness value results further damping improvement compared to thicker spacer layer. The damping capacity was increased and the frequency of the structure lowered since the thinner

structure has lower bending rigidity. The overall comparison of results of first case study is given in (Figure 3-32). The thicker stand-off layer has lower response value for the first three modes at slightly higher frequencies. However the thinner stand-off layer with same topology has higher damping capacity in all modes with higher amplitudes at low frequencies. Additionally although the response amplitude is higher at low frequencies one can see gradual decrease in amplitude with broader peak values.

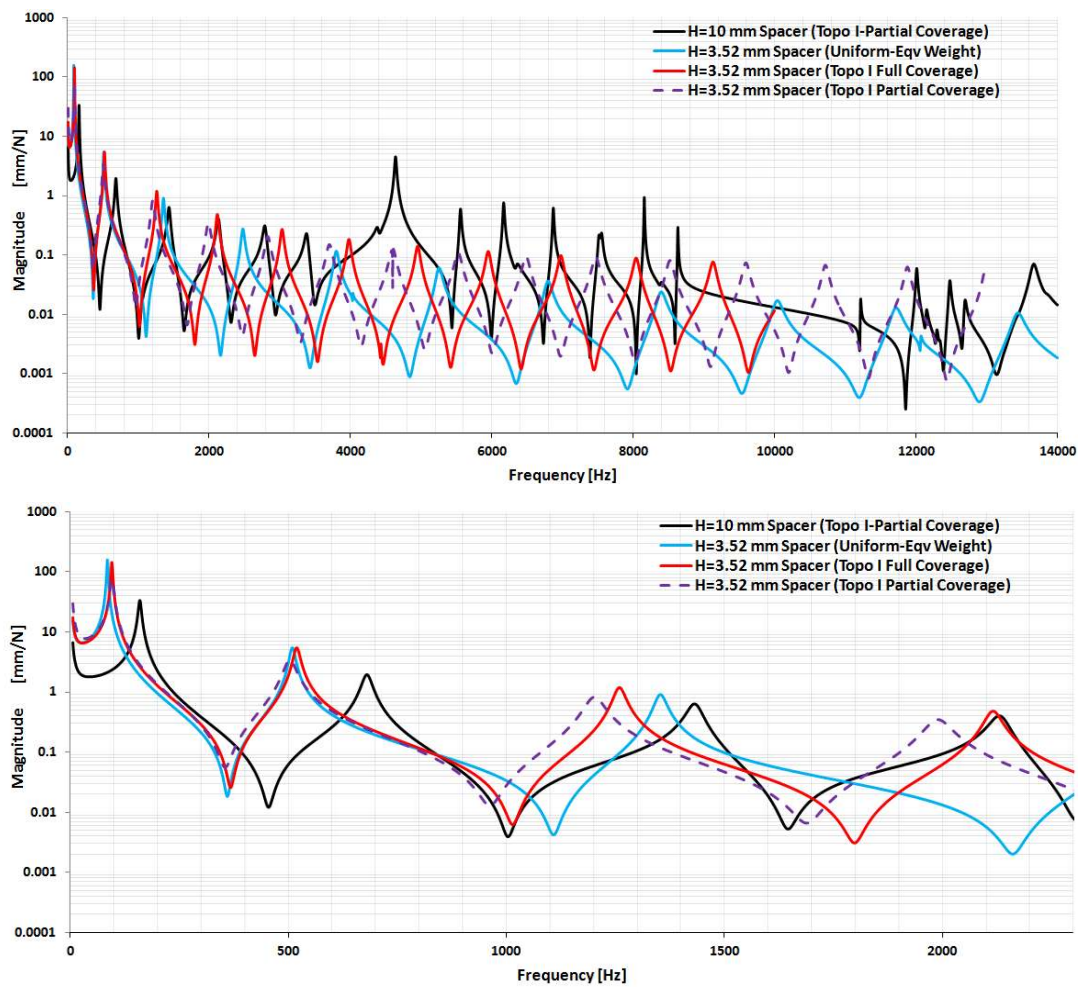


Figure 3-32 Overall comparison of frequency response functions (H=3.52 mm) & (H=10 mm)

The numerical results are summarized in the following Table 3-8 for new thickness value of stand-off layer ($H=3.52$ mm) with same topology as in the previous case. The results include comparison in terms of weight, frequency and loss factors for the first ten modes. Minimizing the thickness of stand-off layer compared to $H=10$ mm stand-off layer, results further %39.27 decrease in weight for the uniform cases. The same topology with lower thickness value increase damping by %9.92 for the first mode, %13.94 for the second mode, %4.55 for the third mode compared to $H=3.52$ mm uniform case. Also for this case, upon 3rd mode there is no achieved relative improvement. The reduction of weight by optimization compared to thin uniform case is %21.43. One can notice that relative percentage increase in damping and decrease in mass via optimization is decreased as the thickness of stand-off layer is reduced. Moreover the improvement for the particular case for the thinner partially treated optimized layout is %113.31 for the first mode, %105.98 for the second mode and %78.79 for the third mode. The relative improvement is continuous until 6th mode for partially treated stand-off with decreasing percentage.

Table 3-8 Summary of the optimization results (CASE I-H=3.52 mm)

(CASE I-H=3.52mm)						
1st Topology Relative Damping Performance w.r.t. Uniform Stand-Off Layer						
Frequency f [Hz]			Loss Factor $\eta=2\zeta$			
H=3.52						
Mode #	Uniform Full Coverage	Optimized Full Coverage	Optimized Partial Coverage	Uniform Full Coverage Weight=100%	Optimized Full Coverage Weight=78.57%	Optimized Partial Coverage Weight=72.18%
Prct [%]						
1++	84.00	94.00	95.00	0.035	0.039	0.075
				-	↑ 9.92%	↑ 113.31%
2++	508.00	518.00	503.00	0.025	0.029	0.052
				-	↑ 13.94%	↑ 105.98%
3++	1353.00	1258.00	1201.00	0.020	0.021	0.035
				-	↑ 4.55%	↑ 78.79%
4-+	2476.00	2115.00	1989.00	0.018	0.017	0.030
				-	↓ -3.87%	↑ 63.54%
5-+	3798.00	3031.00	2828.00	0.017	0.015	0.025
				-	↓ -10.06%	↑ 49.11%
6-+	5253.00	3977.00	3701.00	0.016	0.014	0.022
				-	↓ -15.53%	↑ 34.78%
7--	6794.00	4950.00	4584.00	0.015	0.012	0.010
				-	↓ -19.61%	↓ -33.99%
8-+	8396.00	5949.00	5522.00	0.015	0.011	0.016
				-	↓ -22.07%	↑ 13.10%
9-+	10039.00	6976.00	6483.00	0.014	0.011	0.014
				-	↓ -23.91%	↑ 3.62%
10--	11719.00	8042.00	7469.00	0.013	0.010	0.013
				-	↓ -23.44%	↓ -1.56%

As a summary, if we compare the results obtained for both thickness value of stand-off layers, namely, H=10 mm and H=3.52 mm, the following (Figure 3-33) summarizes the result obtained in terms of frequency response curves. Compared to thicker uniform stand-off layer the thinner partially treated stand-off with optimized configuration has better damping performance in all modes. However the response amplitude is relatively higher.

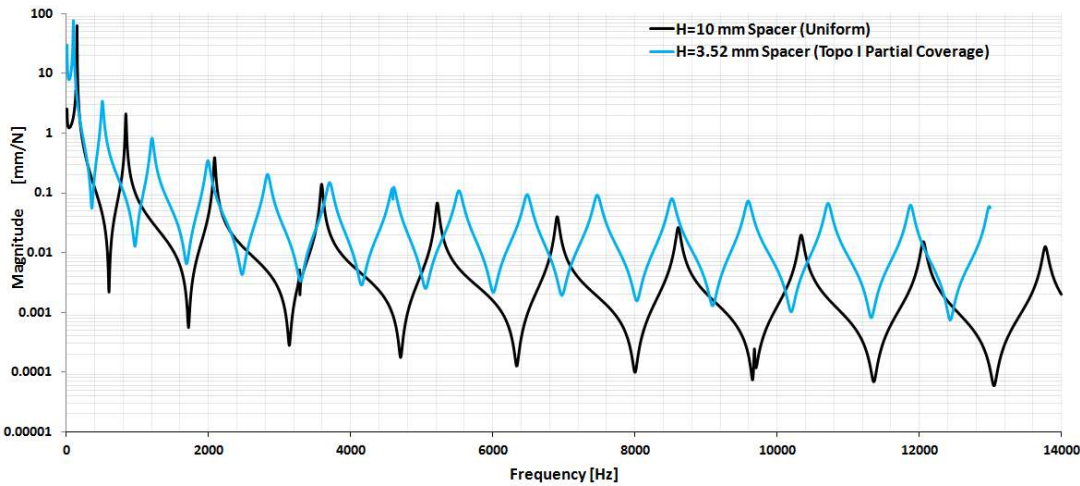


Figure 3-33 Overall comparison of frequency response functions (H=3.52 mm-partially treated) & (H=10 mm-uniform fully treated)

The numerical results are summarized in the following Table 3-9. The thinner uniformly treated beam has relatively high damping capacity compared to thicker configurations and the relative damping improvement is increasing continuously with increasing frequency. Moreover the partial configuration further increase the value of loss factor in all modes compared to uniform cases. This relative increase was expected to be due to increased flexibility that generates relative motion between layers and due to high local strain concentrations, exist within viscoelastic layer upon cutting spacer layer. However in terms of response amplitude, the thicker layer has advantage comparatively.

Table 3-9 Results of Optimization for H=10mm and H=3.52 mm Stand-off Layer

(CASE I-H=10 vs H=3.52mm)

1st Topology Relative Damping Performance

Loss Factor $\eta=2\zeta$

Mode #	H=10			H=3.52				
	Uniform-Full Coverage Prct [%] Weight=100%	Optimized Full Coverage Weight=61.66%	Uniform-Full Coverage Weight=61.66%	Optimized (H=10mm) vs Uniform (H=3.52 mm)	Optimized Partial (H=10mm) vs Uniform (H=3.52 mm)	Uniform-Full Coverage Weight=100%	Optimized Full Coverage Weight=78.57%	Uniform-Eq.Weight Full Coverage Weight=72.18%
1+++	0.018	0.036	0.042	↑ 2.27%	↑ 18.13%	0.035	0.039	0.075
2+++	0.014	0.027	0.033	↑ 8.37%	↑ 31.47%	0.025	0.029	0.052
3+++	0.011	0.019	0.024	↓ -2.02%	↑ 23.23%	0.020	0.021	0.035
4+++	0.009	0.016	0.021	↓ -9.39%	↑ 14.36%	0.018	0.017	0.030
5+++	0.008	0.014	0.018	↓ -14.79%	↑ 6.51%	0.017	0.015	0.025
6+++	0.007	0.013	0.017	↓ -20.50%	↑ 2.48%	0.016	0.014	0.022
7+-	0.007	0.003	0.024	↓ -78.43%	↑ 53.59%	0.015	0.012	0.010
8+-	0.006	0.028	0.005	↑ 94.48%	↓ -62.76%	0.015	0.011	0.016
9+++	0.006	0.004	0.004	↓ -72.46%	↓ -71.01%	0.014	0.011	0.014
10+++	0.005	0.003	0.003	↓ -77.34%	↓ -75.00%	0.013	0.010	0.013

In the middle of Table 3-9 the relative numerical comparison has also been given between thick spacer with new topology and uniform spacer of equal weight. For the full coverage case the damping improvement is only in the order of 2.27% at 1st mode and 8.37% at 2nd mode, while for the partial case up to 7th mode there exist relative improvement in the order of 18.13% at 1st mode, 31.47% at 2nd mode and 23.23% at 3rd mode, 14.36% at 4th mode etc.

3.2.6.2 Case Study II:

In this section different modeling and optimization strategy will be followed. As a second case study the modelling approach proposed by Yellin [107] will be adapted such that the periodic unit cells of topologically optimized stand-off layer can be used as building block of a treated beam.

Previously, at the introductory part the advantage of this methodology was explained as a method of creation of periodically arranged unit cells that return results either amplitude reduction due to suppression of propagating waves or locally resonating attenuation zones due to increased deformation of viscoelastic layer [138,139,140]. For this purpose again a small segment of the beam as, 1/10 of the 250 mm treated beam was considered.

The unit cell exposed to a deformation state statically, that mimics the state of deformation, during cyclic motion by applying sinusoidal load with assumed shear force that is also generated during relative motion. The simply supported boundary condition is applied over the lower left corner of unit cell such that the motion both in $-x$ and $-y$ direction is restrained while the motion of right bottom corner is restrained in $-y$ direction only. This boundary condition mimics the vibration deformation of treated beam under sinusoidal distributed load as shown in Figure 3-34. Moreover, for this case, a distributed shear loading is also assumed applied at the interface nodes between viscoelastic and stand-off layer. This shear load represents the shear load due to shear stress exists during flexural motion. Then the material layout of of this unit cell was found by optimizing the volume of stand-off layer as design space.

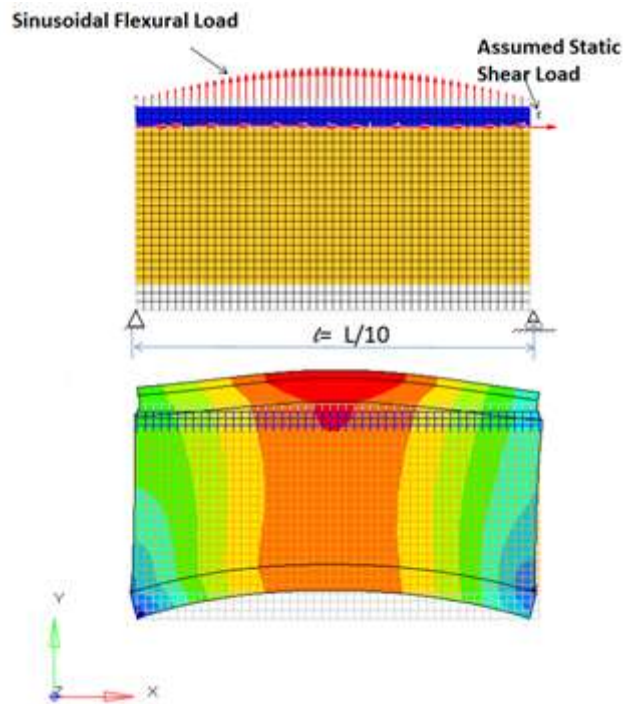


Figure 3-34 Deformation pattern of the unit cell of treated beam with stand-off layer under assumed load cases.

Two static analysis steps are performed prior to the optimization step as base analysis. In optimization step, the property card of stand-off layer is selected as design domain using DESVAR cards in Optistruct. In this case the weighted compliance response card DESRP1 that will be used as objective function was created. In this formulation the two or more static subcases are simultaneously considered during optimization process according to their weights which represents effects of each individual load. The ideal stand-off layer is the one that has infinite shear stiffness while minimum bending stiffness [107]. Therefore the weight parameter for shear load kept maximum relative to the flexural load such that the terms assigned were $\omega_{flex} = 0.5$; $\omega_{shear} = 1$, respectively. For constraining the material volume to be used in final optimized layout, the VOLFRAC response was also created using same card. This card represents the upper bounds of material volume fraction compared to original volume of total design. Therefore in this case the maximum value of 0.30 was set for this response. Upon minimization of weighted compliance the topology extracted for the unit cell is given in Figure 3-35.

The whole treated beam is then recreated by assuming it to be formed from repeated cells as shown in Figure 3-35.

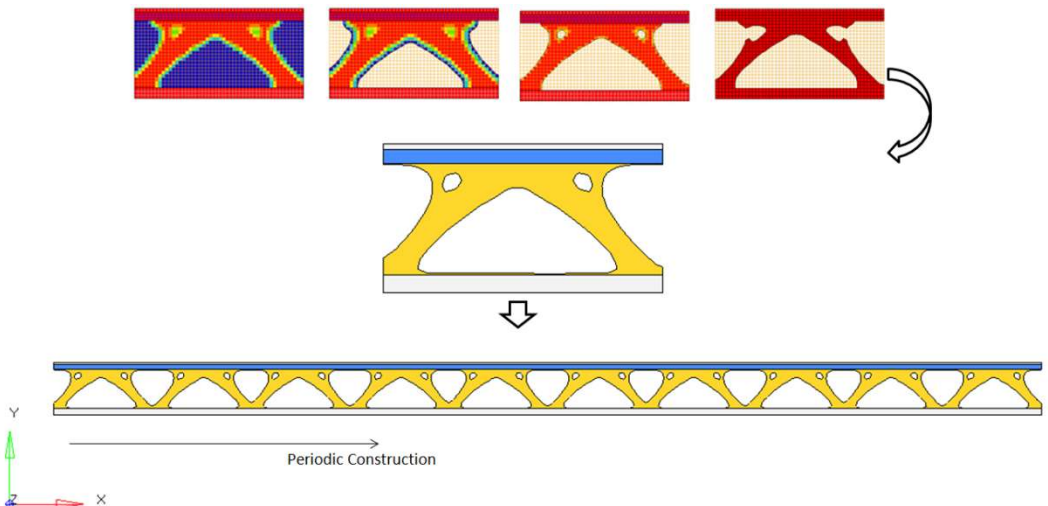


Figure 3-35 Topology optimization result for the treated unit cell (up)-treated beam with periodic units cells (down)

The modal analysis has been performed to visualize the deformation pattern within viscoelastic layer. The following Figure 3-36 and Figure 3-37 shows the mode shapes of cantilever beam created via building repeated optimized unit cell topology. From the deformation state of each cells one can notice that the viscoelastic layer exposed again to irregular deformation pattern and as a result the shear deformation. The irregularity increases for the higher modes because of extracted shape of unit cell and the movement of base vibrating beam. Moreover the local resonances within each unit cell also takes place which cause frequency band gaps in frequency response functions.

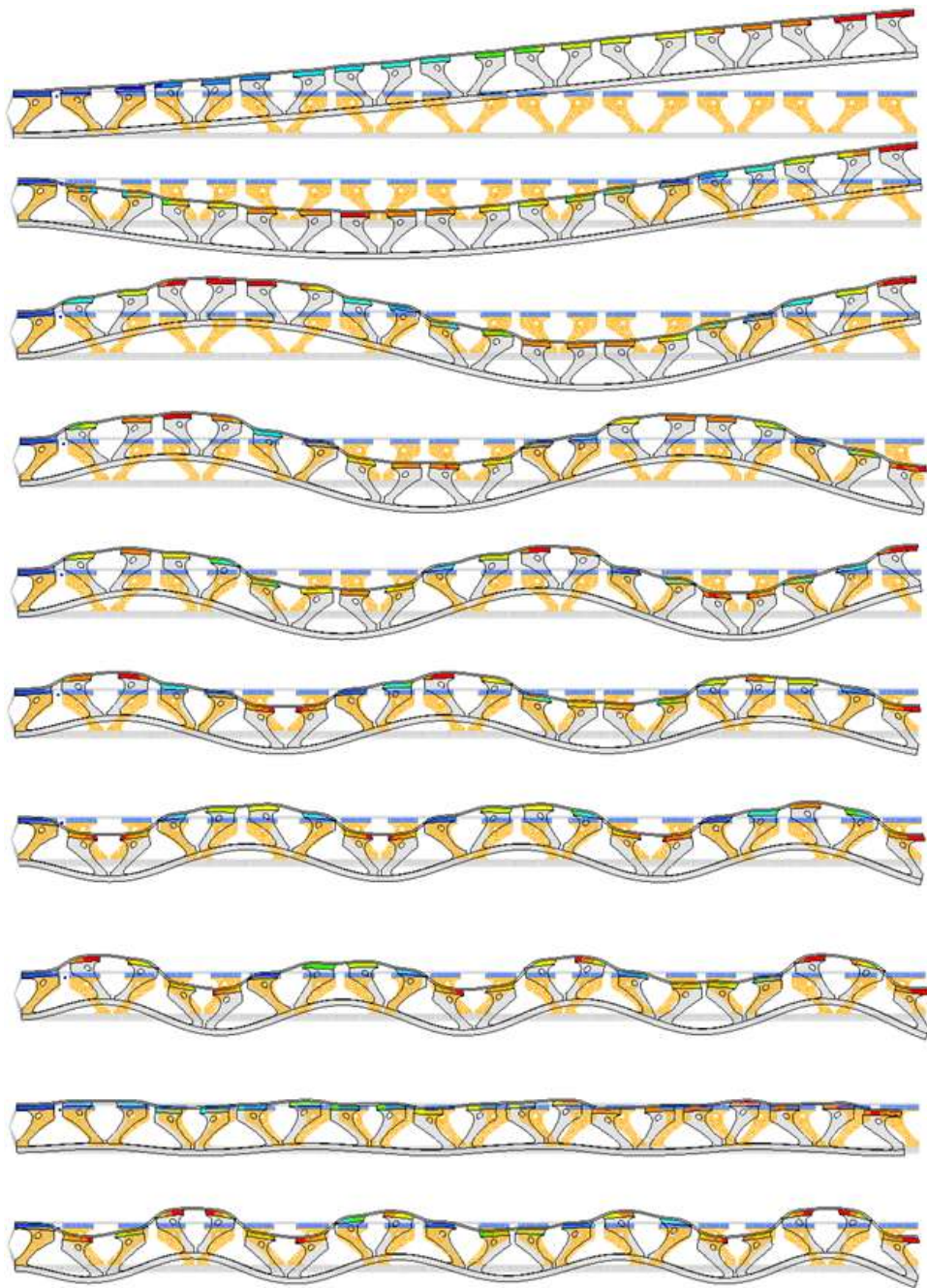


Figure 3-36 Mode shapes of cantilever beam with optimized stand-off (Case II)

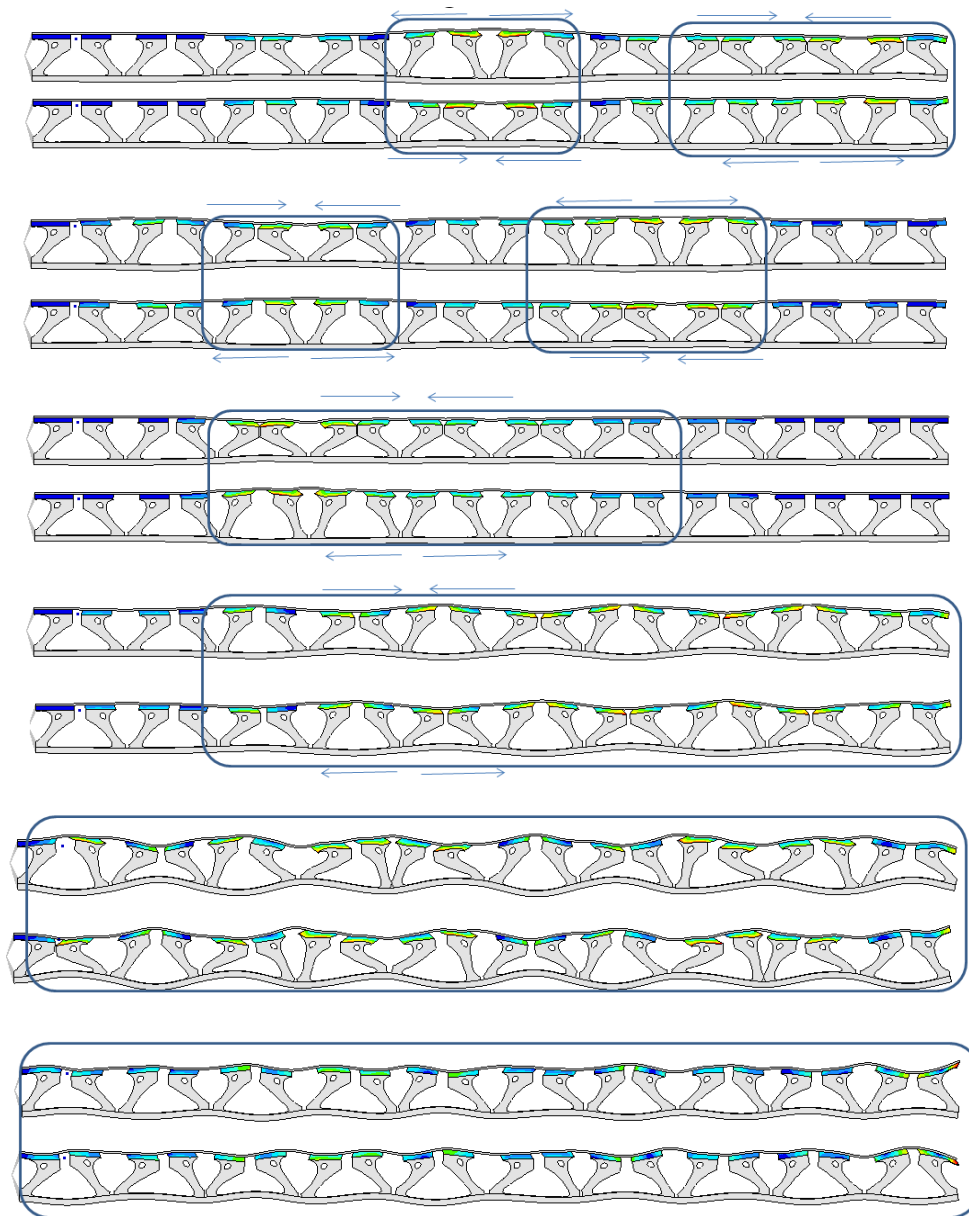


Figure 3-37 Mode shapes of cantilever beam with optimized stand-off (Case II) in the range of 8kHz-12kHz

The following Figure 3-38 shows the frequency response function of whole beam with optimized stand-off layer built with unit cells.

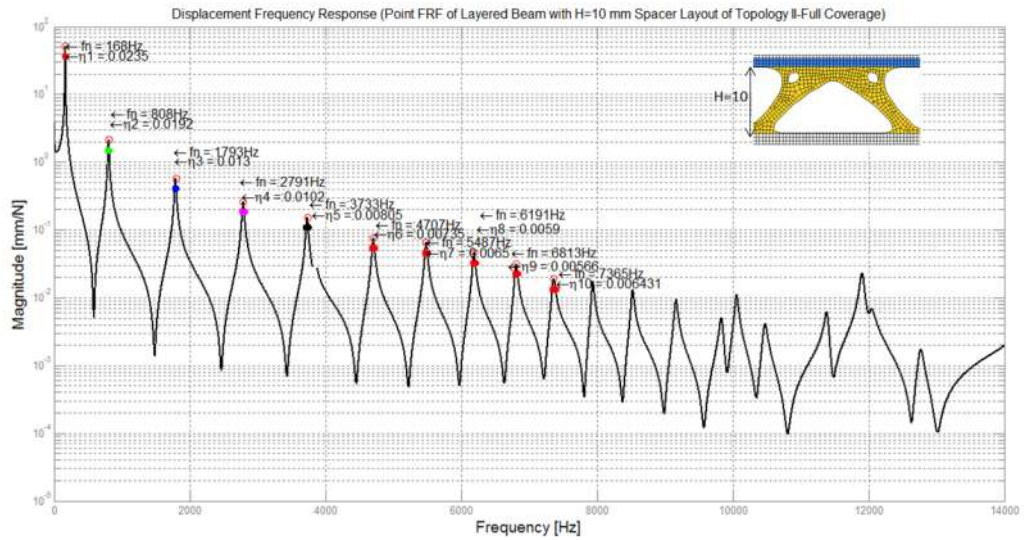


Figure 3-38 Frequency response function of treated beam with stand-off layer with topology of unit cell.

In order to compare the performance of this newly generated stand-off layer with layer that has equivalent mass, a new uniform layer is modeled with less thickness ($H=3.45$ mm) but same weight. The following Figure 3-39 shows the frequency response function of beam with equally weighted uniform stand-off layer.

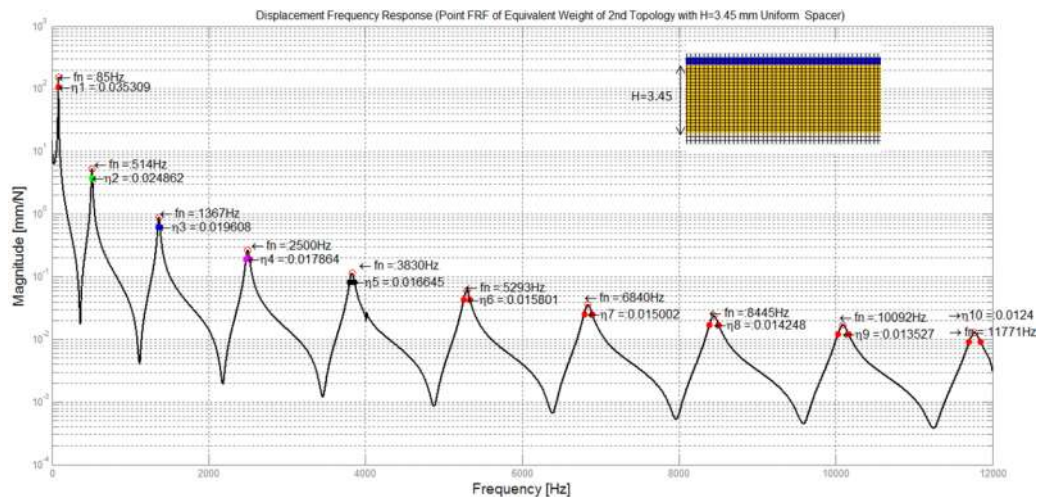


Figure 3-39 Frequency response function of uniform stand-off layer with equivalent mass.

As we followed in previous case study, some cuts were incorporated into new stand-off geometry in suitable locations (Figure 3-40) in order to increase bending flexibility more and local strain energies at the vicinity of the cuts.

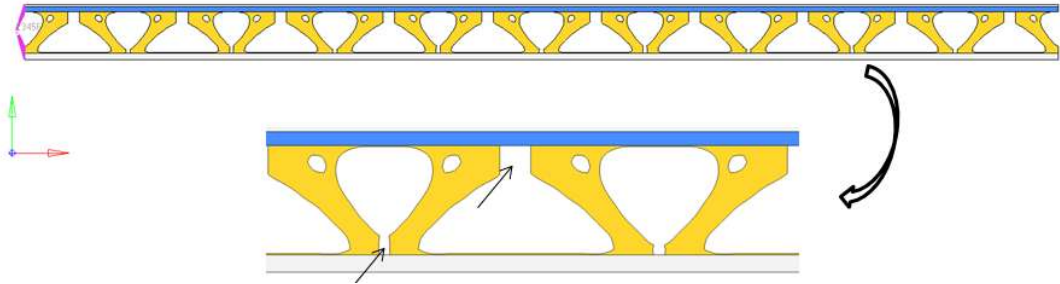


Figure 3-40 Addition of cuts into stand-off layer with unit cell topology.

The viscoelastic layer also partially covered to the stand-off layer and its frequency response function is given Figure 3-41.

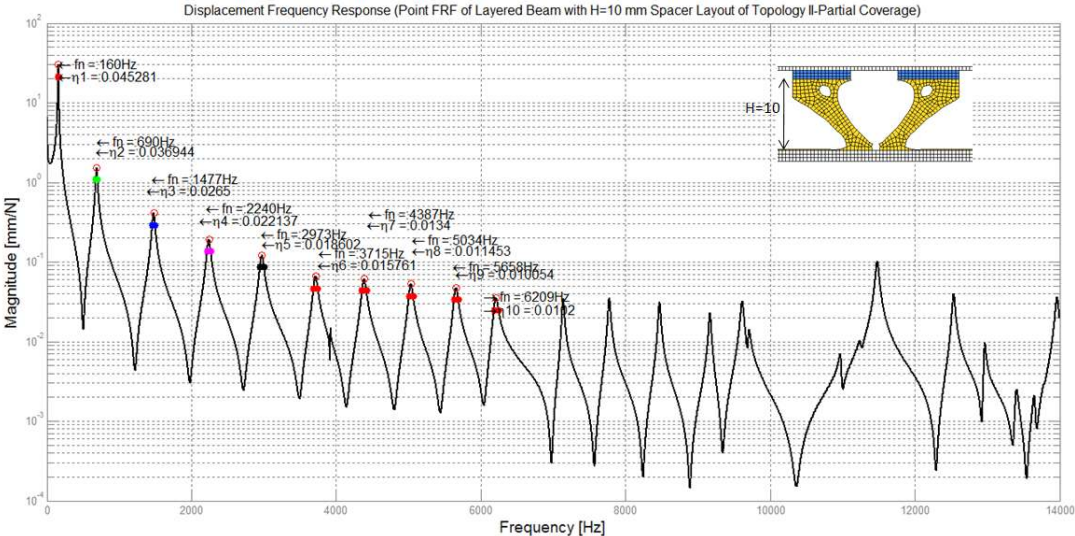


Figure 3-41 Frequency response function of partially treated beam with optimized stand-off layer.

The following Figure 3-42 shows overall comparison of frequency response functions for fully treated original uniform (dashed gray--), fully treated spacer with new topology (black-), partially treated spacer with new topology (orange-) and uniform spacer of equal weight (dashed red--).

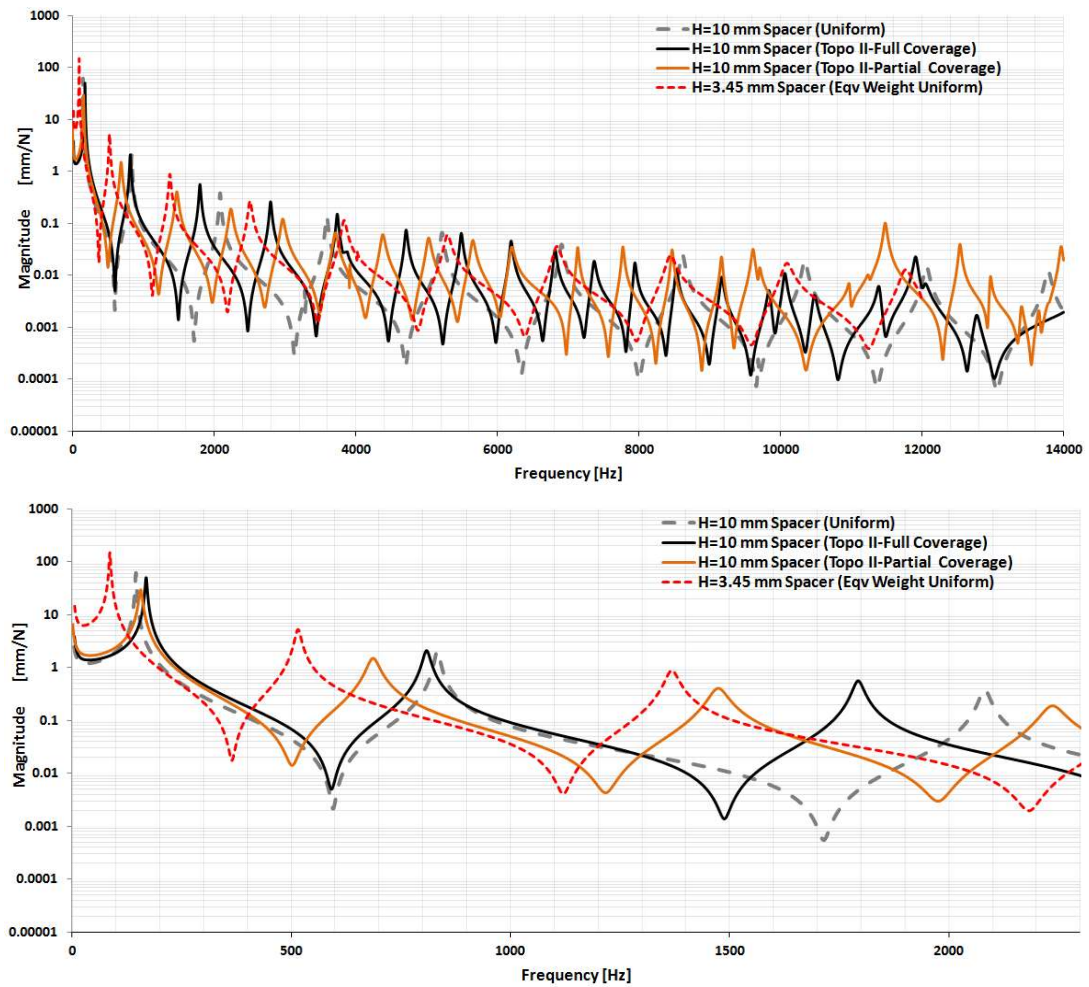


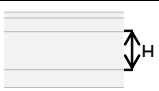
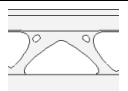


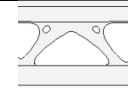
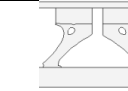
Figure 3-42 Overall comparison of frequency response functions

One can see from Figure 3-42 that the new layout of fully and partially treated thick spacer with new topology has lower amplitude with broader peaks and with overall reduced weight compared to reference beam structure with uniform spacer. However due to reduction of bending rigidity after removal of material from spacer, the frequency of new beam has shifted to the left as in previous case. However upon 10 kHz there exist responses with higher amplitudes with thick partial configuration.

However it is quite visible from response function that thinner layer has again higher response amplitude especially in lower frequencies but they are gradually diminished at higher frequencies. The shape of response curve tends to be broader due to increased damping

In terms of damping performance the numerical results are given for each of the case considered previously in the following Table 3-10. The results include comparison in terms of total weight percentage, frequency and loss factors for the first ten modes. The damping performance of optimized fully and partially treated beam compared to uniform case as considered to be reference configuration. Minimizing weighted compliance results %36.76 mass reduction as well as damping improvement %31.28 for the first mode, %39.13 for the second mode, %21.90 for the third mode for fully treated case and the relative improvement is until 4th mode. Additionally for the partial case with same topology, %41.1 mass reduction as well as damping improvement of %153.07 for the first mode, %167.39 for the second mode, %152.38 for the third mode compared to reference model with 10 mm uniform stand-off layer, was achieved. The improvement is continuous for all modes with gradual decrease in percentage for the partial treatment.

Table 3-10 Summary of the optimization results (CASE II-H=10mm)

(CASE II-H=10mm)						
2nd Topology Relative Damping Performance w.r.t. Uniform Stand-Off Layer						
Frequency f[Hz]			Loss Factor $\eta=2\zeta$			
H=10						
						
Mode #	Uniform Full Coverage	Optimized Full Coverage	Optimized Partial Coverage	Uniform Full Coverage Weight=100%	Optimized Full Coverage Weight=63.24%	Optimized Partial Coverage Weight=58.90%
Prct [%]						
1++	146.00	168.00	160.00	0.018	0.024	0.045
				-	↑ 31.28%	↑ 153.07%
2++	833.00	808.00	690.00	0.014	0.019	0.037
				-	↑ 39.13%	↑ 167.39%
3++	2082.00	1793.00	1477.00	0.011	0.013	0.027
				-	↑ 21.90%	↑ 152.38%
4++	3589.00	2791.00	2240.00	0.009	0.010	0.022
				-	↑ 14.61%	↑ 148.31%
5-+	5216.00	3733.00	2973.00	0.008	0.008	0.019
				-	↓ -1.23%	↑ 129.63%
6-+	6905.00	4707.00	3715.00	0.007	0.007	0.016
				-	↓ -1.35%	↑ 113.51%
7-+	8609.00	5487.00	4387.00	0.007	0.006	0.013
				-	↓ -5.88%	↑ 97.06%
8-+	10338.00	6191.00	5034.00	0.006	0.006	0.012
				-	↓ -4.84%	↑ 85.48%
9-+	12057.00	6813.00	5658.00	0.006	0.006	0.010
				-	↑ 0.00%	↑ 77.19%
10++	13775.00	7365.00	6209.00	0.005	0.006	0.010
				-	↑ 23.08%	↑ 96.15%

If we compare the loss factor values for the thinner stand-off layer with thicker one for the uniform case, one can notice the thinner stand-off layer yields higher loss factor values for all three modes. Therefore, in order to investigate the thickness reduction with new cell topology, the whole beam was recreated using scaled unit cell topology as shown in Figure 3-43.

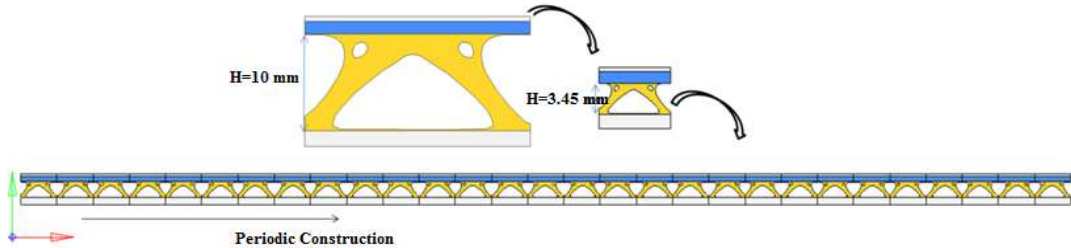


Figure 3-43 Rebuilding of treated beam with scaled unit cell topology

With reduced thickness value, the direct frequency response analysis was repeated and the frequency response functions are generated as shown in Figure 3-44 to Figure 3-45.

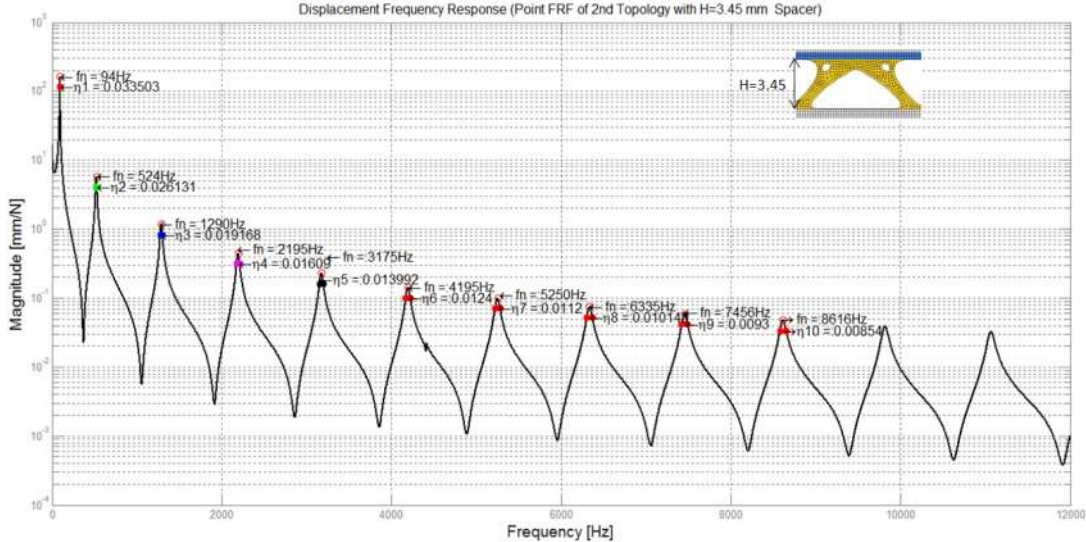


Figure 3-44 Frequency response function of scaled stand-off layer with same unit cell topology

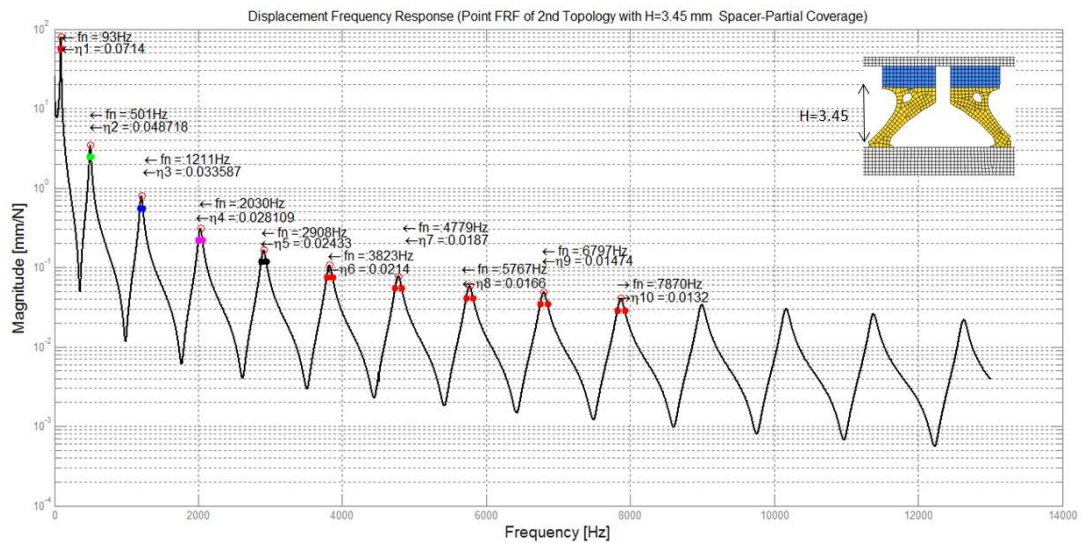


Figure 3-45 Frequency response function of scaled stand-off layer with partially covered same unit cell topology

Comparing all above cases in one plot shows the effectiveness of new topology with reduced thickness in terms of damping (Figure 3-46). The results show that the thicker optimized stand-off layer has advantage of reduced vibration amplitude at lower frequencies. However the thinner stand-off layer with partial treatment has improved damping performance together with reduced vibration amplitudes at higher frequencies. While the damping capacity was increased, the frequency of the structure was lowered because of reduced bending rigidity of the thinner structure.

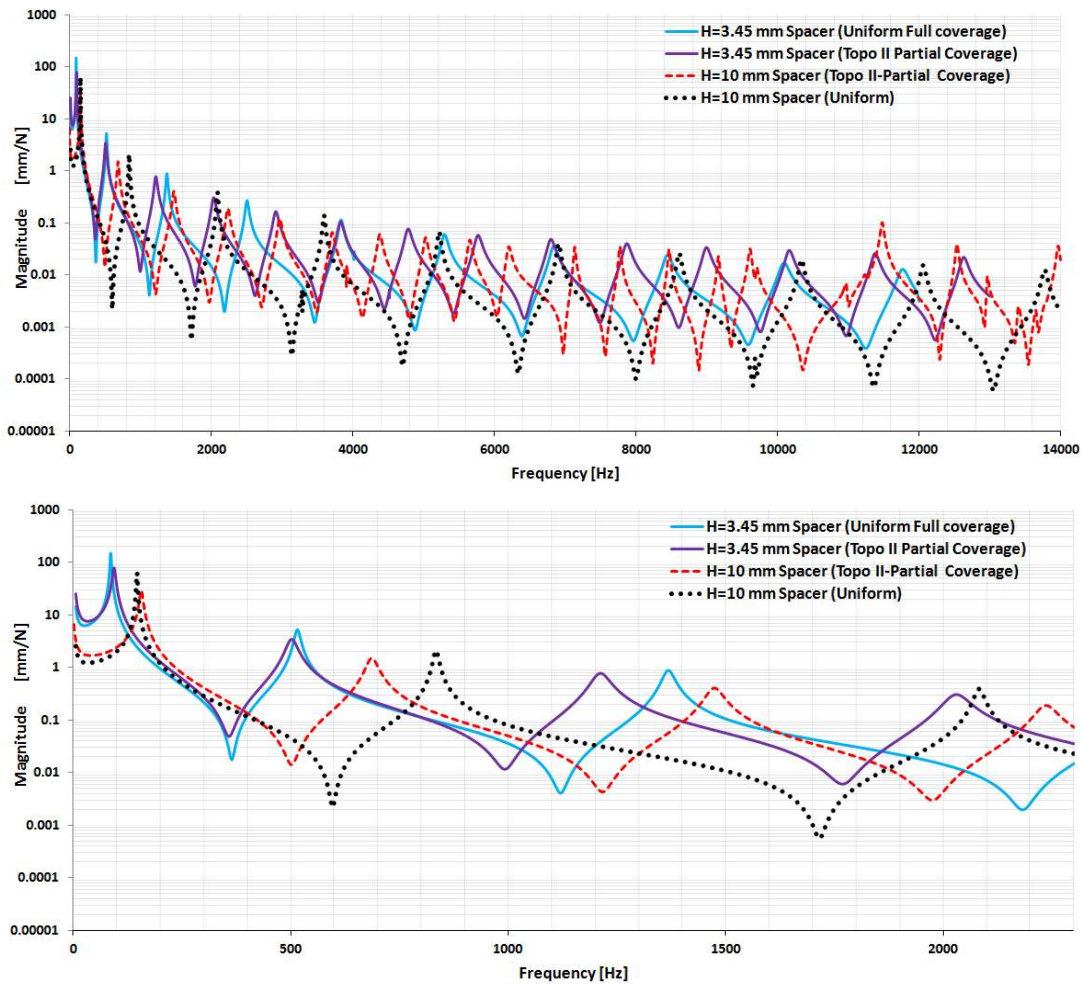

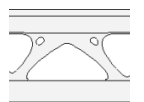
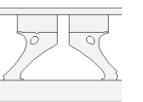
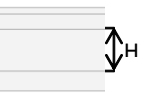

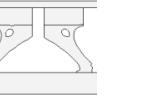


Figure 3-46 Overall comparison of frequency response functions

The following Table 3-11 summarizes the results numerically. The modal loss factors and frequency of resonances as well as loss factors are tabulated for the first ten modes of each configuration for thinner stand-off layer with periodic unit cell topology. For this new topology minimizing the thickness of stand-off layer compared to H=10 mm stand-off layer, results further %52.51 decrease in mass for the uniform cases. However the relative damping increase only exists for partially treated configuration, except for the 2nd mode for full coverage with 4.82% relative improvement only. Compared to uniform case the partial configuration has %101.98 for the 1st mode, %95.58 for the 2nd mode, %71.43 for the 3rd mode compared to H=3.45 mm uniform case. The relative improvement is for all ten modes with gradual decrease in percentage value.

Table 3-11 Summary of the optimization results (CASE II-H=3.45 mm)

(CASE II-H=3.45mm)						
2nd Topology Relative Damping Performance w.r.t. Uniform Stand-Off Layer						
Frequency f [Hz]			Loss Factor $\eta=2\zeta$			
H=3.45						
						
Mode #	Uniform Full Coverage	Optimized Full Coverage	Optimized Partial Coverage	Uniform Full Coverage Weight=100%	Optimized Full Coverage Weight=79.70%	Optimized Partial Coverage Weight=74.44%
Prct [%]						
1-+	85.00	94.00	93.00	0.035	0.034	0.071
				-	↓ -5.10%	↑ 101.98%
2++	514.00	524.00	501.00	0.025	0.026	0.049
				-	↑ 4.82%	↑ 95.58%
3-+	1367.00	1290.00	1211.00	0.020	0.019	0.034
				-	↓ -2.04%	↑ 71.43%
4-+	2500.00	2195.00	2030.00	0.018	0.016	0.028
				-	↓ -10.06%	↑ 56.98%
5-+	3830.00	3175.00	2908.00	0.017	0.014	0.024
				-	↓ -15.66%	↑ 46.39%
6-+	5293.00	4195.00	3823.00	0.016	0.012	0.021
				-	↓ -21.52%	↑ 35.44%
7-+	6840.00	5250.00	4779.00	0.015	0.011	0.019
				-	↓ -25.33%	↑ 24.67%
8-+	8445.00	6335.00	5767.00	0.014	0.010	0.017
				-	↓ -28.87%	↑ 16.90%
9-+	8445.00	7456.00	6797.00	0.014	0.009	0.015
				-	↓ -31.11%	↑ 8.89%
10-+	10092.00	8616.00	7870.00	0.012	0.009	0.013
				-	↓ -31.45%	↑ 5.65%

As summary if we compare the results obtained for both thickness value of stand-off layers, namely, H=10 mm and H=3.45 mm, the following (Figure 3-47) summarizes the result obtained in terms of frequency response characteristic. Compared to thicker uniform stand-off layer, the thinner partially treated stand-off with optimized configuration has better damping performance in all modes with slight increase in response amplitude.

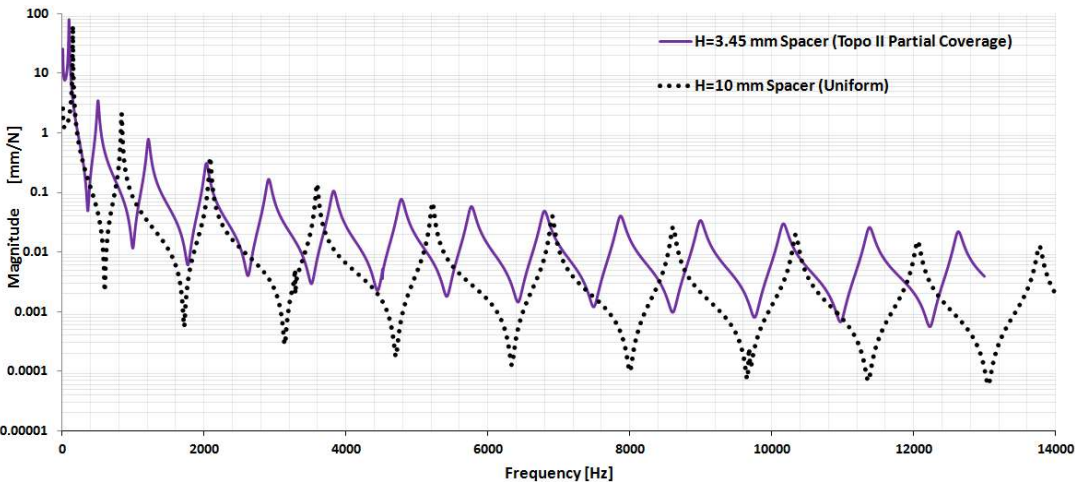


Figure 3-47 Overall comparison of frequency response functions (H=3.45 mm-partially treated) & (H=10 mm-uniform fully treated)

The numerical results are summarized in the following Table 3-12. The relative percentages are calculated by comparing corresponding individual configuration, that is, the uniform, optimized and partial cases were all compared to each other for thick and thin stand-off layer. Based on the numerical results the thinner uniform configuration has higher relative increase in damping with increasing relative percentage value. However the overall damping capacity is highest at thinner partially covered stand-off with same topology of unit cell in all modes of vibration.

Table 3-12 Results of Optimization for H=10mm and H=3.45 mm Stand-off Layer

(CASE II-H=10 vs H=3.45mm)								
2nd Topology Relative Damping Performance								
Loss Factor $\eta=2\zeta$								
Mode #	H=10			H=3.45			Uniform-Eq.Weight Full Coverage	Weight=74.44%
	Uniform-Full Coverage Weight=100%	Optimized Full Coverage Weight=63.24%	Uniform-Full Coverage Weight=58.90%	Optimized (H=10mm) vs Uniform (H=3.45 mm)	Optimized Partial (H=10mm) vs Uniform (H=3.45 mm)	Uniform-Full Coverage Weight=100%		
1+++	0.018	0.024	0.045	↓33.43%	↑28.33%	↑97.21%	0.034	0.071
2+++	0.014	0.019	0.037	↓22.89%	↑48.19%	↑80.43%	0.026	0.049
3+++	0.011	0.013	0.027	↓34.69%	↑35.20%	↑86.67%	0.019	0.034
4+++	0.009	0.010	0.022	↓43.02%	↑23.46%	↑101.12%	0.016	0.028
5+++	0.008	0.008	0.019	↓51.81%	↑12.05%	↑104.94%	0.014	0.024
6+++	0.007	0.007	0.016	↓53.80%	↑0.00%	↑113.51%	0.012	0.021
7+++	0.007	0.006	0.013	↓57.33%	↓-10.67%	↑120.59%	0.011	0.019
8+++	0.006	0.006	0.012	↓58.45%	↓-19.01%	↑129.03%	0.010	0.017
9+++	0.006	0.006	0.010	↓57.78%	↓-25.19%	↑136.84%	0.009	0.015
10+++	0.005	0.006	0.010	↓48.39%	↓-17.74%	↑138.46%	0.009	0.013

In the middle of Table 3-12 the relative numerical comparison has also been given between thick spacer with new topology and uniform spacer of equal weight. For the full coverage case no improvement was achieved in terms of damping while for the partial case up to 6th mode there exist relative improvement in the order of 28.33% at 1st mode, 48.19% at 2nd mode and 35.20% at 3rd mode, 23.46% at 4th mode and 12.05% at 5th mode.

3.2.6.3 Case Study III:

In this section same modelling and optimization strategy will be followed as it was the case in previous case study. The same unit cell geometry of 1/10 of the 250 mm treated beam is considered again under different boundary condition as well as different objective and constraints. The pinned boundary condition is applied over each corner of unit cell such that the motion both in $-x$ and $-y$ direction is restrained. This boundary condition mimics the vibration deformation of treated beam under sinusoidal distributed load only as shown in Figure 3-48.

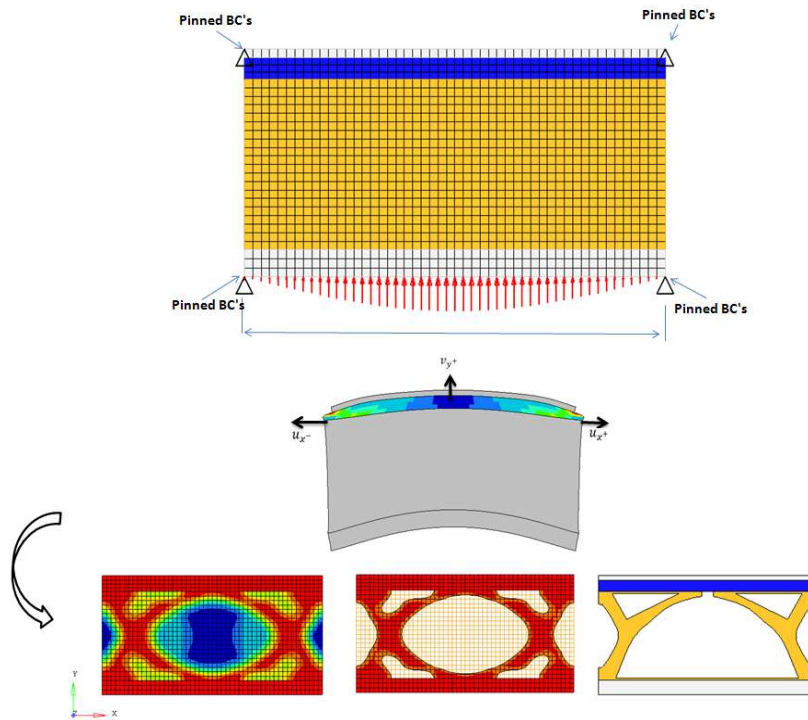


Figure 3-48 Deformation pattern and new topology of the unit cell of treated beam with stand-off layer under assumed load cases.

Static analysis step is performed prior to the optimization step as base analysis under flexural sinusoidal load and pinned boundary condition applied to all vertices of unit cell. In optimization step, the property card of stand-off layer is selected as design domain using DESVAR cards in Optistruct. Then, instead of selecting the

compliance response this time, the three displacement responses were created using DESRP1 cards. Two of the displacement responses were defined to be used as constraints. One of them represents the displacement of top middle node in y direction, u_{y+} , the other two were selected as two right and left top vertices of stand-off layer, such that the right one represents the displacement in positive $-x$ direction, u_{x+} and the left one represents the displacement in negative $-x$ direction, u_{x-} as depicted in Figure 3-48. Based on the fact that the ideal spacer layer has infinite shear stiffness while having lower bending rigidity [107], the two displacement value that are in lateral direction, u_{x+} and u_{x-} were selected as constraints with small value of deformation to induce higher stiffness value in lateral direction. The other displacement response in positive $-y$ direction was selected as objective function such that its value was maximized under reduced volume constraint. This condition in fact creates a material removal that lessens the bending rigidity of unit cell, in other words increase the overall unit cell flexibility while having increased shear stiffness due to the restrained shear motion of stand-off medium at the interface along the beam, which in turn results the deformation of viscoelastic layer during flexural modes of beam, due to its low shear modulus compared to top constraining layer and bottom stand-off layer material.

For constraining the material volume to be used in final optimized layout, the VOLFRAC response was also created. This response represents the upper bounds of material volume fraction to be used in final design concept compared to original volume of total design. Therefore in this case the maximum value of 0.30 was set for this response.

The extracted topology was modified such that the only upper portion was left to support viscoelastic layer (Figure 3-48). After arranging each cell periodically modal analysis has been performed with beam as a whole to visualize the deformation pattern within viscoelastic layer with this new topology. Based on the modal shapes calculated, the increase in deformation within viscoelastic layer is visible. Especially at higher modes while beam has less deformation response the upper portion of

stand-off layer has irregular deformation patterns that is expected to induce shear deformation within viscoelastic layer (Figure 3-50, Figure 3-51).

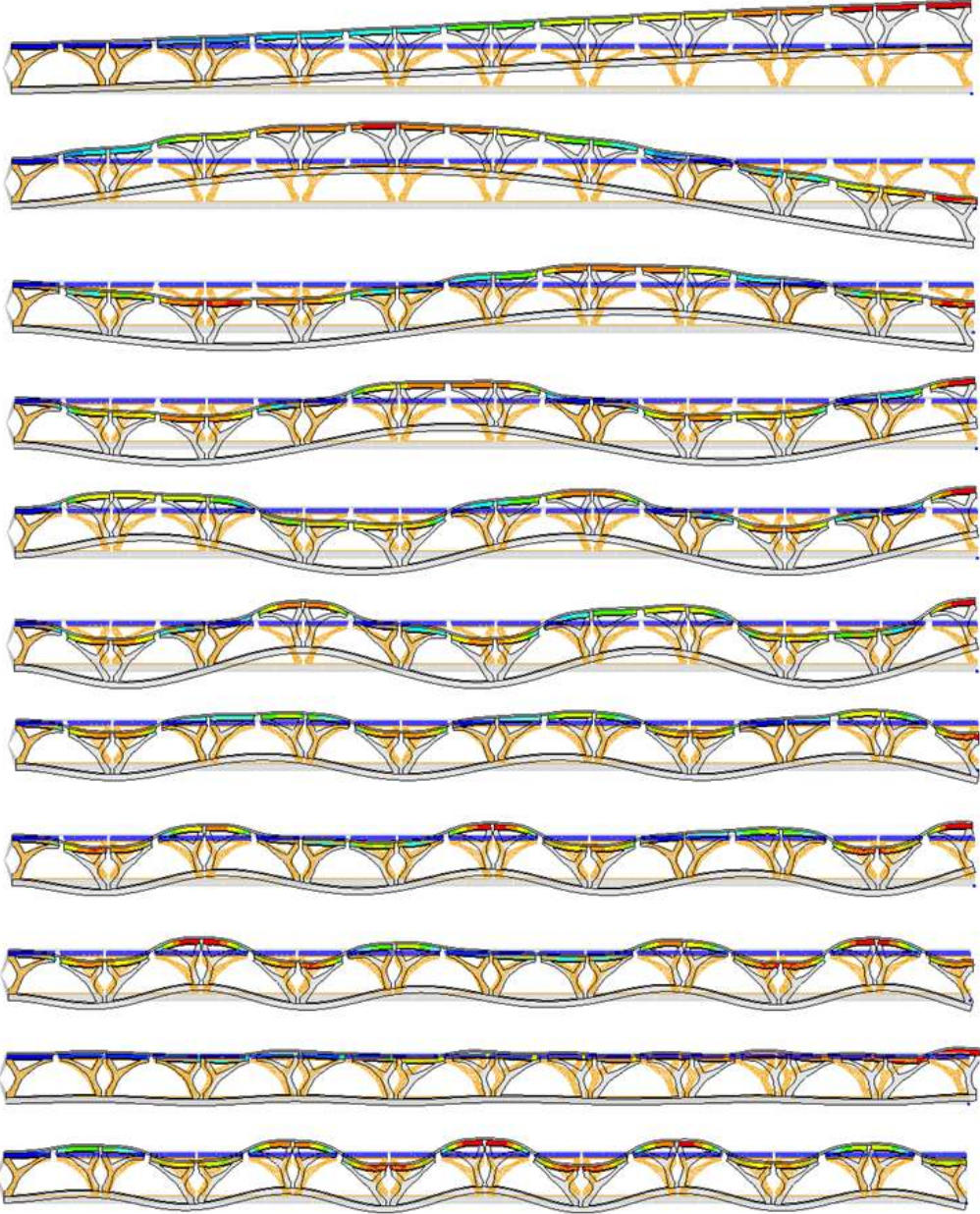


Figure 3-49 First ten mode shapes of treated cantilever beam with optimized stand-off (Case III)

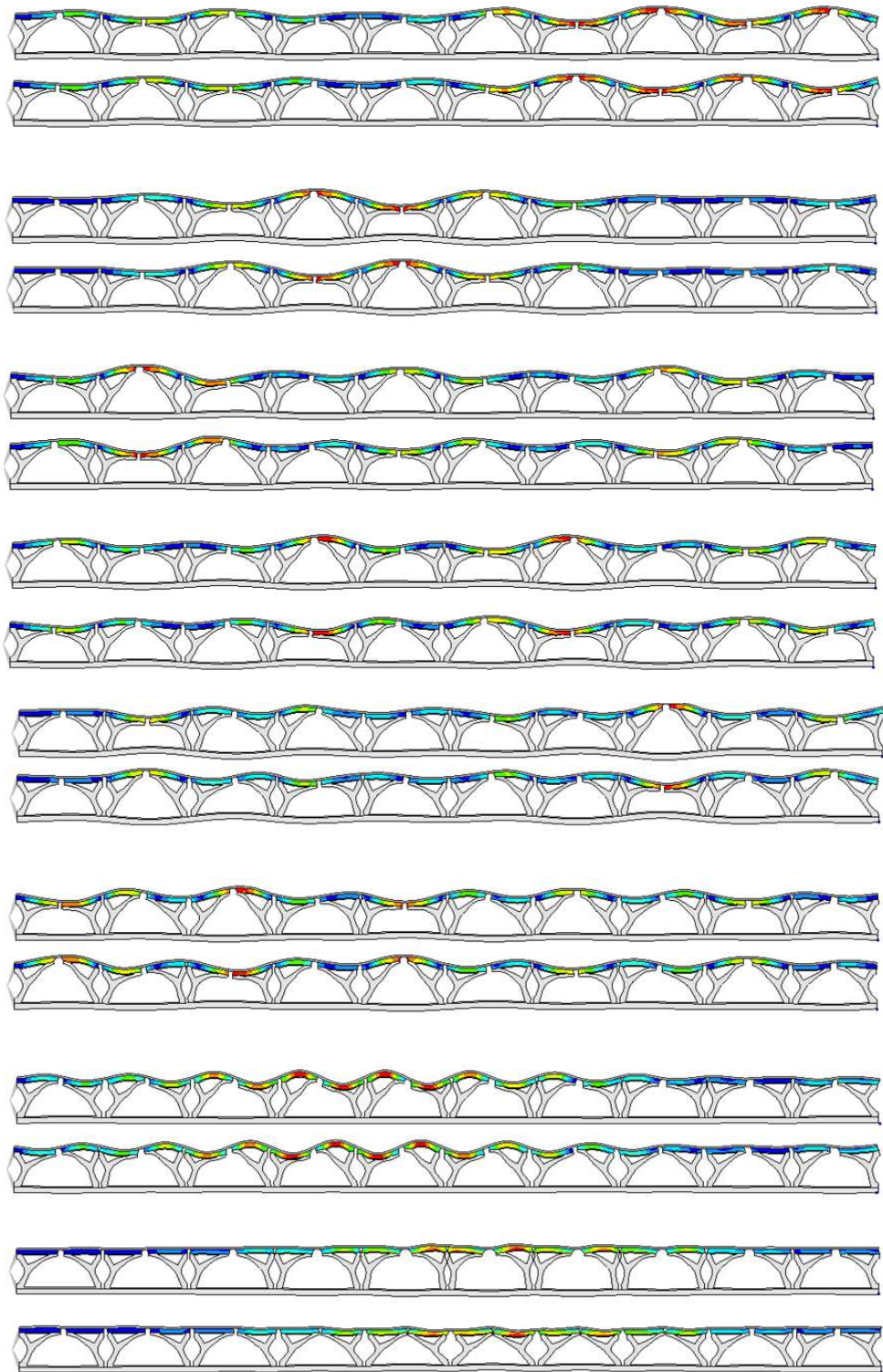


Figure 3-50 Mode shapes of treated cantilever beam at higher modes with optimized stand-off (Case III)

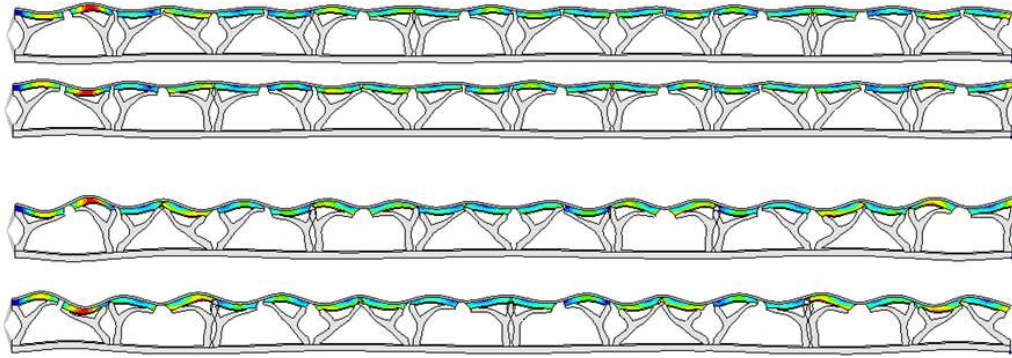


Figure 3-51 Continued

The following Figure 3-52 shows the frequency response function of fully treated beam with optimized stand-off layer for the first ten modes. One can easily see the obvious attenuation zone between 5 kHz and 7.5 kHz and reduction of vibration amplitude beyond this attenuation zone. Moreover the loss factor also higher for the first ten modes compared to beam with uniform fully treated stand-off layer.

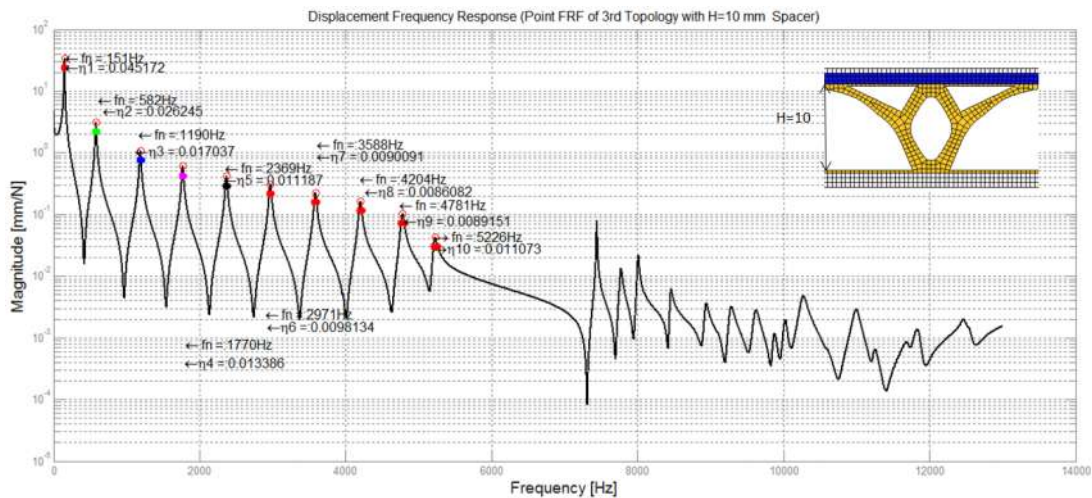


Figure 3-52 Frequency response function of fully treated beam with optimized unit cell topology (Topology III)

Partial coverage with additional cuts in stand-off layer further increase the damping capacity as well as extending the attenuation zone as to be 4 kHz and 7.5 kHz with slight increase in amplitudes beyond which the response amplitude was lowered compared to full treatment.

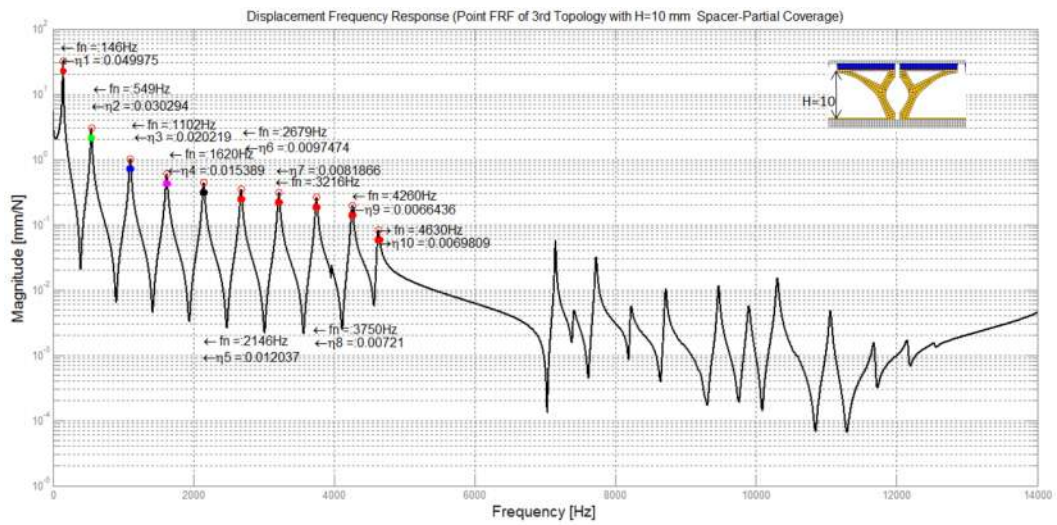


Figure 3-53 Frequency response function of treated beam with optimized unit cell topology with added cuts.

In order to compare the performance of stand-off layer with new unit cell topology with the uniform stand-off layer that has equal weight a new stand-off layer was created with reduced thickness value of $H=2.64$ mm. The frequency response function of latter uniform case is given in Figure 3-54.

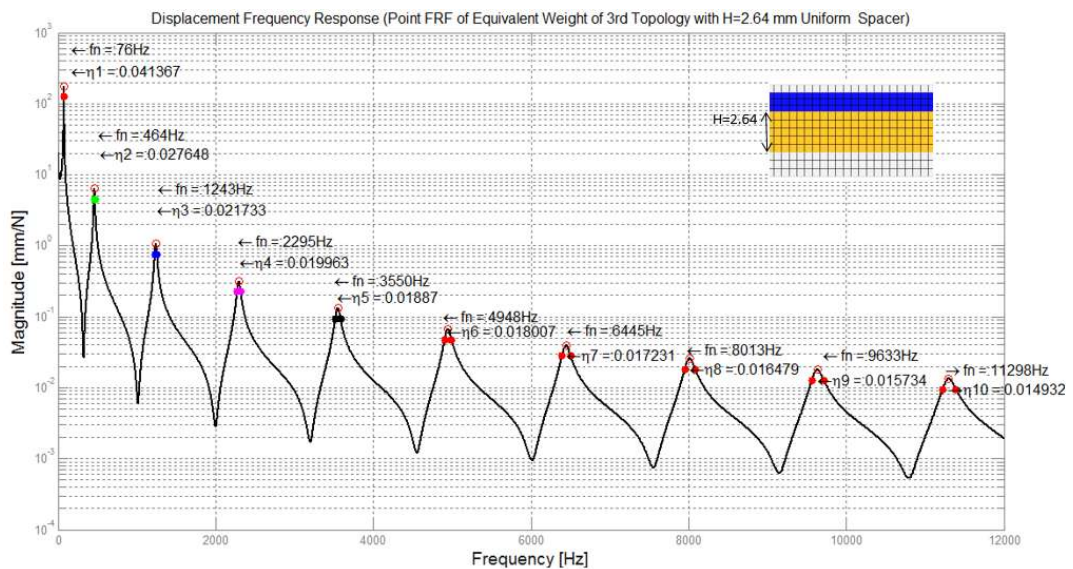


Figure 3-54 Frequency response function of beam with equally weighted uniform stand-off layer (Case III)

All above results are compared in one plot as shown in Figure 3-55. The thinner uniform case has higher amplitude in lower frequencies than at higher frequencies without having an attenuation zone while the thicker full coverage optimized case has lower amplitude in lower frequencies than original uniform base model. Also there exists an attenuation zones for both fully and partially covered thick optimized cases making the amplitudes obviously lower especially at higher frequencies with considerably less weight.

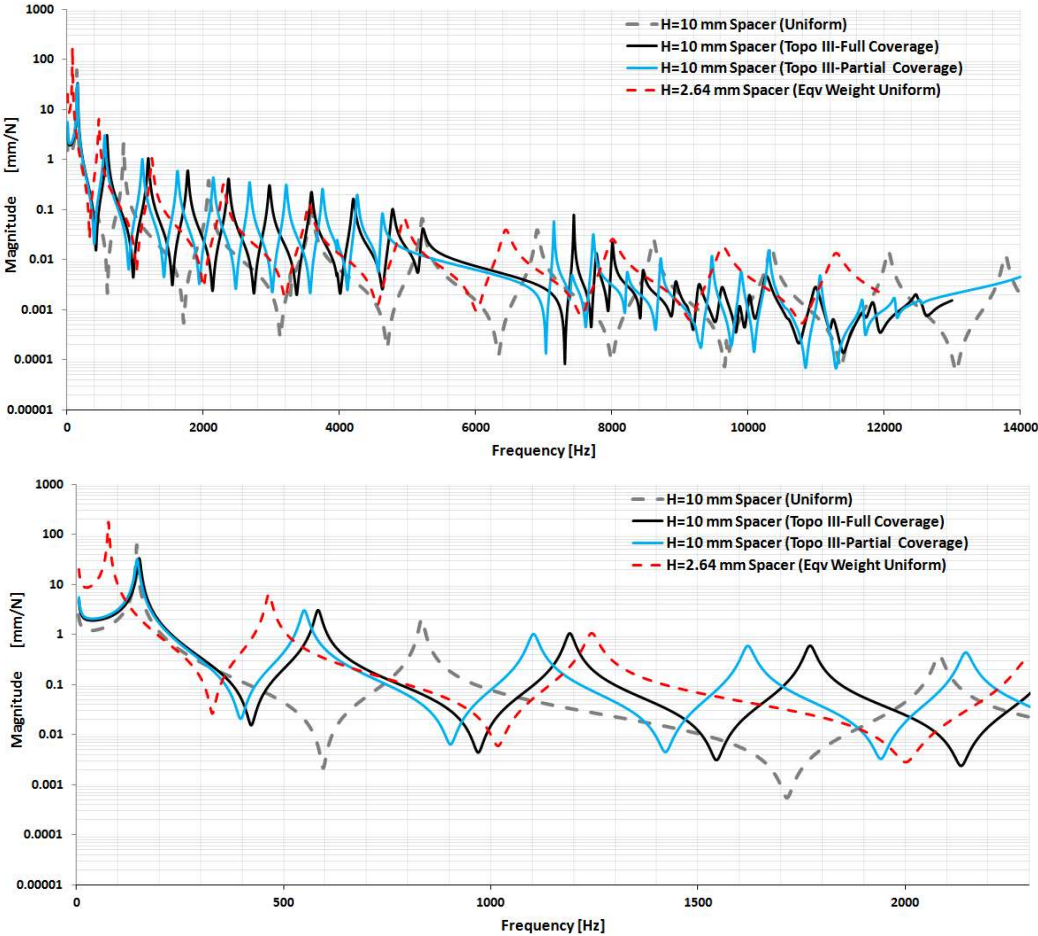


Figure 3-55 Overall comparison of frequency response functions (Case III)

The numerical results for the comparison of above all results are also tabulated in. For the thick layer the results include comparison in terms of weight, frequency and loss factors for the first ten modes. Maximizing displacement in $-y$ direction while constraining the lateral deflection results an optimized layout of stand-off layer which also results %41.84 mass reduction as well as damping improvement %153.21 for the 1st mode, %90.52 for the 2nd mode, %61.20 for the 3rd mode and this improvement also reported not less than the %33 for higher modes for fully treated optimized stand-off layer compared to base analysis model with $H=10$ mm uniform stand-off layer. Additionally relative mass reduction of %45.21 was achieved with partial treatment of same topology and damping improvement is higher in percentage for the same topology for the first ten modes and this relative improvement is numerically %180.1 for the 1st mode, %120.33 for the 2nd mode, %91.54 for the 3rd mode, %72.1 for the 4th mode, %48.33 for the 5th mode with decreasing trend beyond fifth mode.

Table 3-13 Summary of the optimization results (CASE III-H=10mm)

(CASE III-H=10mm)						
3rd Topology Relative Damping Performance w.r.t. Uniform Stand-Off Layer						
Frequency f [Hz]			Loss Factor $\eta=2\zeta$			
H=10						
Mode #	Uniform	Optimized	Optimized	Uniform	Optimized	Optimized
Prct [%]	Full Coverage	Full Coverage	Partial Coverage	Full Coverage	Full Coverage	Partial Coverage
				Weight=100%	Weight=58.16%	Weight=54.79%
1++	146.00	151.00	146.00	0.018	0.045	0.050
				-	↑ 153.21%	↑ 180.10%
2++	833.00	582.00	549.00	0.014	0.026	0.030
				-	↑ 90.52%	↑ 120.33%
3++	2082.00	1190.00	1102.00	0.011	0.017	0.020
				-	↑ 61.20%	↑ 91.54%
4++	3589.00	1770.00	1620.00	0.009	0.013	0.015
				-	↑ 49.75%	↑ 72.10%
5++	5217.00	2369.00	2146.00	0.008	0.011	0.012
				-	↑ 38.44%	↑ 48.33%
6++	6905.00	2971.00	2679.00	0.007	0.010	0.010
				-	↑ 33.03%	↑ 31.67%
7++	8609.00	3588.00	3216.00	0.007	0.009	0.008
				-	↑ 32.97%	↑ 21.15%
8++	10339.00	4204.00	3750.00	0.006	0.009	0.007
				-	↑ 38.09%	↑ 15.61%
9++	12059.00	4781.00	4260.00	0.006	0.009	0.007
				-	↑ 54.22%	↑ 14.36%
10++	13776.00	5226.00	4630.00	0.005	0.011	0.007
				-	↑ 112.42%	↑ 33.96%

In order to investigate the thickness effect of same topology, the scaled model of stand-off layer is recreated as shown in (Figure 3-56) with a thickness value of 2.64 mm that is the same thickness with uniform case with equivalent mass of optimized base model.

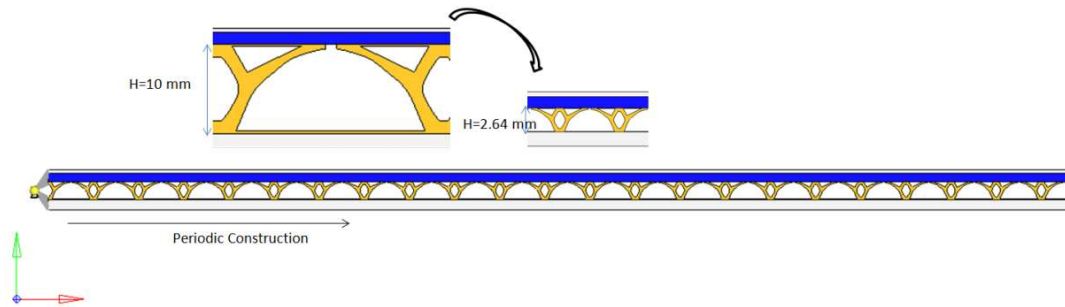


Figure 3-56 Treated beam with scaled model of stand-off layer

The frequency response function of treated beam with reduced thickness value of stand-off layer is given in Figure 3-57. One can notice from this figure that for higher modes of vibration the curve becomes broader and shallower for this topology of stand-off layer.

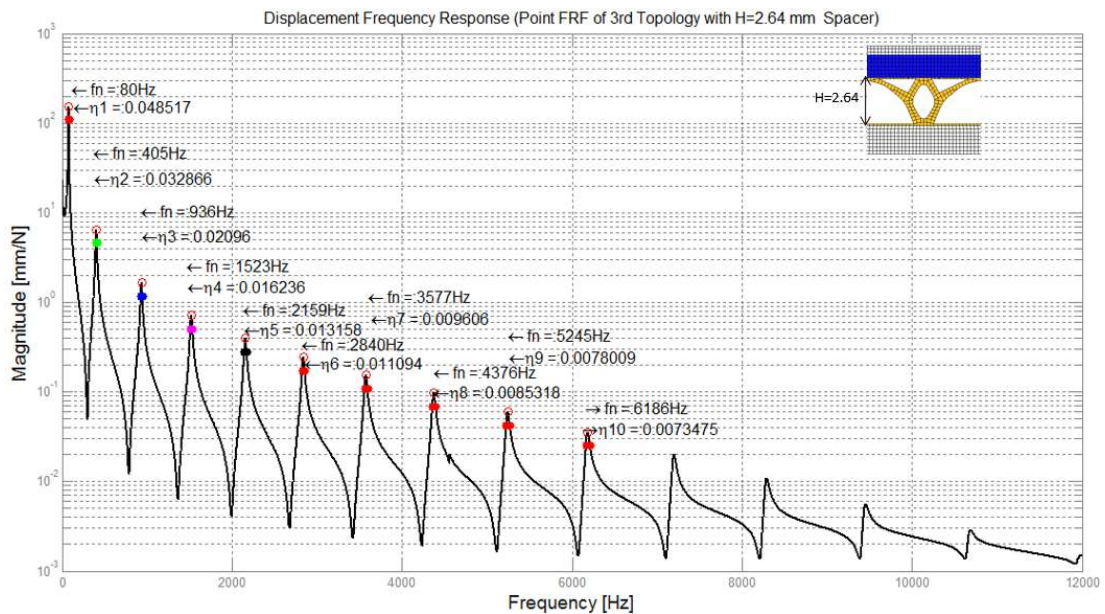


Figure 3-57 Frequency response function of treated beam with reduced thickness value of stand-off layer

Another frequency response function is given in Figure 3-58 for partially treated stand-off layer after addition of cuts between repeated unit cells which gives a little bit more flexibility together with slight increase in loss factors because of increased shear deformation at the vicinity of those cuts.

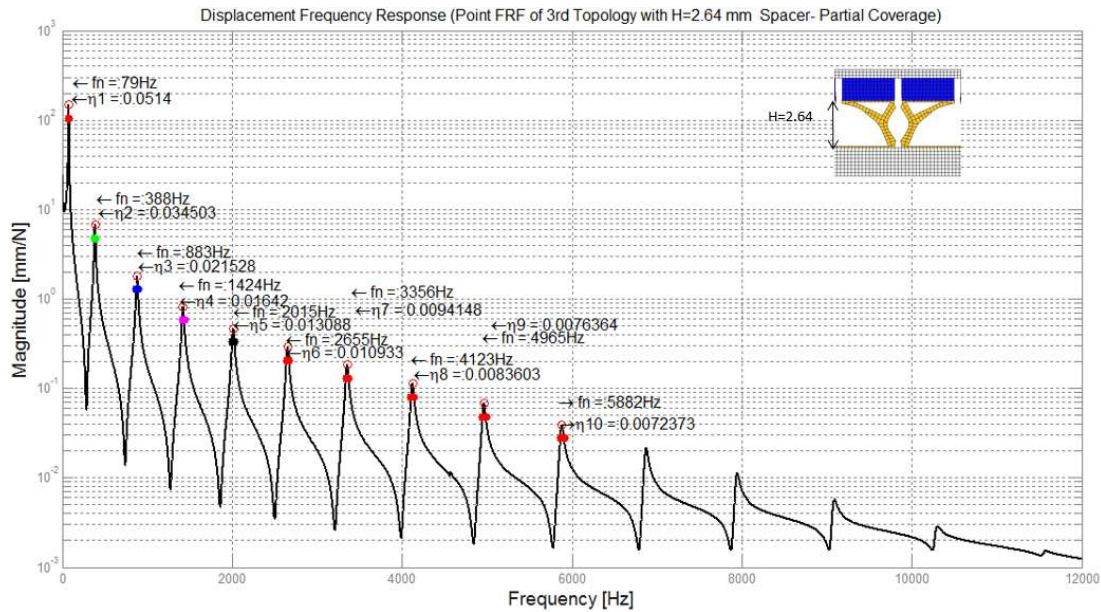


Figure 3-58 Frequency response function of partially treated beam with optimized stand-off layer with cuts

All above results are compared in one plot as shown in Figure 3-59. In this plot one can see that compared to base analysis model the thinner configuration has higher amplitude at lower frequencies while having considerable reduction in amplitude in higher modes of vibration with stand-off layer possessing unit cell topology. Although the thinner configuration has higher amplitude, the relative damping capacity is higher especially for partial thinner configuration. The reduction in amplitude however is further beyond first few modes. Numerically, beyond 5 kHz the amplitude compared to thick uniform case almost diminished.

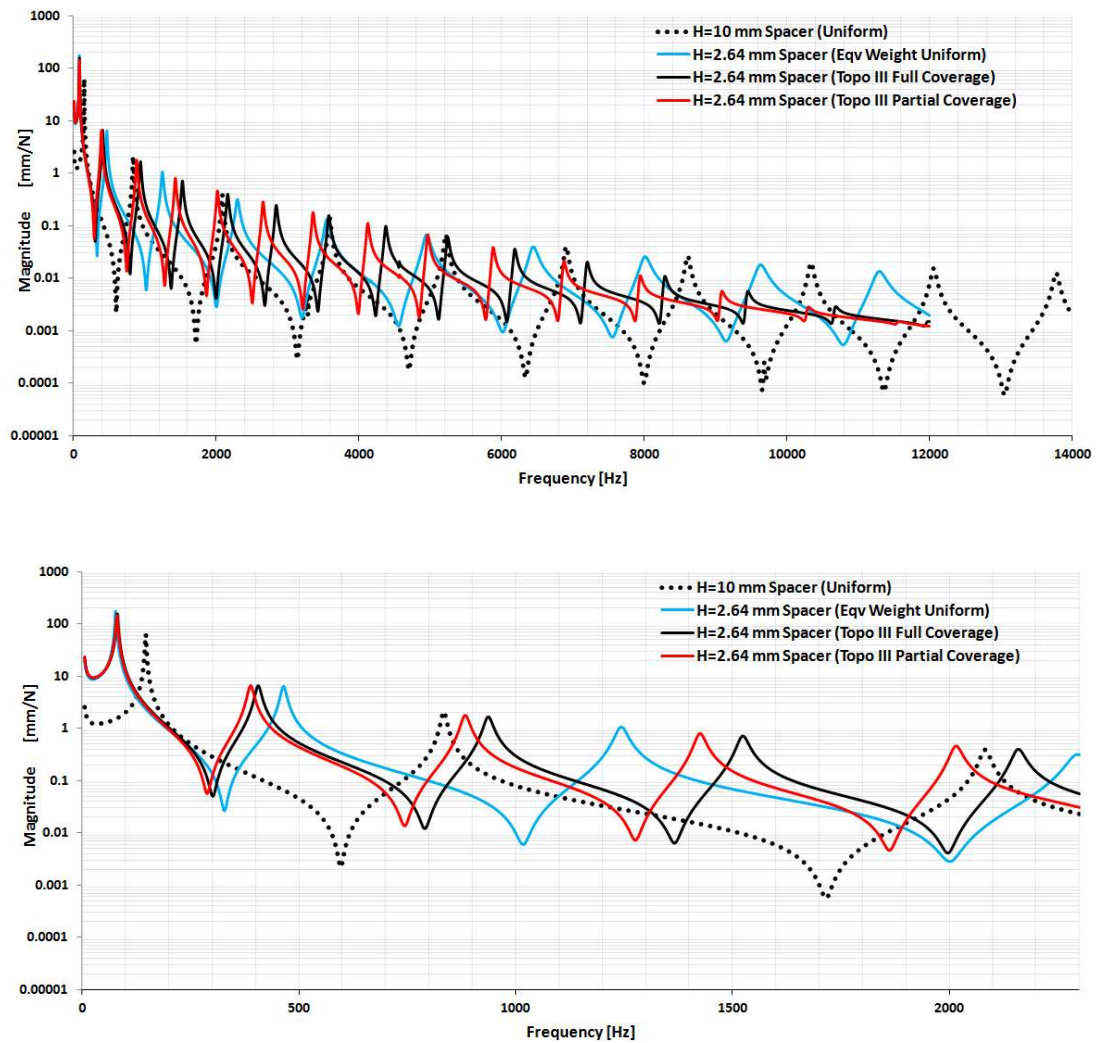


Figure 3-59 Overall comparison of frequency response functions for thinner stand-off layer with same topology (Case III).

The numerical results are summarized in the following Table 3-14 for new thickness value of stand-off layer ($H=2.64$ mm) with same topology as in the previous case. The results include comparison in terms of weight, frequency and loss factors for the first ten modes. Minimizing the thickness of stand-off layer compared to $H=10$ mm stand-off layer, results further %43.84 decrease in mass for the thin uniform case. However compared to thin uniform stand-off layer for both full and partial treatment, the same topology increases damping for the first two modes only and it is relatively by %17.15 for the 1st mode, %19.20 for the 2nd mode. For the partial case it is relatively by %24.15 for the 1st mode, %46.59 for the 2nd mode beyond which the

uniform case has higher damping capacity. The reduction of mass by optimization is %21.95. One can notice that the relative percentage increase in damping and decrease in mass via optimization is decreased as the thickness of stand-off layer is reduced.

Table 3-14 Summary of the optimization results (CASE III-H=2.64 mm)

(CASE III-H=2.64mm)						
3rd Topology Relative Damping Performance w.r.t. Uniform Stand-Off Layer						
Frequency f [Hz]			Loss Factor $\eta=2\zeta$			
H=2.64						
Mode #	Uniform Full Coverage	Optimized Full Coverage	Optimized Partial Coverage	Uniform Full Coverage Weight=100%	Optimized Full Coverage Weight=79.67%	Optimized Partial Coverage Weight=78.05%
1++	76.00	80.00	79.00	0.041	0.049	0.051
				-	↑ 17.15%	↑ 24.15%
2++	464.00	405.00	388.00	0.028	0.033	0.035
				-	↑ 19.20%	↑ 25.00%
3--	1243.00	936.00	883.00	0.022	0.021	0.022
				-	↓ -3.23%	↓ -0.92%
4--	2295.00	1523.00	1424.00	0.020	0.016	0.016
				-	↓ -19.00%	↓ -18.00%
5--	3550.00	2159.00	2015.00	0.019	0.013	0.013
				-	↓ -30.16%	↓ -30.69%
6--	4948.00	2840.00	2655.00	0.018	0.011	0.011
				-	↓ -38.33%	↓ -39.44%
7--	6445.00	3577.00	3356.00	0.017	0.010	0.009
				-	↓ -44.19%	↓ -45.35%
8--	8013.00	4376.00	4123.00	0.017	0.009	0.008
				-	↓ -48.48%	↓ -49.09%
9--	9633.00	5245.00	4965.00	0.016	0.008	0.008
				-	↓ -50.32%	↓ -51.59%
10--	11298.00	6186.00	5882.00	0.015	0.007	0.007
				-	↓ -51.01%	↓ -51.68%

As a summary if we compare the results obtained for both thickness value of stand-off layers, with $H=10$ mm and $H=2.64$ mm, the following Figure 3-60 summarizes the result obtained in terms of frequency response characteristic. Compared to thicker uniform stand-off layer, although the amplitudes in lower frequencies higher compared to thicker case, the thinner partially treated stand-off with optimized configuration has better damping performance for the first ten modes as well as obvious considerable amplitude reduction in higher modes.

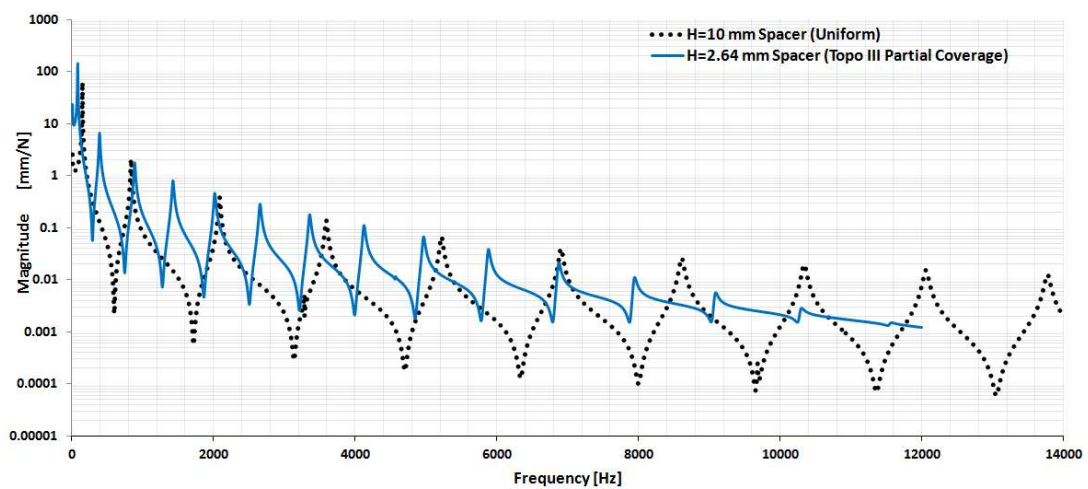


Figure 3-60 Overall comparison of frequency response functions ($H=2.64$ mm-partially treated) & ($H=10$ mm-uniform fully treated)

Numerical results associated with damping capacity of thin and thick stand-off layer for the new layout of spacer layer was compared in the following Table 3-15. Results show relative increase in damping in all configuration of thin stand-off layer compared to same but thicker layout of spacer. The thin uniform, full and partial treatment cases have higher relative increase in all ten modes among which the uniform thin case has larger capacity of damping. When we consider the over all damping performance however, the thin partially treated configuration has higher loss factors compared to thick uniform spacer layer configuration.

Table 3-15 Results of Optimization for H=10mm and H=2.64 mm Stand-off Layer

(CASE III-H=10 vs H=2.64mm)								
3rd Topology Relative Damping Performance								
Loss Factor $\eta=2\zeta$								
Mode # Prct [%]	H=10			Optimized (H=10mm) vs Uniform (H=2.64 mm)		H=2.64		
	Uniform-Full Coverage Weight=100%	Optimized Full Coverage Weight=58.16%	Uniform-Full Coverage Weight=54.79%	Optimized Partial (H=10mm) vs Uniform (H=2.64 mm)	Optimized Full Coverage Weight=79.67%	Uniform-Full Coverage Weight=100%	Uniform-Eq.Weight Full Coverage Weight=78.05%	
1+++	0.018	0.045	0.050	↑ 9.18%	↑ 20.77%	0.041	0.049	0.051
	-	-	-	↑ 131.92%	↑ 7.30%	↑ 2.80%		
2+++	0.014	0.026	0.030	↓ -5.07%	↑ 9.78%	0.028	0.033	0.035
	-	-	-	↑ 100.70%	↑ 25.57%	↑ 13.86%		
3+++	0.011	0.017	0.020	↓ -21.66%	↓ -6.91%	0.022	0.021	0.022
	-	-	-	↑ 105.77%	↑ 23.53%	↑ 6.44%		
4+++	0.009	0.013	0.015	↓ -33.00%	↓ -23.00%	0.020	0.016	0.016
	-	-	-	↑ 123.51%	↑ 20.90%	↑ 6.49%		
5+++	0.008	0.011	0.012	↓ -40.74%	↓ -36.51%	0.019	0.013	0.013
	-	-	-	↑ 133.61%	↑ 17.86%	↑ 9.17%		
6+++	0.007	0.010	0.010	↓ -45.56%	↓ -46.11%	0.018	0.011	0.011
	-	-	-	↑ 144.34%	↑ 13.27%	↑ 12.37%		
7+++	0.007	0.009	0.008	↓ -47.67%	↓ -52.33%	0.017	0.010	0.009
	-	-	-	↑ 154.12%	↑ 6.67%	↑ 14.63%		
8+-	0.006	0.009	0.007	↓ -47.88%	↓ -56.36%	0.017	0.009	0.008
	-	-	-	↑ 164.94%	↓ -1.16%	↑ 16.67%		
9+-	0.006	0.009	0.007	↓ -43.31%	↓ -57.96%	0.016	0.008	0.008
	-	-	-	↑ 172.05%	↓ -12.36%	↑ 15.15%		
10+-	0.005	0.011	0.007	↓ -25.50%	↓ -53.02%	0.015	0.007	0.007
	-	-	-	↑ 185.15%	↓ -34.23%	↑ 2.86%		

In the middle of Table 3-15 the relative numerical comparison has also been given between thick spacer with new topology and uniform spacer of equal weight. For the full coverage case the damping improvement is only at 1st mode and it is in the order of 9.18%, for the partial case however it is only at 1st and 2nd mode and numerically is 20.77% and 9.78% respectively.

3.2.6.4 Case Study IV:

In this last section of topology optimization another different optimization strategy has been investigated using different objective function. The same cantilever beam model given in first case study was used here under same in-plane sinusoidal flexural load that force the beam to deform statically as one of its lowest fundamental mode, that is, its first bending mode as well as inducing shear motion between layers (Figure 3-61). It was aimed for the stand-off layer to get such a material distribution after optimization that induce same static deformation pattern during its first mode of vibration within viscoelastic layer so that the higher damping could be achieved in lower frequencies due to induced state of shear within damping layer for maximum damping.

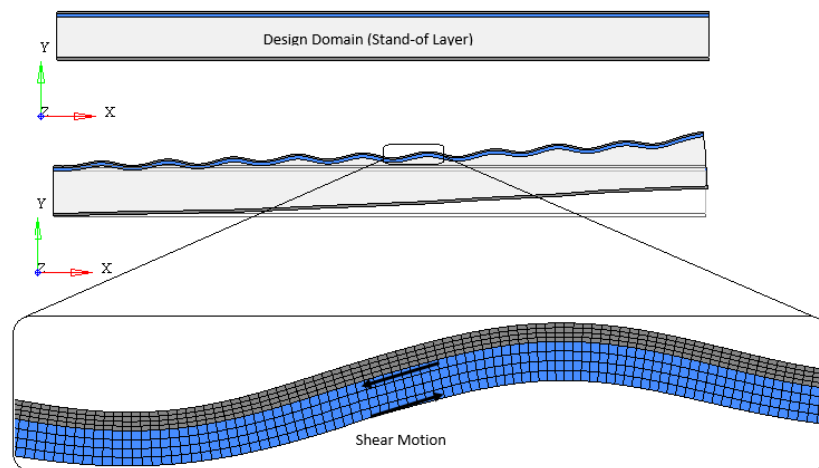


Figure 3-61 State of deformation under sinusoidal static load
(Exaggerated deformation)

In order to investigate this possibility, first, a static analysis has been performed to extract tip deflection, u_{y+} , of the beam (Figure 3-62) which was in the order of 7.5 mm. Then the pre-stressed modal analysis step was created in order to extract natural frequencies under static distributed sinusoidal load. Therefore the frequency optimization procedure could be followed by maximizing the first modal frequency of cantilever beam, which amounts to the increased shear stiffness [147] for stand-off

layer, to reduce vibration amplitude of the beam since at higher modes the relative amplitudes are lowered. At the same time the VOLFRAC, and static displacement response cards have been created as constraints such that it is expected to increase stiffness while having flexibility of deformation due to reduction of material in design space. Maximum bound of VOLFRAC response was set to 0.3. As the material is removed the deflection will be increased at the tip of the beam due to decreased flexural rigidity, therefore to limit the deflection in order not to get unfeasible solution, another constraint is used for the limitation of tip deflection assumed to be as maximum of 10 mm compared to first nominal value of 7.5 mm obtained after static analysis step.

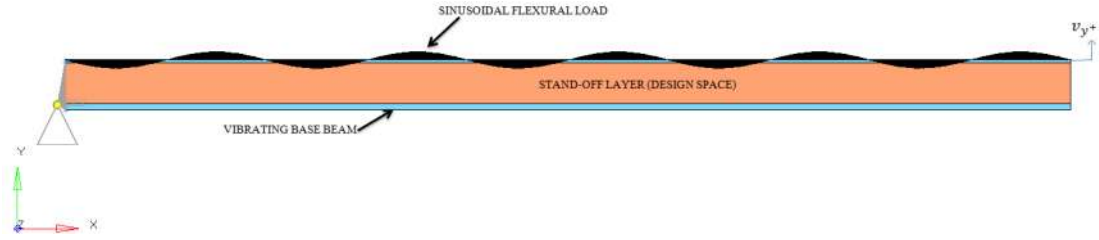


Figure 3-62 Finite element model of cantilever beam under sinusoidal loading

The resulting topology and refined geometry of stand-off layer after maximizing the first natural frequency under given constraints of treated beam is given in Figure 3-63. The cross-shape geometry has been extracted through interpretation of resulting topology.

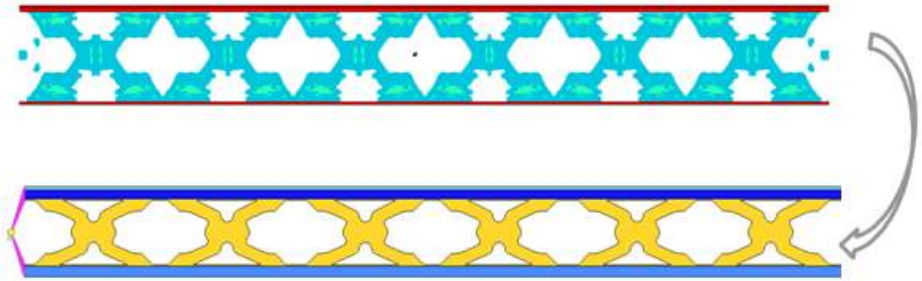


Figure 3-63 Resulting topology and refined geometry of stand-off layer

Based on the mode shapes calculated, the increase in deformation within viscoelastic layer is visible. Especially at higher modes while beam has less deformation response the upper portion of stand-off layer has irregular deformation patterns that is expected to induce shear deformation within viscoelastic layer (Figure 3-64, Figure 3-65).

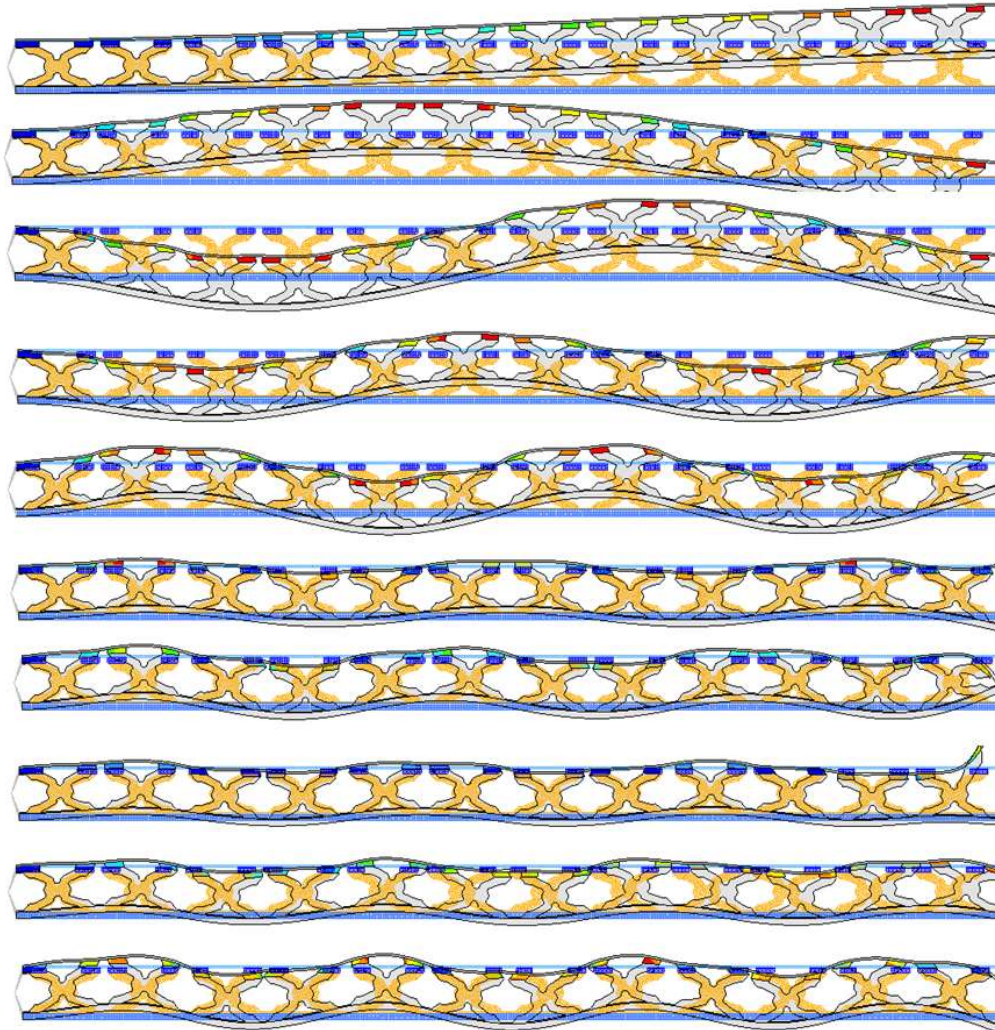


Figure 3-64 Mode shapes of treated beam with optimized stand-off layer (Case IV)

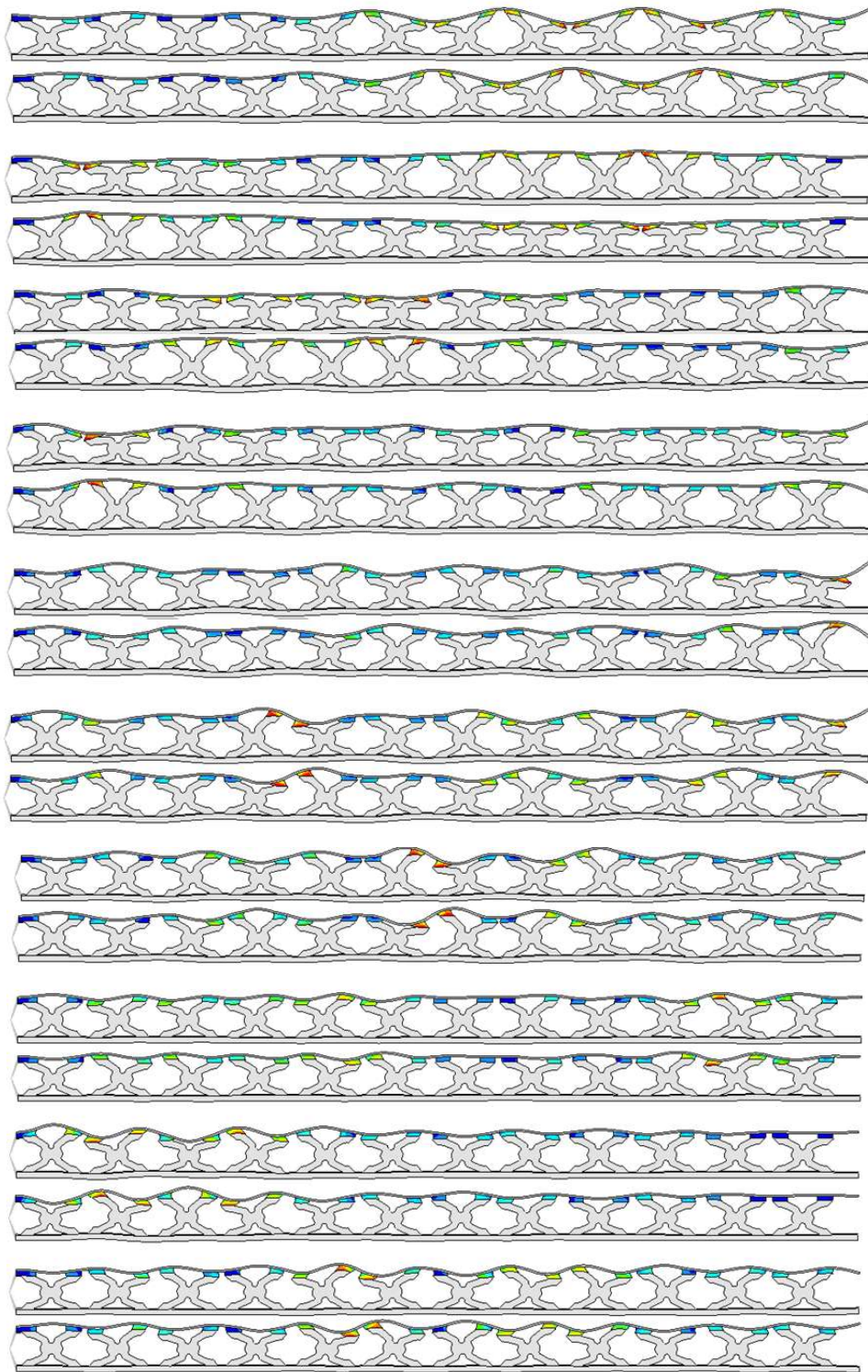


Figure 3-65 Mode shapes of treated beam with optimized stand-off layer at higher modes (Case IV)

The following Figure 3-66 and Figure 3-67 show the frequency response of fully and partially treated beam with new topology of stand-off layer .

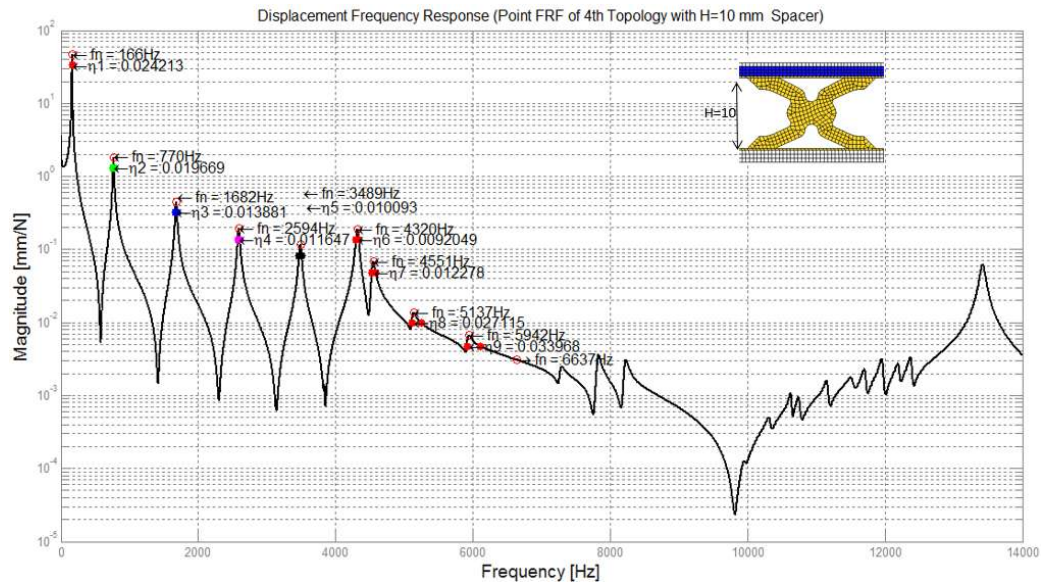


Figure 3-66 Frequency response function of treated beam with optimized stand-off layer.

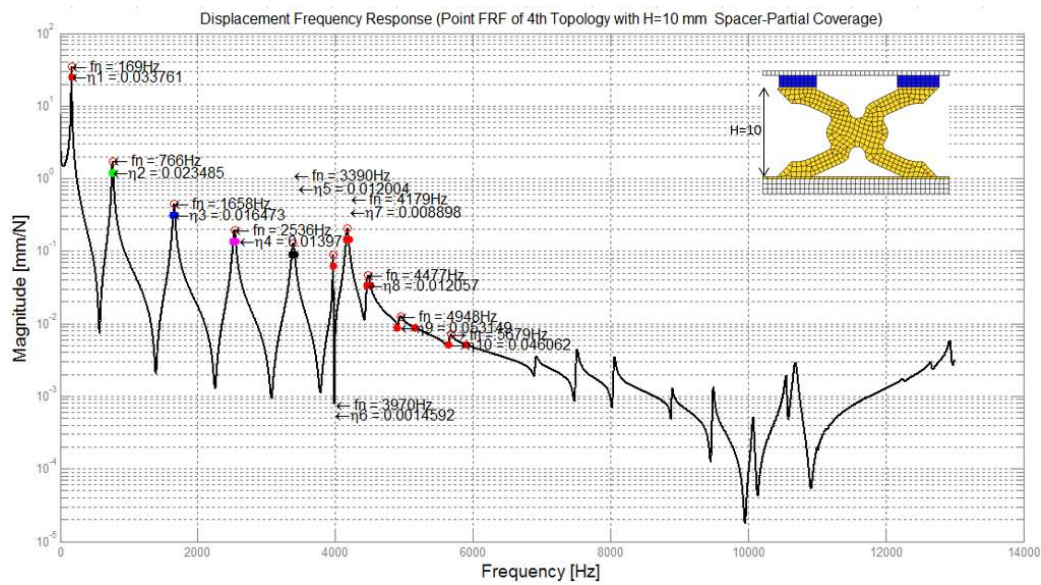


Figure 3-67 Frequency response function of partially treated beam with optimized stand-off layer

It is obvious from the frequency response plots that the attenuation zones exists in both fully and partially treated beams. The starting frequency is around 4 kHz and the reduction of amplitude show itself after 7th mode between 4.5 kHz and 12.5 kHz.

In order to compare the performance new topology of stand-off layer with the uniform stand-off layer that has equal weight, a new stand-off layer was created with reduced thickness value of H=3.79 mm. The frequency response function of latter uniform case is given in Figure 3-68.

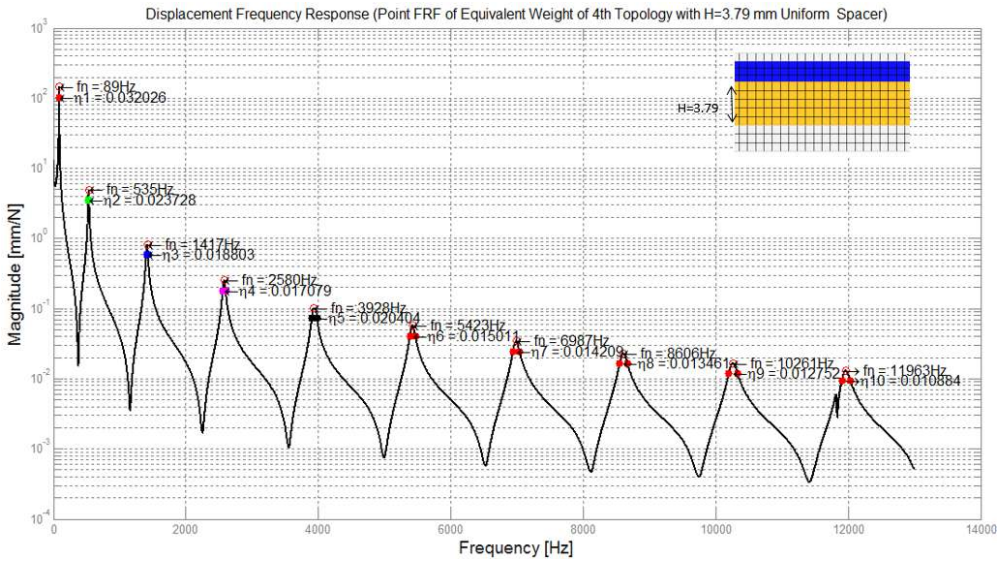


Figure 3-68 Frequency response function of equally weighted treated beam with uniform stand-off layer

All above results are compared in one plot as shown in Figure 3-69. In this plot one can see that compared to base analysis model with H=10 mm stand-off, the optimized stand-off layer with new layout of spacer has slight amplitude reduction starting from lowest modes and this reduction is obvious between 4.5 kHz and 12.5 kHz which can be considered as anti-resonance region with large frequency band beyond which the amplitudes are high again. As was the case in previous cases, it was again concluded that the thinner uniform stand-off layer has higher response

amplitude but greater damping capacity in lower frequency range compared to thicker one and its response curve getting broader for higher modes.

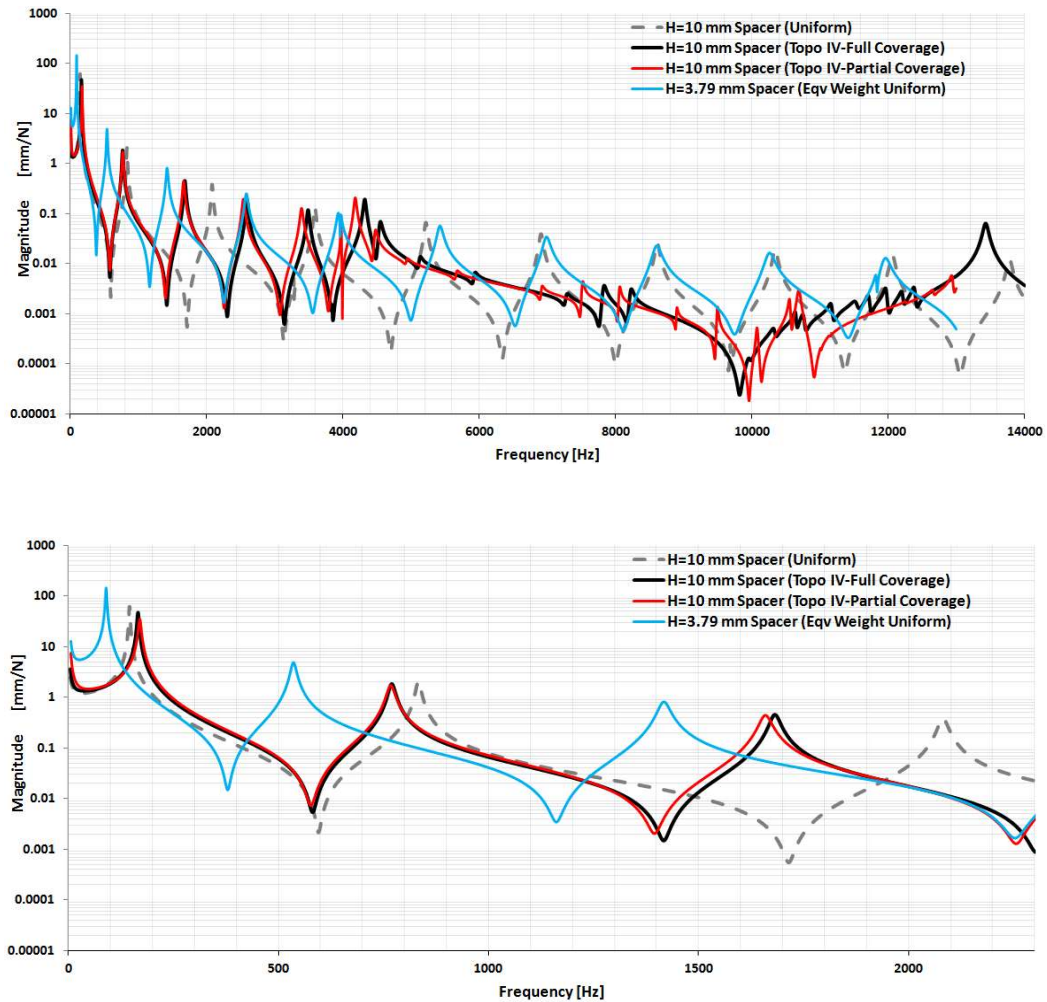
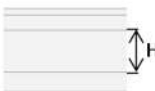
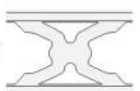
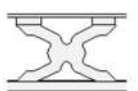
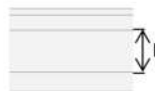
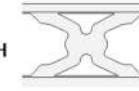
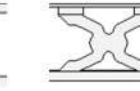


Figure 3-69 Overall comparison of frequency response functions (Case IV)

In terms of damping capacity the numerical results are summarized in the following Table 3-16. The results include comparisons in terms of weight, frequency and loss factors for the first ten modes. The optimized layout of stand-off layer results %35.84 mass reduction as well as damping improvement by %35.57 for the 1st mode, %43.25 for the 2nd mode, %31.80 for the 3rd mode and this improvement was also reported to be continuous compared to base analysis model with H=10 mm uniform stand-off layer. The relative mass reduction is %41.1 and damping improvement is higher in percentage for the partial treatment of same topology for which the relative damping

improvement is %89.35 for the 1st mode, %70.88 for the 2nd mode, %56.46 for the 3rd mode. For higher modes due to attenuation zones diminished peaks exists which makes calculation of damping factors not applicable.

Table 3-16 Summary of the optimization results (CASE IV-H=10mm)

(CASE IV-H=10mm)						
4th Topology Relative Damping Performance w.r.t. Uniform Stand-Off Layer						
Frequency f [Hz]			Loss Factor $\eta=2\zeta$			
H=10						
						
Mode #	Uniform Full Coverage	Optimized Full Coverage	Optimized Partial Coverage	Uniform Full Coverage Weight=100%	Optimized Full Coverage Weight=64.16%	Optimized Partial Coverage Weight=58.90%
1++	146.00	166.00	169.00	0.018	0.024	0.034
				-	↑ 35.57%	↑ 89.35%
2++	833.00	770.00	766.00	0.014	0.020	0.024
				-	↑ 43.25%	↑ 70.88%
3++	2082.00	1682.00	1658.00	0.011	0.014	0.017
				-	↑ 31.80%	↑ 56.46%
4++	3589.00	2594.00	2536.00	0.009	0.012	0.014
				-	↑ 29.64%	↑ 56.46%
5++	5217.00	3489.00	3390.00	0.008	0.010	0.012
				-	↑ 24.84%	↑ 48.33%
6+-	6905.00	4320.00	3970.00	0.007	0.009	0.002
				-	↑ 24.88%	↓ -79.64%
7++	8609.00	4551.00	4179.00	0.007	0.012	0.009
				-	↑ 81.72%	↑ 31.49%
8++	10339.00	5137.00	4477.00	0.006	0.027	0.012
				-	↑ 335.15%	↑ 94.29%
9++	12059.00	5942.00	4948.00	0.006	0.034	0.053
				-	↑ 489.14%	↑ 820.10%
10++	13776.00	6637.00	5679.00	0.005	NA	0.046
				-	-	↑ 782.23%

From numerical and graphical results shows that thinner stand-off layer has greater damping capacity than thicker one. Therefore in order to quantify the performance of new topology with thinner case, the same topology of stand-off layer was scaled to $H=3.79$ mm which is the thickness of equally weighted stand-off layer with optimized topology of stand-off layer with $H=10$ mm.

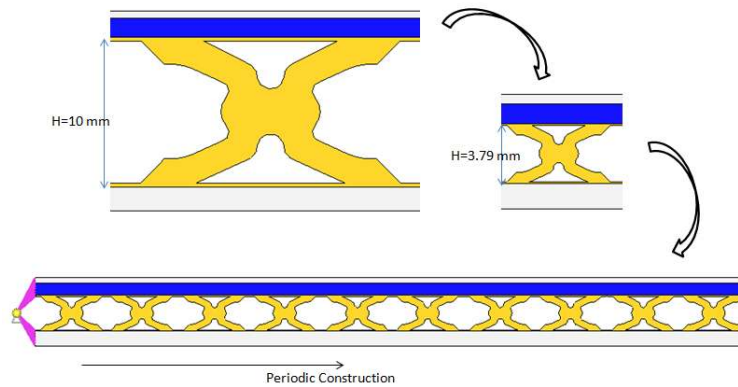


Figure 3-70 Treated beam with scaled model of optimized stand-off layer

The frequency response function of fully treated beam with reduced thickness value of stand-off layer is given in Figure 3-71.

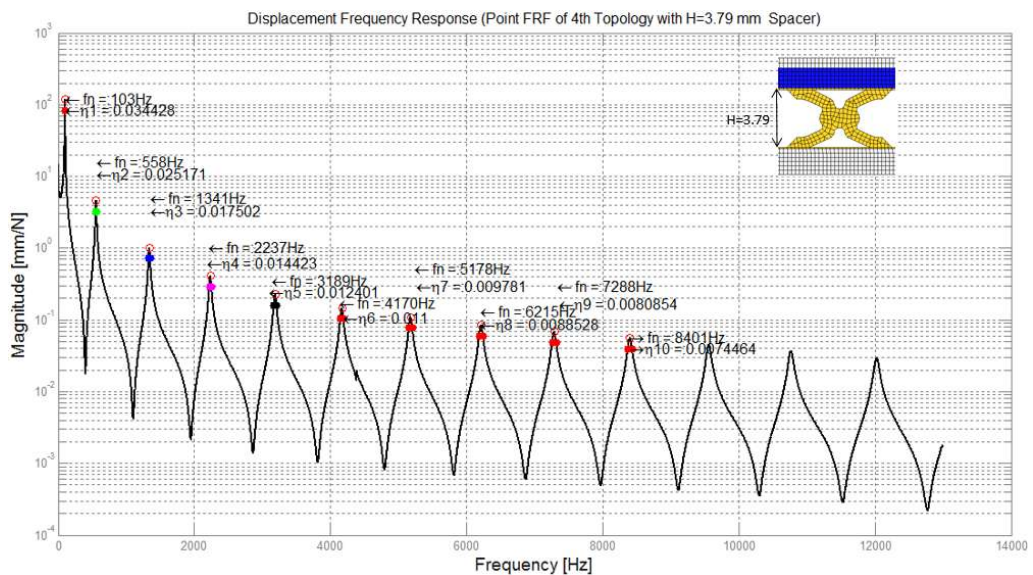


Figure 3-71 Frequency response function of treated beam with reduced thickness value of stand-off layer

The frequency response function is given for partially treated beam in Figure 3-72 together with its equally weighted counterpart with a corresponding thickness value of $H=1.523$ mm. The frequency response plot of this latter treated beam with uniform stand-off layer is given in Figure 3-73

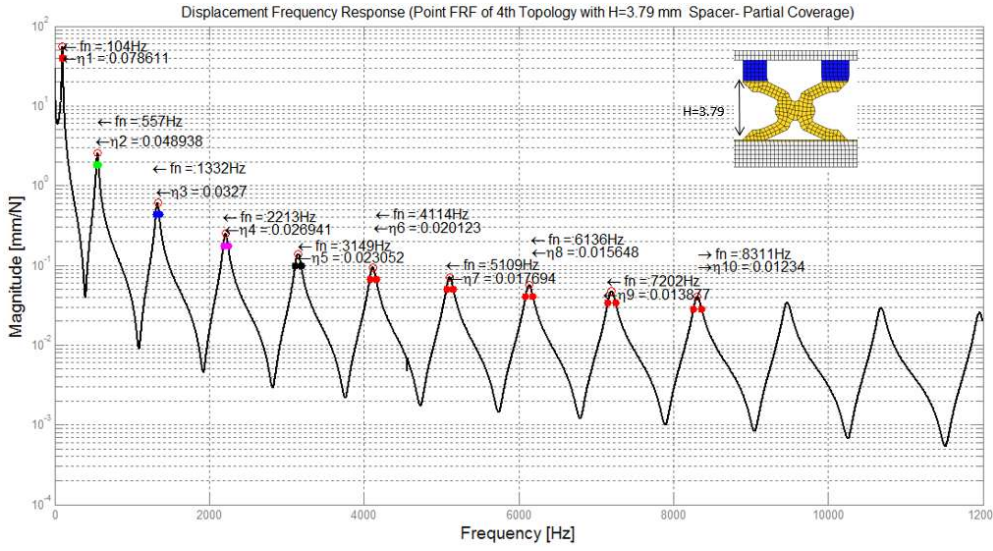


Figure 3-72 Frequency response function of partially treated beam with optimized stand-off layer with cuts (Case IV)

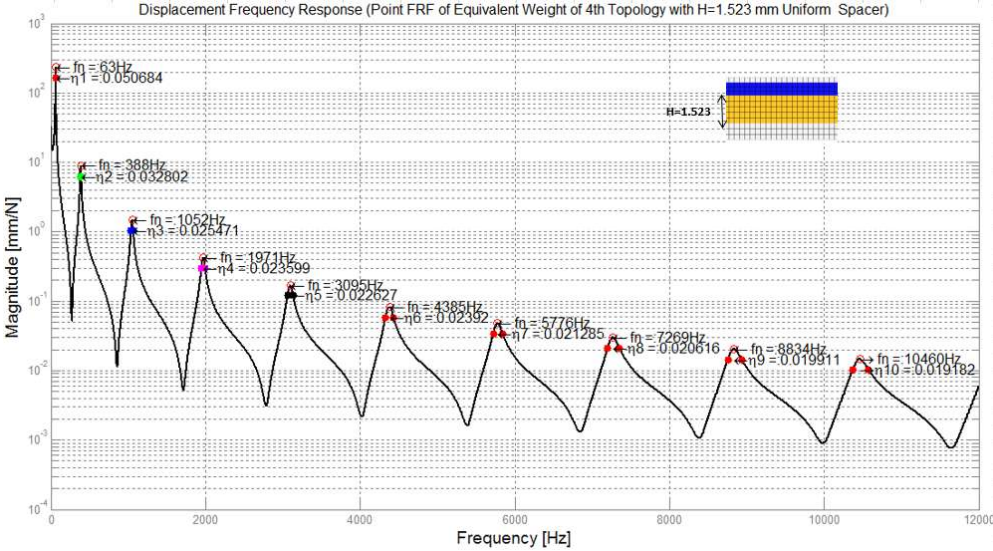


Figure 3-73 Frequency response function of treated beam with uniform equally weighted stand-off layer (Case IV $H=1.523$ mm)

Comparing all above results for this case study yields the following plot given in Figure 3-74. For this new topology minimizing the thickness of stand-off layer compared to H=10 mm stand-off layer, results further %36.76 decrease in mass for the uniform cases. Based on the results achieved for this topology, the thinner (H=3.79 mm) partially treated case (red dashed line) has lower response amplitude even at low frequencies with its natural frequencies were shifted to the left compared to thicker uniform stand-off layer. Further reduction in thickness however increase response amplitude (Figure 3-74).

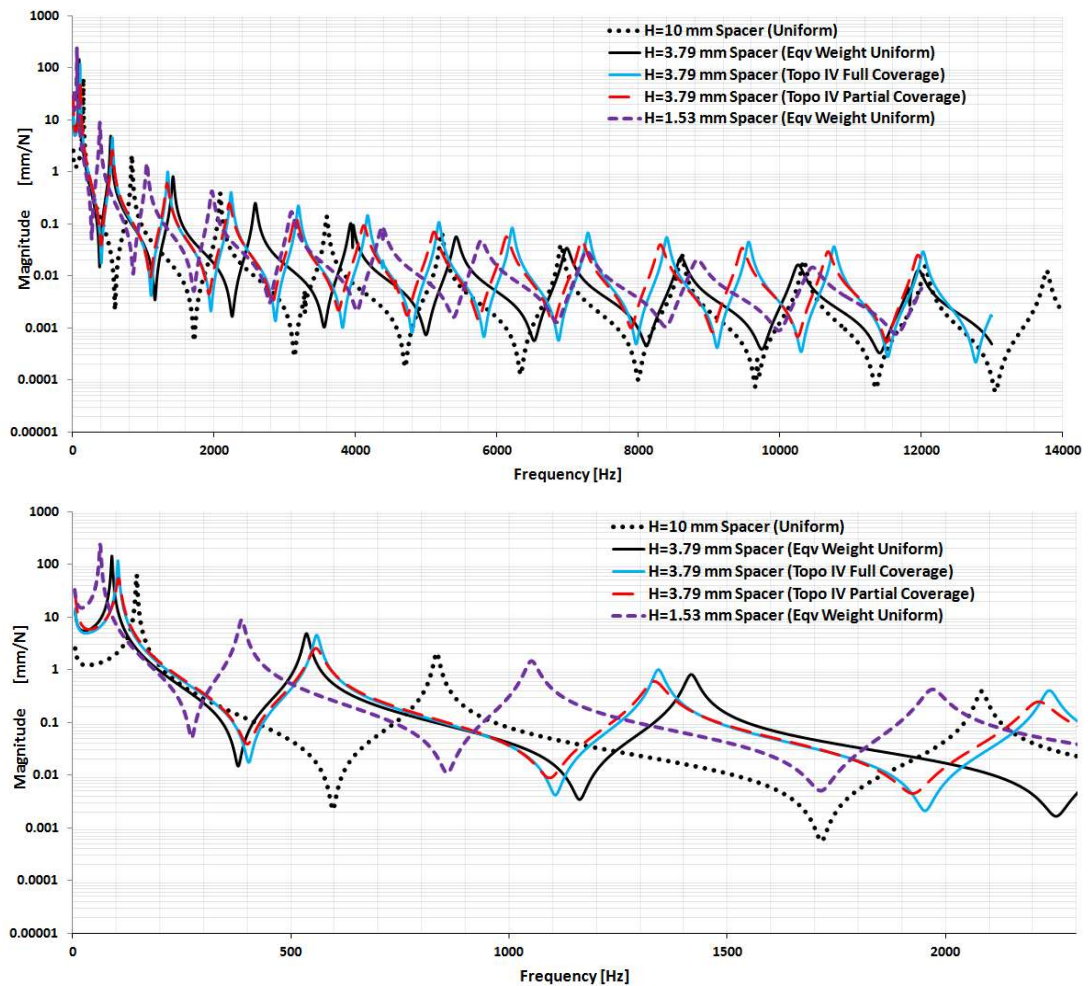
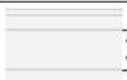

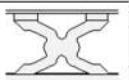


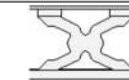


Figure 3-74 Overall comparison of frequency response functions

For the thinner case partially treated beam also has advantage with higher damping capacity in all modes by %145.63 for the 1st mode, %106.33 for the 2nd mode and % 73.94 for the third mode while with fully treated case no relative improvement was achieved except for the first two modes by 7.5% for the first mode and 6.33% for the second mode as given in Table 3-17.

Table 3-17 Summary of the optimization results (CASE IV-H=3.79 mm)

(CASE IV-H=3.79mm)						
4th Topology Relative Damping Performance w.r.t. Uniform Stand-Off Layer						
Frequency f [Hz]			Loss Factor $\eta=2\zeta$			
Mode # Prct [%]	Uniform Full Coverage		Optimized Full Coverage		Optimized Partial Coverage	
	Prct [%]	Weight=100%	Prct [%]	Weight=81.59%	Prct [%]	Weight=74.01%
	H=3.79					
						
1++	89.00	103.00	104.00	0.032	0.034	0.079
				-	↑ 7.50%	↑ 145.63%
2++	535.00	558.00	557.00	0.024	0.025	0.049
				-	↑ 6.33%	↑ 106.33%
3-+	1417.00	1341.00	1332.00	0.019	0.018	0.033
				-	↓ -6.91%	↑ 73.94%
4-+	2580.00	2237.00	2213.00	0.017	0.014	0.027
				-	↓ -15.79%	↑ 57.31%
5-+	3928.00	3189.00	3149.00	0.020	0.012	0.023
				-	↓ -39.22%	↑ 13.24%
6-+	5423.00	4170.00	4114.00	0.015	0.011	0.020
				-	↓ -27.33%	↑ 34.00%
7-+	6987.00	5178.00	5109.00	0.014	0.010	0.018
				-	↓ -30.99%	↑ 24.65%
8-+	8606.00	6215.00	6136.00	0.014	0.009	0.016
				-	↓ -34.07%	↑ 15.56%
9-+	10261.00	7288.00	7202.00	0.013	0.008	0.014
				-	↓ -36.72%	↑ 8.59%
10-+	11963.00	8401.00	8311.00	0.011	0.007	0.012
				-	↓ -32.11%	↑ 12.84%

As a summary if we compare the results obtained for both thickness value of stand-off layers, with $H=10$ mm and $H=3.79$ mm, the following (Figure 3-74) summarizes the result obtained in terms of frequency response characteristic. Compared to thicker uniform stand-off layer, the thinner partially treated stand-off with optimized configuration has better damping performance in all modes with slight increase in amplitude.

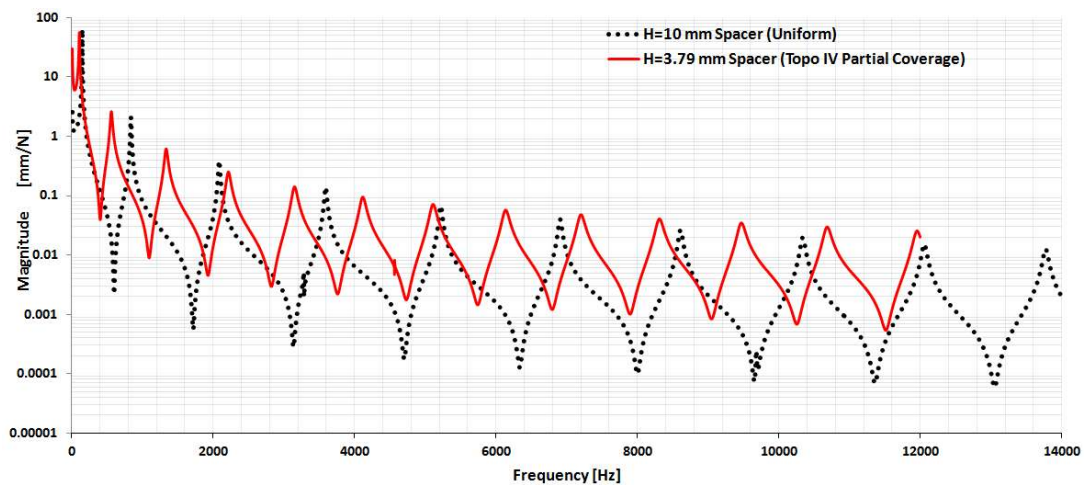


Figure 3-75 Overall comparison of frequency response functions ($H=3.79$ mm-partially treated) & ($H=10$ mm-uniform fully treated)

The following Table 3-18 summarizes relative improvement numerically in terms of damping capacity for both cases. The results show obvious relative increase in damping for the thinner configurations compared to thicker configurations. Among the thinner configuration the damping capacity considerably increases for the first three modes with minimum weight among all configurations. The relative percentage increase in damping compared to corresponding counterpart configuration is %132.54 for the 1st mode, %108.09 for the 2nd mode and % 98.18 for the 3rd mode.

Table 3-18 Results of Optimization for H=10mm and H=3.79 mm Stand-off Layer

(CASE IV-H=10 vs H=3.79mm)								
4th Topology Relative Damping Performance								
Loss Factor $\eta=2\zeta$								
Mode # Prct [%]	H=10			H=3.79				
	Uniform- Full Coverage Weight=100%	Optimized Full Coverage Weight=64.16%	Uniform- Full Coverage Weight=58.90%	Optimized (H=10mm) vs Uniform (H=3.79 mm)	Optimized Partial (H=10mm) vs Uniform (H=3.79 mm)	Uniform- Full Coverage Weight=100%	Optimized Full Coverage Weight=81.59%	Uniform-Eq.Weight Full Coverage Weight=74.01%
1+++	0.018	0.024	0.034			0.032	0.034	0.079
	-	-	-	↓ 24.38%	↑ 5.62%	↑ 79.26%	↑ 42.15%	↑ 132.54%
2+++	0.014	0.020	0.024			0.024	0.025	0.049
	-	-	-	↓ 16.88%	↓ -0.84%	↑ 72.34%	↑ 27.92%	↑ 108.09%
3+++	0.011	0.014	0.017			0.019	0.018	0.033
	-	-	-	↓ 26.06%	↓ -12.23%	↑ 78.27%	↑ 25.90%	↑ 98.18%
4+++	0.009	0.012	0.014			0.017	0.014	0.027
	-	-	-	↓ 32.16%	↓ -18.13%	↑ 91.10%	↑ 24.14%	↑ 92.14%
5+++	0.008	0.010	0.012			0.020	0.012	0.023
	-	-	-	↓ 50.49%	↓ -41.18%	↑ 152.15%	↑ 22.77%	↑ 92.50%
6+++	0.007	0.009	0.002			0.015	0.011	0.020
	-	-	-	↓ 38.67%	↓ -90.00%	↑ 103.62%	↑ 18.48%	↑ 1240.00%
7+++	0.007	0.012	0.009			0.014	0.010	0.018
	-	-	-	↓ 13.38%	↓ -37.32%	↑ 109.80%	↓ -20.33%	↑ 98.88%
8+--	0.006	0.027	0.012			0.014	0.009	0.016
	-	-	-	↑ 100.74%	↓ -10.37%	↑ 116.77%	↓ -67.16%	↑ 28.93%
9+--	0.006	0.034	0.053			0.013	0.008	0.014
	-	-	-	↑ 165.63%	↑ 314.84%	↑ 121.79%	↓ -76.18%	↓ -73.82%
10+--	0.005	NA	0.046			0.011	0.007	0.012
	-	-	-	-	↑ 322.94%	↑ 108.60%	-	↓ -73.32%

The following Table 3-19 and Table 3- summarizes the relative damping improvement that was achieved by reduction of thickness of uniform stand-off layer compared to reference treated beam with thicker uniform stand-off layer, numerically for the first ten modes of vibrating cantilever beam. Comparison was made in terms of weight and relative percentage increase in loss factors for the first ten modes.

Table 3-19 Relative Damping Performance of Fully Treated Uniform Thinner Stand-off Layers

H=10 mm Uniform Full Coverage (Total Weight=4.38E-06 TON)				H=3.79 mm Uniform Full Coverage (Total Weight=2.77E-06 TON)		
Reference	Mode #	Loss Factor [%]	Weight Reduction [%]	Mode #	Relative Loss Factor Improvement [%]	
-	1	0.018	-36.76%	1	78.92%	
	2	0.014		2	71.94%	
	3	0.011		3	79.09%	
	4	0.009		4	91.94%	
	5	0.008		5	141.40%	
	6	0.007		6	103.09%	
	7	0.007		7	109.38%	
	8	0.006		8	117.90%	
	9	0.006		9	124.93%	
	10	0.005		10	111.48%	

H=3.52 mm Uniform Full Coverage (Total Weight=2.66E-06 TON)			H=3.45 mm Uniform Full Coverage (Total Weight= 2.66E-06 TON)		
Weight Reduction [%]	Mode #	Relative Loss Factor Improvement [%]	Weight Reduction [%]	Mode #	Relative Loss Factor Improvement [%]
-39.27%	1	87.38%	-39.27%	1	97.26%
	2	77.90%		2	80.17%
	3	84.96%		3	86.75%
	4	98.81%		4	100.67%
	5	102.88%		5	105.54%
	6	111.51%		6	113.76%
	7	118.59%		7	121.09%
	8	127.87%		8	130.60%
	9	135.65%		9	138.56%
	10	127.63%		10	139.75%

Table 3-19 Continued

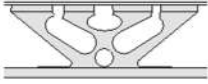
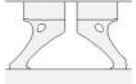

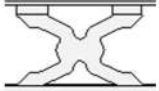
H=2.64 mm Uniform Full Coverage (Total Weight=2.46E-06 TON)			H=1.53 mm Uniform Full Coverage (Total Weight=2.18E-06 TON)		
Weight Reduction [%]	Mode #	Relative Loss Factor Improvement [%]	Weight Reduction [%]	Mode #	Relative Loss Factor Improvement [%]
-43.84%	1	131.10%	-50.23%	1	183.15%
	2	100.35%		2	137.70%
	3	106.98%		3	142.59%
	4	124.33%		4	165.17%
	5	133.06%		5	179.42%
	6	143.58%		6	216.81%
	7	153.87%		7	213.37%
	8	166.61%		8	233.26%
	9	177.32%		9	250.51%
	10	189.06%		10	270.73%

Based on the tabulated results as we decrease the thickness the relative damping capacity was increased that is reported to be relatively maximum for the case of H=1.523 mm for maximum relative percentage weight reduction of %50.23. However from the frequency response plots it was obvious that the thinner stand-off configuration yields higher response amplitude with lower natural frequency due to reduced bending rigidity. Another results is that the damping capacity has an increasing trend towards to higher modes for all configurations which is expected because of higher ripple is induced as well as increased relative motion within the viscoelastic layer that increase the shear deformation as the main cause of energy dissipation which results higher loss factor.

Another overall conclusion can be drawn by comparing the relative damping performances of all extracted topologies for the stand-off layer. The main conclusion was that the partial treatment resulted higher damping capacity. Therefore in the

following Table 3-20 the corresponding configurations are compared by reporting relative percentage increase in damping with respect to uniform reference thicker stand-off with the height of H=10 mm.

Table 3-20 Summary of Relative Damping Improvement w.r.t. Thick Uniform Stand-off Layer (H=10mm)

TOPOLOGY I H=3.52 mm Partial Coverage			TOPOLOGY II H=3.45 mm Partial Coverage		
					
Weight Reduction [%]	Mode #	Relative Loss Factor Improvement [%]	Weight Reduction [%]	Mode #	Relative Loss Factor Improvement [%]
-56.16%	1	320.67%	-54.79%	1	298.32%
	2	274.64%		2	252.90%
	3	237.14%		3	220.00%
	4	232.58%		4	215.73%
	5	211.11%		5	200.00%
	6	193.24%		6	189.19%
	7	48.53%		7	175.00%
	8	164.52%		8	167.74%
	9	150.88%		9	157.89%
	10	142.31%		10	151.92%
TOPOLOGY III H=2.64 mm Partial Coverage			TOPOLOGY IV H=3.79 mm Partial Coverage		
					
Weight Reduction [%]	Mode #	Relative Loss Factor Improvement [%]	Weight Reduction [%]	Mode #	Relative Loss Factor Improvement [%]
-56.16%	1	187.94%	-53.20%	1	340.31%
	2	150.87%		2	255.58%
	3	103.87%		3	210.07%
	4	83.28%		4	200.62%
	5	61.92%		5	185.53%
	6	47.96%		6	172.85%
	7	38.88%		7	161.51%
	8	34.88%		8	150.49%
	9	31.69%		9	140.86%
	10	37.79%		10	135.39%

It was obvious from the frequency response plots that the response at the lowest resonance modes of vibrating structures dominates the overall dynamic response of the structure in terms of high amplitude. Therefore controlling the fundamental mode of vibration, that is, damping of the lowest response is much more essential. From this point of view one can see from the tabulated results (Table 3-20) that first case topology has better damping capacity in first three mode of vibration with highest mass reduction. The second candidate was found to be fourth topology with its relative higher damping performance at 1st mode of vibration.

3.2.7 Parametric Optimization

3.2.7.1 Introduction

In previous optimization method the topology optimization has been followed in which the density of each element in design space was considered as continuous design variables which were also related to the material within the design domain. Using the topology optimization several design concept with different material topologies were extracted and investigated in terms of damping performance as well as weight reduction. It was observed from the results that the thickness of stand-off layer was one of the important design parameter that yields higher damping capacity. As also found from the previous numerical results, contrary to fact that increase of stand-off height to increase the strain within the viscoelastic layer does not always increase the damping capacity and there is an optimum value for this parameter [54].

In this part of the thesis study another design optimization strategy, which is parametric design optimization, will be followed such that design parameter such as height of stand-off layer will be defined as discrete design variable to find its optimum value. Moreover the elasticity modulus will also be selected as design parameter in order to investigate the effect of material type together with its best choice for the best damping performance.

For this purpose, as in the previous case studies a 2D four layered cantilever beam model was studied. The system loss factors were related with geometrical and material parameters of finite element model of vibrating beam in plain strain case (Figure 3-76).

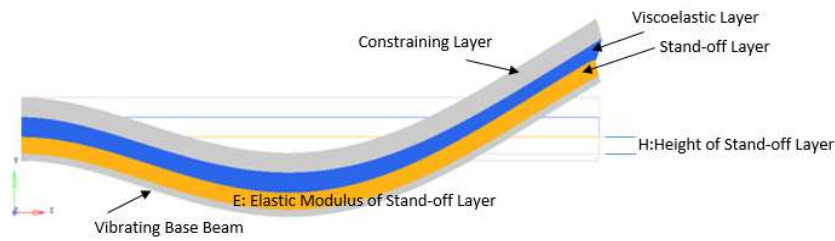


Figure 3-76 2D Finite element (shaded) model of cantilever vibrating beam

3.2.7.2 Development of Methodology

As one of the design methodology the parametric optimization technique has been followed and the proposed design cycle is given in (Figure 3-77). In this design cycle the modal strain energy method (MSE) proposed by Johnson and Kienholz [64] in conjunction with finite element method has been utilized. Basically the objective is to develop a systematic design approach that considers multiple design alternatives in a more robust way. The loss factors were extracted analytically using Modal Strain Energy Method by requesting the modal strain energies of all individual layers using finite element method which was also parametrically changed. Linking those geometrical and material parameters that were used in finite element with those loss factors found from mentioned method, the effects of each parameters can easily be analyzed. Moreover using well known optimization algorithms that use those parameters as design variable, the best optimum ones can also be easily determined.

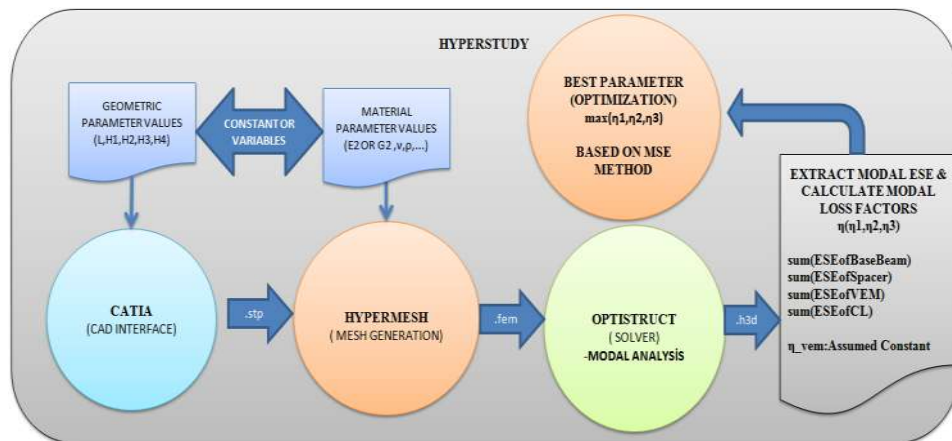


Figure 3-77 Parametric design cycle

The design process mentioned in this section was built in HyperStudy[®] environment that is one of the efficient platform enables design engineers to conduct design of experiment studies as well as discrete design parameter optimization using embedded algorithms such as Genetic Algorithm, Global Response Surface Method [148] etc by controlling all prescribed parameters. Moreover different design and analysis softwares can also be linked together to build faster and flexible design process by eliminating time consuming trial and error procedures in a traditional design cycle (Figure 3-77).

The design and analysis cycle that is depicted in Figure 3-77 is shown in a more extended form in Figure 3-78.

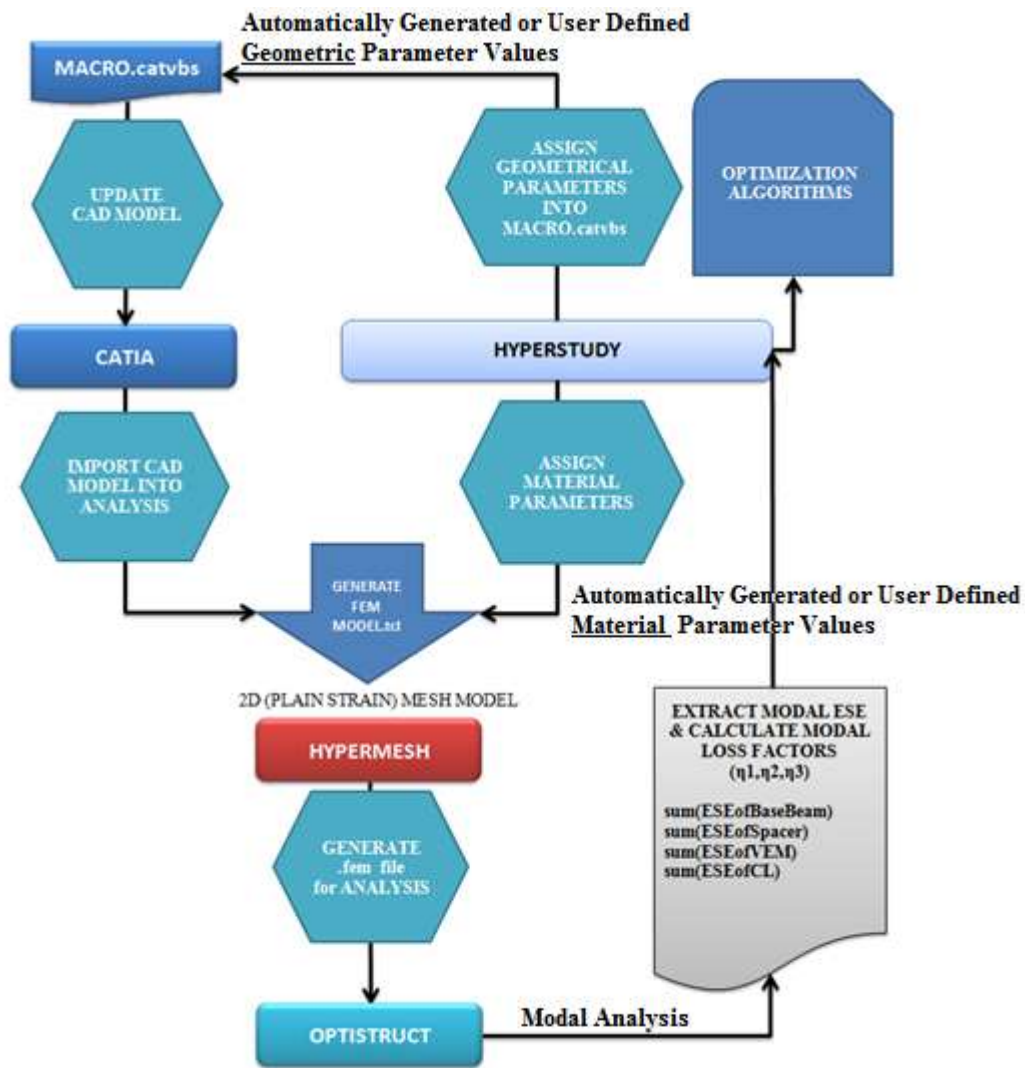


Figure 3-78 Parametric design and optimization cycle

The design strategy was started by generation of 2D four layered treated beam model with stand-off layer using CATIA V5-R22[®] design environment. As shown in Figure 3-79, the geometric parameters, which are the thickness values were all selected as design parameter. Those parameters were also controlled by HyperStudy[®] with a MACRO.catvbs file that has been recorded during generation of 2D design with those parameters.



Figure 3-79 Parametric design of 2D treated beam in CATIA®

After automatic generation of beam model using automatically generated geometric parameters between predefined lower and upper bounds, it was imported into Hypermesh® environment in which the automatic generation of finite element model has also been performed with its prescribed boundary condition, mesh size and analysis type that is in our case, the fixed-free, 0.1 mm and modal analysis, respectively, by execution of MODEL.tcl file using hmbatch.exe. Material properties of finite element model was controlled by HyperStudy® also at this step. Again, automatically generated modulus of elasticity data between predefined lower and upper bounds was assigned for the element material property MAT1 card. All above steps were controlled by HyperStudy® using Model.tpl file as shown in Figure 3-80.

```

(parameter(BaseBeamLength, "L", 200.00000, 150.00000, 300.00000))
(parameter(BaseBeamHeight, "H1", 1.60000, 1.20000, 3.00000))
(parameter(SpacerHeight, "H2", 5.00000, 3.00000, 15.00000))
(parameter(VEMHeight, "H3", 0.12700, 0.10000, 1.00000))
(parameter(CLHeight, "H4", 0.10000, 0.10000, 1.00000))
(parameter(E core, "ElasticModulus of SOL", 62.00, 5.00, 3000.00))

Language="VBSCRIPT"
Sub CATMain()
Set partDocument1 = .CATIA.ActiveDocument
Set part1 = partDocument1.Part
Set parameters1 = part1.Parameters
Set length1 = parameters1.Item("BaseBeamLength")
length1.Value = 250.000000
part1.Update
Set parameters2 = part1.Parameters
Set length2 = parameters2.Item("BaseBeamHeight")
length2.Value = 1.60000
length2.Value = {templex on}(BaseBeamHeight, *8.5f){templex off}
part1.Update
.
.
*setvalue mats id=2 STATUS=1 1=62.00
*setvalue mats id=2 STATUS=1 1={templex on}(E core, *4.2f){templex off}
.
.

```

Figure 3-80 Content of HyperStudy Model.tpl file

Upon modification of all geometric and material parameter with Model.tpl file an analysis file with an extension of .fem was generated to be run via Optistruct. The modal analysis has been performed using .fem file by invoking Optistruct.bat file. The modal strain energies were requested by ESE (ALL)=ALL command within analysis run file (.fem) for all elements within the treated beam design. At this step the challenge was to select elements within each layer, base beam layer, stand-off layer, viscoelastic layer and constraining layer respectively. Because at each design iteration the since the geometry of the design updated the number of elements within that boundary were also changing. Therefore a tempex code was written that select corresponding elements ID's within each component of finite element model of treated beam which were later used to extract strain energies of each component from Model.res file using a translator, hmresdmp.exe, which translates HyperMesh binary results (.res) into ASCII file format. It was then possible to get required strain energies for each component automatically using element ID's. Once the strain energy values for each element were extracted the sum of total strain energies were computed within HyperStudy[®] layer by layer for the first ten modes. Moreover the modal frequencies, mass and volume information were also extracted as well as analytical calculation of loss factors based on the output modal strain energies as shown in Figure 3-81.

Active	Label	Variable	Expression	Value	Comment
<input checked="" type="checkbox"/>	BaseBeamESE@Mode1	r_1	sum(v_1)	... 29429.585	...
<input checked="" type="checkbox"/>	BaseBeamESE@Mode2	r_2	sum(v_2)	... 561424.63	...
<input checked="" type="checkbox"/>	BaseBeamESE@Mode3	r_3	sum(v_3)	... 2785426.3	...
<input checked="" type="checkbox"/>	BaseBeamESE@Mode4	r_4	sum(v_4)	... 7820402.7	...
<input checked="" type="checkbox"/>	BaseBeamESE@Mode5	r_5	sum(v_5)	... 1.82e+07	...
<input checked="" type="checkbox"/>	BaseBeamESE@Mode6	r_6	sum(v_6)	... 3.70e+07	...
<input checked="" type="checkbox"/>	BaseBeamESE@Mode7	r_7	sum(v_7)	... 6.86e+07	...
<input checked="" type="checkbox"/>	BaseBeamESE@Mode8	r_8	sum(v_8)	... 2.37e+08	...
<input checked="" type="checkbox"/>	BaseBeamESE@Mode9	r_9	sum(v_9)	... 1.19e+08	...
<input checked="" type="checkbox"/>	BaseBeamESE@Mode10	r_10	sum(v_10)	... 1.91e+08	...
<input checked="" type="checkbox"/>	SpacerESE@Mode1	r_11	sum(v_11)	... 3479.3244	...
<input checked="" type="checkbox"/>	SpacerESE@Mode2	r_12	sum(v_12)	... 241093.20	...
<input checked="" type="checkbox"/>	SpacerESE@Mode3	r_13	sum(v_13)	... 1974196.5	...
<input checked="" type="checkbox"/>	SpacerESE@Mode4	r_14	sum(v_14)	... 7449339.8	...
			⋮		
<input checked="" type="checkbox"/>	Loss Factor @Mode 1	r_63	$(0.001*r_1+0.008*r_11+r_53*r_21+0.001*r_31)/(r_1+r_11+r_21+r_31)$... 0.1178662	...
<input checked="" type="checkbox"/>	Loss Factor @Mode 2	r_64	$(0.001*r_2+0.008*r_12+r_54*r_22+0.001*r_32)/(r_2+r_12+r_22+r_32)$... 0.2285638	...
<input checked="" type="checkbox"/>	Loss Factor @Mode 3	r_65	$(0.001*r_3+0.008*r_13+r_55*r_23+0.001*r_33)/(r_3+r_13+r_23+r_33)$... 0.1653177	...
<input checked="" type="checkbox"/>	Loss Factor @Mode 4	r_66	$(0.001*r_4+0.008*r_14+r_56*r_24+0.001*r_34)/(r_4+r_14+r_24+r_34)$... 0.1232864	...
<input checked="" type="checkbox"/>	Loss Factor @Mode 5	r_67	$(0.001*r_5+0.008*r_15+r_57*r_25+0.001*r_35)/(r_5+r_15+r_25+r_35)$... 0.0885148	...
			⋮		

Figure 3-81 Extraction of strain energies and modal loss factors within HyperStudy[®]

Throughout the design process constant material properties were used for the viscoelastic layer since modal strain energy method utilizes the undamped mode shapes of the treated beam [64]. Corresponding loss factor values are used for each of modal frequency values. The values of loss factor were read from Figure 3-11 by considering each modal frequency of treated beam. The other material properties were selected to be same as given in Table 3-5.

3.2.7.3 Verification of Methodology

In order to verify the results of above methodology a three layer symmetric sandwich cantilever (Figure 3-82) beam model that has also been used by several other investigators [113, 114, 115] was used in comparison. It is particularly well characterized and suited for use in comparison with loss factors obtained by MSE and other approximate methods used by other investigators. Loss factors for the first three modes of the damped sandwich cantilever beam having the same material and geometrical properties were determined with FEA using proposed 2D design cycle (Figure 3-78). Calculated loss factors for the first three modes of the cantilever beam were compared to results obtained by other investigators.

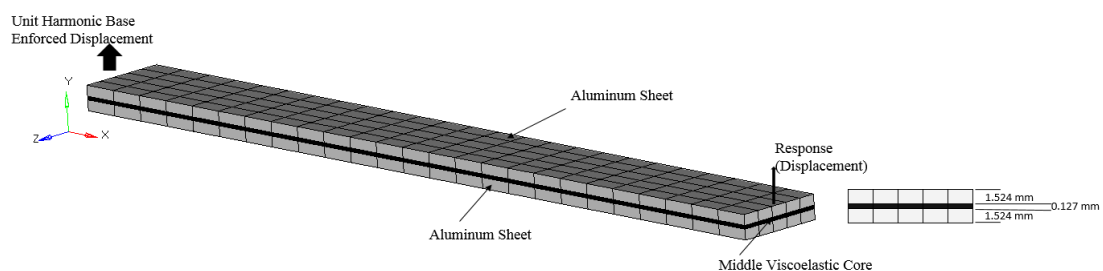


Figure 3-82 3D Finite element model of cantilever beam with viscoelastic core

The material and geometrical properties of cantilever sandwich beam that were used in analysis are given in the following Table 3-21.

Table 3-21 Material properties of sandwich beam [114]

	Aluminum	Viscoelastic Core
Thickness [mm]	1.524	0.127
Young's Modulus [Mpa]	69000	2.1
Poisson's Ratio	0.3	0.499
Loss Factor	0.0001	1.0
Density [kg/m ³]	2800	970

shows the comparison of results obtained with desing cycle with those of already published results for the cantilever beam shown in (Figure 3-82). In analysis the loss factor and material properties of viscoelastic layer has been choosen as constant. The beam is modelled in 2D with given dimensions and material properties. In order to compare the 2D analysis results, another 3D finite element model has been built and direct frequency response analysis was performed (Figure 3-82). The loss factors are calculated from the frequency responde function plots using half power bandwidth method after performin direct frequency response analysis. For this purpose a special MATLAB code has been written to accomplish this task such that the code finds the peaks of FRF plots and detects half-power bandwidth points from which it calculates the loss factors (Figure 2-17).

Table 3-22 Comparison of the loss factor results¹

$\eta_2=0.1$								
Model Comparison								
	Loss Factor				Frequency (Hz)			
	Plain Strain 2D FEM MSE (a)	3D FEM Direct Freq. Resp. (a)	Cho et. al. PLWPT (b)	Soni & Bogner 3D FEM (c)	Plain Strain 2D FEM MSE (a)	3D FEM Direct Freq. Resp. (a)	Cho et. al. PLWPT (b)	Soni & Bogner 3D FEM (c)
Mode I	0.0296	0.0320	0.02799	0.02817	66.10	65	64.28	64.2
Prct Err%	-	7.50%	5.75%	5.08%	-	1.69%	2.83%	2.96%
Mode II	0.0244	0.0250	0.02426	0.02425	306.33	300	297.48	297
Prct Err%	-	2.40%	0.58%	0.62%	-	2.11%	2.97%	3.14%
Mode III	0.0155	0.0160	0.01546	0.01534	770.88	754	747.98	747.2
Prct Err%	-	3.13%	0.26%	1.04%	-	2.24%	3.06%	3.17%
$\eta_2=0.3$								
Mode I	0.0873	0.0821	0.08127	0.08175	66.10	65	64.62	64.7
Prct Err%	-	6.33%	7.42%	6.79%	-	1.69%	2.29%	2.16%
Mode II	0.0717	0.0714	0.07227	0.07203	306.33	301	297.80	298
Prct Err%	-	0.42%	0.79%	0.46%	-	1.77%	2.86%	2.80%
Mode III	0.0448	0.0458	0.04635	0.04593	770.88	756	748.06	748.2
Prct Err%	-	2.18%	3.34%	2.46%	-	1.97%	3.05%	3.03%
$\eta_2=1.0$								
	Loss Factor				Frequency (Hz)			
	Plain Strain 2D FEM MSE (a)	3D FEM Direct Freq. Resp. (a)	Soni & Bogner 3D FEM (c)	Analytical 6th Order Theory (d)	Plain Strain 2D FEM MSE (a)	3D FEM Direct Freq. Resp. (a)	Soni & Bogner 3D FEM (c)	Analytical 6th Order Theory (d)
Mode I	0.2892	0.2014	0.2019	0.2022	66.10	68	67.4	67.4
Prct Err%	-	43.59%	43.24%	43.03%	-	2.79%	1.93%	1.93%
Mode II	0.2371	0.2009	0.2180	0.2177	306.33	310	307	302.8
Prct Err%	-	18.02%	8.76%	8.91%	-	1.18%	0.22%	1.17%
Mode III	0.1472	0.1403	0.1500	0.1502	770.88	769	762	748.6
Prct Err%	-	4.92%	1.87%	2.00%	-	0.24%	1.17%	2.98%

¹ (a) Present Study

(b) Cho KD, Han JH, Lee I. Vibration and damping analysis of laminated plates with fully and partially covered damping layers. J. Reinf. Plast Compos 2000; 19:1176–200.

(c) N.L. Soni, F.K. Bogner, (1982), Finite element vibration analysis of damped Structures, American Institute of Aeronautics and Astronautics Journal 20(5),700-707

(d) D. K. RAO , (1978) ,Frequency and loss factors of sandwich beams under various boundary conditions, Journal of Mechanical Engineering Science 20, 271-282.

As summarized in Table 3-22, analyzes were performed for three different loss factor values for the viscoelastic layer, 0.1, 0.3 and 1.0 for the same geometrical configuration, respectively. The error associated with loss factors that were found by 2D methodology for the lowest loss factor case, 0.1, is maximum 7.5% for the first mode, 2.4% for the second mode, 3.13 for the third mode. For the average loss factor, 0.3, the results are; maximum 7.42% for the first mode, 0.79% for the second mode, 3.34 for the third mode. And for the maximum loss factor case, 1.0, the results are; maximum 43.59% for the first mode, 18.02% for the second mode, 4.92% for the third mode. From the results we can conclude that as the loss factor of viscoelastic layer was increased the error achieved was also gets higher meaning that 2D modal strain method can only be used confidentially for the viscoelastic materials that has low loss factor values. On the other hand regardless of value of loss factor for the viscoelastic layer, 3D finite element method yields always closer results either to value of other researchers or analytical results. In addition to loss factor comparison the frequency deviation from others was %3.17 which is quite acceptable.

The comparison of 2D plain strain results with others shows that the design cycle can be used with enough confidence for design purpose especially for viscoelastic materials that possesses low loss factor values. Although the error is high for the high loss factor materials, in literature review section it was noted that the MSE method was proved to be efficient to find out relative effectiveness of design alternatives or various design configurations. Therefore the design cycle is used to find the effect of the geometrical parameters as well as material properties of each layer. For this purpose the height and Young's Modulus of stand-off layer were selected as design variable. Several other parameters can also be selected as design variable as long as they can be controlled in automatic modelling and analysis procedure as shown in Figure 3-83. All design variables were defined within a prescribed lower and upper bounds among which the geometry and material properties were selected for any single design alternative during iterations conducted by search algorithms.

Define design variables								
Add Design Variable Remove Design Variable								
	Active	Label	Varname	Lower Bound	Initial	Upper Bound	Comment	Category
1	<input checked="" type="checkbox"/>	L	m_1_BaseBeamLength	150.00000 ...	200.00000 ...	300.00000	Controlled ▼
2	<input checked="" type="checkbox"/>	H1	m_1_BaseBeamHeight	1.2000000 ...	1.6000000 ...	3.0000000	Controlled ▼
3	<input checked="" type="checkbox"/>	H2	m_1_SpacerHeight	3.0000000 ...	5.0000000 ...	15.000000	Controlled ▼
4	<input checked="" type="checkbox"/>	H3	m_1_VEMHeight	0.1000000 ...	0.1270000 ...	1.0000000	Controlled ▼
5	<input checked="" type="checkbox"/>	H4	m_1_CLHeight	0.1000000 ...	0.1000000 ...	1.0000000	Controlled ▼
6	<input checked="" type="checkbox"/>	ElasticModulus of SOL	m_1_E_core	5.0000000 ...	62.000000 ...	3000.0000	Controlled ▼
7	<input checked="" type="checkbox"/>	PoissonRatio of SOL	m_1_nu	0.3000000 ...	0.3700000 ...	0.4300000	Controlled ▼
8	<input checked="" type="checkbox"/>	Density of SOL	m_1_rho_core	1.38e-09 ...	1.54e-09 ...	1.69e-09	Controlled ▼
9	<input checked="" type="checkbox"/>	MeshSize	m_1_M	0.1000000 ...	0.5000000 ...	1.0000000	Controlled ▼
10	<input checked="" type="checkbox"/>	Equivalence	m_1_MergeMesh	0.0700000 ...	0.0800000 ...	0.0900000	Controlled ▼

Figure 3-83 Definition of geometrical and material parameters as discrete design variables.

3.2.7.3.1 Case Study I

As expected and realized from the previous case studies, it is obvious that there is an optimum spacer height for any given configuration of layered composite beam that maximize the loss factors at each of ten modes. Also the elastic modulus of spacer layer has effect on the value of loss factors. To extract the effect of both, for a fixed geometrical and material properties for other layers the dimension of stand-off height and value of Young's Modulus of stand-off layer were randomly altered between lower and upper bounds conducting design of experiment numerically for the cantilever sandwich beam model shown in Figure 3-84 . Design of experiment study conducted in HyperStudy® was an intelligent procedure that creates sets of solution out of assigned parameters that characterize the effect of each design variable.



Figure 3-84 Cantilever sandwich beam model and its design variables (E_2 & H_2)

The following plots, Figure 3-85 to Figure 3-88 show the loss factor variation with respect to mode numbers for each of predefined thickness values for the stand-off layer which were varied from 1.5 mm to 4 mm, additionally for each of thickness values, effect of different Young's Modulus values have also been reported graphically.

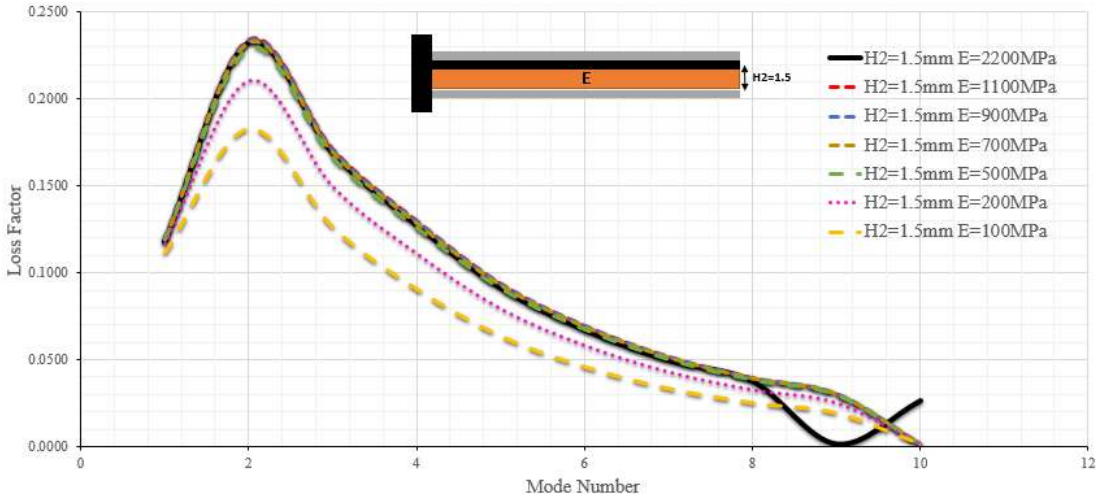


Figure 3-85 Variation of loss factor value for different modulus value for the first ten modes (H=1.5 mm)- E_{opt} =500-2200 MPa

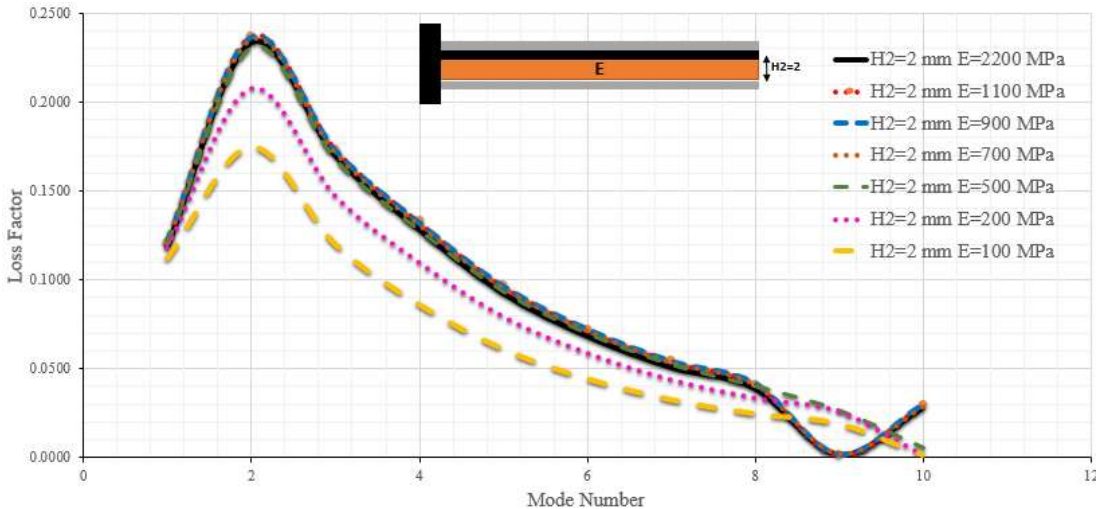


Figure 3-86 Variation of loss factor value for different modulus value for the first ten modes (H=2 mm)- E_{opt} =500-2200 MPa

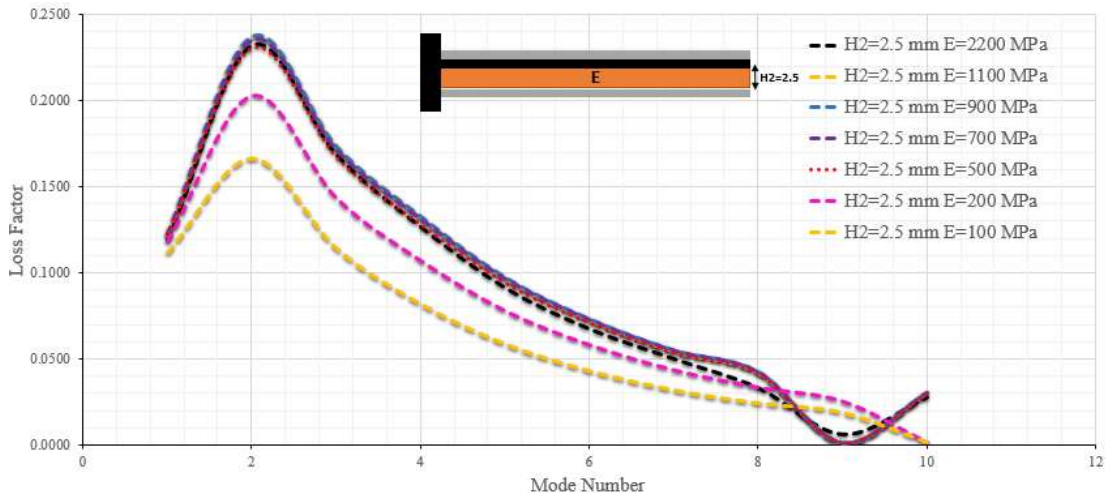


Figure 3-87 Variation of loss factor value for different modulus value for the first ten modes (H=2.5 mm) - E_{opt} =500-1100 MPa

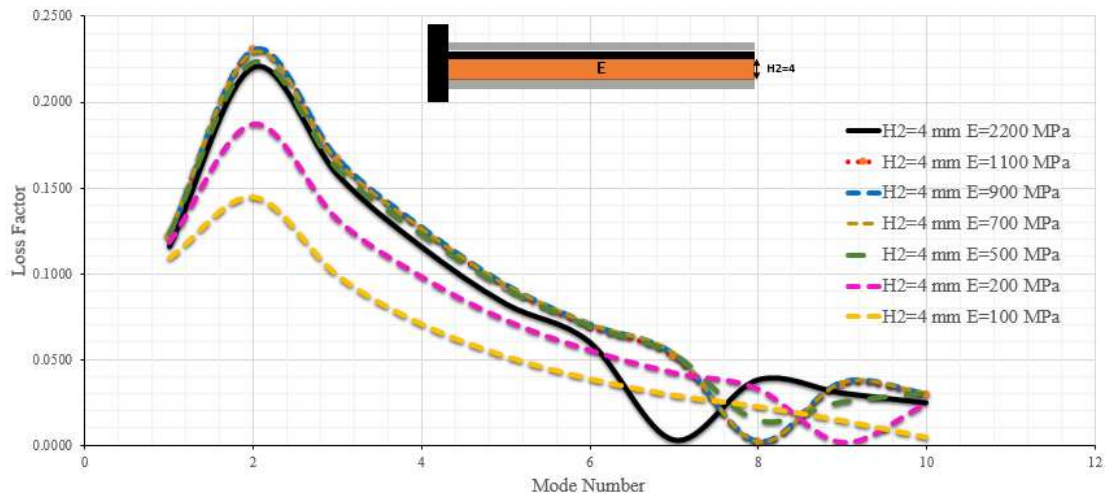


Figure 3-88 Variation of loss factor value for different modulus value for the first ten modes (H=4 mm) - E_{opt} =500-1100 MPa

The common conclusion that can be drawn from the above graphs is that the highest modal loss factor was achievable at the 2nd mode of cantilever beam regardless of thickness value of stand-off layer. Moreover the elastic modulus of stand-off layer greatly effects the value of loss factor which has also an optimum value for highest loss factor that is around $E_2 \approx 500 - 2200 \text{ MPa}$.

For target modulus value, $E_2=2200 \text{ MPa}$ the thickness variation can be extended as shown in Figure 3-89. It can be seen from the plots that there is also an optimum range of height value for stand-off layer for maximum damping capacity and it is around $H_2 \approx 2.5 - 3 \text{ mm}$ and the highest loss factor show itself at the 2nd mode. For an optimum modulus value as we increase the thickness beyond 2.5-3 mm the damping performance is decreased. This conclusion quite well agree with the previous results that were achieved for the topology optimization section of this chapter such that the thinner topology of stand-off layer had highest value of damping. However that should also be noted that the thicker the stand-off layer higher the reduction in response amplitude.

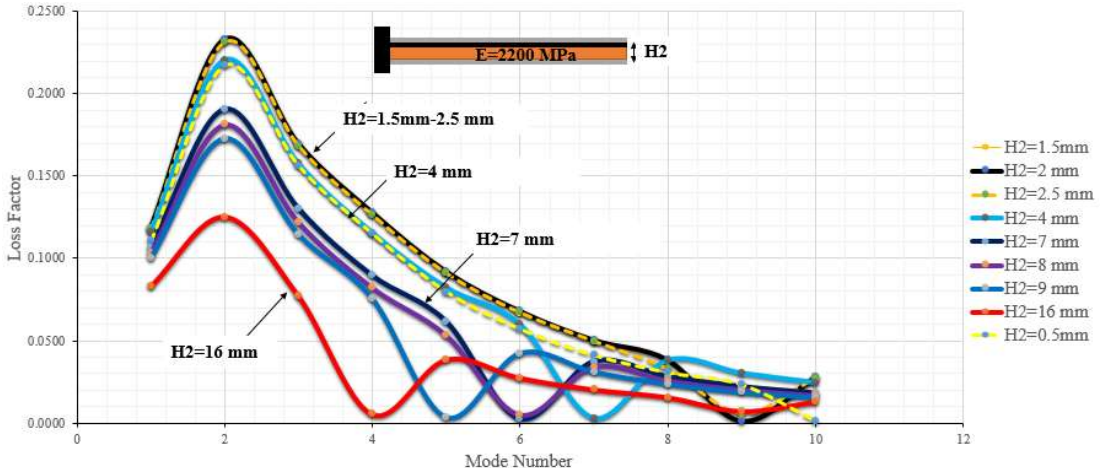


Figure 3-89 Effect of spacer height and elastic modulus on loss factor

In the following pages the loss factor variation with respect to stand-off height for the first ten modes was reported. From the graphs one can easily see that each mode has its maximum value around 2.5 mm-3 mm. Beyond the 3rd mode for the certain thickness values there exists sudden drop in loss factor due to longitudinal mode of vibration at which the shear deformation within viscoelastic layer almost diminish because each layer elongate and contract without relative motion between them. This also shows the fact that the main mechanism of damping is due to the shear deformation. Also this drop completely related with boundary condition, that is in our case fixed-free which allows such mode of vibration.

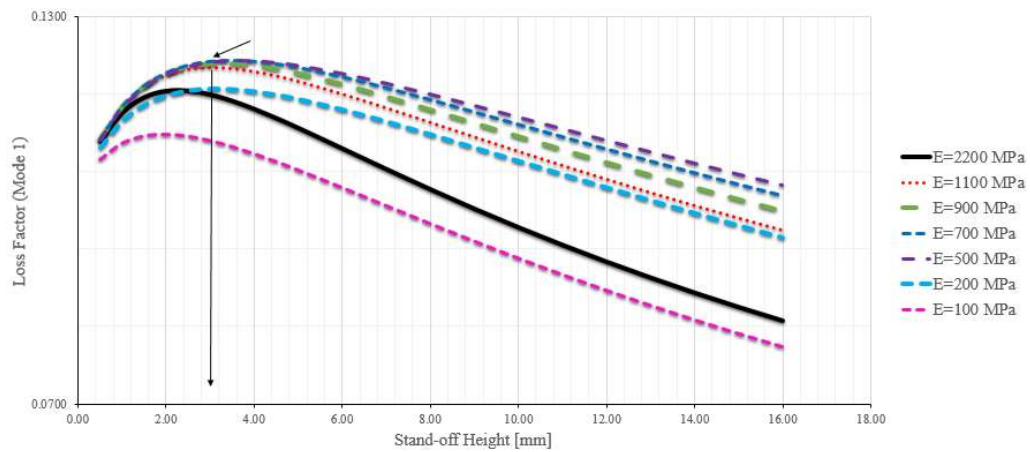


Figure 3-90 Effect of spacer height and elastic modulus on loss factor at 1st mode

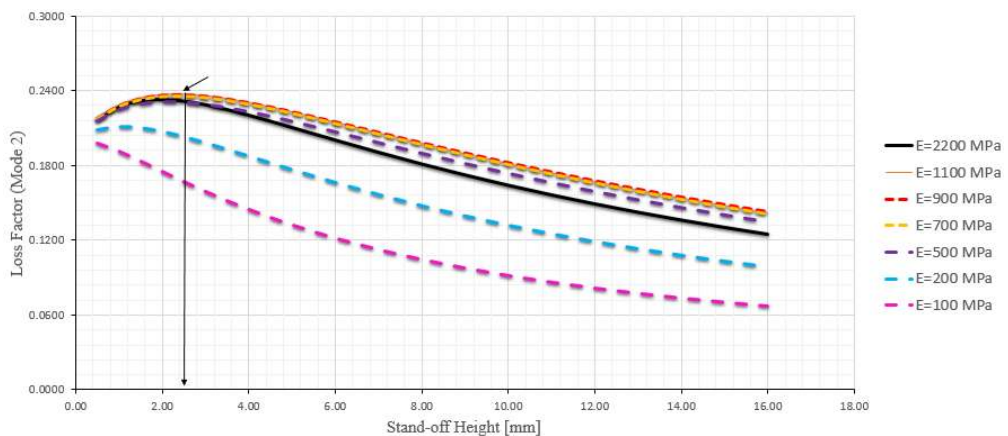


Figure 3-91 Effect of spacer height and elastic modulus on loss factor at 2nd mode

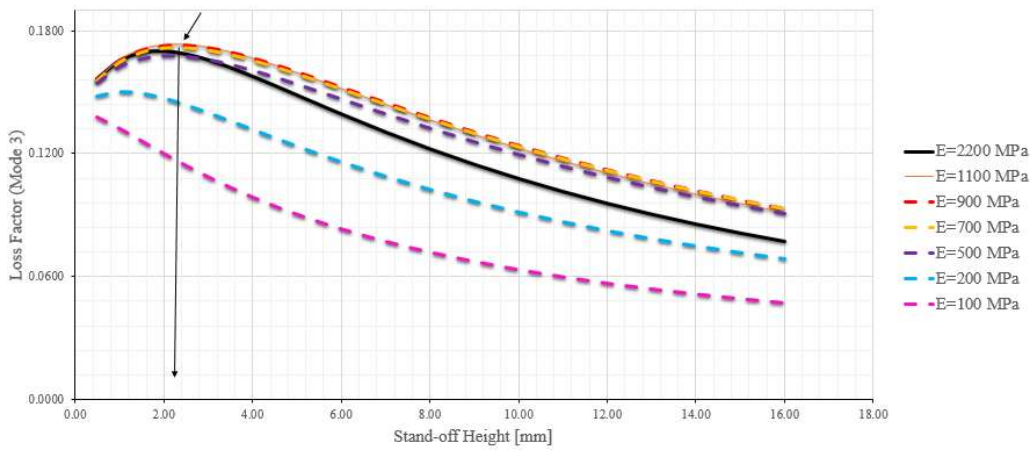


Figure 3-92 Effect of spacer height and elastic modulus on loss factor at 3rd mode

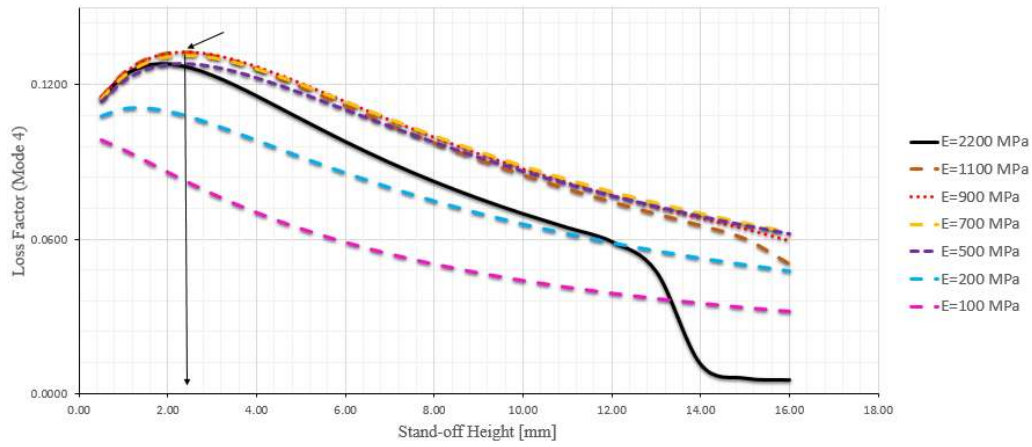


Figure 3-93 Effect of spacer height and elastic modulus on loss factor at 4th mode

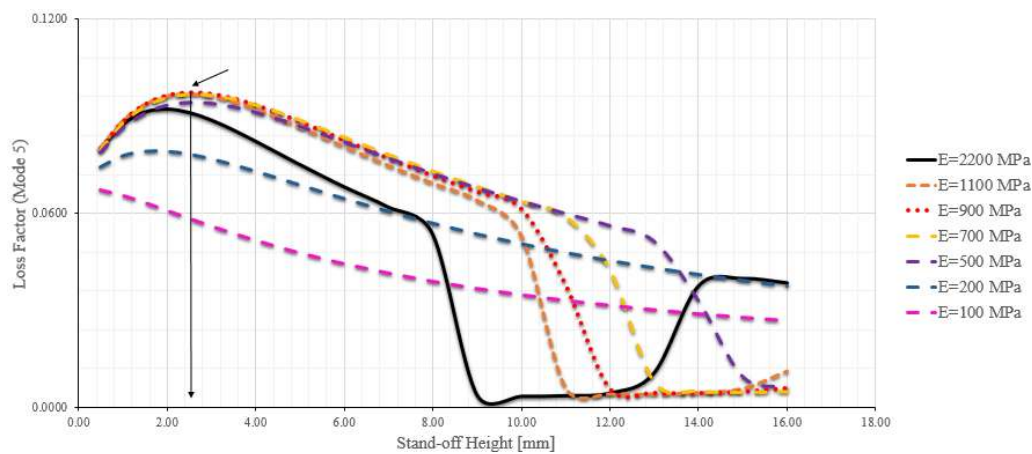


Figure 3-94 Effect of spacer height and elastic modulus on loss factor at 5th mode

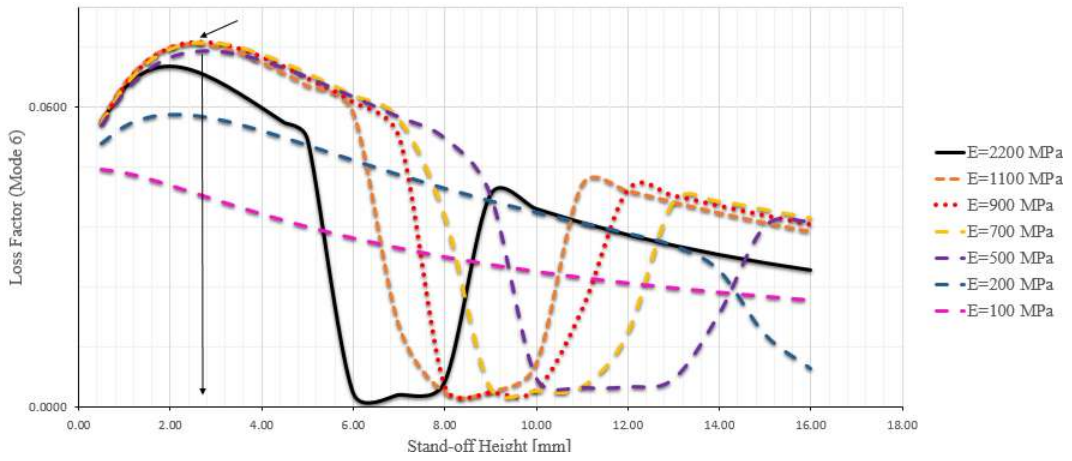


Figure 3-95 Effect of spacer height and elastic modulus on loss factor at 6th mode

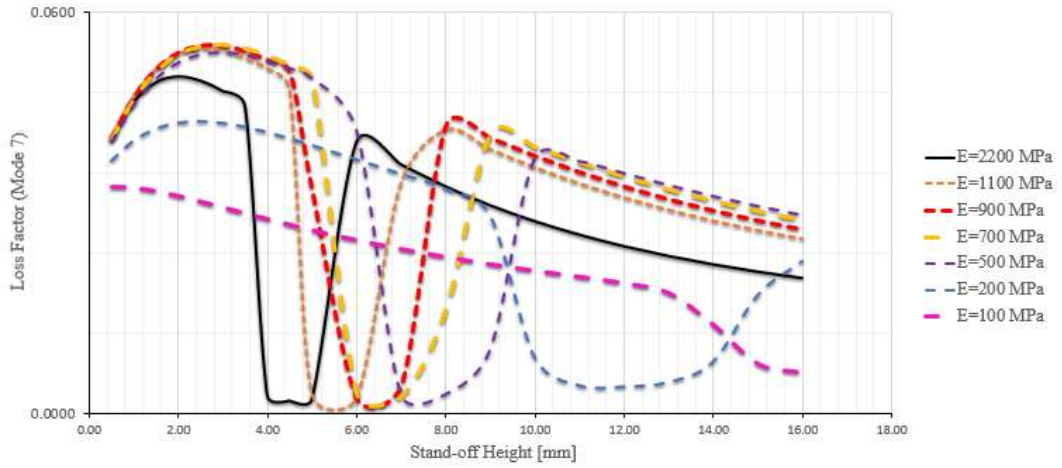


Figure 3-96 Effect of spacer height and elastic modulus on loss factor at 7th mode

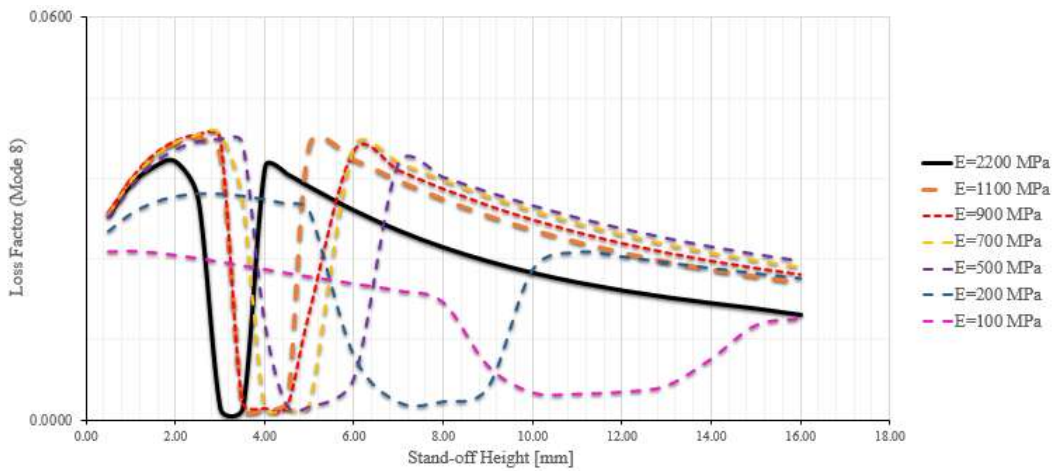


Figure 3-97 Effect of spacer height and elastic modulus on loss factor at 8th mode

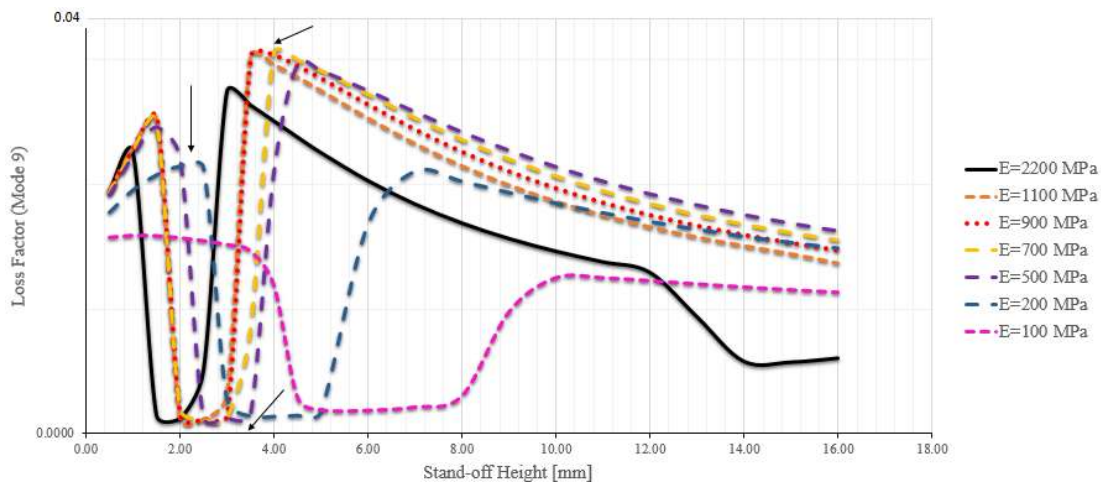


Figure 3-98 Effect of spacer height and elastic modulus on loss factor at 9th mode

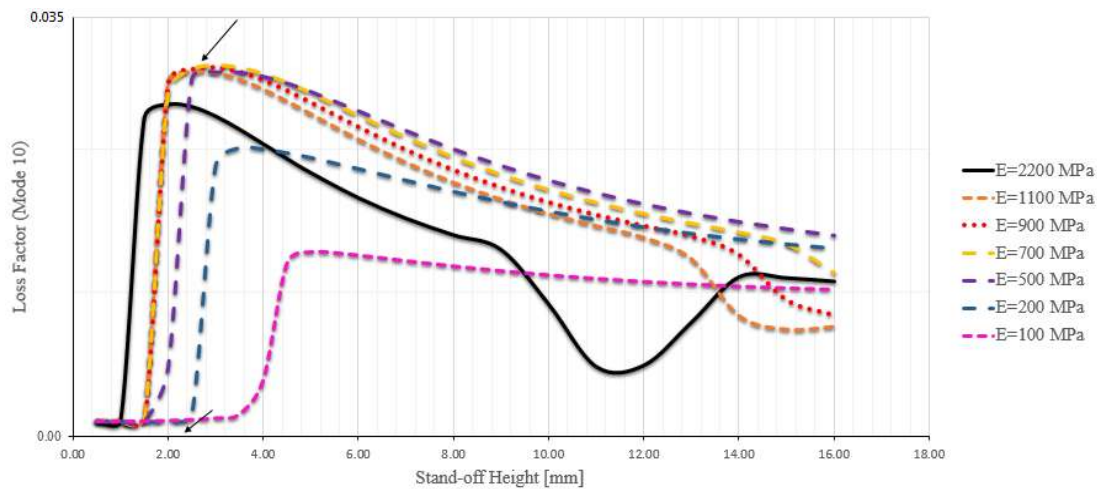


Figure 3-99 Effect of spacer height and elastic modulus on loss factor at 10th mode

The graphical results show the effect of both Young's Modulus and height of stand-off layer over the loss factor for the first ten modes. For the first mode of cantilever beam one can notice that the maximum loss factor for given configuration exists around $H_2=2.5-3$ mm with $E_2=500-2200$ MPa.

In order to extract the effect of modulus explicitly the loss factor variations were plotted with respect to elastic modulus data in Figure 3-100 to Figure 3-109. For almost all modes of vibration it was seen that for constant stand-off height there is an optimum modulus value for the stand-off material. For the first three modes for

$H_2=2.5-4$ mm the $E_2=500$ MPa value yields a maximum peak for loss factor beyond which the loss factor decreases. At higher modes $H_2=1.5-2.5$ mm yields maximum loss factor for almost all values of elastic modulus value beyond $E_2=500$ MPa if we neglect the slight gradual drop in loss factors. However for thicker stand-off layers this decrease much more dominant. Also there exists sudden drop in loss factor at some certain modulus and mode values due to longitudinal mode of vibration at which the shear deformation within viscoelastic layer almost diminish because each layer elongate and contract without relative motion between them.

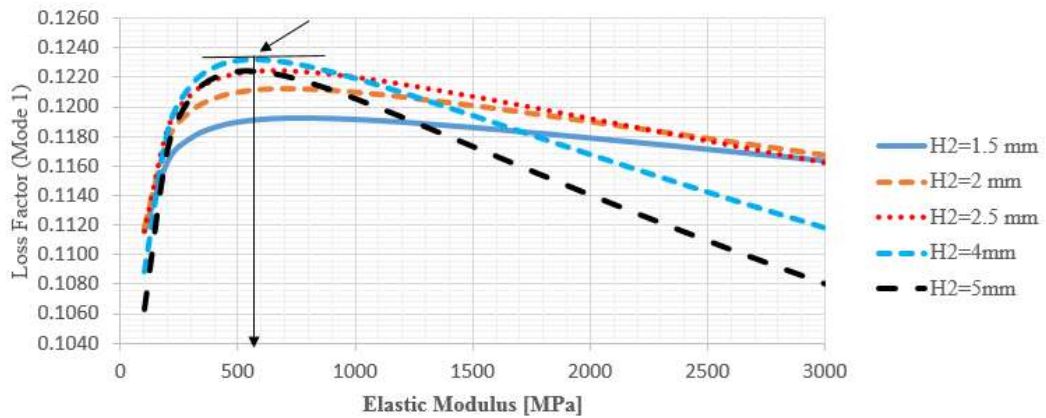


Figure 3-100 Effect of elastic modulus and spacer height on loss factor at 1st mode

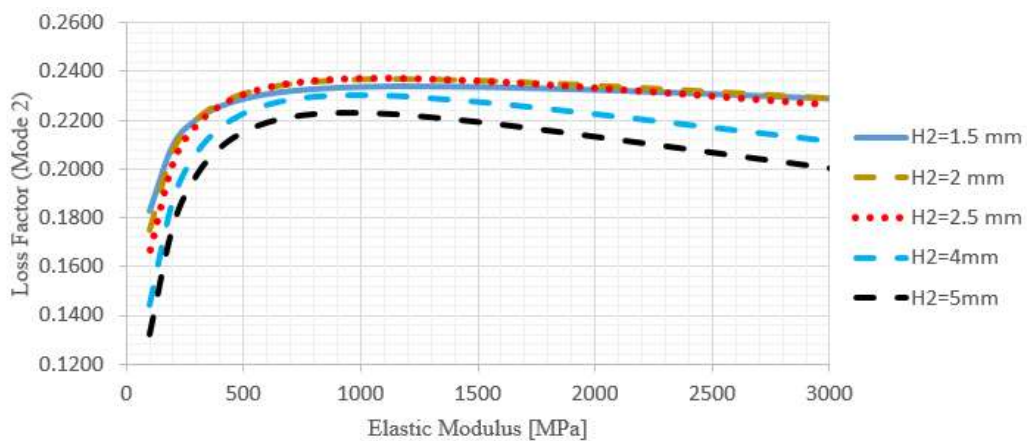


Figure 3-101 Effect of elastic modulus and spacer height on loss factor at 2nd mode

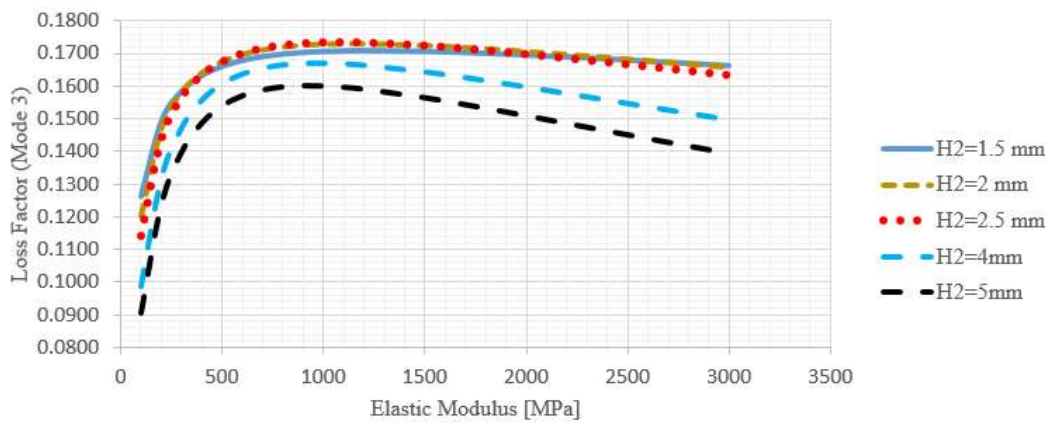


Figure 3-102 Effect of elastic modulus and spacer height on loss factor at 3rd mode

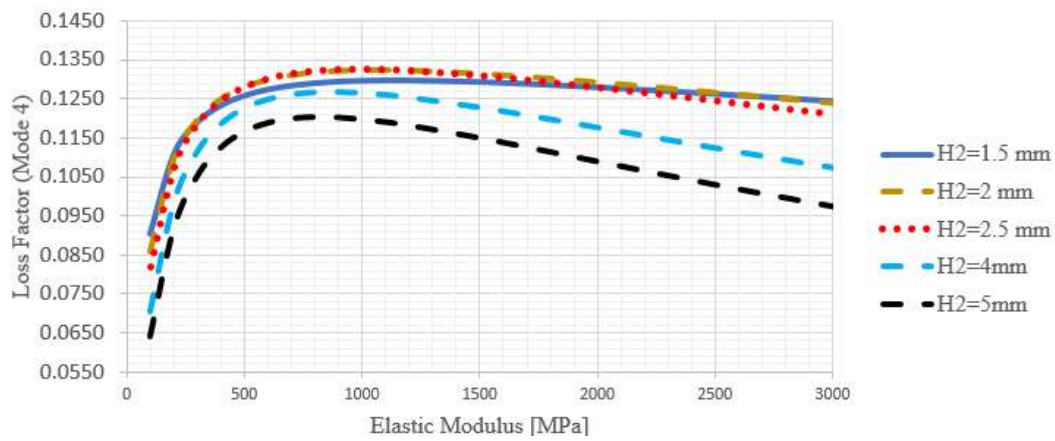


Figure 3-103 Effect of elastic modulus and spacer height on loss factor at 4th mode

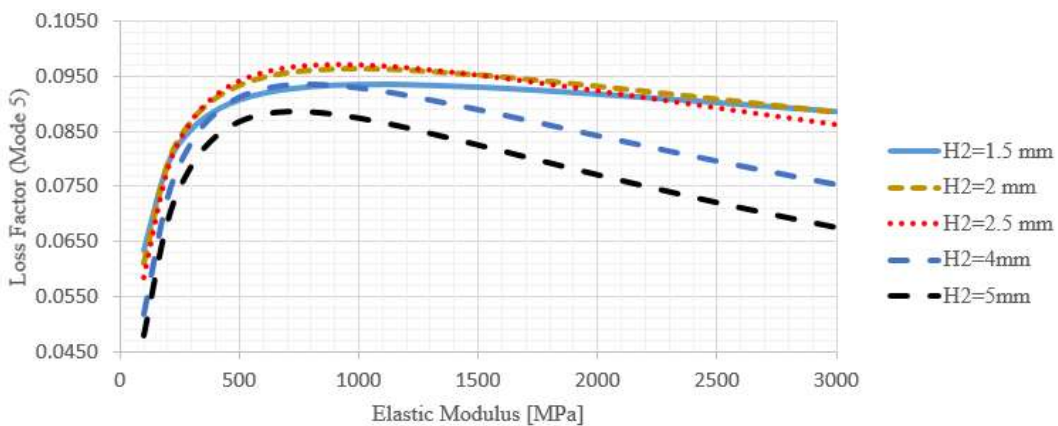


Figure 3-104 Effect of elastic modulus and spacer height on loss factor at 5th mode

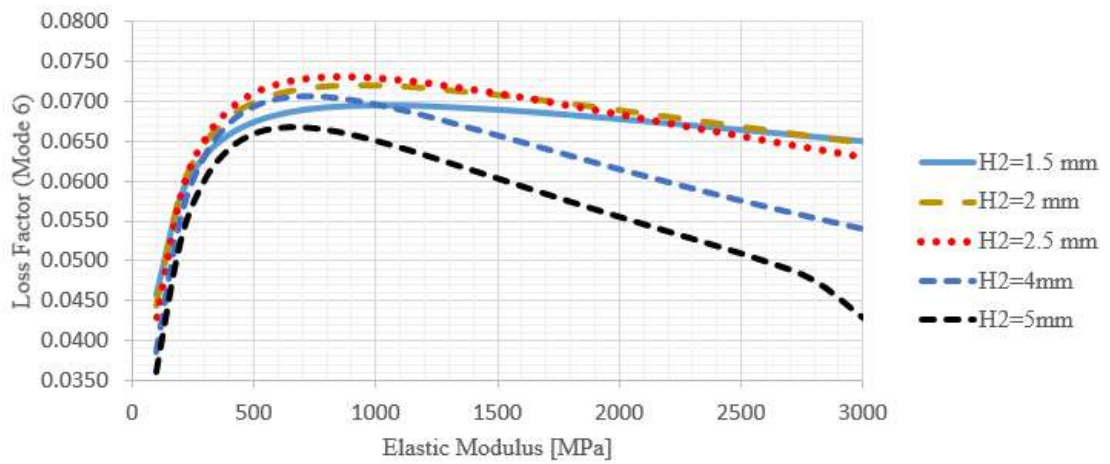


Figure 3-105 Effect of elastic modulus and spacer height on loss factor at 6th mode

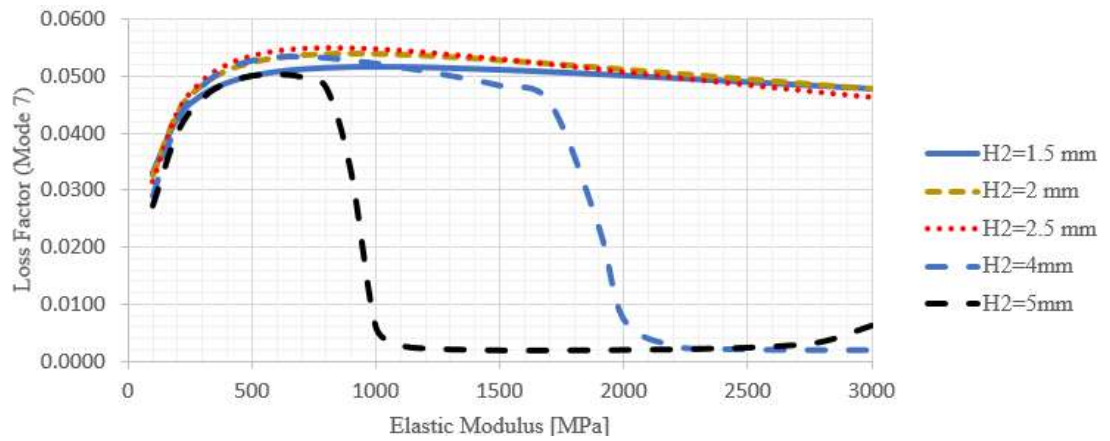


Figure 3-106 Effect of elastic modulus and spacer height on loss factor at 7th mode

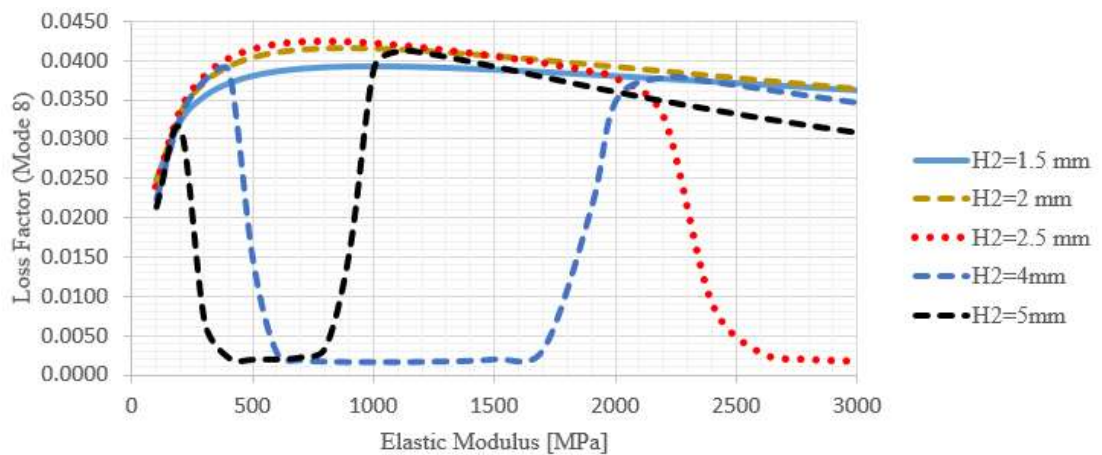


Figure 3-107 Effect of elastic modulus and spacer height on loss factor at 8th mode

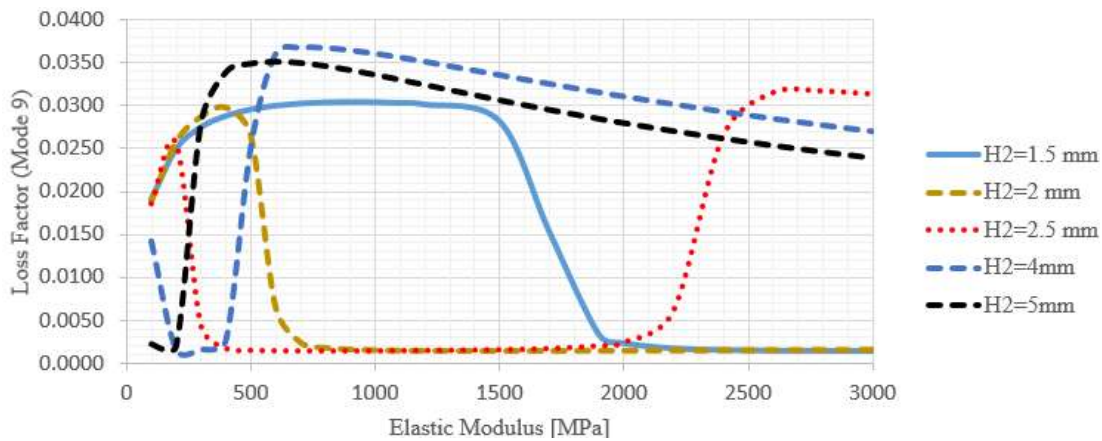


Figure 3-108 Effect of elastic modulus and spacer height on loss factor at 9th mode

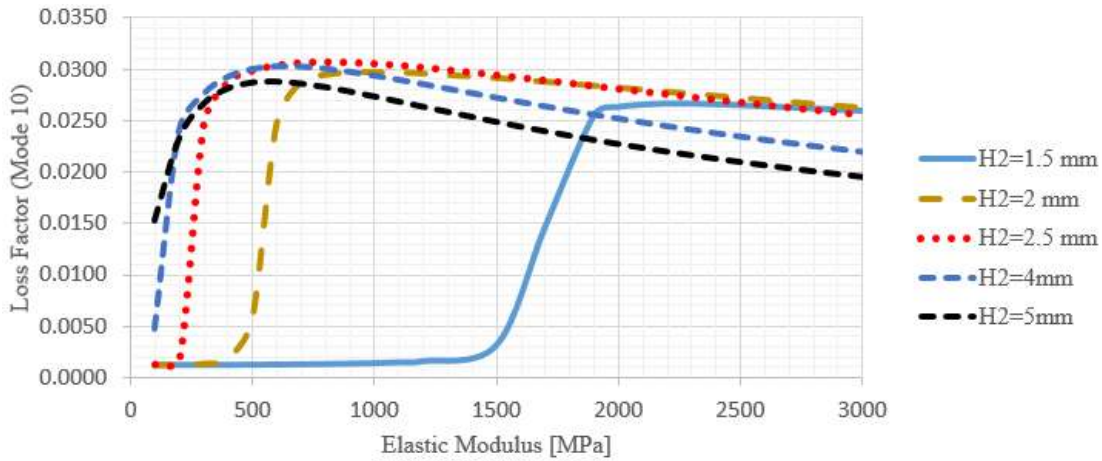


Figure 3-109 Effect of elastic modulus and spacer height on loss factor at 10th mode

The above all results suggest that for increase in all modal loss factor for the first three modes, the height of stand-off layer should be around H2=2.5 mm which implies increase of stand-off height further from a certain value is unnecessary in terms of damping capacity. Moreover the modulus of stand-off material, in other words the stiffness, greatly effects the results especially at first mode which has an optimum peak value beyond which the loss factor decreases dramatically for the fixed-free boundary condition.

3.2.7.3.2 Case Study II

In this case study a new automatized parameter study was performed using the previously mentioned design cycle. The study of Koruk et.al [66] and Yellin et.al [107] was adapted such that the stand-off layer which is our design domain was divided into certain number of separate design domains which forms the slotted configuration of stand-off layer which was created as a combination of some design parameters in CATIAV5-R22 environment as shown in

Figure 3-110. The first design parameter was selected to be as the height of the stand-off layer as was the case in previous study. In this case additional design parameters were created in order to find the best dimensions of slotted configuration through the use of optimization algorithms embedded in HyperStudy[®] environment with a more systematic method instead of following trial and error procedure. For this purpose the spacer domain divided into 21 cells. Each cell was thought to be like a window opening whose width controlled with a parameter value of cut-extrude option, used in Generative Shape Design Module in CATIAV5-R22, to remove the material from the design domain which in the ends creates the slots in stand-off layer and the remaining portion as columns. The width of those cuts assigned into a parameter p_i , $i=1$ to 21, as shown in

Figure 3-110. The value of each parameter was selected between 1 and 10 as lower and upper bounds respectively (Figure 3-112). As those parameters were changed by the optimization algorithms, the new model, based on new design parameters, p_i 's, automatically updated within CATIA using the newly created MACRO.catvbs and was sent to directly to the analysis environment using the same approach used in previous case study (Figure 3-78).

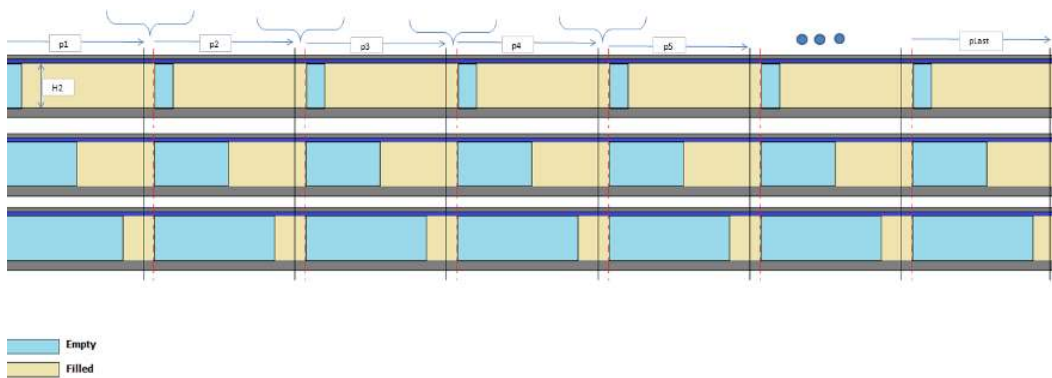


Figure 3-110 Design parameters of slotted stand-off layer

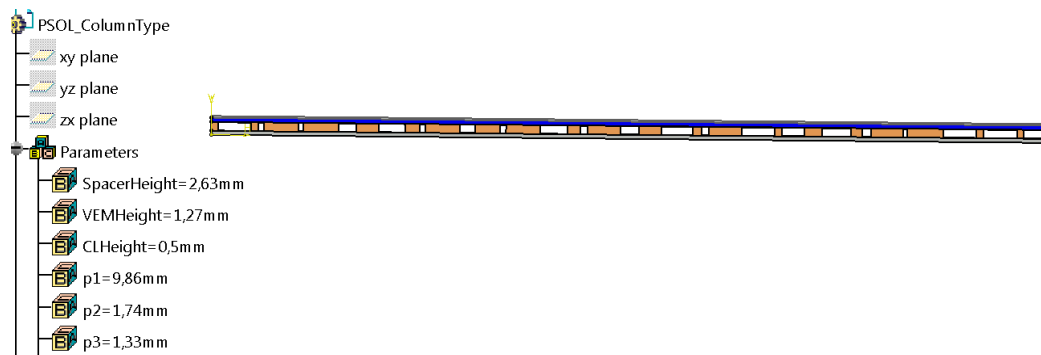


Figure 3-111 Parametric model of slotted configuration of treated beam

Define design variables									
Add Design Variable									
	Active	Label	Varname	Lower Bound	Initial	Upper Bound			
1	<input checked="" type="checkbox"/>	H2	m_1_SpacerHei...	2.0000000	2.6400000	20.0000000
2	<input checked="" type="checkbox"/>	p1	m_1_p1	1.0000000	1.0000000	10.0000000
3	<input checked="" type="checkbox"/>	p2	m_1_p2	1.0000000	1.0000000	10.0000000
4	<input checked="" type="checkbox"/>	p3	m_1_p3	1.0000000	1.0000000	10.0000000
5	<input checked="" type="checkbox"/>	p4	m_1_p4	1.0000000	1.0000000	10.0000000
6	<input checked="" type="checkbox"/>	p5	m_1_p5	1.0000000	1.0000000	10.0000000
7	<input checked="" type="checkbox"/>	p6	m_1_p6	1.0000000	1.0000000	10.0000000
8	<input checked="" type="checkbox"/>	p7	m_1_p7	1.0000000	1.0000000	10.0000000
	:	:	:	:	:	:			
22	<input checked="" type="checkbox"/>	p21	m_1_p21	1.0000000	1.0000000	7.0000000

Figure 3-112 Design variables in parameter optimization of slotted configuration

After defining the values of all design variables between certain ranges as shown in the Figure 3-112, the objective function was defined in a number of ways. At first, the four objective functions were created and selected as to be the maximization of loss factors for all first three modes of the treated beam since these modes dominates the overall dynamic response. Additionally another objection was defined to minimize the total volume of finite element model under cantilever boundary condition (Figure 3-113).

	Active	Label	Varname	Type	Apply On
1	<input checked="" type="checkbox"/>	Maximize Loss Factor @ Mode I	obj_1	Maximize	Loss Factor @Mode I (r_18)
2	<input checked="" type="checkbox"/>	Maximize Loss Factor @ Mode II	obj_2	Maximize	Loss Factor @Mode II (r_19)
3	<input checked="" type="checkbox"/>	Maximize Loss Factor @ Mode III	obj_3	Maximize	Loss Factor @Mode III (r_20)
4	<input checked="" type="checkbox"/>	MinimizeVolume	obj_4	Minimize	TOTAL VOLUME (r_14)

Figure 3-113 Objective functions definitions in optimization

Based on the objective and constraint functions HyperStudy® enables engineers to select different kinds of built-in optimization algorithms. In our case since multiple objective functions were created among which two of them were ready to be selected as depicted in Figure 3-114. The Global Response Surface Method (GRSM), which is one of the special optimization algorithms, developed by Altair Engineering Inc. was selected as it provides either single or multi objective optimization. The defaults settings were used throughout calculations.

Specifications				
	Mode	Label	Varname	Details
1	<input type="radio"/>	Adaptive Response Surface Method	ARSM	Only single-obj...
2	<input checked="" type="radio"/>	Global Response Surface Method	GRSM	
3	<input type="radio"/>	Sequential Quadratic Programming	SQP	Only single-obj...
4	<input type="radio"/>	Method of Feasible Directions	MFD	Only single-obj...
5	<input type="radio"/>	Genetic Algorithm	GA	Only single-obj...
6	<input type="radio"/>	Multi-Objective Genetic Algorithm	MOGA	
7	<input type="radio"/>	Sequential Optimization and Reliability Assessment	SORA	Only single-obj...
8	<input type="radio"/>	ARSM based SORA	SORA_ARSM	Only single-obj...
9	<input type="radio"/>	Single Loop Approach	SLA	Only single-obj...
10	<input type="radio"/>	Xopt	xopt	User Defined

Figure 3-114 Built-in optimization algorithms

GRSM method simply creates hundreds of sample design alternatives out of given design by changing the design variables which are related with response of the system (Figure 3-115).The method then fits a response surface on which it finds the optimum [148].

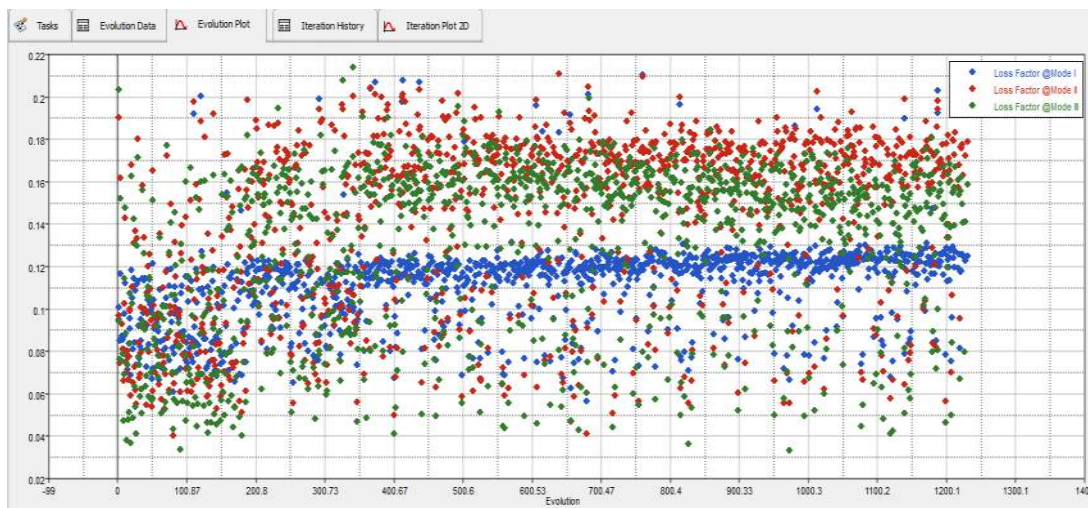


Figure 3-115 Evaluation history of optimization method.

Based on the GRSM method the optimal parameters of slotted configuration of stand-off layer were extracted, among hundreds of sample designs, as to be the values given in Table 3-23. Compared to design of experiment study conducted in previous case study, the optimal height of the stand-off layer was found to be as $H=2.51$ mm which is quite in agreement with the optimum value which was found to be around $H=2.5-3$ mm. For the highest damping the best slot dimensions are also extracted, in other words, best location and length of the viscoelastic patches that should be attached over the spacer layer (Figure 3-116). Those locations are known to be the area where the highest strain energy is cumulated during flexural motion (Figure 3-117).

Table 3-23 Optimum values of parameters for the slotted configuration (GRSM)

H2	p1	p2	p3	p4	p5	p6	p7	p8	p9	p10	p11	p12	p13	p14	p15	p16	p17	p18	p19	p20	p21
2.51	8.73	8.13	9.27	2.97	9.50	3.15	7.20	2.91	6.09	1.22	8.59	2.45	2.25	3.99	7.72	8.77	8.74	8.41	8.87	2.86	2.04

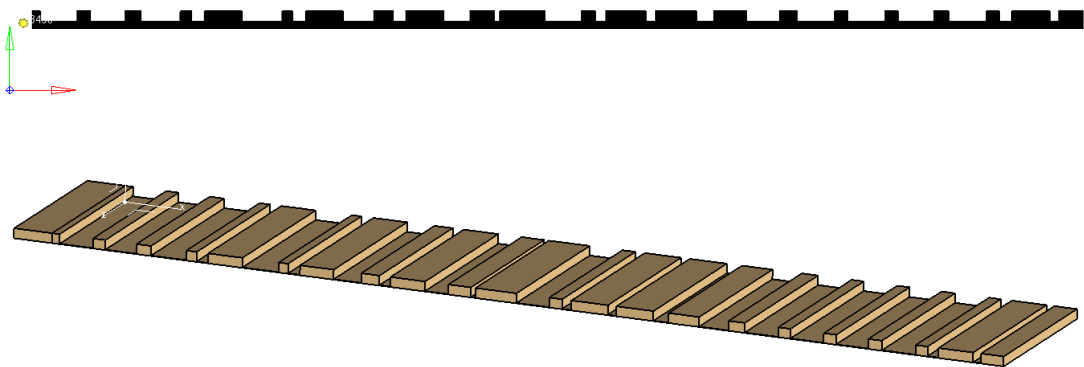


Figure 3-116 Optimized slotted configuration of stand-off layer ($H=2.513$ mm)

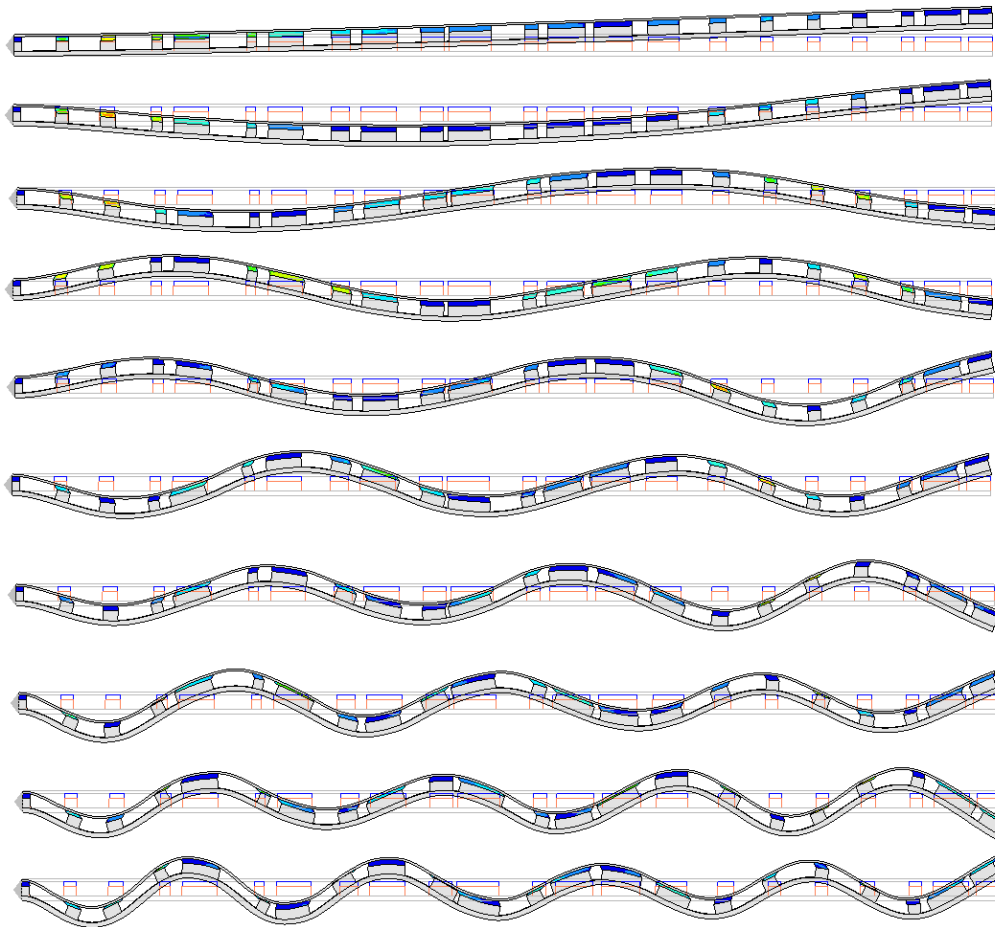


Figure 3-117 Mode shapes of treated cantilever beam with optimized slotted stand-off layer ($H_2=2.513$ mm)

Based on the mode shapes extracted, the material distribution obtained was cumulated at the regions where high strain energy is induced (Figure 3-117).

Recalling the use of approximate constant material properties for the viscoelastic layer, in order to assess the damping performance of this optimized slotted configuration, direct frequency response analysis with the frequency dependent material properties was performed. Point frequency displacement responses for different thickness values were extracted for the stand-off layer to see the effect of geometrical parameters and compare the damping performance of optimized slotted configuration with respect to those uniform stand-off layers with $H=10$ mm, $H=4$

mm and $H=2.51$ mm together with $H=1.32$ mm uniform spacer of equivalent weight respectively.

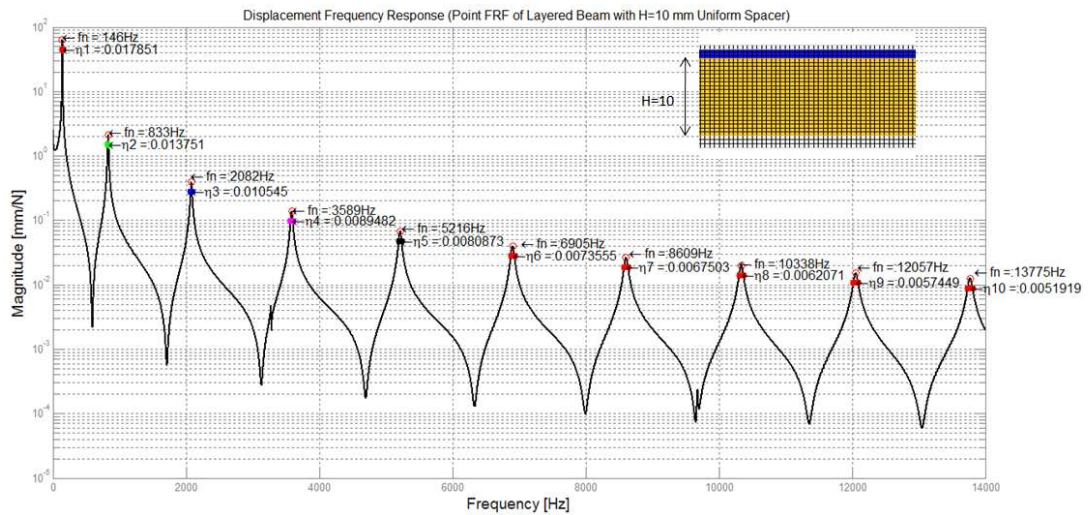


Figure 3-118 Displacement response of treated beam with uniform stand-off ($H=10$ mm).

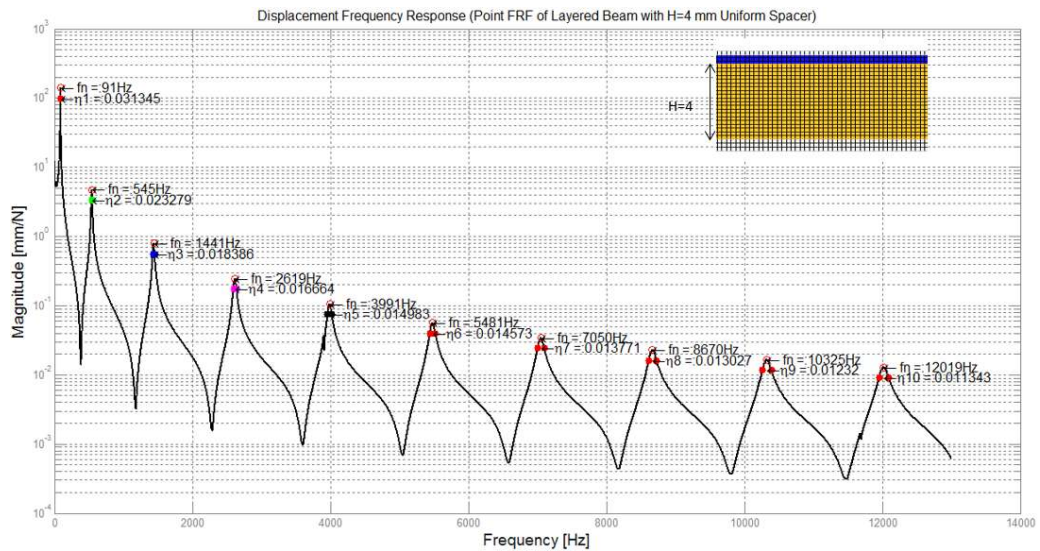


Figure 3-119 Displacement response of treated beam with uniform stand-off ($H=4$ mm).

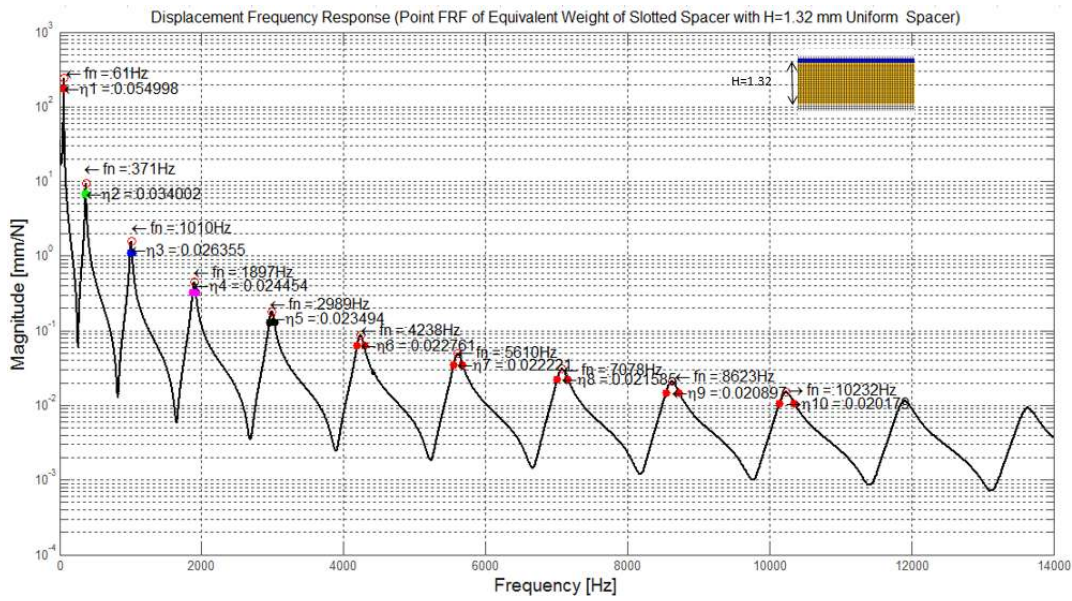


Figure 3-120 Displacement response of treated beam with uniform stand-off (H=1.32 mm).

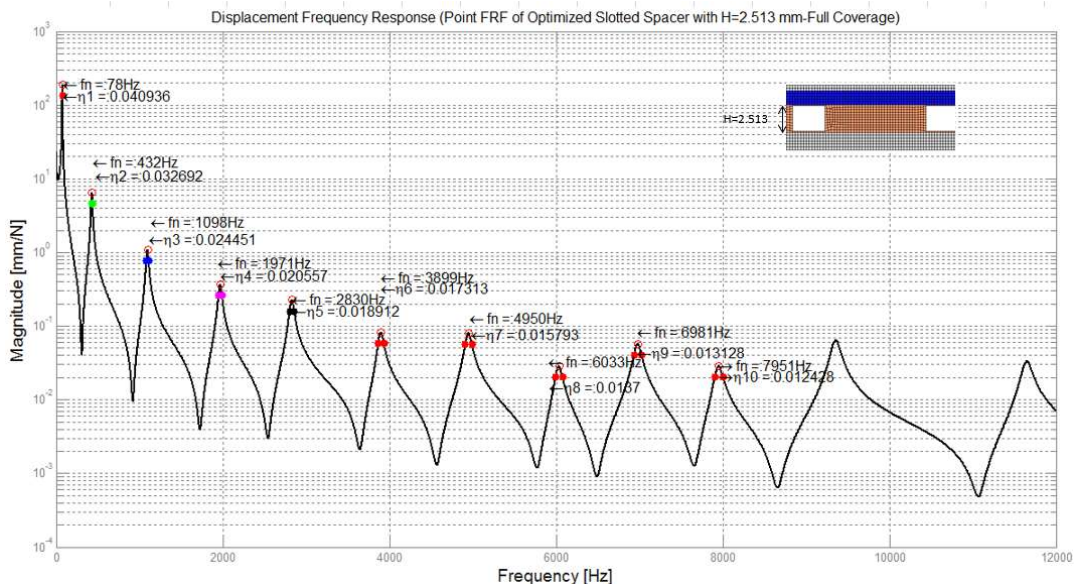


Figure 3-121 Displacement response of treated beam with optimized slotted stand-off (H=2.513 mm -Full Coverage).

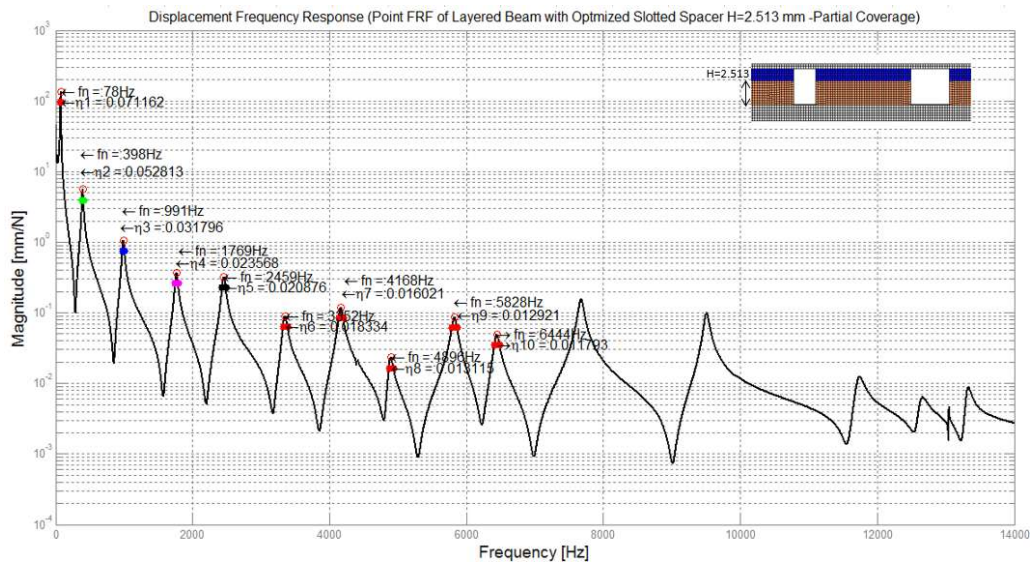


Figure 3-122 Displacement response of treated beam with optimized slotted stand-off (H=2.513 mm -Partial Coverage).

The overall comparison of frequency response functions of all treated beams with different height and configuration of stand-off layer that were considered above can be given in a single plot as shown in Figure 3-123. Again for the thinner configuration, the displacement response amplitude is relatively higher while the damping capacity is also higher. One can see also from the frequency response function that the optimized slotted configuration has higher damping capacity and lower response amplitude compared to $H_2=4$ mm and its counterpart $H_2=1.32$ mm with same weight.

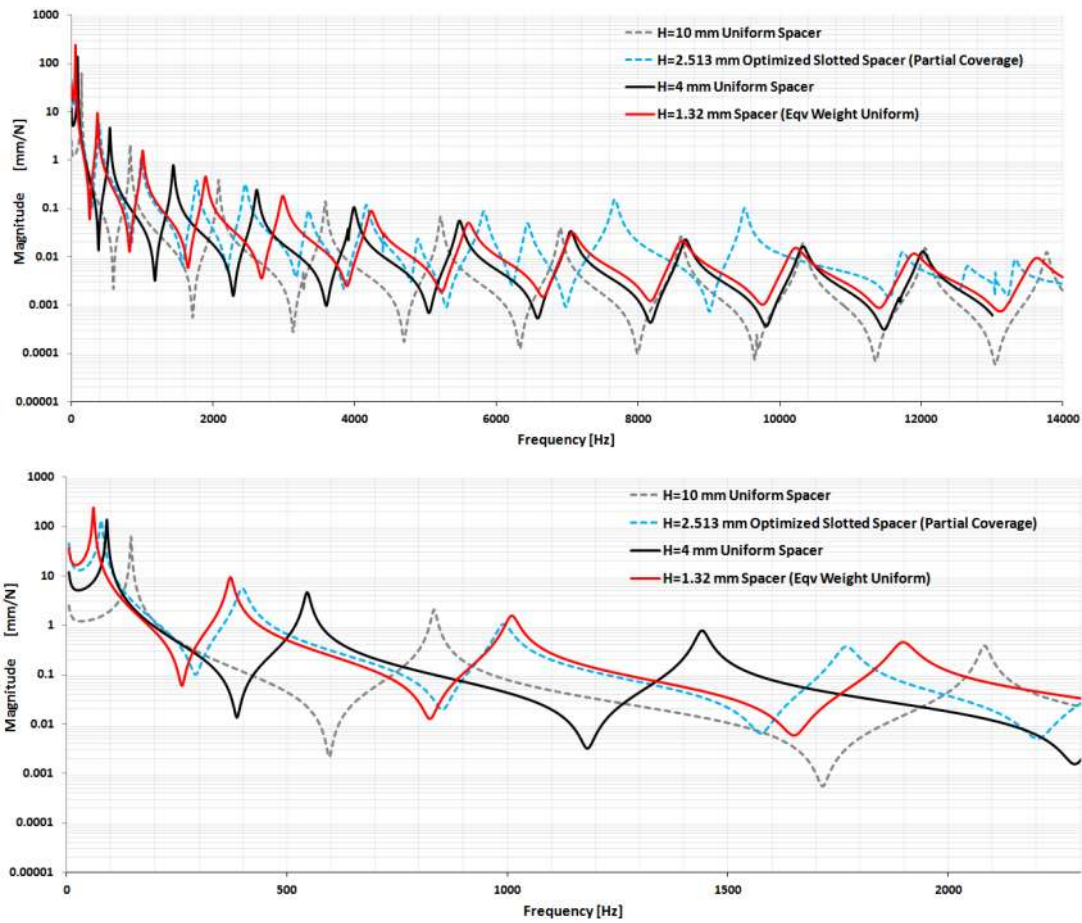








Figure 3-123 Overall comparison of treated beams with uniform and optimized stand-off.

Additionally, the partial treatment of optimized slotted configuration has considerable lowered response amplitude beyond 10 kHz although there are two peak regions with higher displacement amplitude between 7 kHz and 10 kHz.

The Table 3-24 summarizes the numerical values for the relative damping improvement with respect to uniform case. According to the results, the optimized slotted has relatively higher damping only between 2nd and 4th mode while partial treated configuration has relatively much higher damping capacity at first 5 modes compared to uniform thin stand-off layer (H=2.513 mm).

Table 3-24 Relative damping performance of optimized slotted stand-off layer

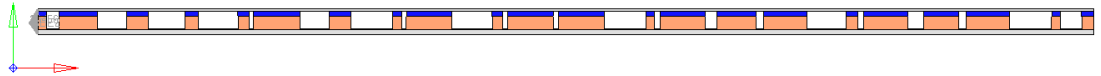
(Slotted Stand-off Optimization-H=2.513 mm) Global Response Surface Method						
Relative Damping Performance w.r.t. Uniform Stand-Off Layer						
Frequency f [Hz]			Loss Factor $\eta=2\zeta$			
H=2.513						
						
Mode #	Uniform Full Coverage	Optimized Full Coverage	Optimized Partial Coverage	Uniform Full Coverage Weight=100%	Optimized Full Coverage Weight=87.87%	Optimized Partial Coverage Weight=69.03%
Prct [%]						
1-+	75.00	78.00	78.00	0.041	0.041	0.071
				-	↓ -0.97%	↑ 72.39%
2++	453.00	432.00	398.00	0.028	0.033	0.053
				-	↑ 15.65%	↑ 86.74%
3++	1217.00	1098.00	991.00	0.022	0.025	0.032
				-	↑ 10.40%	↑ 43.29%
4++	2252.00	1971.00	1769.00	0.020	0.021	0.024
				-	↑ 1.02%	↑ 15.73%
5-+	3489.00	2830.00	2459.00	0.019	0.019	0.021
				-	↓ -2.09%	↑ 8.27%
6--	4870.00	3899.00	3352.00	0.018	0.017	0.018
				-	↓ -6.26%	↓ -0.85%
7--	6352.00	4950.00	4168.00	0.018	0.016	0.016
				-	↓ -10.75%	↓ -9.62%
8--	7907.00	6033.00	4896.00	0.017	0.014	0.013
				-	↓ -19.26%	↓ -22.79%
9--	9516.00	6981.00	5828.00	0.016	0.013	0.013
				-	↓ -19.35%	↓ -20.58%
10--	11172.00	7951.00	6444.00	0.015	0.012	0.012
				-	↓ -19.86%	↓ -23.73%

In order to compare the efficiency of optimization algorithms available within HyperStudy® the search for the optimum parameters has been repeated for different optimization algorithms, Genetic Algorithm (GA) and Multi Objective Genetic Algorithm (MOGA) respectively. Genetic algorithm provides single objective function which was selected as to be the maximization of loss factor for the first mode of cantilever beam without any other constraints or objection since the first mode has highest response amplitude that dominates the overall vibration response of the vibrating beam hence cause inherent structural weakness. Therefore the first mode loss factor was maximized (Table 3-25)

Table 3-25 Optimum values for slotted configuration: Genetic Algorithm (GA)

Add Objective		Remove Objective					
Active	Label	Varname	Type	Apply On	Evaluate From		
<input checked="" type="checkbox"/>	Maximize ESE @ Mdoe I	obj_1	Maximize	Loss Factor @Mode I (r_18)	SOLVER		
<input type="checkbox"/>	Maximize ESE @ Mdoe II	obj_2	Maximize	Loss Factor @Mode II (r_19)	SOLVER		
<input type="checkbox"/>	Maximize ESE @ Mdoe III	obj_3	Maximize	Loss Factor @Mode III (r_20)	SOLVER		
<input type="checkbox"/>	MinimizeVolume	obj_4	Minimize	TOTAL VOLUME (r_14)	SOLVER		

H2	p1	p2	p3	p4	p5	p6	p7	p8	p9	p10	p11	p12	p13	p14	p15	p16	p17	p18	p19	p20	p21
3.12	2.90	6.89	8.80	9.35	1.04	6.89	10.00	1.15	9.56	1.23	1.13	9.98	1.25	2.72	1.69	9.33	1.53	3.77	1.79	9.91	5.09



Based on the mode shapes extracted, the material distribution obtained was cumulated at the regions where high strain energy is induced (Figure 3-124).

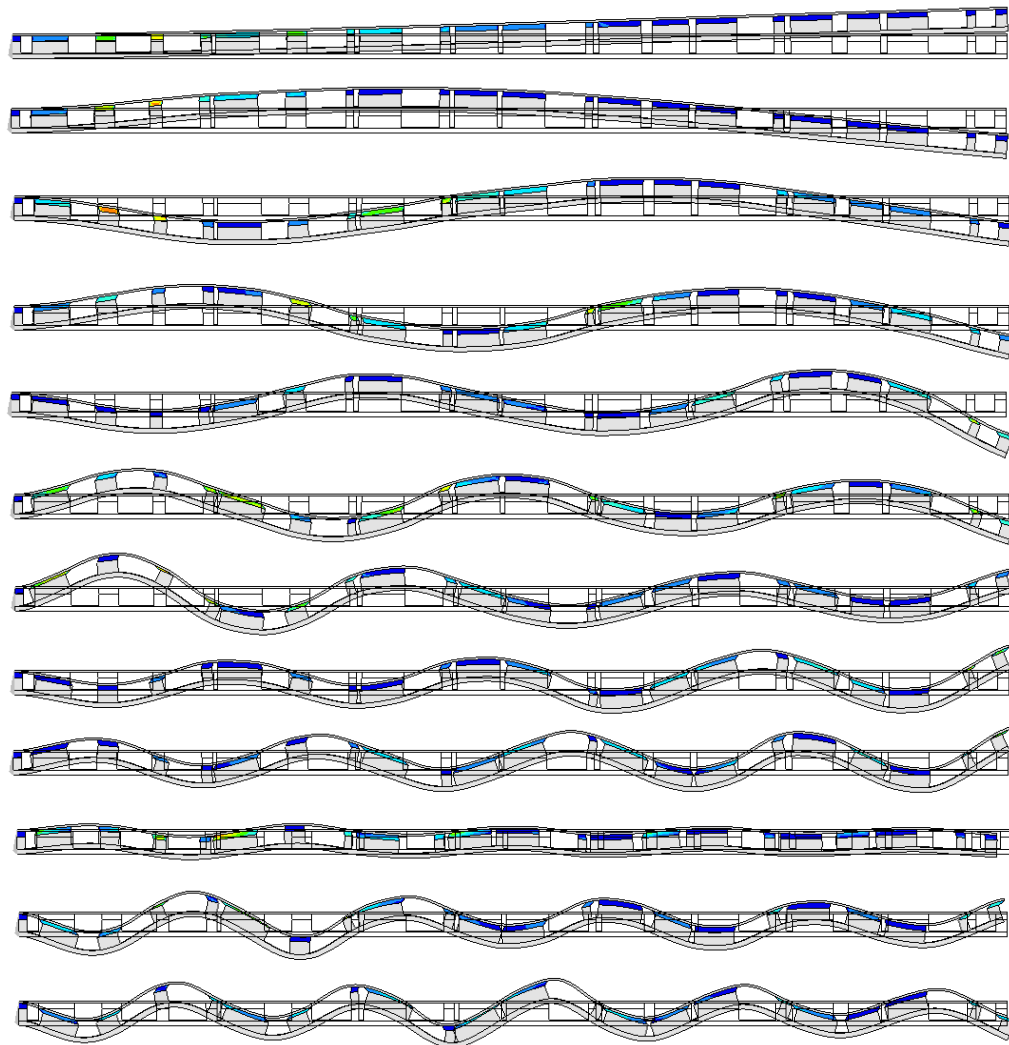


Figure 3-124 Mode shapes of treated cantilever beam with optimized slotted stand-off layer ($H_2=3.12$ mm)

To extract the modal loss factors for all ten modes the frequency response analysis was performed for the partial treatment. As shown in Figure 3-125, the frequency response amplitudes are higher at lower modes compared to results of GRSM ($H=2.513$ mm). However the GA results ($H=3.12$ mm) such configuration that it yields an extended anti-resonance region between 6.2 kHz and 12 kHz suppressing corresponding modes at this range while GRSM yielded two higher peaks at same location but beyond 12 kHz GRSM results improved amplitude reduction.

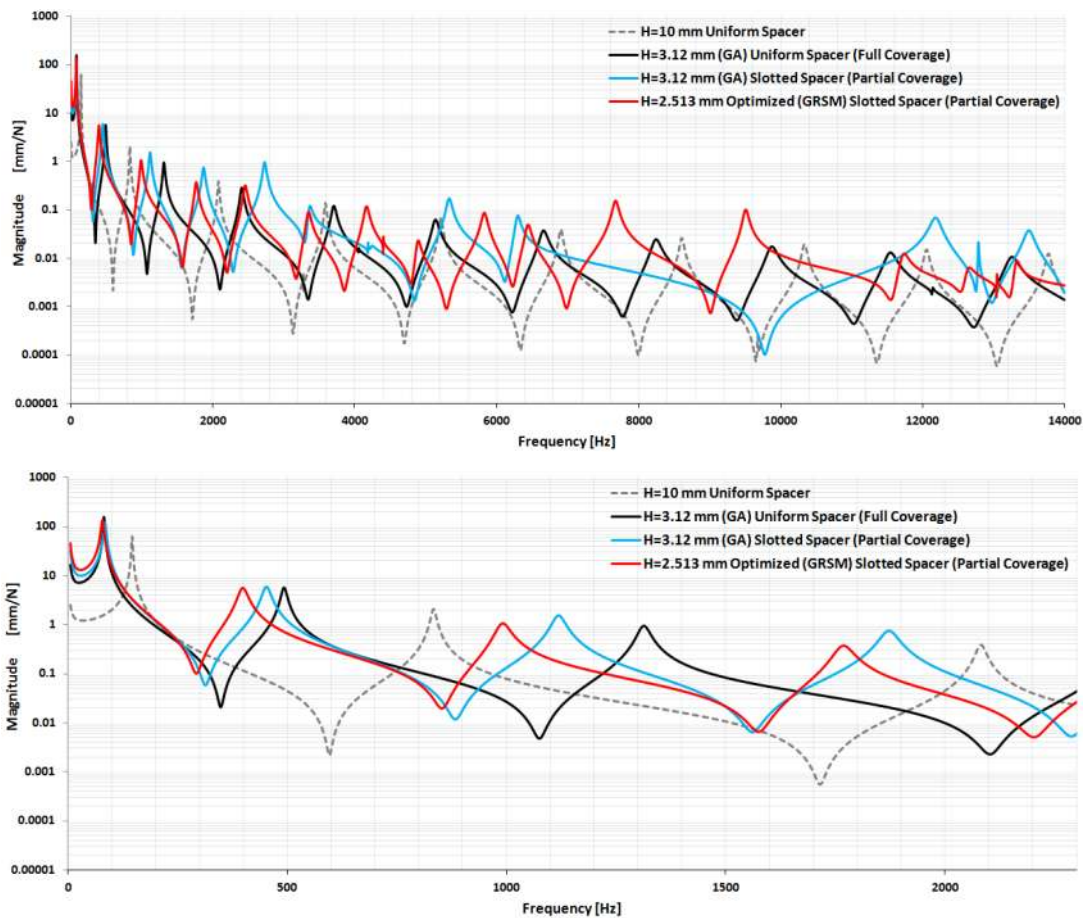








Figure 3-125 Comparison of results of optimization algorithms: GRSM vs GA

The numerical results for the relative damping capacity compared to its uniform case is given in Table 3-26. According to the results, the optimized slotted has relatively higher damping only between 2nd and 7th mode which shows extended but lower performance compared to GRSM result, while partial treated configuration has relatively much higher damping capacity at first 4 modes, which are also numerically lower than GRSM result, compared to uniform thin stand-off layer (H=3.12 mm).

Table 3-26 Relative damping performance of optimized slotted stand-off layer (GA)

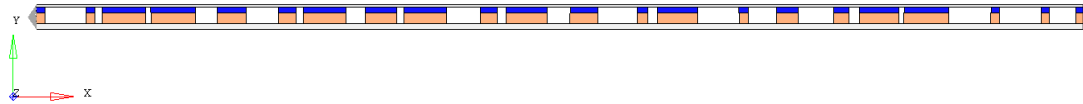
(Slotted Stand-off Optimization-H=3.12 mm) Genetic Algorithm						
Relative Damping Performance w.r.t. Uniform Stand-Off Layer						
Frequency f [Hz]			Loss Factor $\eta=2\zeta$			
						
Mode #	Uniform Full Coverage	Optimized Full Coverage	Optimized Partial Coverage	Uniform Full Coverage Weight=100%	Optimized Full Coverage Weight=77.09%	Optimized Partial Coverage Weight=71.01%
Prct [%]						
1-+	81.00	83.00	84.00	0.039	0.038	0.063
				-	↓ -2.11%	↑ 63.21%
2++	492.00	468.00	452.00	0.026	0.029	0.042
				-	↑ 13.52%	↑ 60.23%
3++	1313.00	1182.00	1119.00	0.021	0.023	0.026
				-	↑ 10.80%	↑ 25.37%
4++	2411.00	2033.00	1872.00	0.019	0.020	0.021
				-	↑ 8.14%	↑ 12.30%
5+-	3707.00	3021.00	2732.00	0.018	0.018	0.017
				-	↑ 1.43%	↓ -5.11%
6++	5140.00	3803.00	3372.00	0.017	0.020	0.020
				-	↑ 20.71%	↑ 18.56%
7++	6662.00	4865.00	4247.00	0.016	0.029	0.049
				-	↑ 79.83%	↑ 210.69%
8--	8248.00	5916.00	5332.00	0.015	0.015	0.014
				-	↓ -0.64%	↓ -9.93%
9--	9879.00	7267.00	6299.00	0.014	0.014	0.011
				-	↑ 0.00%	↓ -23.61%
10 +	11549.00	7642.00	12185.00	0.014	NA	0.011
				-	NA	↓ -15.56%

As a final optimization technique, multi objective optimization the MOGA was selected as the base search algorithm with which the maximum loss factor for the first mode together with minimal volume objectives were selected. The extracted results for the geometrical parameters of slotted stand-off layer are given in Table 3-27 with totally different geometrical values compared to previous configuration.

Table 3-27 Optimum values for slotted configuration: Multi Objective Genetic Algorithm (MOGA)

+ Add Objective		- Remove Objective					
	Active	Label	Varname	Type	Apply On		
1	<input checked="" type="checkbox"/>	Maximize ESE @ Mdoe I	obj_1	Maximize	Loss Factor @Mode I (r_18)		
2	<input type="checkbox"/>	Maximize ESE @ Mdoe II	obj_2	Maximize	Loss Factor @Mode II (r_19)		
3	<input type="checkbox"/>	Maximize ESE @ Mdoe III	obj_3	Maximize	Loss Factor @Mode III (r_20)		
4	<input checked="" type="checkbox"/>	MinimizeVolume	obj_4	Minimize	TOTAL VOLUME (r_14)		

H2	p1	p2	p3	p4	p5	p6	p7	p8	p9	p10	p11	p12	p13	p14	p15	p16	p17	p18	p19	p20	p21
2.63	9.86	1.74	1.33	5.18	7.70	1.68	4.59	1.82	8.11	2.19	5.45	9.47	2.26	9.84	6.70	8.47	2.50	1.21	9.94	9.98	6.25



The frequency response results are given in Figure 3-126. The overall results are compared to uniform stand-off layer with H=10 mm as well as previous optimized slotted configurations. According to the results, the damping performance achieved, for the partial treatment, by the slotted configuration is higher with the results of GRSM method compared to other methods. On the other hand the Genetic Algorithm (GA) also yields the better result than the Multi Objective Genetic Algorithm (MOGA).

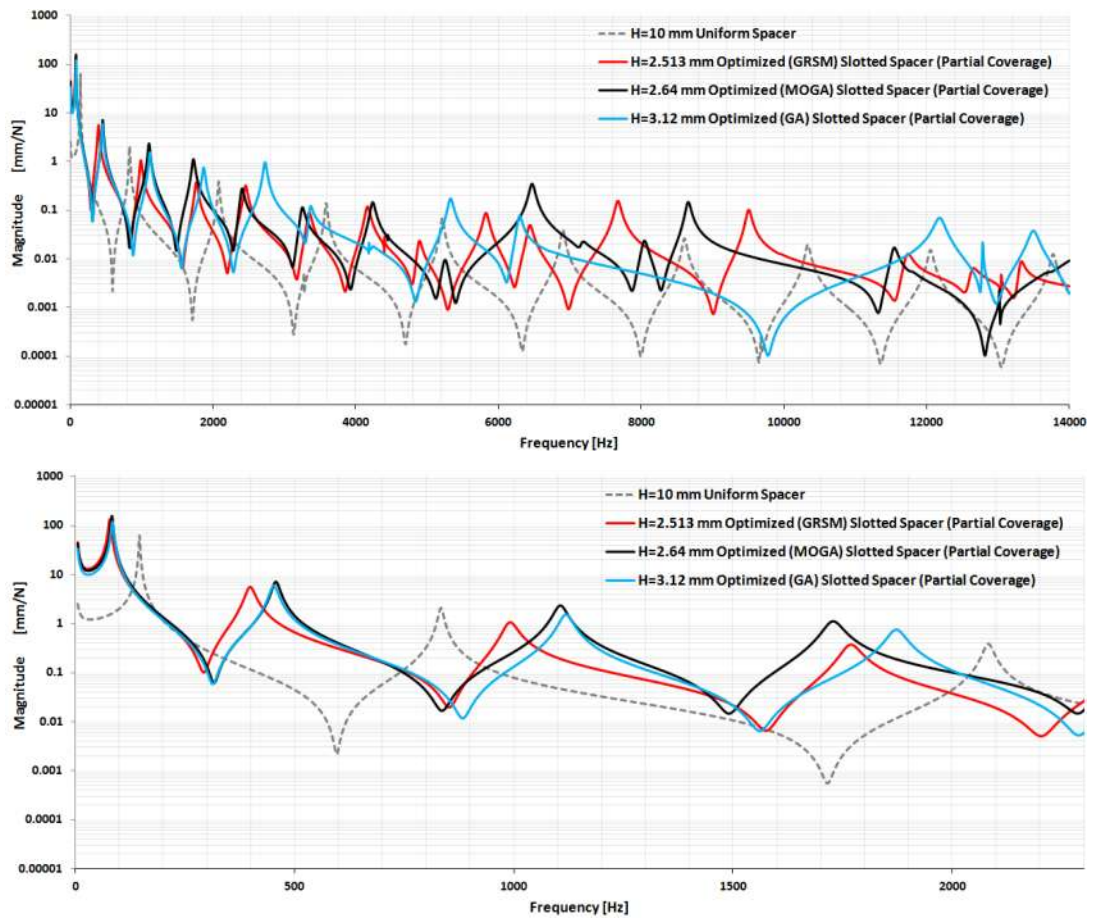


Figure 3-126 Comparison of results of optimization algorithms: GRSM-GA-MOGA


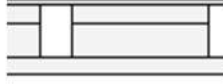
The numerical results associated with final MOGA search algorithm for the relative damping capacity compared to its uniform case is given in Table 3-28. According to the results, the optimized slotted has slightly higher damping until 7th mode which is almost same with uniform counterpart with less weight. Also partial treatment shows relatively higher damping but with lower increase compared to GRSM and GA results.

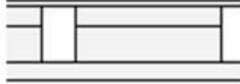
Table 3-28 Relative damping performance of optimized slotted stand-off layer (MOGA)

1++	76.00	79.00	83.00	0.041	0.041	0.057		
				-	↑ 0.08%	↑ 37.55%		
2++	464.00	454.00	457.00	0.028	0.030	0.038		
				-	↑ 7.06%	↑ 36.00%		
3++	1243.00	1135.00	1106.00	0.022	0.023	0.026		
				-	↑ 6.75%	↑ 19.63%		
4++	2295.00	1882.00	1728.00	0.020	0.022	0.024		
				-	↑ 9.19%	↑ 19.71%		
5++	3550.00	2684.00	2410.00	0.019	0.021	0.022		
				-	↑ 9.12%	↑ 15.48%		
6++	4948.00	3612.00	3256.00	0.018	0.019	0.019		
				-	↑ 5.41%	↑ 7.07%		
7--	6445.00	4795.00	4241.00	0.017	0.017	0.015		
				-	↓ -2.68%	↓ -11.37%		
8--	8013.00	5750.00	5256.00	0.017	0.016	0.014		
				-	↓ -5.63%	↓ -18.33%		
9--	9634.00	7163.00	6474.00	0.016	0.015	0.012		
				-	↓ -7.64%	↓ -25.98%		
10++	11299.00	7824.00	7193.00	0.015	0.023	0.030		
				-	↑ 52.35%	↑ 97.59%		

As a summary of the previous results, the overall damping performance of each final configurations, which were extracted by different optimization algorithms, compared to thick uniform reference stand-off layer with corresponding relative percentage damping increase and relative percentage weight reduction is given in Table 3-29. The numerical results shows improvement achieved in damping with slotted configuration obtained by GRSM especially at first modes.

Table 3-29 Relative damping performance of optimized slotted stand-off layers with respect to thick uniform spacer (H=10 mm)

(GRSM) H=2.513 mm Partial Coverage			(GA) H=3.12 mm Partial Coverage		
					
Weight Reduction [%]	Mode #	Relative Loss Factor	Weight Reduction [%]	Mode #	Relative Loss Factor
		Improvement [%]			Improvement [%]
-61.28%	1	298.86%	-57.60%	1	252.92%
	2	283.94%		2	201.77%
	3	201.54%		3	143.69%
	4	163.74%		4	134.68%
	5	158.33%		5	106.42%
	6	148.41%		6	168.77%
	7	136.39%		7	629.85%
	8	110.35%		8	118.38%
	9	123.53%		9	90.60%
	10	125.82%		10	118.17%

(MOGA) H=2.64 mm Partial Coverage		
		
Weight Reduction [%]	Mode #	Relative Loss Factor
		Improvement [%]
-60.23%	1	218.75%
	2	173.41%
	3	146.54%
	4	167.09%
	5	169.46%
	6	161.99%
	7	126.05%
	8	116.77%
	9	102.73%
	10	468.38%

3.3 Comparison of Optimization Results

Up to now we have been considered two main optimization methodology namely, topology optimization and parametric optimization for the design of vibrating structures for optimum dynamic behavior in terms of damping performance as well as amplitude reduction. Below, the frequency response functions (Receptance) of each of the best candidate designs were given for the sake of comparison of their vibration characteristics (Figure 3-128). It can be concluded from the results that stand-off layer with the topology of first case study with a 3.52 mm height gives higher damped response which is slightly greater than another configuration which is optimized slotted stand-off layer with a height of 2.513 mm. Moreover the first topology has considerable amplitude reduction in higher modes. In terms of response amplitude however especially at lower resonance frequencies the thicker optimized stand-off layer has better performance with less damping capacity and same weight.

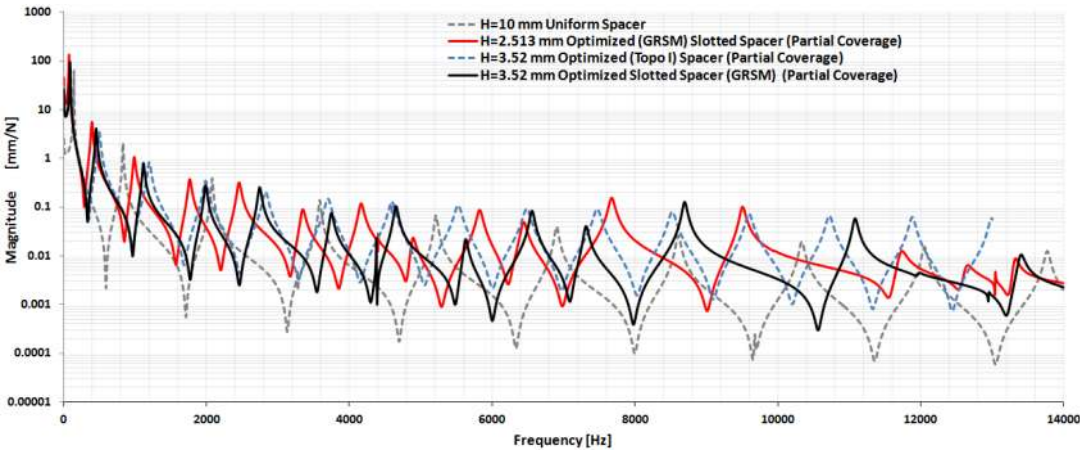


Figure 3-127 Frequency response function comparison of best candidate designs.

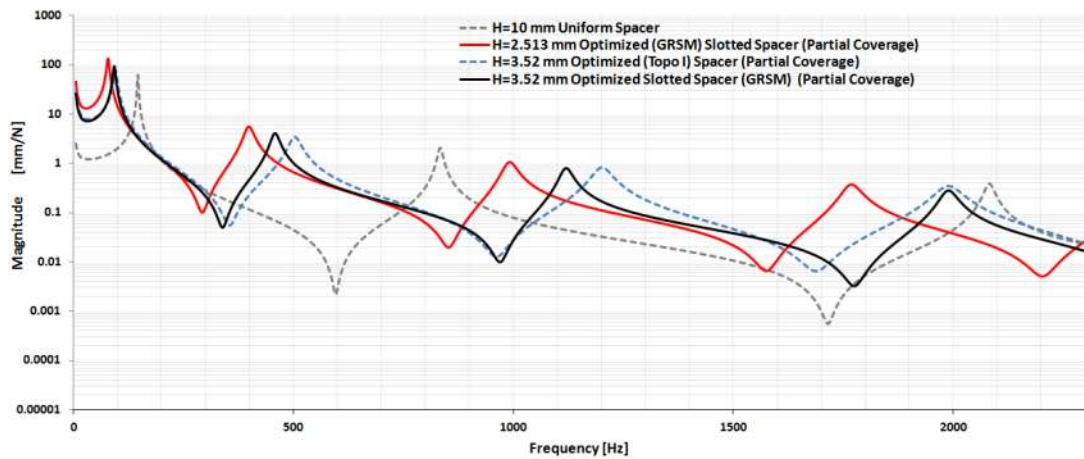
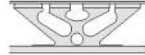




Figure 3-128 Continued

Table 3-30 Overall comparison of optimized designs in terms of damping

 TOPOLOGY I H=3.52 mm Partial Coverage			 (GRSM) H=3.52 mm Partial Coverage			 (GRSM) H=2.513 mm Partial Coverage		
Weight Reduction [%]	Mode #	Relative Loss Factor Improvement [%]	Weight Reduction [%]	Mode #	Relative Loss Factor Improvement [%]	Weight Reduction [%]	Mode #	Relative Loss Factor Improvement [%]
-56.16%	1	320.67%	-51.94%	1	224.71%	-61.28%	1	298.86%
	2	274.64%		2	207.77%		2	283.94%
	3	237.14%		3	136.00%		3	201.54%
	4	232.58%		4	109.38%		4	163.74%
	5	211.11%		5	102.42%		5	158.33%
	6	193.24%		6	93.06%		6	148.41%
	7	48.53%		7	74.20%		7	136.39%
	8	164.52%		8	45.93%		8	110.35%
	9	150.88%		9	58.83%		9	123.53%
	10	142.31%		10	60.94%		10	125.82%

The numerical results for the relative percentage damping improvement as well as weight reduction with respect to reference thick uniform stand-off layer were tabulated for the first ten modes in Table 3-30. For the sake of comparison of parametric results with topology optimization results, the optimized slotted design

response was generated for the same thickness value of first topology optimization, that is for $H=3.52$ mm. One can see from the tabulated result that for the same thickness value, topology optimization has yielded better material distribution which results higher damping capacity for almost all modes with considerable higher weight reduction compared to optimized slotted configuration. The relative percentage increase in loss factor for the first mode is %320.67 for the topologically optimized stand-off with %56.16 weight reduction while it was %224.71 for the optimized slotted configuration with %51.94 weight reduction. However, the thinner slotted design has better damping performance compared to same slotted configuration which makes it second candidate for design.

In order to see the damped response of best candidate design in vibration reduction purpose the result of optimized solution was compared with the bare beam response (Figure 3-129). One can easily see the considerable amount of vibration response reduction with optimized topology of stand-off layer with minimum thickness, in other words with less weight. The damping improvement for the first mode was reported as %102.87 at the first mode, %600.29 at the second mode and %1501.81 at the third mode which are the lowest dominating responses.

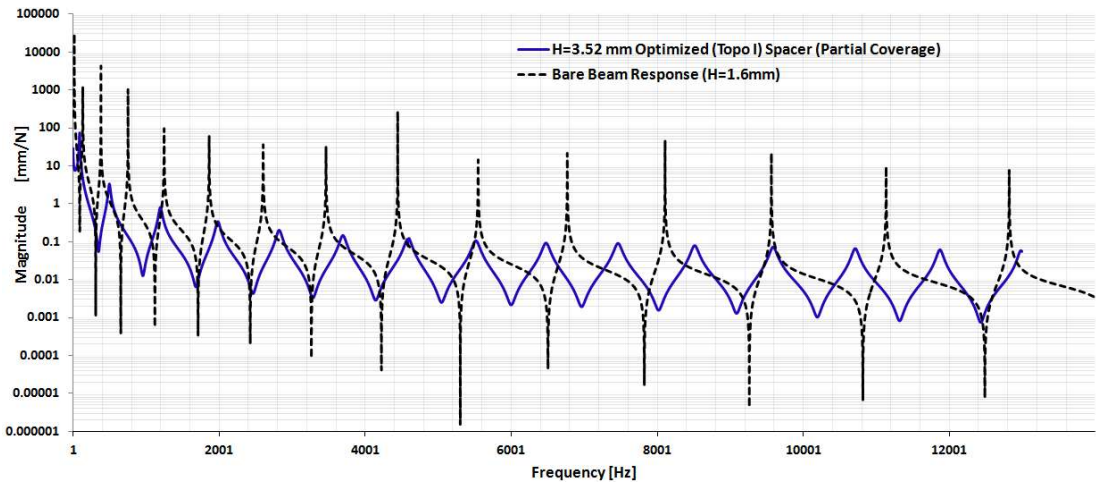


Figure 3-129 Frequency response function of bare and treated beam with optimum stand-off layer

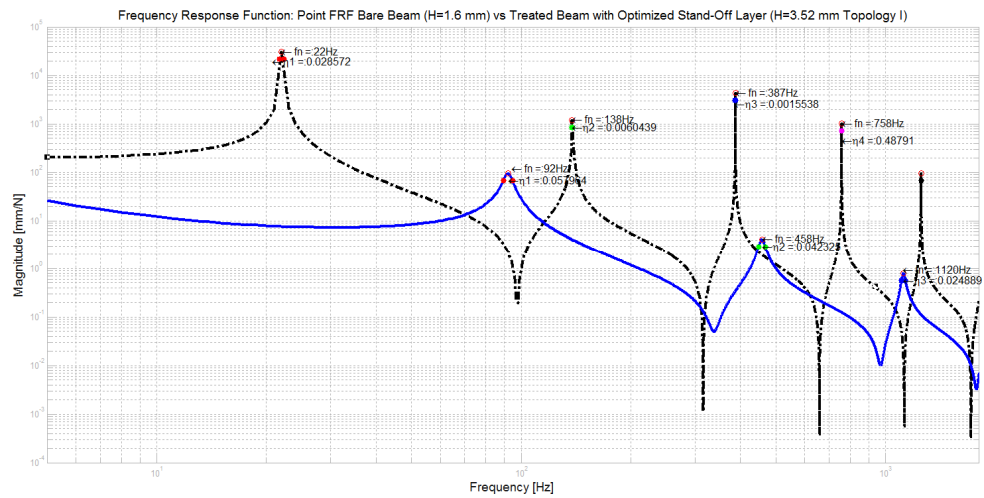


Figure 3-130 (Continued)

The response of best candidate designs for the optimum dynamic response were plotted and compared in the following Figure 3-131 and Figure 3-133 with both bare base beam and layered beam with thick uniform case as reference models. One can see from the response curves the thick uniform beam has comparatively lower response amplitude but with less damping capacity whereas the thin optimized candidate designs for spacer layer induce higher damping capacity with slight amplitude increase especially at lower modes. The relative increase in response amplitude gradually decreases and at higher frequencies there exists dramatic reduction of amplitude with optimum thin layers.

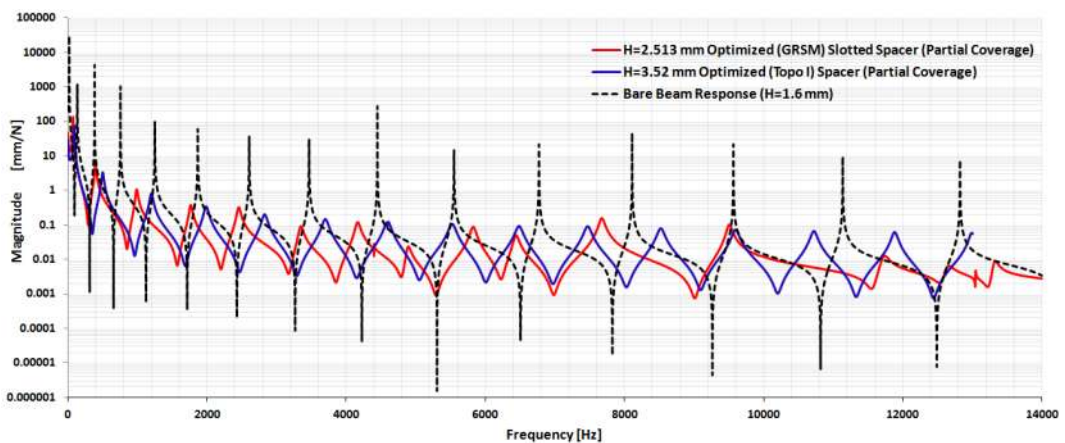


Figure 3-131 Frequency response function of bare and treated beam with optimum design candidates for stand-off layer

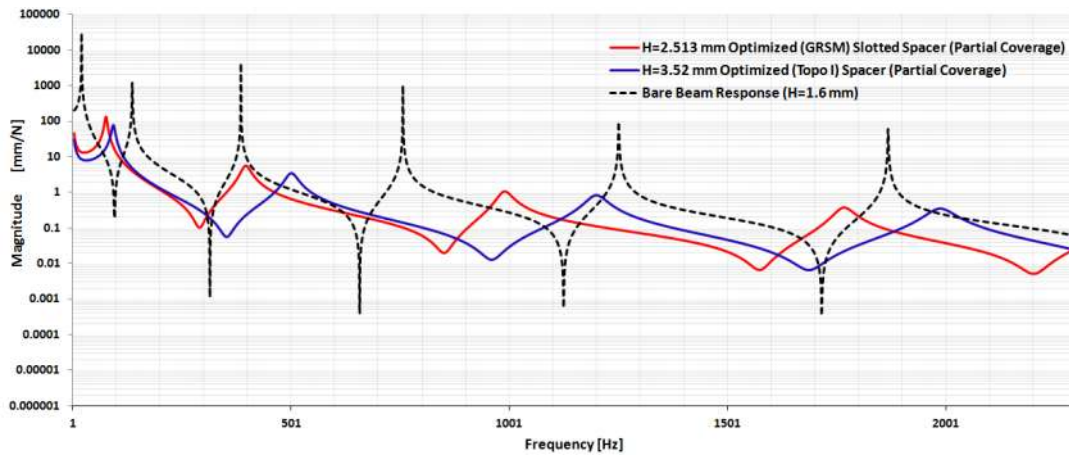


Figure 3-132 (Continued)

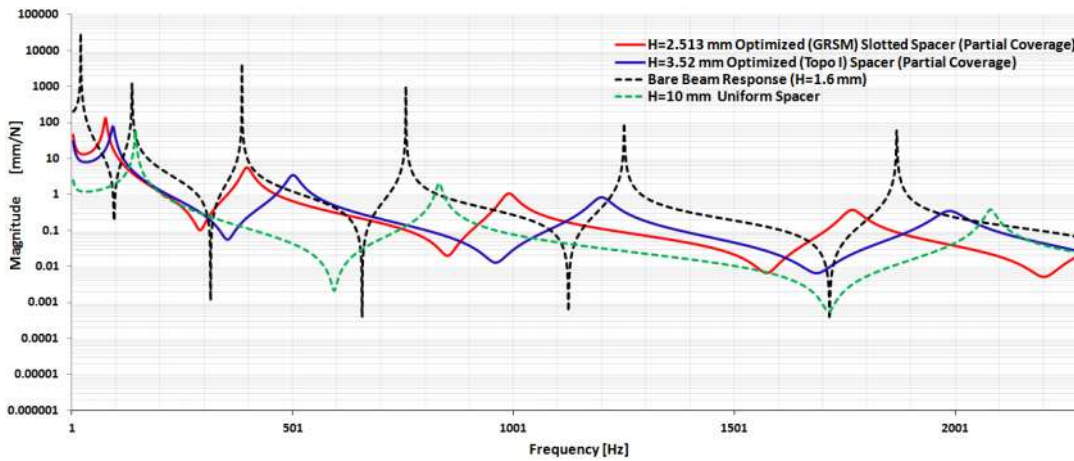


Figure 3-133 Frequency response function of bare and treated beam with optimum stand-off layer

As a general result of the numerical design process of this study the Figure 3-133 summarizes the optimum dynamic response of candidate designs. From the response curve one can see that 3.52 mm partially covered spacer with layout of optimized topology of first case study gives best response amplitude as well as maximum damping capacity with minimum weight.

CHAPTER 4

VIBRATION TEST FOR VALIDATION

4.1 Experimental Study

Up to now the design process has been carried out using numerical approach. Additionally the experimental studies play an important role either to verification of approach used or final qualification of developed products. In this section of thesis study it is aimed to conduct a vibration experiment in order to verify the methodology used and to extract the damping performance of optimized slotted stand-off layer as shown in Figure 4-1. For this purpose the samples of treated beam structures were produced adhering to numerical models. The viscoelastic material used was selected to be one provided from Soundcoat[®] Company, which is DYAD 601 with a thickness of 1.27 mm. As a constraining layer a 0.5 mm thick 2024-T3 aluminum samples were used. On the other hand for the stand-off layer ABS plastic (ABS P430) was used since it has quite suitable modulus of elasticity for use in practical application for the maximum damping performance based on the results achieved in first case study of parametric optimization. Moreover, the ABS plastic has another advantage ensuring to be used in 3D printing technology. Finally for vibrating beam a 1.6 mm thick 2024-T3 aluminum sheet was selected with overall dimensions of 250 mm x 45 mm. Upon production of each sample, a sine-sweep vibration test has been conducted under unit harmonic base excitation of treated beam fixed to a fixture that is also attached to the shaker table in environmental conditions laboratory.

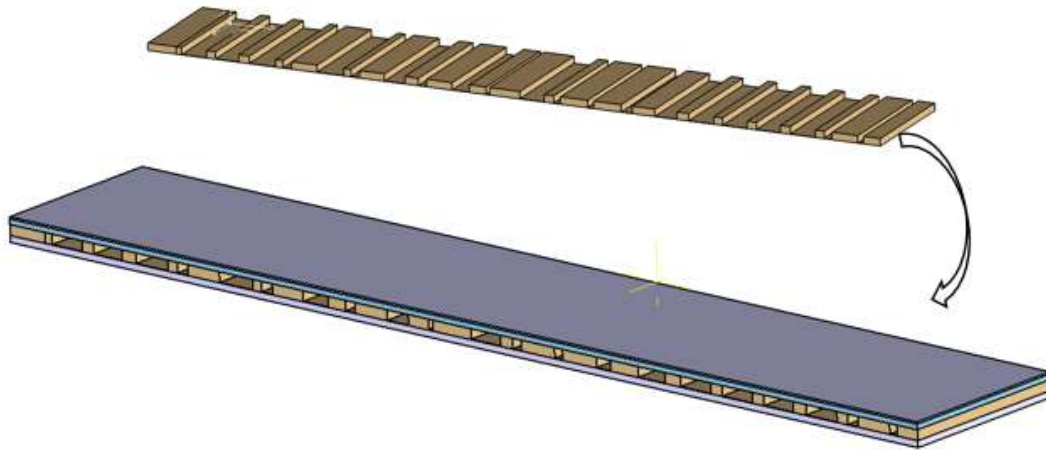


Figure 4-1 3D view of treated beam with optimized configuration of slotted stand-off layer

The vibration response of each samples were measured using instrumentation available in laboratory such as accelerometers, cables and data acquisition system together with shaker table from LDS[®] Company. Upon measuring the tip response of treated beams under fixed-free boundary condition, the frequency response functions are extracted which will be later on used in order to calculate loss factors using Half Power Bandwidth Method. The following sections explain the steps followed in details.

4.1.1 Production of Test Samples

The metallic test specimens for vibrating base beam and constraining layer were prepared in prescribed dimensions (250mm x 45mm) by cutting them from aluminum sheets that were also later machined altogether to tune the dimensions of each to exact values as shown in Figure 4-2.

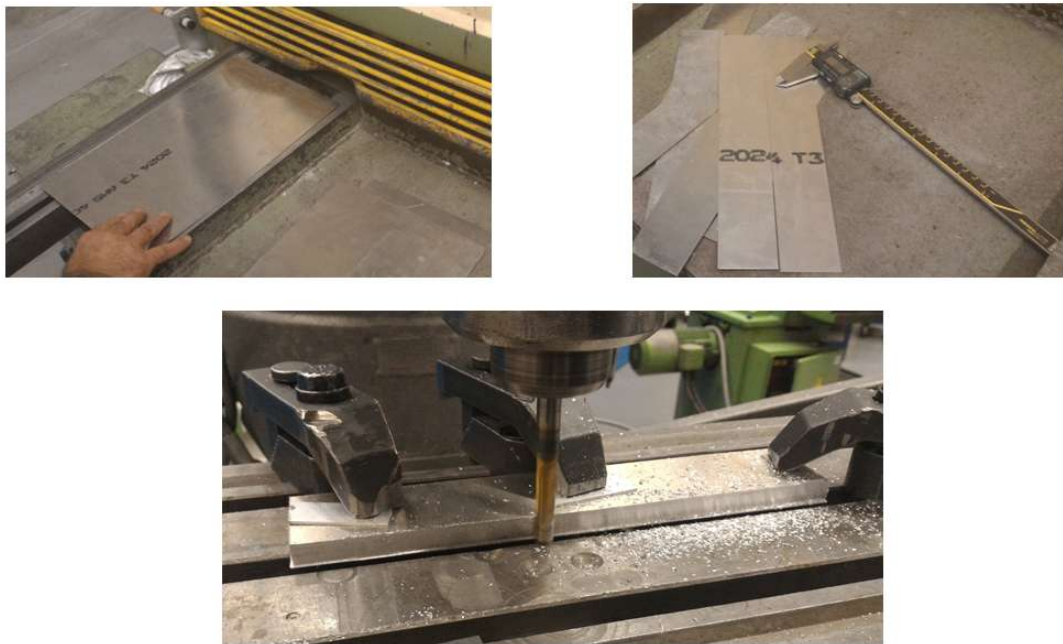


Figure 4-2 Cutting and machining of aluminum sheets

For the stand-off layer with optimized slotted configuration ABS-P430 polymeric material was used and its production was completely accomplished by using 3D printing technology which is one of the additive manufacturing method used worldwide in production of complex 3D parts extracted from topology optimization. In this method the 3D part is divided into sections in certain dimensions from bottom to top using software then the source material is melted pixel by pixel over the 2D surface that represents the 2D section of 3D part. At each section the process is continuously repeated until the whole model is generated from bottom to top. Prototype of any complex geometry that is represented in CAD environment digitally

can easily be produced with additive material layer by layer instead of using cutting, machining etc [3D print]. For this process a special machine, Fortus 250mc, was used and two samples of optimized slotted stand-off layer was manufactured from 2D layout of optimized slotted stand-off layer using 3D printing technology (Figure 4-3). The production time for each of sample (250 mm x 45 mm) was recorded to be 4 hour.



Figure 4-3 3D prototypes of optimized slotted stand-off layer

In order to be used in performance comparisons 3 more uniform stand-off layers were also manufactured. Upon manufacturing of metallic base and constraining layers together with polymeric stand-off layers the final step left was the assembling of all layers into single treated beam. For the slotted configuration either full or partial coverage was applied over the surface of the printed layers carefully. The viscoelastic sheet, DYAD 601-Soundcoat[®], was cut into dimensions adhering to

width of each single column that was given in Table 3-23. Then a special adhesive, Loctite 401[®] from Henkel Inc. was used to glue the layers altogether (Figure 4-4).



Figure 4-4 Assemblage of each individual layers to form treated beams

After assembling all the layers together the samples were ready to be tested as shown in Figure 4-5.

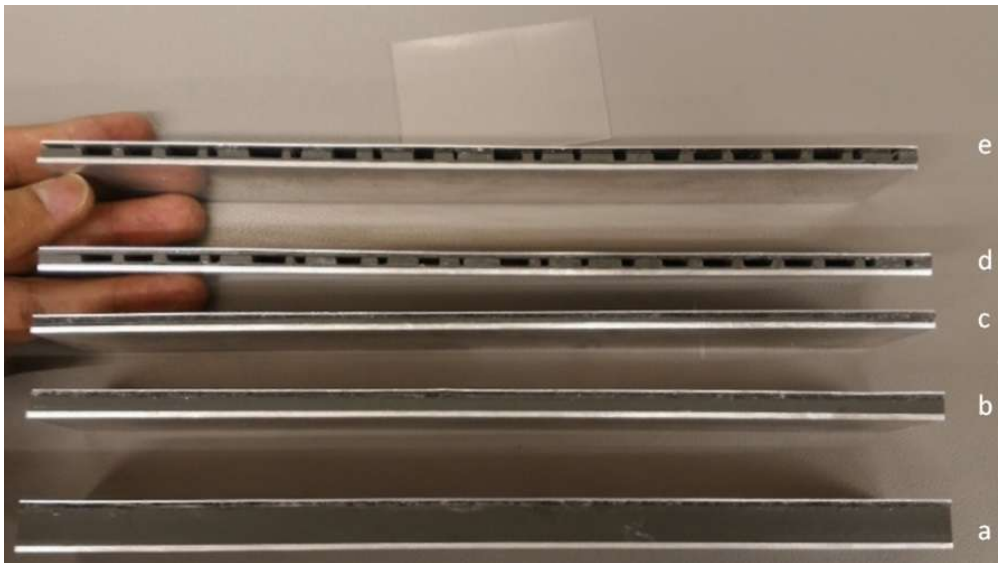


Figure 4-5 Manufactured treated beam samples: (a) 10 mm uniform, (b) 4 mm uniform, (c) 1.32 mm uniform,(d) 2.513 mm slotted-full coverage, (e) 2.513 mm slotted partially covered stand-off layer.

4.1.2 Vibration Test

As well as verifying the analytical or numerical predictions for their dynamic behavior of structural parts, the vibration test is also conducted for assessing the performance of products qualitatively by replicating the dynamic environment encountered in physical operational conditions in order to see whether the design under test meets the design requirements. In a vibration test a design under test is simply attached to the stiff fixture that is also fixed to the shaker table which is excited electromechanically by means of signal generator. The excitation signal can be of sine, random, or shock input in a deterministic shape of square, triangular pulses.

In order to assess the damping performance of treated beams that was previously manufactured, the swept sine vibration test was conducted in order to identify the natural frequencies of treated beam as well as loss factors from frequency response functions generated based on measurement throughout the vibration test. During such

kind of test, one of the important considerations that should be taken into account is that the fixture should be free of resonance especially at the frequency range of test in order not to amplify the test input due to resonance of fixture itself that may results erroneous measurements. For this purpose the fixture used was designed accordingly and checked its resonance frequencies via modal analysis as a pretest analysis step as shown in (Figure 4-6). The finite element model of the test fixture was built with same material and boundary conditions applied during fixation of fixture over shaker table. According to results, the first mode of test fixture was found to be around 1958 Hz and the second mode was around 2609 Hz which are sufficiently higher values above the interested frequency range which was up to 1400Hz for the thickest treated beam under fixed-free boundary condition which was also determined by pretest trials.

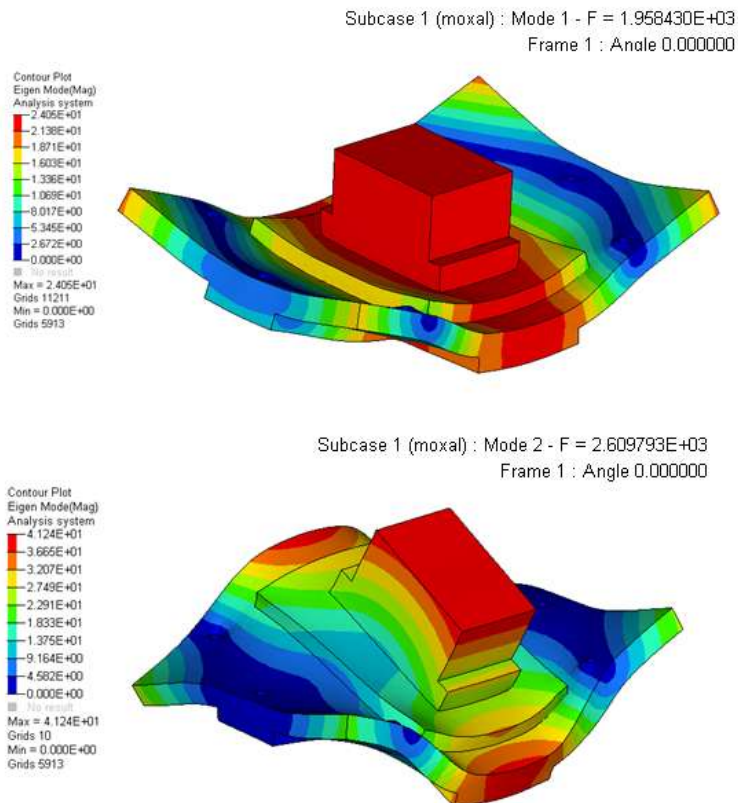


Figure 4-6 Modal analysis of test fixture: 1st Mode: 1958 Hz (Up), 2nd Mode: 2609 Hz (Down)

After design and analysis of test fixture the model was also manufactured by aluminum blocks that were screwed to each other. Later on the treated beams clamped from one end of the beams to the fixture via using plate and bolts creating a cantilever beam condition. The test fixture also fixed to surface of the shaker table via bolts. The beam is shown mounted to the shaker table as in Figure 4-7 . This configuration is used to perform vibration tests in the Z-direction, as it was done in numerical direct frequency response analysis.

Another important consideration during test is instrumentation consists of sensors such as accelerometers to measure response level and control the input level. Particularly the control accelerometer was used to monitor and control the input vibration level delivered correctly to the shaker table while the tip sensor attached to the treated beam was used to measure the acceleration response of beam from which the frequency response functions are generated.

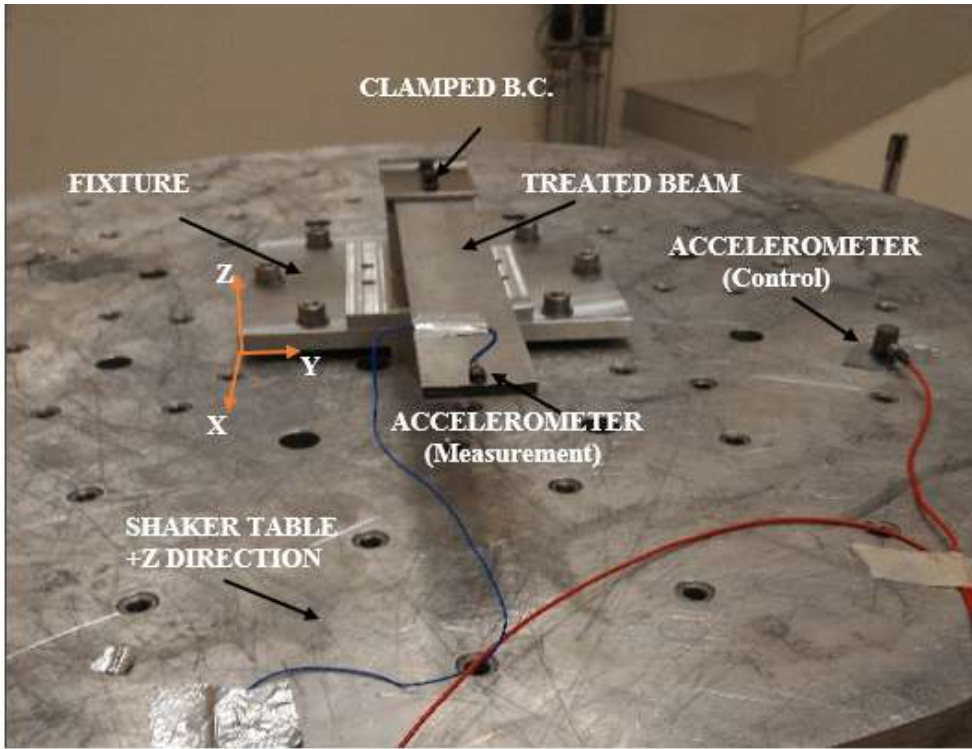


Figure 4-7 Treated beam attached to the shaker in fixed-free boundary condition

For the response measurement PCB type miniature mono-axial accelerometer from Piezotronics Inc. with a sensitivity of 9.215mV/g was used. It was securely glued to the tip of the beam using special wax provided by manufacturer.

One of the popular test technique used for identification of natural frequencies and damping factors through extracting the frequency response function is swept sine test which is also known as modal survey vibration test. During test an enforced unit harmonic acceleration load is applied to the test structure by sweeping a lower bound of frequency to the upper bound. During test the responses are measured using suitable accelerometer in required direction. In our case a unit 1g sinusoidal harmonic acceleration load was applied at a rate of 1 octave/min in the frequency range of 10 Hz to 2000Hz in +Z direction which is the limit range of shaker table, perpendicular to the surface of shaker table as shown in Figure 4-7. The sweep rate indicates how fast the frequency of loading was changed during survey.

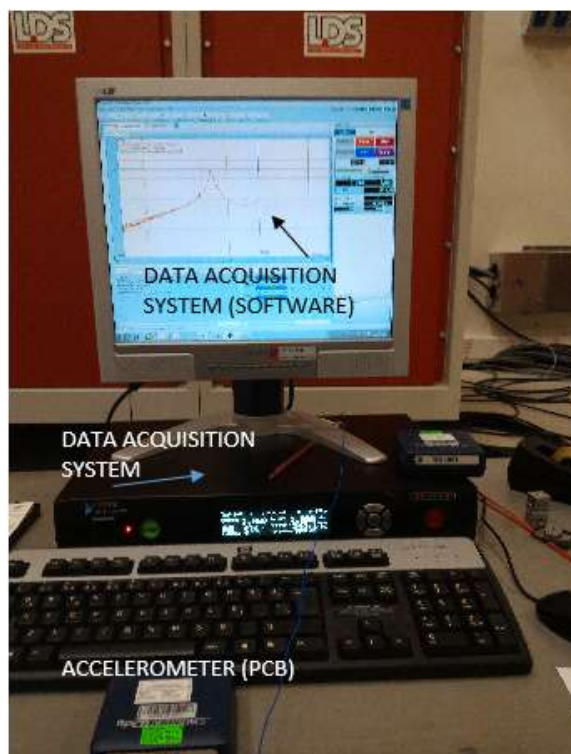


Figure 4-8 Data acquisition system used in vibration test

Data acquisition system forms the backbone of the vibration test such that it drives the shaker table with specified value of harmonic loading, controls it and provides measurement and recording of responses simultaneously. It consist of sensors, cables, signal conditioners, an input/output board and a specifically developed software ensuring data processing in real time as shown in Figure 4-8. Throughout the test the acceleration response was measured using mono-axial miniature accelerometer in +Z direction and recorded simultaneously. A high-pass filter was applied to the response accelerometer at 5 Hz. After processing of each data samples the frequency response functions were generated.

The frequency response plots were also generated for enforced unit base acceleration excitation in order to have comparable results with shaker test to be conducted for this configuration. This time, a 1g unit harmonic base acceleration was applied to the fixed point of cantilever beam and the response was selected to be as acceleration at the tip point of cantilever beam (Figure 4-9). This simulation resembles the vibration test conducted on shaker table.

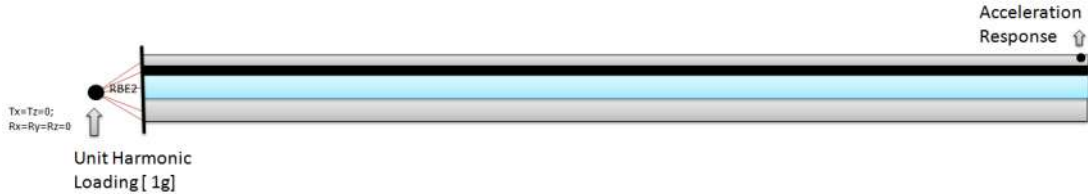


Figure 4-9 Generation of frequency response function

In the following section the test results are summarized both in graphical and numerical form. The frequency response function of each beam sample was reported from which the loss factor values for the first three modes were extracted using Half Power Bandwidth Method accordingly.

4.2 Results and Comparisons

Upon completion of vibration test which took approximately 9 min for each of samples, the frequency response functions were automatically generated by the data acquisition system. They are combined into one single graph for the sake of easy comparison as shown in Figure 4-10. According to results shown the experimental results showed a good agreement in terms of damping performance as predicted via numerical approach. However the frequency of resonances were found to be quite different compared to numerical results. As predicted in first case study the 4 mm fully covered uniform stand-off layer has better damping performance compared to thicker counterpart (H=10 mm). Also the H=2.513 mm optimized fully covered slotted stand-off layer provided higher damping together with lower total weight, in only first mode compared to H=4 mm stand-off contrary to the results achieved numerically Moreover the optimized stand-off with partially treated case provided higher damping performance even compared to its equally weighted counterpart as predicted numerically (Figure 4-12).

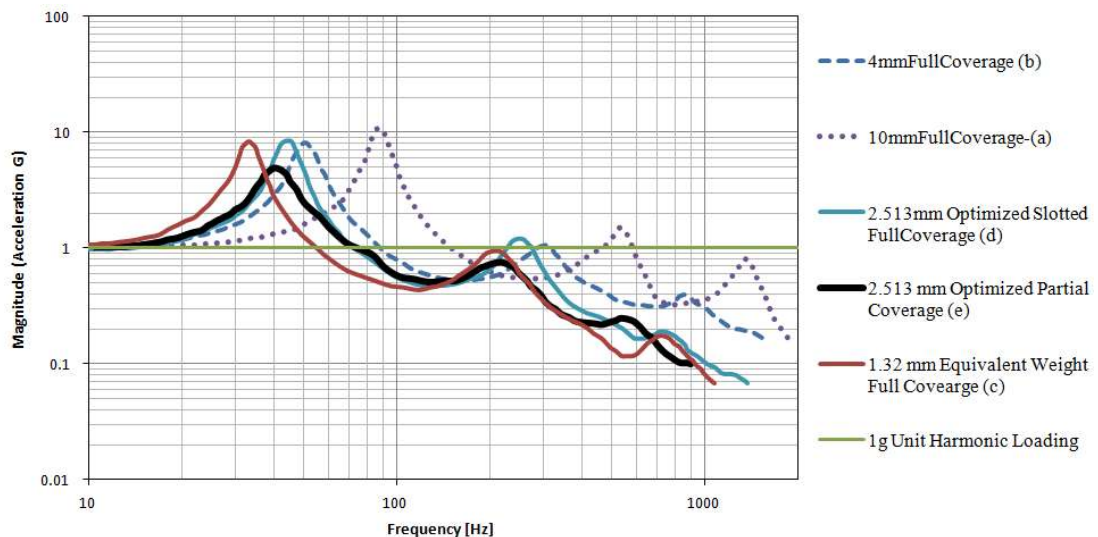
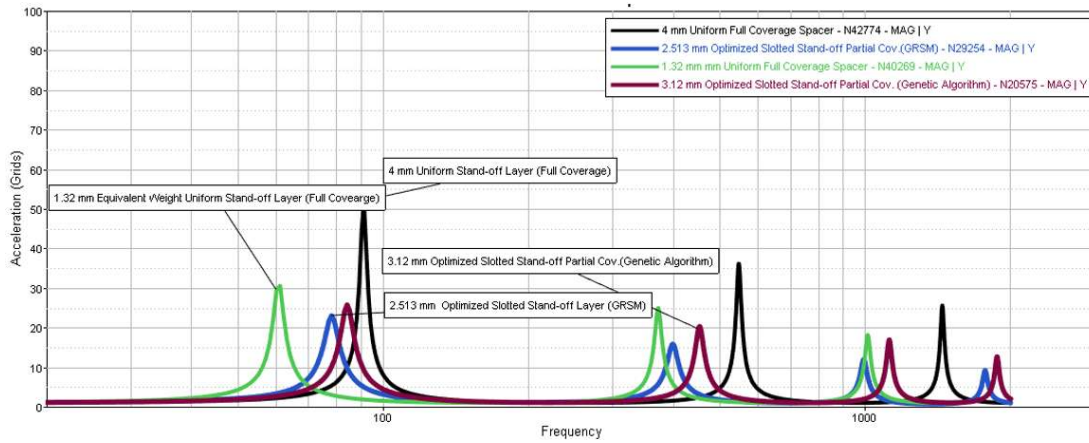
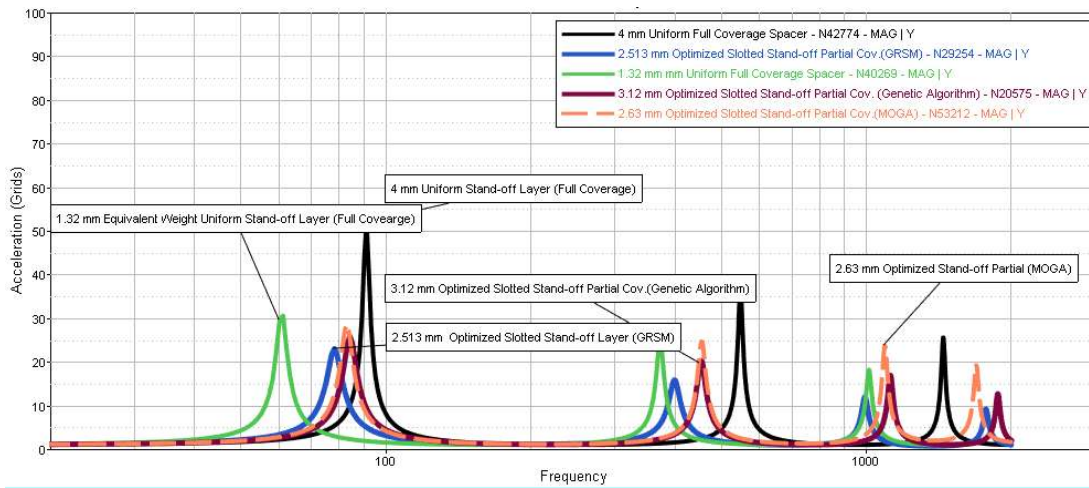


Figure 4-10 Vibration test results: Frequency response functions of each sample

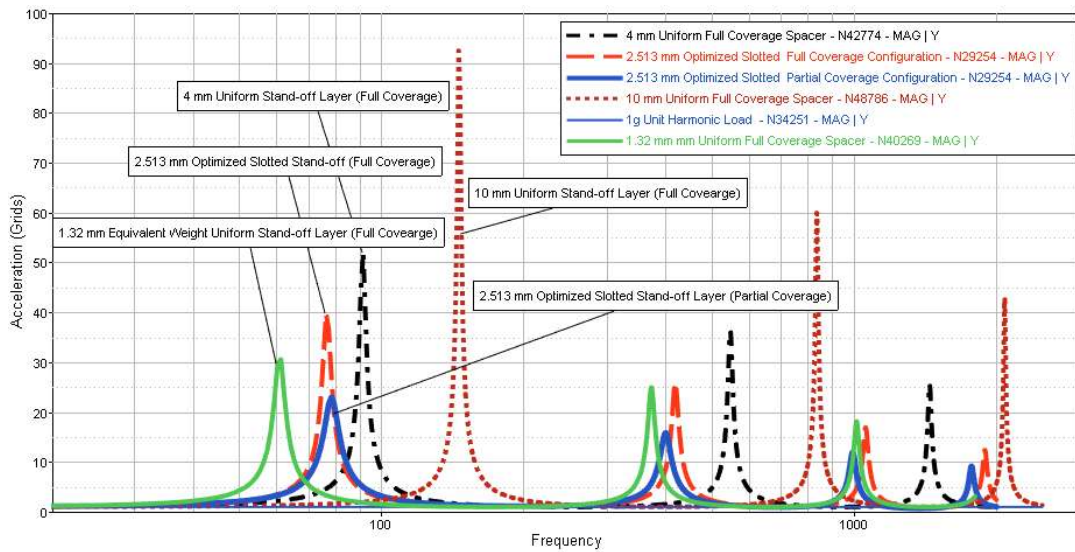


(a)



(b)

Figure 4-11 Acceleration response of treated beams with uniform and optimized slotted stand-off: (a) GRSM vs GA , (b) GRSM,GA,MOGA, (c) GRSM vs Uniform Spacer



(c)

Figure 4-12 (Continued)

The result obtained from experimental study also verifies the numerical response functions given in Figure 4-12-(c). From graphical result one can see that the relative responses show same trend, that is, the acceleration response of optimized slotted configuration is lower than thicker uniform stand-off layer in both numerical and experimental studies which verifies the effectiveness of optimized slotted stand-off layer.

The Figure 4-13 summarizes the variation of loss factor values given in Table 4-1 and Table 4-2 which were obtained from numerical and experimental frequency response functions. It is obvious from results that the maximum loss factor was achieved with the optimized slotted configuration with a thickness of $H_2=2.513\text{mm}$ in both cases and the experimental results are higher in all three modes compared to numerical results which were obtained analyzing geometry created based on approximate numerical model, that is, Modal Strain Energy (MSE) method. Therefore the numerical results already contains some errors. However it is verified by experimental results that the methodology quite useful in predicting the best candidate design in terms of damping even if the numerical results contains some error.

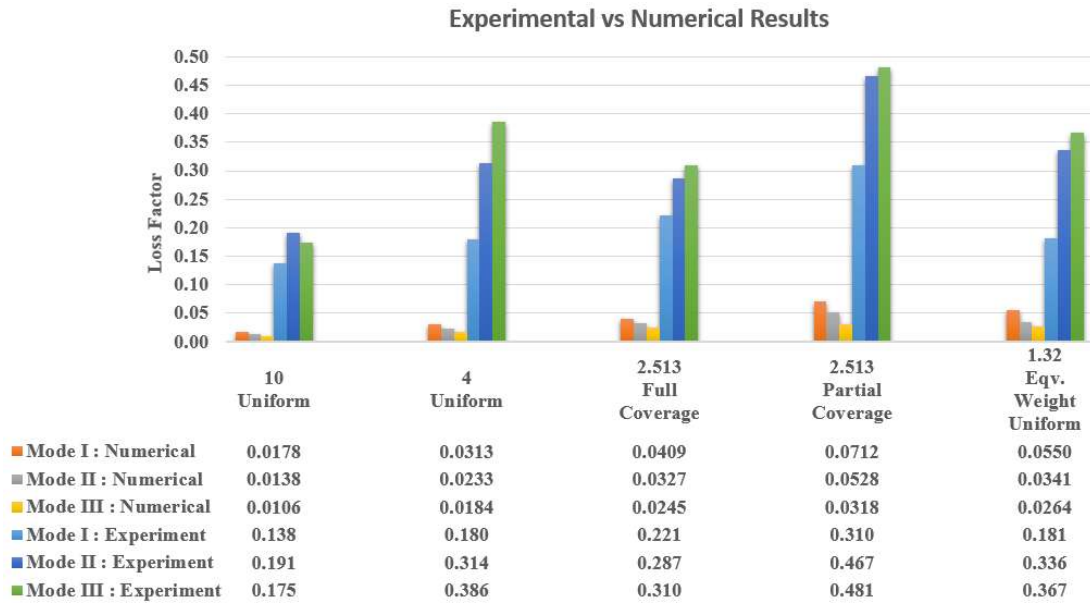


Figure 4-13 Comparison of numerical and experimental results

Table 4-1 Loss factors and frequency results for optimized beam with slotted stand-off (Numerical Results)

Stand-off Height [mm]	Coverage	Configuration	η_1	η_2	η_3
10.0	Full	Uniform	0.0178	0.0138	0.0106
4.0	Full	Uniform	0.0313	0.0233	0.0184
2.513	Full	Optimized Slotted	0.0409	0.0327	0.0245
2.513	Partial	Optimized Slotted	0.0712	0.0528	0.0318
1.32	Full	Uniform (Eq. Weight)	0.0550	0.0341	0.0264

Table 4-2 Relative comparison of damping performances of tested beams

Stand-off Height [mm]	Coverage	Configuration	η_1	η_2	η_3
10.0	Full	Uniform	0.138	0.191	0.175
4.0	Full	Uniform	0.180	0.314	0.386
2.513	Full	Optimized Slotted	0.221	0.287	0.310
2.513	Partial	Optimized Slotted	0.310	0.467	0.481
1.32	Full	Uniform (Eq. Weight)	0.181	0.336	0.367

The numerical results for the loss factors for the first three modes of the beams were tabulated in Table 4-1. Compared to thicker one the H=4 mm stand-off layer has 30.43% higher damping capacity in first mode, 64.40% in second mode and 120.57% in third mode together with 35.43% mass reduction relatively. In case of optimized slotted configuration with H=2.513 mm the damping performance was further increased such that 22.78% in first mode, 8.60% in second mode and 19.69% increase in third mode respectively in full coverage case with a 33.80% further reduction in mass. When we consider the partial coverage case for the same optimized slotted stand-off, a 9.88% further mass reduction was achieved in addition to the further increase in values of loss factors as 40.27% in first mode, 62.72% in second mode and 55.16% in third mode. Moreover comparing the results of optimized case with partial treatment to the results of equally weighted uniform stand-off which has height of H=1.32 mm also yields 21.01% total mass reduction as well as 71.27% damping improvement in first mode, 38.99% in second mode and 31.06% in third mode. The overall relative damping performance increase compared to initial thicker base analysis model was noted as 124.64% in the first mode 144.50% in second mode, 174.86% in third mode with an overall relative mass reduction value of 61.48%.

CHAPTER 5

CONCLUSION AND FUTURE WORK

Mechanical design process starts with a need and continues with solution of fundamental engineering problems that can be of static strength or dynamic vibration problem in nature and mostly followed by an objection or design goal to be achieved. Achieving an engineering design goal requires extensive research and development stage based on design requirements. The process continues with planning, selection of material, conceptual design with engineering judgement and from basic to advanced analysis stages and finally followed by the production of prototype to be tested to reveal whether it satisfies functional or operational requirements and if not the an iteration should be followed until the requirements are satisfied. Therefore the design process is an iterative and time consuming inherently. Fortunately there are many developed engineering tools such as mathematical approaches and softwares to maximize the efficiency in product development as well as obtaining best candidate design solution.

In the present work extensive research and development activity has been followed in order to solve vibration problem encountered in radar antenna structures that are assumed to be attached to thin shell, panel like structures. Specifically aim was to minimize the vibration displacement amplitude which cause the scattering of radar beam, interference of signals etc. For the solution of this kind of problem it was aimed to increase the damping capacity of the base structure which was assumed to be exposed harmonic loadings, therefore the peak amplitude of response function.

First extensive literature survey has been conducted on one of the passive vibration isolation technique, namely, surface damping treatments. Its theoretical background

and analysis techniques were all reviewed in detail with related published data. Then it was decided to focus on surface damping treatments with spacer layer which was found to be one of the effective method in increasing damping of vibrating thin shell, panel like structures. Based on the research it was revealed that there were little or no systematic approach had been conducted in design and analysis of layered beam with spacer layer and it was decided to investigate optimization methodologies on advancement of damping while reducing weight for the passive surface damping treatment with stand-off layer.

Apart from traditional methodology the systematic approach in design and analysis of surface damping treatment has been followed as much as possible in order to enhance the damping performance of vibrating structures such that numerical approach, namely topology optimization and automated parametric study have been used in order to find best material distribution for the spacer layer as well as to investigate effect of different overall design parameters such as material and dimensions and lastly to overcome time consuming trial and error process. The developed systematic approach has also been validated based on the published data and proved to be useful with less effort in finding the best optimum design based on maximum damping and minimum weight requirements, the latter is being indispensable for weight critical applications.

In this study the research activity is composed of three parts. In the first part, one of the numerical method namely topology optimization technique has been utilized in order to find best material distribution of stand-off layer with minimal weight using different modelling technique and objective function as well as constraints. Then the overall damping performance of the resulting topologies has been investigated and compared to each other in terms of total weight and damping loss factors extracted from frequency response functions using Half Power Bandwidth method upon performing direct frequency response analysis which computes the harmonic forced response of each candidate design. In the second part, another numerical method which is parametric design strategy together with known optimization algorithms

have been used to find best optimum geometrical and material parameters that maximize the loss factor for the first three modes since the first modes dominate the overall structural dynamic response. The Modal Strain Energy (MSE) has been used in conjunction with Finite Element Method to calculate the loss factors. Moreover to see the effects of extracted geometries from numerical studies in higher modes, the frequency of interest has been selected such a way that it covers the first 10 modes of the vibrating structure. Throughout the numerical studies cantilever boundary condition has been used for layered beam structure since it is easy to model, simulate and manufacture to be used in experimental study that was conducted at the third and last part of the research, in order to validate the design procedure that has been followed. Also, the objective of experiment has been primarily to qualify the design, manufactured based on numerical results that were achieved in the second part of the study.

It was revealed from this study that;

- The numerical approaches such as topology optimization and search algorithms together with finite element technique are effective methods to find the best material distribution within spacer layer and geometrical parameters which will in the end give rise in damping of structures with minimum material consumption with less effort without any trial and error procedures.
- It was concluded from the response curves that for the passive surface damping treatment with stand-off layer there is a trade-off between stiffness and damping such that increase of stiffness, in other words increase of height of spacer, results less damping capacity within the vibrating structure. The reason for this is the restricted relative motion due to increased rigidity (rigidity is proportional to cube of height of spacer) which also results increase of structural weight. Instead as mentioned in previous study [106,107] in order to decrease weight and increase damping there must be

sufficient flexibility of whole treated structure that will in turn results relative motion between layers which induce shear strain within viscoelastic layer which was also known to be basic mechanism of energy dissipation with compliant viscoelastic materials through hysteresis effect. This results also means that there must be an optimum height and material for the spacer layer and from the results we concluded that thinner layer with optimum layout of spacer gives higher damping capacity. The result of topology optimization revealed that 3.52 mm height with optimized layout of first case study comparatively yielded best damping capacity. This also reveals that material distribution of spacer layer greatly effects the damping performance of the vibrating structure with constrained layer damping treatment.

- In order to investigate the optimum height of spacer layer, a systematic design cycle, which was based on a combined use of analytical and numerical method that was known to be MSE (Modal Strain Energy Method), also verified based on the published results in literature, revealed that the optimum height of uniform spacer layer lies between 2.5-3 mm which is almost consistent height with the result of first case study conducted in topology optimization step. Moreover the material for the spacer layer should have sufficient rigidity for maximum damping [106] and this study reveals that the modulus of spacer layer between 500-2200 MPa yields best results at least in cantilever beam condition that was the specific boundary condition applied. Also it was found that the maximum damping for the cantilever boundary condition exist in the 2nd mode of vibration.
- The systematic approach has been used in order to find best number of slots and its dimensions for the slotted spacer layer eliminating trial and error in finding best geometrical parameters. In finding those results GRSM (Global Response Surface Method) yielded comparatively best results among other search algorithms such as GA (Genetic Algorithm) and MOGA (Multi Objective Optimization Algorithm)

- An experimental study also conducted for the evaluation of the performance of optimized slotted configuration of spacer layer. The results only verified that the numerical approach based on MSE method can only be used in prediction of best design alternative. Although two approach converged to the same configuration the numerical results obtained suggest that the predictions made by numerical method are quite lower than the experimental results. This may be due to use of approximate constant material properties in numerical approach as well as errors associated with finite element modelling technique. But final configuration obtained numerically gives same trends with experiments with the overall relative damping performance increase compared to initial thicker base analysis model was noted as 124.64% in the first mode 144.50% in second mode, 174.86% in third mode with an overall relative mass reduction value of 61.48%.
- It was quantitatively seen that loss factor is greatly affected by the material layout of the spacer layer.

REFERENCES

- [1] Melvin, W. L., Scheer, J. A, Principles of Modern Radar, Vol.II: Advanced Techniques, Edison, NJ:Scitech, (2013).
- [2] Meikle, H. (2008), Modern Radar Systems. Boston: Artech House, Inc.
- [3] Thomas F. Eibert, John L. Volakis, (2002), "Antennas, Radar and Mobile Communications", Scattering, Pages 384-406
- [4] Retrieved from:
http://zaielacademic.net/networking_wireless/wireless_antennas.htm, [Accessed on 10th of June 2015]
- [5] Retrieved from:
<http://my.ece.ucsb.edu/York/Bobsclass/201C/Handouts/Chap3.pdf>, [Accessed on 10th of June 2015]
- [6] Retrieved from:
<http://www.radartutorial.eu/01.basics/Radar%20Principle.en.html>, [Accessed on 10th of June 2015]
- [7] Retrieved from: https://en.wikipedia.org/wiki/Radiation_pattern, [Accessed on 10th of June 2015]
- [8] Retrieved from:
<http://www.digikey.com/en/articles/techzone/2011/mar/understanding-antenna-specifications-and-operation>, [Accessed on 15th of June 2015]
- [9] Merrill I. Skolnik (1990), Radar Handbook, Chapter 6 , 2nd ed. New York, McGraw-Hill
- [10] Retrieved from:<http://www.aliexpress.com/item-img/Short-Roof-Car-Radio-Antenna/32336116998.html> [Accessed on 17 th of June 2015]

- [11] Retrieved from: http://www.nasa.gov/centers/dryden/Features/ads-_tests_complete_prt.htm, [Accessed on 17 th of June 2015].
- [12] Retrieved from: <http://theaviationist.com/2012/12/17/awacs-konya>, [Accessed on 17 th of June 2015]
- [13] Retrieved from: https://www.youtube.com/watch?v=vWQC41wpuIo_, [Accessed on 20 th of June 2015]
- [14] Lionel D. Alford and Robert C. Knarr, (1999), “General flight test theory applied to aircraft modifications”, *Acquisition Review Quarterly*, pp. 157-167.
- [15] A. K. Noor (ed), *Structures Technology for Future Aerospace Systems*, Vol. 188 of *Progress in Astronautics and Aeronautics*, American Institute of Aeronautics and Astronautics, 2000.
- [16] Constantine A. Balanis, *Antenna Theory*, 3rd ed., Wiley-India publications.
- [17] Patnam, H. R., (2007), "Emerging trends in Microstrip Antenna Technology," *Applied Electromagnetics Conference, 2007. AEMC 2007. IEEE*, pp.1, 4.
- [18] K.S. Beenamole, (2009), *Microstrip Antenna Designs for Radar Applications* DRDO Science Sepctrum, pp. 84-86.
- [19] Danial Ehyaie, (2011), *Novel Approaches to the Design of Phased Array Antennas*, Phd. Thesis, The University of Michigan.
- [20]. Anouar Dalli, Lahbib Zenkouar, Seddik Bri, “Comparison of circular sector and rectangular patch antenna arrays in C-band,” *Journal of Electromagnetic Analysis and Applications*, 2012, 4, 457-467
- [21] G.Zeng,S.Li,Z. Wei,W. Lu et al. (eds.), *Research on Conformal Phased Array Antenna Pattern Synthesis*, *Proceedings of the 2012 International Conference on Information Technology and Software Engineering*, *Lecture Notes in Electrical Engineering* 210,Chapter2,pp.13-21
- [22] Vijay K. Varadan, Vasundara V. Varadan,(1997) ,*Design and development of smart skin conformal antenna with MEMS structural sensors and actuators*, *Proc.*

SPIE 3046, Smart Structures and Materials: Smart Electronics and MEMS, 94
doi:10.1117/12.276632.

[23] DLR Institute of Communications and Navigation Efficient Simulation
Procedures for the Design of Conformal Antennas,

Retrieved from:http://www.dlr.de/kn/en/desktopdefault.aspx/tabid-2203/3256_read-9234, [Accessed on 4th of July 2015]

[24] Z. Xie, F. Peng, P. Zhang, W. Zhao, (2014), A smart Skin Antenna Structure for
Global Navigation Satellite System, Applied Mechanics and Materials Vols.464,
pp:316-320

[25] Seong Ho Son and Soon Young Eom and Woonbong
Hwang,(2008),Development of a smart-skin phased array system with a honeycomb
sandwich microstrip antenna ,Smart Materials and Structures, Vol. 17,No.3,p.035012

[26] Z. Xie, F. Peng, P. Zhang, W. Zhao, (2014),A smart Skin Antenna Structure for
Global Navigation Satellite System, Applied Mechanics and Materials
Vols.464,pp:316-320

[27] Richard L. Chaney, Douglas R. Hackler, Dale G. Wilson, Brian N.
Meek,(2013), Advanced Conformal Load-Bearing Antenna Structures, American
Semiconductor, Inc. Retrieved from: <http://www.americansemi.com/flexform/>,
[Accessed on 7 th of July 2015]

[28] J. Wenger, "Automotive radar - status and perspectives," in Compound
Semiconductor Integrated Circuit Symposium, 2005. CSIC '05. IEEE, 2005, p. 4

[29] Allen J. Lockyer, Kevin H. Alt, Jayanth N. Kudva, Robert W. Kinslow, Allan C.
Goetz, (1997), Conformal load-bearing antenna structures (CLAS): Initiative for
multiple military and commercial applications. Proc. SPIE 3046, Smart Structures
and Materials: Smart Electronics and MEMS, 182.

[30] Kim, Y.; Walton, E.K.,(2006) "Automobile conformal antenna design using
non-dominated sorting genetic algorithm (NSGA)," Microwaves, Antennas and
Propagation, IEE Proceedings , vol.153, no.6, pp.579,582.

[31] Retrieved from:

<http://www.freescale.com/webapp/sps/site/overview.jsp?code=AUTRMWT>,
[Accessed on 10 th of July 2015]

[32] *Future Submarine Force* Retrieved from:

<http://www.navy.mil/navydata/cno/n87/future/conformal.html>, [Accessed on 15 th of July 2015]

[33] John E. Sirmalis, (1997), Extendible planar phased array mast, The United States Of America As Represented By The Secretary Of The Navy Patent, US5977918 A (Patent)

[34] Boyns J, (1972), Submarine-to-satellite communications antenna, US Navy Patent, US3754268 A(Patent)

[35] Jacob Longacre, Gerald Exley, and Craig McMillan, Voices From the Deep The New Age of Submarine Communications, Retrieved from:

<http://www.navy.mil/navydata/cno/n87/usw/autumn98/voices.htm>, [Accessed on 15 th of July 2015]

[36] Bisplinghoff, R. L., Ashley, H., and Halfman, R. L., (1955), *Aeroelasticity*, Dover.

[37] A.J. Lockyer, J.N. Kudva, D. Kane, B.P. Hill, C.A. Martin, A.C. Goetz, et al.(1994),” A qualitative assessment of smart skins and avionic/structures integration”, Proc. SPIE 2189, Smart Structures and Materials, 172 pp. 172–183

[38] J. Tuss, A. Lockyer, K. Alt, F. Uldrich, R. Kinslow, J. Kudva, et al. (1996),”Conformal loadbearing antenna structure” Collection of technical papers AIAA/ASME/ASCE/AHS/ASC structures, structural dynamics and materials conference pp. 836–843.

[39] M.A. Hopkins, J.M. Tuss, A.J. Lockyer, K. Alt, R. Kinslow, J.N. Kudva, (1997), "Smart skin conformal load-bearing antenna and other smart structures developments " Collection of technical papers–AIAA/ASME/ASCE/AHS/ASC structures, structural dynamics and materials conference , pp. 521–530.

- [40] A.J. Lockyer, K.H. Alt, D.P. Coughlin, M.D. Durham, J.N. Kudva, A.C. Goetz, et al.(1999), "Design and development of a conformal load-bearing smart-skin antenna: overview of the AFRL Smart Skin Structures Technology Demonstration (S3TD)", Proceedings of SPIE – the International Society for Optical Engineering, 3674, pp. 410–424
- [41] P. Knott, C. Locker, and S. Algermissen, “Antenna element design for a conformal antenna array demonstrator,” in 2011 Aerospace Conference, 2011, pp. 1–5.
- [42] Adapted from [41] and 3D Aircraft CAD Model Retrieved from: <http://www.turbosquid.com/3d-model/airbus/airbus-a320?synonym=a320>, [Accessed on 20 th of July 2015]
- [43] H.Schippers, H.V.Tongeren, Jaco Verpoorte and G.Vos, (2001), Distortion of Conformal Antennas on Aircraft Structures, Smart Structure and Materials, Proc. of SPIE, Vol.4334
- [44] P. Brahma, P. Nandi, A. Senapati and J. S. Roy, (2015), "Reduction of Side Lobe Level of Thinned Phased Array Antenna using Genetic Algorithm", International Journal of Computer Applications (975-8887), Volume 112 – No. 8. Retrived from: <http://research.ijcaonline.org/volume112/number8/>, [Accessed on 25 th of July 2015]
- [45] Congsi Wang, Baoyan Duan , Fushun Zhang & Minbo Zhu (2009) Analysis of performance of active phased array antennas with distorted plane error, International Journal of Electronics, 96:5, 549-559
- [46] Harmouch, A., Kamali, W, El Moucary, C. (2011) "Sidelobe Reduction in Offset Dish Parabolic Antennas Using Metallic Scatters", Progress in Electromagnetics Research Symposium (PIERS), Marrakesh, Morocco, pp. 1835-1839
- [47] P. Knott, C. Locker, S. Algermissen, and W. Gruner, “Research on vibration control and structure integration of antennas in NATO/RTO/SET-131,” in 2010 IEEE Antennas and Propagation Society International Symposium, 2010, pp. 1–4

- [48] Calusdian, James,(1988),”Radiation Patterns of Aantennas Installed on Aircrafts” , Msc.Thesis, Naval Postgraduate School Monterey CA 93943-5000.
- [49] P. Knott, "Deformation and Vibration of Conformal Antenna-arrays and Compensation Techniques," Paper presented at Multifunctional Structures/Integration of Sensors and Antennas, Paper 19, Neuilly-sur-Seine, France, 2006.
- [50] H. Schippers, J.H. van Tongeren, P. Knott, T. Deloues, P. Lacomme, and M.R. Scherbarth, "Vibrating Antennas and Compensation Techniques Research in NATO/RTO/SET 087/RTG 50," IEEE Aerospace Conference, 3-10 March 2007
- [51] H. Schippers, J.H. van Tongeren, G. Vos, "Development of Smart Antennas on Vibrating Structures of Aerospace Platforms," Paper presented at Multifunctional Structures/Integration of Sensors and Antennas, Paper 20, Neuilly-sur-Seine, France, 2006.
- [52] Lesueur, G.; Caer, D.; Merlet, T.; Granger, P., (2009), "Active compensation techniques for deformable phased array antenna," Antennas and Propagation, 2009. EuCAP 2009. 3rd European Conference on , vol., no., pp.1578-1581.
- [53] J.Verpoorte, H.Schippers, C.G.H. Roeloffzen, David A.I.Marpung, Smart Antennas in Aerospace Applications, 2010 URSI International Symposium on Electromagnetic Theory.
- [54] D J Mead, *Passive Vibration Control*, Wiley, 1998.
- [55] Ashish M. Dharme, Pravin P. Hujare, (2014), Analysis of Performance of FLD and CLD Technique
- [56] M D Rao, (2003), Recent applications of viscoelastic damping for noise control in automobiles and commercial airplanes, *Journal of Sound and Vibration*, 262 (3), 457 – 474, 2003
- [57] Retrived from: <http://www.smac-sas.com/smac-aero/>, [Accessed on 28 th of July 2015]

- [58] Retrived from: <http://www.zoneenterprisesusa.com/products-zone-butyl-and-sealant.html>, [Accessed on 30 th of July 2015]
- [59] Kerwin Jr E. M., Damping of flexural waves by a constrained viscoelastic layer. *Journal of Acoustical Society of America* 1959; 31:952– 962
- [60] Ross D, Ungar E.E, Kerwin E.M Jr. Damping of plate flexural vibrations by means to viscoelastic laminae, structural damping. In: Ruzicka JE, editor. *Colloquium on structural damping, ASME annual meeting, 1959.*
- [61] Ungar E.E, Kerwin Jr EM. Loss factors of viscoelastic systems in terms of energy concepts. *Journal of Acoustical Society of America* 1962 ; 34:954–958
- [62] D.J. Mead, S. Markus,(1969) The forced vibration of a three-layer damped sandwich beam with arbitrary boundary conditions, *Journal of Sound and Vibration*, vol. 10, p.p. 163-75
- [63] Lumsdaine, A. And Scott, R.A., “Shape Optimization Of Unconstrained Viscoelastic Layers Using Continuum Finite Elements”, *Journal of Sound and Vibration*, Vol. 216, No.1, p.29-52, (1998).
- [64] Johnson, C.D. and Kienholz, D.A. (1982), “Finite Element Prediction of Damping in Structures with Constrained Viscoelastic Layers”, *AIAA Journal*, 20(9), pp.1284-1290
- [65] Lumsdaine, “Topology optimization of constrained damping layer treatments,” in *Proceedings of the ASME International Mechanical Engineering Congress and Exposition*, pp. 149–156, New Orleans, La, USA, November 2002
- [66] Koruk, H. and Sanliturk, K.Y., “Optimisation of damping treatments based on big bang–big crunch and modal strain energy methods”, *Journal of Sound and Vibration*, Vol.333, p.1319–1330, (2014)
- [67] Kang, Z., Zhang, Z., Jiang, S. and Cheng, G.,(2012) “On topology optimization of damping layer in shell structures under harmonic excitations” *Structural and Multidisciplinary Optimization*, Vol.46, No.1, p.51-67.

- [68] Zhanpeng Fang and Ling Zheng, (2015),” Topology Optimization for Minimizing the Resonant Response of Plates with Constrained Layer Damping Treatment”, *Shock and Vibration*, Volume 2015, Article ID 376854
- [69] Chia, C.M., Rongong, J.A and Worden, K., (2009) “Strategies for using cellular automata to locate constrained layer damping on vibrating structures”, *Journal of Sound and Vibration*, Vol.319, p.119–139
- [70] Parfitt, G. G.; Lambeth, D.,*The Damping of Structural Vibrations*, Aeronautical Research Council, “A.1” Report (U); Ministry of Aviation, U.K., 1960.
- [71] D. S. Nokes and F. C. Nelson 1968, ” Constrained layer damping with partial coverage” *The Shock and Vibration Bulletin* 38(03) ,5-10.
- [72] Plunkett, R., Lee, C.T., Length Optimization for Constrained Viscoelastic Layer Damping, *J. Acoust. Soc. Amer.*, Volume 48 Number 1 (Part 2) ,150-61 1970.
- [73] Trompette, P. and Fatemi, J., “Damping of beams. Optimal distribution of cuts in the viscoelastic constrained layer”, *Structural Optimization*, Vol.13, p.167-171, (1997)
- [74] J.-l. Marcelin, S. Shakhesi , F. Pourroy, Optimal Constrained Layer Damping of Beams: Experimental and Numerical Studies,*Shock and Vibration*, Vol. 2, No.6, pp. 445-450 (1995)
- [75]. Kung, S.W. and Singh, R., *Vibration Analysis Of Beams With Multiple Constrained Layer Damping Patches*, *Journal of Sound and Vibration*, Volume 212, No.15, p.781-805, (1998)
- [76]. Zheng, H., Cai, C., and Tan, X.M., “Optimization of partial constrained layer damping treatment for vibrational energy minimization of vibrating beams, *Computers and Structures*, Vol. 82, p.2493–2507, (2004)
- [77] Lepoittevin, G. and Kress, G., “Optimization of segmented constrained layer damping with mathematical programming using strain energy analysis and modal data”, *Materials and Design*, Vol.31, p.14–24, (2010)

- [78] Zheng, H., Pau, G.S.H. and Wang, Y.Y., “A comparative study on optimization of constrained layer damping treatment for structural vibration control”, *Thin-Walled Structures*, Vol. 44, p.886–896, (2006)
- [79] Avinashkadam, (2014), ”Finite Element Analysis of Damping Performance of VEM Materials Using CLD Technique”, *Int. Journal of Engineering Research and Applications* ISSN : 2248-9622, Vol. 4, Issue 7 (Version 6), pp.150-153
- [80] Xie, Z, Shepard, W.S. and Woodbury, K.A., “Design optimization for vibration reduction of viscoelastic damped structures using genetic algorithms, *Shock and Vibration*, Vol.16, p.455-466, (2009)
- [81] Duane E. Veley, S. S. Rao, (1994) Two-dimensional finite element modeling of constrained-layer damping, *Proc. SPIE 2193, Smart Structures and Materials: Passive Damping*, 276.
- [82] Subramanian, S., Surampudi, R., Thomson K.R., and Vallurupalli, S., “Optimization of Damping Treatments for Structure Borne Noise Reduction”, *Sound and Vibration*, p.14-17, (2004)
- [83] Maoût, N.L., Verron, E. and Bégueé, J., (2011), “Simultaneous geometrical and material optimal design of hybrid elastomer/composite sandwich plates”, *Composite Structures*, Vol.93, p.1153–1157
- [84] Wang, B.Q., Wang, B.L. and Huang, Z.Y., “Topology optimization for constrained layer damping plates using evolutionary structural optimization method”, *Advanced Materials Research*, Vol.894, p.158-162, (2014)
- [85] Serabatir, D.A., Bayraktar, F. and Sanliturk, K.Y., (2007), “Structural damping optimization using viscoelastic materials”, *INTER-NOISE*
- [86] Boucher, M.A. , Smith, C.w., Scarpa, F., Rajasekaran, R. and Evans, K.E., (2013) , “Effective topologies for vibration damping inserts in honeycomb structures”, *Composite Structures*, Vol.106, p.1-14
- [87] F. Agnese, F. Scarpa, (2014) Macro-composites with star-shaped inclusions for vibration damping in wind turbine blades, *Composite Structures* 108,978-986

- [88] Pai, Rohan Vinay, (2003), "Parameter Study on Topology Optimization of Constrained Layer Damping Treatments. " Master's Thesis, University of Tennessee.
- [89] Pai,R.A.Lumsdaine,M.Parsons,"Design and Fabrication of Optimal Constrained Layer Damping Topologies", Smart Structures and Materials Damping and Isolation, Proc. of SPIE Vol. 5386
- [90] Kim, S.Y., Mechefske, C.K. and Kim, I.Y., "Optimal damping layout in a shell structure using topology optimization", Journal of Sound and Vibration, Vol.332 p.2873-2883, (2013)
- [91] Rong, J.H., Tang, Z.L., Xie, Y.M. and Li, F.Y., "Topological optimization design of structures under random excitations using SQP method", Engineering Structures, Vol.56, p.2098–2106, (2013)
- [92] Lei, Y., Zheng, W., Huang, Q. and Li, C., "Topology optimization of passive constrained layer damping on plates with respect to noise control", Advanced Materials Research, Volumes:774-776, p.3-6, (2013)
- [93] Wenjiong Chen, Shutian Liu, (2014), "Topology optimization of microstructures of viscoelastic damping materials for a prescribed shear modulus, Structural and Multidisciplinary Optimization August 2014, Volume 50, Issue 2, pp 287-296.
- [94] Al-Ajmi M (2004) Homogenization and topology optimization of constrained layer damping treatments. Ph.D. dissertation, University of Maryland
- [95] Whittier, J .S. (1959), The Effects of Configurational Additions Using Viscoelastic Interfaces on the Damping of a Cantilever Beam: WADC TR 58-568, ASTIA Doc. 214381
- [96] Patel, B.M., Warnaka, G.E, Mead, D.J., (1978) ,"New Structural Damping Technique For Vibration Control", The Shock And Vibration Bulletin Part 2 Isolation and Damping, Impact, Blast, p.39-52
- [97] Corsaro, R.D. and Sperling, L.H., Sound and Vibration Damping with Polymers, Volume 424 American Chemical Society, (1990).

- [98] Painter, G.W. U.S. Patent 3 079 277, 1963
- [99] Falugi, M., Moon, Y., and Arnold, R., (1989) "Investigation of a Four Layer Viscoelastic Constrained Layer Damping System," USAF/WL/FIBA/ASIAC, Report No. 189.1A.
- [100] Parin, M., Rogers L., Moon Y. I., and Falugi M., (1989) "Practical Stand-Off Damping Treatment for Sheet Metal", Proceeding of Damping '89, Vol. II, Paper No. IBA.
- [101] Rogers, L., and Parin, M., (1995) "Experimental Results for Stand-off Passive Vibration Damping Treatment," Passive Damping and Isolation, Proceedings SPIE Smart Structures and Materials, Vol. 2445, pp. 374–383
- [102] Yellin JM, Shen IY. (1998), An analytical model for a passive stand-off layer damping treatment applied to an Euler-Bernoulli beam, Proceedings of SPIE. Vol. 3327 1998 pp. 349–57
- [103] A.W. van Vuure, I. Verpoest, F.K.Ko, (2001), "Sandwich-fabric panels as spacers in a constrained layer structural damping application", Composites Part B 32, 11-19
- [104] Peter Y.H. Huang, Per G. Reinhall, I. Y. Shen and Vipin Kumar, (2001), "Use of Microcellular Foam Materials in Constrained Layer Damping Treatments", Cellular Polymers, Vol.20, No.2
- [105] Yellin JM, Shen IY, Reinhall PG, Huang PYH. (1999), An experimental investigation of a passive stand-off layer damping treatment applied to an Euler-Bernoulli beam Proceedings of SPIE, pp. 228–33.
- [106] Jessica M. Yellin, I.Y. Shen, and Per G. Reinhall, (2000), "An analytical model for a one-dimensional slotted stand-off layer damping treatment", Proceedings of SPIE Vol. 3989, 132-141

- [107] Yellin, J. M., Shen, I. Y. and Reinhall, P. G. (2005). Experimental and finite element analysis of stand-off layer damping treatments for beams, in K. W. Wang (ed.), *Smart Structures and Materials 2005: Damping and Isolation*, Vol. 5760 of *Proceedings of the SPIE - The International Society for Optical Engineering*, San Diego, CA, US, pp. 89–99
- [108] A.Gandhi Pavanasam, (2002) *Optimization of Standoff Constrained Layer Damping for Sandwich Composite Panels*, Msc Thesis, Mepco Schlenk Engineering College, Sivakasi, India.
- [109] A. Chaudry, A. Baz, (2006), "Vibration Control of Beams using Stand-Off Layer Damping: Finite Element Modeling and Experiments ",*Smart Structures and Materials* ,Proc. of SPIE Vol. 6169 61690R-1
- [110] Naveed Ahmad, Rakesh K. Kapania, Complex modes in damped sandwich beams using beam and elasticity theories, *Advances in Aircraft and Spacecraft Science*, Vol.2, No.1 (2015) 57-76
- [111] X.Huang, S.Zhou, G.Sun, G.Li,Y.M.Xie, Topology optimization for microstructures of viscoelastic composite materials, *Comput. Methods Appl. Mech. Engrg.* 283 (2015) 503–516.
- [112] *Vibration Damping*, Ahid D.Nashif, David I.G.Jones, and John P.Henderson, John Wiley & Sons, Inc., NY.,1985 pp-36
- [113] Dukkipati R.V, Srinivas J.,*Textbook of Mechanical Vibrations* ,2nd Ed.Phi Learning,2012.
- [113] De Silva CW. *Vibration: fundamentals and practice*. Boca Raton: CRC Press LLC; 2000
- [114] Metu ME532 Lecture Notes,2014
- [115] M.Colakoglu, Factors Effecting Internal Damping of Aluminum *Journal Of Theoretical and Applied Mechanics* 42, 1, pp. 95-105, Warsaw 2004

- [116] Hui Lu, Xianping Wang, Tao Zhang, Zhijun Cheng and Qianfeng Fang, Design, Fabrication, and Properties of High Damping Metal Matrix Composites—A Review, *Materials* 2009, 2, 958-977
- [117] E. Sarlin, Y. Liu, M. Vippola, M. Zogg, P. Ermanni, J. Vuorinen, T. Lepistö, (2012), Vibration damping properties of steel/rubber/composite hybrid structures, *Composite Structures*, 94, 3327-3335.
- [118] Danton Gutierrez-Lemini,(2013), *Engineering Viscoelasticity*, Springer-Verlag New York Inc. pp.2-3
- [119] E. Rivin, *Stiffness and Damping in Mechanical Design*, Marcel Dekker, New York, 1999.
- [120] R. S. Lakes, *Viscoelastic Materials*, Cambridge University Press 2009
- [121] Evaristo Riande, Ricardo Diaz-Calleja, Margarita Prolongo, Rosa Masegosa, Catalina Salom, *Polymer Viscoelasticity: Stress and Strain in Practice*, November 5, 1999 by CRC Press
- [122] C.Beards, *Structural Vibration: Analysis and Damping*, "Transverse Vibration of Thin Uniform Beam", Sec.4.2 ,pp:133-134
- [123] [Online] Retrieved from:
http://www.serendi-cdi.org/serendipedia/index.php?title=Dynamic_Beam_-_Physics&oldid=1910 [Accessed on 6.02.2016]
- [124] Rao Y., Sadasiva V.K., Nakra B.C., Vibrations of unsymmetrical sandwich beams and plates with viscoelastic plates, 1974, *Journal of Sound andVibration*, 34(3), 309-326
- [125] Lecture Notes [online] Retrieved from:http://www.ce.memphis.edu/7117/notes/presentations/chapter_06a.pdf [Accessed on 12.12.2015]
- [126] B.J.Mac Donald , *Practical Stress Analysis with Finite Elements* 2nd Edition

- [127] Ansel C. Ugural, Saul K. Fenster, *Advanced Mechanics of Materials and Applied Elasticity*, (2011), 5th Ed., Prentice Hall, USA
- [128] Lecture notes [Online] Retrieved from : www.rpi.edu/~des/FEM2&3D.ppt
[Accessed on: 15.12 2015]
- [129] Reddy, J.N. (2005), *An Introduction to the Finite Element method*, 3rd Edition, McGraw-Hill, New York, NY, USA
- [130] S. S. Rao, *Mechanical vibrations*, Prentice Hall, Upper Saddle River, N.J., 2011
- [131] Angelo De Fenza, Phd Thesis, (2011), *Experimental and Numerical Estimation of Damping In Composite Plates with Embedded Viscoelastic Treatments*
Department of Aerospace Engineering, University of Naples Federico II.
- [132] Optistruct 13.0 User Guide [Online] Retrieved from:
ftp://ftp.altair.com.cn/priv/support/hw12.0/hw12.0_installation/hw12_docs/OptiStruct/OptiStruct_12.0_User_Guide.pdf [Accessed on 23.12.2015]
- [133] D.J.Mead, (2007), The measurement of the loss factors of beams and plates with constrained and unconstrained damping layers: A critical Assesment. *Journal of Sound and Vibration* (300) 744-762
- [134] E.Hinton, et al., *Analysis and Optimization of Prismatic and Axisymmetric Shell Structures*, Springer-Verlag London 2003
- [135] Retrieved from: <http://www.tog.ie/wp-content/uploads/2015/05/product-cad-design-computer-7986312.jpg> [Accessed on 28.12.2015]
- [136] Kirsch, Uri, (1993), *Structural Optimization, Fundamentals and Applications*, Springer-Verlag Berlin Heidelberg
- [137] Bendsøe, M.P. and Sigmund, O., “Material Interpolation Schemes in Topology Optimization,” *Archives in Applied Mechanics*, Vol. 69, (9-10), 1999, pp. 635-654
- [138] Olhoff and Du, 2013, *Introductory Notes on Topological Design Optimization of Vibrating Continuum Structures*

- [139] Claus C. Claeys, Karel Vergote, Paul Sas, Wim Desmet, (2013), On the potential of tuned resonators to obtain low-frequency vibrational stop bands in periodic panels, *Journal of Sound and Vibration*, Volume 332, Issue 6, Pages 1418–1436
- [140] M.I. Hussein, K. Hamza, Gregory M. Hulbert, K. Saitou, (2007), Tailoring of two-dimensional band-gap materials for broadband frequency isolation, *Proceedings of ASME, IDETC/CIE, Las Vegas, Nevada, USA*
- [141] Z. Liu, X. Zhang, Y. Mao, Y. Zhu, Z. Yang, C. Chan, P. Sheng, Locally resonant sonic materials, *Science* 289 (5485)(2000) 1734–1736
- [142] Dede, E.M. and Hulbert, G.M., “Mid-frequency response of structures with integral compliant mechanisms: Verification and validation”, *Journal of Sound and Vibration*, Vol.313, p.493–509, (2008)
- [143] Hyperworks 13.0 User Guide
- [144] Materials and their mechanical properties are retrieved from: The Soundcoat Company, Deer Park, L.I., N.Y. 11729-5701, Contact Person: Rebecca Brutus.
- [145] 3D printing Software helps you design for 3D printing manufacturability by Leslie Langnau, March 7, 2013 [Online] Retrieved from: <http://www.designworldonline.com/software-helps-you-design-for-3d-printing-manufacturability/>
- [146] G. I. N. Rozvany. Aims, scope, methods, history and unified terminology of computer aided topology optimization in structural mechanics. *Struct. Multidisc. Optim.*, 21:90,108, 2000
- [147] Jacqueline Sanchez Hubert, *Vibration and Coupling of Continuous Systems: Asymptotic Methods* Springer, 1989.
- [148] Global Response Surface Method [Online] Retrieved from: <http://www.altairuniversity.com/2014/02/13/one-click-optimization> [Accessed on 10.02.2016]